University of Strathclyde

Strathclyde Institute of Pharmacy and Biomedical Sciences

Preparation and Evaluation of Tumour-targeted Delivery Systems for Tocotrienol

by

Ju Yen Fu

A thesis presented in fulfilment of the requirements for the degree of Doctor of Philosophy

2010

For those who are inspired, "There are only two ways to live your life. One as though nothing is a miracle, the other is as though everything is a miracle." ~ Albert Einstein.

TABLE OF CONTENTS

CHAPTER 1: INTRODUCTION

CHAPTER 2: PREPARATION AND CHARACTERIZATION

CHAPTER 5: CONCLUSION AND FUTURE WORKS

LIST OF FIGURES

ABBREVIATIONS

ABC	ATP-binding cassette
ANH	Alliance for NanoHealth
CARS	Coherent anti-Stokes Raman scattering
CEHC	Carboxyethylhydrochroman
CLSM	Confocal laser scanning microscopy
CMC	Critical micelle concentration
CME	Clathrin-mediated endocytosis
COX	Cyclooxygenase
CvME	Caveolae-mediated endocytosis
DLVO	Derjaguin-Landau-Verwey-Overbeek
DMEM	Dulbecco's Modified Eagle Medium
DMSI	Dimethylsuberimidate dihydrochloride
DMSO	Dimethyl sulfoxide
DOPE	Dioleoyl-phosphatidylethanolamine
DR	Death receptor
EGF	Epidermal growth factor
EPR	Enhanced permeability and retention effect
ERK	Extracellular signal-regulated kinases
FADD	Fas-associated death domain
FCS	Foetal calf serum
FGF	Fibroblast growth factor
GF	Growth factor
HAEC	Human aortic endothelial cell
HDL	High density lipoprotein
HLB	Hydrophilic lipophilic balance
HMG-CoA	3-hydroxy-3-methyl-glutaryl-CoA
HPLC	High performance liquid chromatography
IC_{50}	Growth inhibitory concentration
IR	Infrared
JNK	c-Jun N-terminal kinase
LDL	Low density lipoprotein
MAPK	Mitogen-activated protein kinase
MDR	Multidrug resistance
MLV	Multilamellar vesicles
MTT	3-(4,5-dimethylthiazol-2-yl)-2,5-diphenyl-tetrazolium bromide
NADPH	Pyridinic coenzyme
NCI	National Cancer Institute
NF-κB	Nuclear factor kappa-light-chain-enhancer of activated B cells
NIH	America National Institute of Health

nu/nu	Nude athymic
OPO	Optical parametric oscillator
PAMAM	Polyamidoamines
PBS	Phosphate-buffered saline
PDI	Polydispersity index
PE	Phosphatidylethanolamine
PEG	Polyethylene glycol
PFAD	Palm fatty acid distillate
P-gp	P-glycoprotein
PLA	Poly(lactide)
PLGA	Poly(lactide-co-glycolide)
PMT	Photomultiplier detector tubes
PPI	Polypropyleneimine
RECIST	Response evaluation criteria in solid tumours
RES	Reticulo-endothelial system
ROS	Reactive oxygen species
RPMI	Roswell Park Memorial Institute
scid/scid	Severe combined immunodeficient
Solulan C24	Cholesteryl poly(24)oxyethylene ether
Span 60	Sorbitan monostearate
SR-BI	Scavenger receptor class B type I
SREBP	Sterol regulatory element binding protein
TEF	Tocotrienol-enriched fraction
TEM	Transmission electron microscopy
Tf	Transferrin
TfR	Transferrin receptor
TNF	Tumour necrosis factor
TPGS	Tocopheryl polyethylene glycol succinate
TRAIL	Tumour necrosis factor-related apoptosis-inducing ligand
TRF	Tocotrienol-rich fraction
VEGF	Vascular endothelial growth factor
VLDL	Very low density lipoprotein
α-TTP	α-tocopherol transfer protein

ABSTRACT

Tocotrienol, a group of compounds present in vitamin E, has gained much attention in recent years for its tumour suppressive properties on cancer cells. However, its therapeutic potential was hampered by the limited ability to reach tumours specifically after intravenous administration. In this study, we aim to develop a formulation of tocotrienol that could be specifically delivered to tumours upon intravenous administration through the use of a tumour-targeted delivery system. Transferrin is an iron transporter whose receptors are often over-expressed in cancer cells due to high iron demand for tumour growth. Conjugation of transferrin to drug delivery systems appeared to be an attractive tool for selective receptor-mediated tumour delivery of therapeutic drugs. The objectives of this study are therefore (1) to prepare and characterize transferrin-bearing vesicles encapsulating tocotrienol and (2) to evaluate *in vitro* and *in vivo* the therapeutic and targeting efficacies of this therapeutic system. This work corresponds to the first preparation of a tumour-targeted delivery system able to encapsulate tocotrienol. The grafting of transferrin to tocotrienol-loaded vesicles demonstrated an improved therapeutic efficacy of tocotrienol to at-least 15-fold compared to free tocotrienol *in vitro*. Intravenous administration of tocotrienol therapeutic systems led to significant tumour regression and improvement in animal survival in murine xenograft models without visible toxicity. In conclusion, our findings showed that tocotrienol encapsulated in transferrin-bearing vesicles is a highly promising therapeutic system, leading to possible eradication of tumours as a result of significant improvement in tocotrienol therapeutic efficacy.

Chapter 1

Introduction

1.1   TOCOTRIENOL

The role of vitamin E as a micronutrient essential for reproduction was discovered in 1922 by Evans and Bishop (Evans and Bishop, 1922). Although vitamin E was first shown to prevent the loss of spermatogenesis in males and the failure to retain zygotes in female rats (Evans and Bishop, 1922), it was later established as a potent antioxidant as well as a key vitamin in neurological dysfunction (Briglius-Florhé and Traber, 1999). Natural vitamin E is defined as a mixture of tocopherol and tocotrienol, essentially occurring in four isoforms, namely alpha (α-), beta (β-), gamma (γ-) and delta (δ-). Structurally, tocopherol and tocotrienol share a common polar chromanol head with two fused rings, one phenolic acid and one heterocyclic ring, linked to an isoprenoid-derived hydrophobic tail (Ghosh *et al.*, 2009). As shown in figure 1.1, the four isoforms differ by the location of methyl groups on the aromatic rings. Tocotrienols are distinguished from tocopherols by the side chain with three *trans* double bonds at positions 3', 7' and 11' whereas tocopherol has a saturated carbon chain. The presence of unsaturated side chain imposes greater curvature and flexibility on tocotrienol molecules, which is believed to facilitate membrane association (Sen *et al.*, 2007). It is very likely that this feature leads to some biological functions not shared by tocopherol, including protection against stroke and neurodegeneration progress, as well as cholesterol-lowering properties (Khanna *et al.*, 2003; Khanna *et al.*, 2005; Sen *et al.*, 2007).

A

	R1	R2
α	CH₃	CH₃
β	CH₃	H
γ	H	CH₃
δ	H	H

B
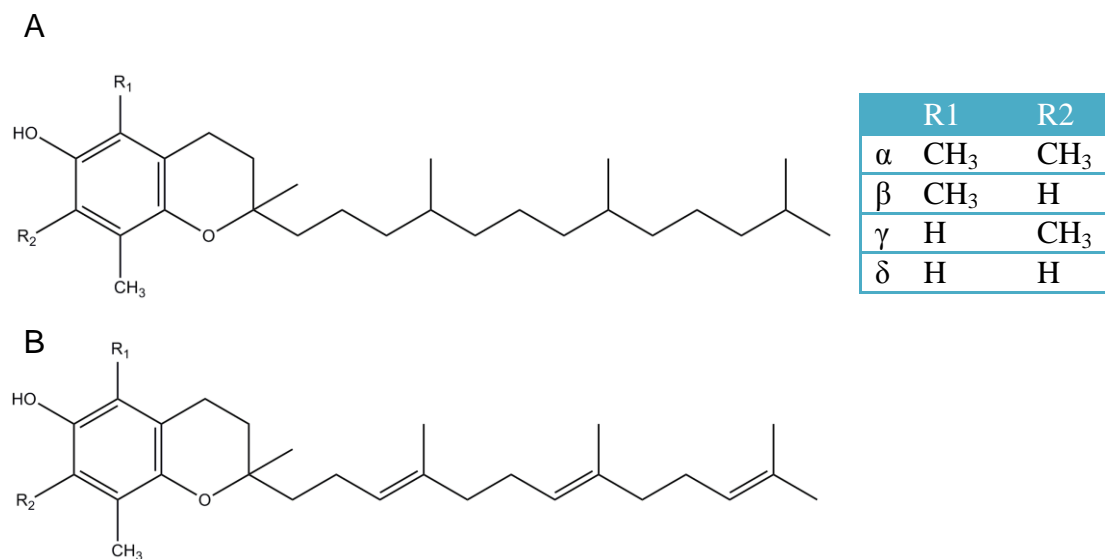
Figure 1.1: Chemical structures of (A) Tocopherols and (B) Tocotrienols.

While tocopherols are found abundantly in vegetable oils (soybean, olive and sunflower seed oils), primary sources of tocotrienols are palm oil, rice bran oil, barley, oat and Annatto (Schauss, 2009). Table 1.1 is the content of vitamin E isoforms obtained from natural sources. Crude palm oil is believed to be the largest natural source of tocotrienol after Annatto (90 % δ-tocotrienol and 10 % γ-tocotrienol). The biosynthesis of tocopherols and tocotrienols is localised in the plastids of seeds and chloroplasts of leaves, via condensation of homogentisic acid (HGA) derived from the shikimate pathway and geranylgeranyl diphosphate derived from the methylerythritol phosphate pathway (Qi *et al.*, 2005). Thus, the availability of HGA was believed to be the determining factor in tocopherol and tocotrienol synthesis (Qi *et al.*, 2005).

Table 1.1: Contents of tocopherols and tocotrienols in natural sources.

	Tocotrienols (mg/100g)					Tocopherols (mg/100g)				
	α	β	γ	δ	Total	α	β	γ	δ	Total
Palm oil	20.5	-	43.9	9.4	**73.8**	15.2	-	-	-	**15.2**
Rice bran	23.6	-	34.9	-	**58.5**	32.4	1.8	5.3	-	**39.5**
Wheat germ	2.4	16.5	-	-	**18.9**	117.9	39.8	49.3	11.8	**218.8**
Barley	67	12	12	-	**91**	35	5	5	-	**45**
Coconut oil	0.5	0.1	1.9	-	**2.5**	0.5	-	-	0.6	**1.1**
Soy bean oil	-	-	-	-	**0**	10.1	-	59.3	26.4	**95.8**
Olive oil	-	-	-	-	**0**	5.1	-	-	-	**5.1**
Peanut oil	-	-	-	-	**0**	13.0	21.6	2.1	-	**36.7**
Safflower oil	-	-	-	-	**0**	38.7	-	38.7	-	**77.4**

(Adapted from Ghosh et al., 2009).

Although tocopherol can be produced using chemical synthesis by condensing isophytol with tri-, di-, or monomethyl hydroquinone, equimolar of racemic mixtures with eight stereoisomers are obtained, whereas natural sources of tocopherol only yield one stereoisomer (Ghosh *et al.*, 2009). Hence, for four tocopherol isomers, a total of 32 stereoisomers are produced when synthesized via chemical process instead of four isomers that should be occurring in natural sources of tocopherol. A recent statement from the America National Institute of Health (NIH) revealed that the synthetic form of tocopherol is only about half as effective in its biological activity as the natural form (Levin and Clouatre, 2009). This was further confirmed in animal and human studies that natural vitamin E are retained

longer in the body and has higher bioavailability over synthetic forms (Kosowski and Clouatre, 2009).

1.1.1 Biological activity of tocotrienol

- *Antioxidant*

The recognition of vitamin E as an antioxidant was long established back in the 1930s (Schauss, 2009). Free radicals and other reactive species of oxygen (ROS) are highly reactive and thereby destructive molecules, commonly known to be the underlying mechanism of many diseases such as atherosclerosis, diabetes, cancer and aging (Simone and Palozza, 2009). For example in lipid peroxidation, free lipid peroxyl radical serves as a chain carrier for propagation (Wang *et al.*, 1999):

$$LO_2\bullet + LH \rightarrow LOOH + L\bullet$$

Where $LO_2\bullet$ is the free lipid peroxyl radical, LH is the target lipid, LOOH is the lipid hydroperoxide and $L\bullet$ is a lipid radical, which will then react with oxygen to generate another lipid peroxyl radical:

$$L\bullet + O_2 \rightarrow LO_2\bullet$$
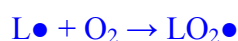
Tocopherol and tocotrienol are antioxidants that can safely interact with free radicals to terminate the chain reaction by donating one of their electrons to neutralise the free radicals. However they do not become radicals after losing an electron because they are stable in either form. Instead, they act as a scavenger to prevent cell and tissue damage caused by oxidative stress (Simone and Palozza, 2009).

$$LO_2\bullet + TOH \rightarrow LOOH + TO\bullet$$
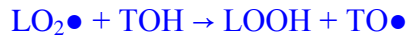
Where TOH represents tocopherol or tocotrienol and TO● is the peroxyl form of tocopherol or tocotrienol (Wang *et al.*, 1999).

Numerous studies showed that tocotrienol has greater reactivity against oxidative stress compared to tocopherol, up to 40-60 times higher (Yoshida and Niki, 2009). Many suggested that it might be due to the higher mobility of tocotrienol owing to the three double bonds, thus better incorporated in cell membranes leading to elevated cellular uptake compared to tocopherol (Noguchi *et al.*, 2009; Simone and Palozza, 2009). Tocotrienol as a potent antioxidant has been extensively explored in various human diseases, especially in the protection against cardiovascular disease.

- *Cardiovascular disease*

Atherosclerosis is the process of cholesterol plaque deposition on interior artery lining, when vessels become narrower and eventually blocked by the fatty deposit. As a consequence, extensive damage to heart tissue often leads to the development of ischemic heart disease and myocardial infarction (Das *et al.*, 2009). The initiation of atherosclerosis is the accumulation of low density lipoprotein (LDL) in the endothelium. LDL is a cholesterol carrier, which becomes the oxidised form in the endothelium of the arteries (ox-LDL) when in contact with free radicals (Cao *et al.*, 2009). Accumulation of ox-LDL often triggers a series of inflammation response, whereby monocytes are recruited, promoting cholesterol acumulation while

propagating the inflammatory process, eventually leading to the formation of atherosclerosis plaque in the endothelium of blood vessel lining (Cao *et al.*, 2009). Tocotrienol plays an important role in slowing the process of atherosclerosis by preventing the oxidation of LDL, as an early prevention of plaque deposition (Das *et al.*, 2009). In addition to reducing ox-LDL, tocotrienol was also found to inhibit the adherence of monocytes to the endothelium (Naito and Yoshikawa, 2009). In human aortic endothelial cells (HAEC), treatment with tocotrienol demonstrated a significant inhibition of monocyte-endothelial interactions (Naito and Yoshikawa, 2009). Moreover, tocotrienol was also found to reduce the levels of total cholesterol and LDL (major precursors in cardiovascular risk factors) by 30 % and 67 % in rats induced with hypercholesterolemia (Juturu, 2009). The mechanism of tocotrienol in cholesterol regulation is discussed as follow.

- *Regulation in cholesterol biosynthesis*

High blood cholesterol or hypercholesterolemia, is a metabolic malfunction derived from genetic disorder or high cholesterol dietary, also a major cause for development of diseases such as atherosclerosis and Alzheimer's disease (Cao *et al.*, 2009). Cholesterol is synthesized from acetate precursor acetyl-CoA, which is converted to HMG-CoA (3-hydroxy-3-methyl-glutaryl-CoA) via condensation. HMG-CoA reductase plays an important role to reduce HMG-CoA to mevalonate, where further condensation takes place to form lanosterol and finally cholesterol (Figure 1.2) (Cao *et al.*, 2009). Tocotrienol, but not tocopherol, has the ability to alter cholesterol biosynthesis pathway by affecting the HMG-CoA reductase activity, also known as the rate limiting steps in cholesterol synthesis (Schauss, 2009). Upon

treatment with tocotrienol, upstream protein of HMG-CoA reductase, sterol regulatory element binding protein (SREBP), was found to be restrained in the reticular endothelium (Cao *et al.*, 2009). Degradation of HMG-CoA reductase was also detected with tocotrienol treatment (Cao *et al.*, 2009). In a human study conducted by Bristol-Myers Squibb, 4-weeks supplementation of tocotrienol was found to reduce cholesterol level by 15-22 % and LDL level by 10-20 % (Tan and Mueller, 2009).
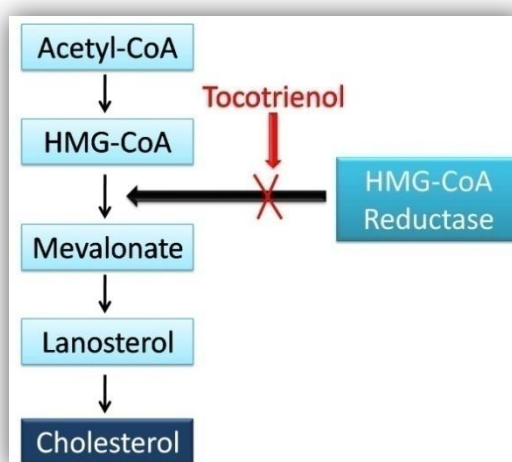
Figure 1.2: The role of tocotrienol in suppressing cholesterol biosynthesis.

- *Protection against neurodegeneration*

Numerous pathophysiological conditions in the brain and neural tissues such as Alzheimer's and Parkinson's diseases arise from oxidative damage. Antioxidant defences are thus regarded as a critical step for sufficient neuroprotection, as such vitamin E has been an important subject of study in neurological research. Glutamate-toxicity is a major contributor to neurodegeneration, when HT4 hippocampal neural cells were challenged by glutamate, tocotrienol provides

complete neuroprotection against glutamate-induced cell death (Sen *et al.*, 2000). In the same study, α-tocotrienol was found to be the most potent vitamin E isoform for neuroprotection at nanomolar concentrations, a phenomenon not evident with tocopherol (Sen *et al.*, 2000). It was suggested that the antioxidant property of tocotrienol should not have an activity at such low dose, which leads to the hypothesis that tocotrienol exerts its neuroprotective effect via antioxidant-independent pathway. This hypothesis was further confirmed when tocotrienol was found to regulate specific neurodegenerative signalling process via inhibiting c-Src kinase and 12-lipoxygenase activity (Sen *et al.*, 2009). Overexpression of c-Src kinase activity as a result of glutamate treatment markedly sensitised HT4 neuronal cells to induce cell death whereas 12-lipoxygenase is the major enzymatic activity in arachidonic acid metabolism, of which arachidonic acid and its metabolites are neurotoxic and that massive amounts are released in response to brain ischemia or trauma (Sen *et al.*, 2009). Therefore, suppression of c-Src kinase and 12-lipoxygenase activity by tocotrienol eventually leads to effective neuroprotection against glutamate-induced damage to neural cells.

- *Anticancer activity*

The anti-cancer properties of tocotrienol have been the focus of tocotrienol research for over a decade. In animal studies, administration of tocotrienol, but not tocopherol, suppressed the growth of human breast cancer and colorectal cancer (Nesaretnam, 2008). Various studies suggested that the anti-cancer property associated with vitamin E is in fact a distinctive characteristic of tocotrienol. In this

work, we exploit the potential of tocotrienol as a therapeutic agent for cancer therapy using tocotrienol-rich fraction (TRF) extracted from palm oil.

1.1.2 Tocotrienol and cancer

Palm oil-derived tocotrienol was first reported in 1989 to have the ability to prevent chemically induced mammary tumorigenesis in rats by Sundram *et al.* (Sundram *et al.*, 1989). This chemopreventive characteristic was further confirmed in the early 90's when tocotrienol efficiently prevented the growth of implanted tumours in mammary tumours and hepatic tumours (Komiyama *et al.*, 1989; Guthrie *et al.*, 1997; Schauss, 2009). In 1995, Nesaretnam *et al.* proved that this unique ability to inhibit cancer cell growth was restricted to tocotrienol, but not tocopherol (Nesaretnam *et al.*, 1995). Following promising evidence obtained *in vitro* against human oestrogen receptor-negative MDA-MB-435 breast cancer cells, tocotrienol was subsequently found to be efficacious against prostate cancer cells (LNCaP, DU145, PC-3), adenocarcinoma cells (HeLa), colon carcinoma (RKO), fibrosarcoma cells (HT1080) and Hep3B hepatoma cells (Nesaretnam *et al.*, 1995; Inokuchi *et al.*, 2003; Mizushina *et al.*, 2006; Sakai *et al.*, 2006; Srivastava and Gupta, 2006). *In vivo,* oral supplementation of tocotrienol led to a significant delay in tumour growth in murine B16 melanomas, which was further confirmed by Nesaretnam *et al.* (2004) on tumour model of breast cancer cells (MCF-7) (He *et al.*, 1997). Wada *et al.* (2005) then showed that reduced liver and lung carcinogenesis was observed upon oral administration of tocotrienol. Since then, tocotrienol has gained much attention for its anti-cancer properties. To date, tocotrienol was found active against gastric cancer cells, colon carcinoma cells, pancreatic carcinoma cells, liver cancer cells and

prostate cancer cells *in vitro* (Har and Cheong, 2005; Sun *et al.*, 2008; Yap *et al.*, 2008; Hussein and Mo, 2009; Xu *et al.*, 2009).

Nevertheless, compounds derived from food sources are often classified as chemopreventive agents due to their ability to delay the onset of carcinogenic process by suppressing the transformative, hyperproliferative and inflammatory processes that initiate carcinogenesis (Dorai and Aggarwal, 2004). In the case of tocotrienol, most studies involved the use of tocotrienol as therapeutic adjuvant. For example, synergistic anti-proliferative effects were observed using combined treatment of γ-tocotrienol with chemotherapy drugs and celecoxib, a selective cyclooxygenase (COX)-2 inhibitor (Chang *et al.*, 2009; Shirode and Sylvester, 2010). Statins including simvastation, lovastatin and mevastatin showed no anti-cancer effect when used alone but demonstrated a significant cell cycle arrest and inhibition of cell growth when used in combination with tocotrienol (Wali *et al.*, 2009). Consistently, further study by Yang *et al.* (2010) showed synergistic anti-proliferative effect of tocotrienol when combined with atorvastatin and celecoxib in human colon cancer cells HT 29 and HCT116. Moreover, recent studies by Kunnumakkara *et al.* (2010) and Yap *et al.* (2010) showed that tocotrienol when used in combination therapy, has the ability to potentiate gemcitabine- and docetaxel-induced apoptosis in pancreatic cancer cells and prostate cancer cells, thus enhancing the anti-tumour properties of the respective chemotherapy. Meanwhile, tocotrienol was also exploited for its synergistic effect on radiation sensitization on prostate tumours as well as in augmenting the effectiveness of dendritic cell vaccines in mouse mammary cancers (Kumar *et al.*, 2009; Hafid *et al.*, 2010).

A general delay in tumour growth was observed when tocotrienol was used alone as a chemopreventive agent, as shown in murine hepatoma tumours by Hiura *et al.* (2009). In mice bearing B16 melanoma tumours, co-administration of tocotrienol and lovastatin induced apparent reduction in tumour weight upon oral administration (McAnally *et al.*, 2007). In fact, the Malaysian Palm Oil Board in association with Hospital Kuala Lumpur embarked on a clinical trial of tocotrienol in 2006 for combination therapy with tamoxifen (conventional chemotherapy for breast cancer). This 5-year clinical trial involved 240 women aged between 40-60 years old diagnosed with early breast cancer. Patients were given oral administration of tamoxifen in conjunction with tocotrienol or tamoxifen plus placebo. Although there seems to be no association between tocotrienol and breast cancer recurrence, the risk of mortality due to breast cancer was 60 % lower with tocotrienol treatment group. Five-year breast cancer specific survival and disease free survival were also slightly improved with adjuvant tocotrienol therapy (Nesaretnam *et al.*, 2010).

1.1.3 Mechanism of action

According to previous research efforts to elucidate the mechanism of action of tocotrienol, its anti-cancer properties at the molecular level appeared rather complex. Among the proposed pathways, induction of apoptosis was said to play a major role (Figure 1.3). Early research in the molecular biology of tocotrienol was promising when caspases 8 and 3 from the caspase cascade were found to be upregulated (Sakai *et al.*, 2004; Sylvester and Shah, 2005). The caspase cascade with 'initiator' caspases 8 and 9 and 'effector' caspases 3, 6 and 7 are actively inducing

apoptosis via various pathways, one of which is initiated by Bax protein (Sylvester and Shah, 2005). An increase in Bax protein enhances the mitochondrial membrane permeability, leading to cytochrome c release, an essential factor in activation of caspase 3 (Sakai *et al.*, 2006). A study by Agarwal *et al.* (2004) showed an increase in Bax protein in colon carcinoma RKO cells when treated with tocotrienol. In this study, cells appeared shrunk with condensed chromatin and DNA fragmentation, a clear indication of apoptosis (Agarwal *et al.*, 2004). Upregulation of Bax protein upon tocotrienol treatment was consistent in hepatoma Hep3B, colon carcinoma HT-29 and gastric cancer SGC-7901 cells (Sun *et al.*, 2008; Xu *et al.*, 2009). In conjunction with an upregulation of tumour suppressor gene p53, extracellular signal-regulated kinases (ERK) 1 and reactive oxygen species (ROS), elevated Bax protein also led to an upregulation of death receptor (DR) 4 and 5 in the tumour necrosis factor-related apoptosis-inducing ligand (TRAIL) pathway, triggering the activation of apoptosis (Kannappan *et al.*, 2010).

As mentioned above, tocotrienol was found to increase caspase 8 activity. However, in an effort to elucidate the upstream of caspase 8 activation, which is closely associated with the FADD (Fas-associated death domain) pathway, tocotrienol was found to have no effect on Fas, FasL and FADD (Shah and Sylvester, 2004). It was then confirmed that tocotrienol-induced caspase 8 activation was due to the suppression of anti-apoptotic proteins, i.e. PI3K or PI3K-dependant kinase, phosphor-Akt, FLIP, Bcl-xl, Bcl-2 and several other proteins (Shah and Sylvester, 2004; Sylvester and Shah, 2005; Ahn *et al.*, 2007; Kannappan *et al.*, 2010). Anti-apoptotic proteins, often overexpressed in tumour cells, are usually able to sequester

pro-apoptotic proteins, thus hampering the normal development of cell death (Kostanová-Poliaková and Sabova, 2005; Richardson and Kaye, 2008). Therefore, inhibition of anti-apoptosis proteins by tocotrienol was expected to promote apoptosis.
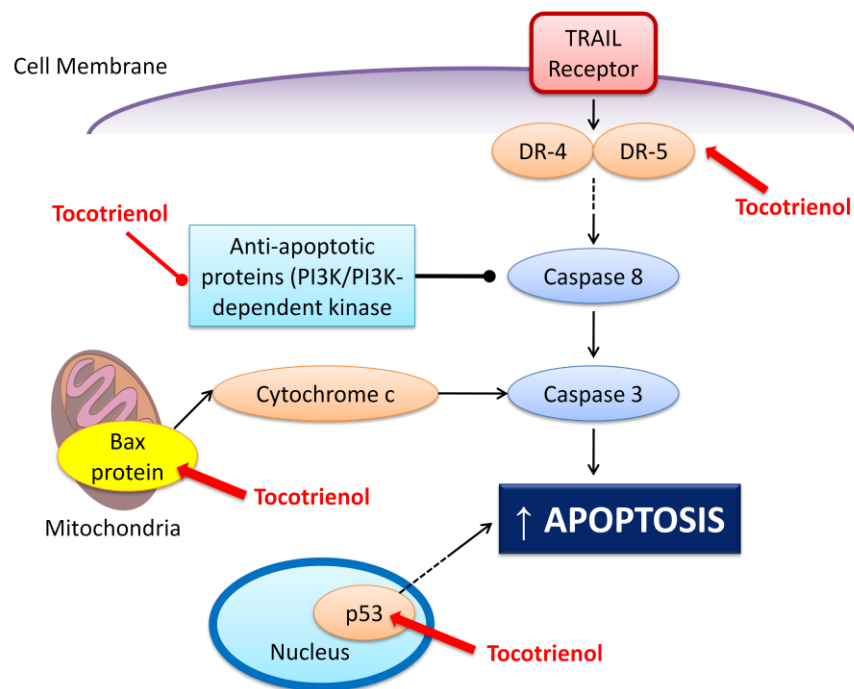
Figure 1.3: Tocotrienol-mediated upregulation of apoptosis. Mechanisms involved increased expression of p53, DR4 and 5, Bax protein as well as suppression of anti-apoptotic proteins.

Moving from apoptosis, a study by Sun *et al.* (2008) showed that treatment with therapeutic doses of tocotrienol interfered with the mitogen-activated protein kinase (MAPK) pathway. The MAPK pathway is essentially responsible for cell proliferation, differentiation, apoptosis and transformation (Seger and Krebs, 1995). Substrates and downstream proteins of MAPK pathway such as ERK, p38, JNK (c-Jun N-terminal kinase) and c-Myc are generally upregulated in cancer cells (Seger and Krebs, 1995; Marampon *et al.*, 2006; Wagner and Nebreda, 2009). When gastric

adenocarcinoma SGC-7901 cells were incubated with tocotrienol, upstream proteins of MAPK pathway Raf-1, ERK1/2 proteins and c-Myc expression were significantly suppressed (Figure 1.4) (Sun *et al.*, 2008). Transcription factor c-Myc was known to reduce cell cycle progression and influence apoptosis when downregulated, playing an important role in halting cell proliferation (Marampon *et al.*, 2006). In 2007, Ahn *et al.* suggested that tocotrienol has the ability to block tumour necrosis factor (TNF)-induced phosphorylation pathways in nuclear factor kappa-light-chain-enhancer of activated B cells (NF-κB) subunit p65, suppressing its nuclear translocation, thus limiting cell cycle progression and survival (Figure 1.4) (Ahn *et al.*, 2007; Xu *et al.* 2009). Cell cycle arrest was further proven in HT-29 cells, Bca breast cancer cells, HeLa cells and a series of prostate cancer cells (Srivastava and Gupta, 2006; Xu *et al.*, 2009; Wu *et al.*, 2010; Yap *et al.*, 2010).
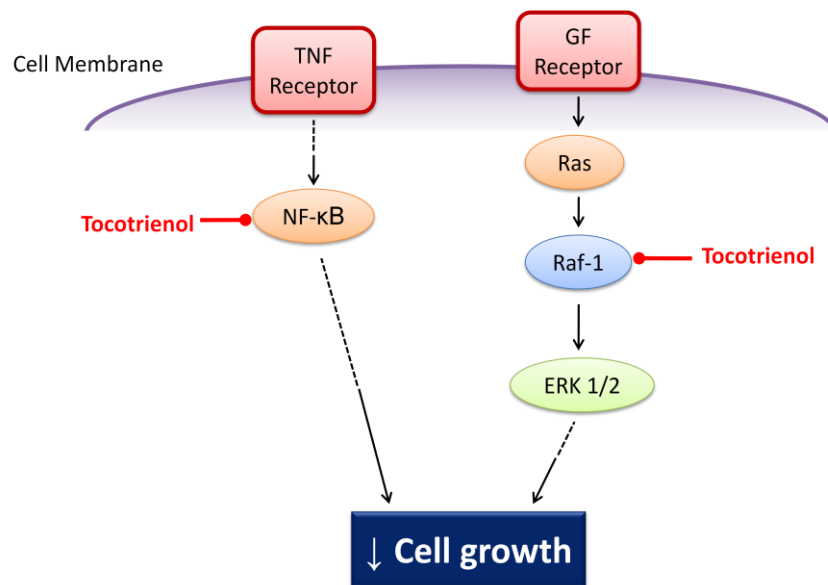
Figure 1.4: Postulated cell growth inhibition mechanism of tocotrienol via inhibition of downstream proteins from growth factor (GF) receptor and tumour necrosis factor (TNF) receptor pathways.

On the other hand, the tumour suppressor p53 protein is well known for its role in regulating survival via several pathways, essentially maintaining the genome stability and normal cell growth. The main function of p53 is to trigger cell cycle arrest for DNA repair when cells encounter stresses like DNA damage or oncogenic assault (Chen *et al.*, 2010). During cancer progression however, p53 is hijacked in all forms of tumours either trapped in negative regular or directly mutated or deleted (Chen *et al.*, 2010). Studies in THP-1 monocytes and colon carcinoma RKO cells showed that treatment of cells with tocotrienol restored the function of p53, activating a sequence of apoptosis and cell death pathways (Agarwal *et al.*, 2004; Munteanu *et al.*, 2007).

Both tumour and normal tissues need blood supply for oxygen, nutrients and waste removal (Shchors and Evan, 2007). Angiogenesis is an essential process in which the vascular tree is remodelled by the growth of new capillaries from pre-existing vessels, satisfying the metabolic demands of tissue (Papetti and Herman, 2002). Under normal circumstances, angiogenesis is a highly ordered process under tight regulation (Papetti and Herman, 2002). Tumour cells, however, have the ability to induce their own blood supply from pre-existing vasculature, allowing the tumour cells to survive and propagate in a hostile environment (Papetti and Herman, 2002). Angiogenesis is initiated when specific angiogenic molecules, i.e. vascular endothelial growth factor (VEGF), fibroblast growth factor (FGF) and epidermal growth factor (EGF) are released from tumour cells (Miyazawa *et al.*, 2009). VEGF in particular was reported to enhance angiogenesis via alteration of vascular

permeability (Veikkola *et al.*, 2000). In 2008, a study by Shibata *et al.* showed that tocotrienol almost completely suppressed the endothelial cell tube formation and migration, presumably due to inhibition of VEGF receptors (Figure 1.5) (Shibata *et al.*, 2008). Furthermore, inhibitory effect of tocotrienol on tube formation in bovine aortic endothelial cells was also shown to be partly mediated by suppression of DNA polymerase λ (Mizushina *et al.*, 2006). DNA polymerases are the only biological macromolecules able to duplicate genetic information stored in the DNA, thus playing a crucial role during DNA replication or DNA repair (Crespan *et al.*, 2010). *In vivo*, angiogenic response assessed using the dorsal air sac method showed a direct anti-angiogenic effect induced by tocotrienol when studied using chick chorioallantoic cells (Miyazawa *et al.*, 2009).
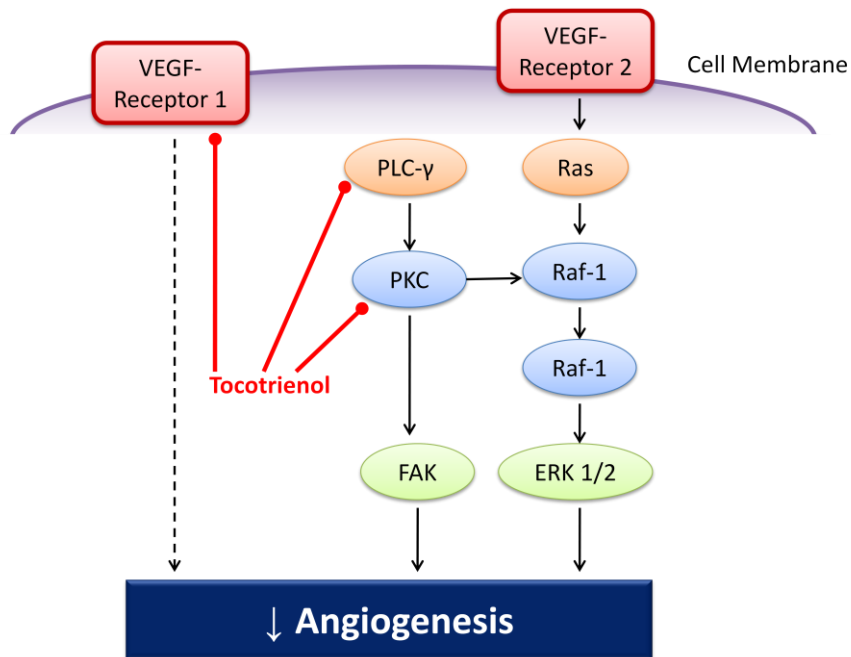
Figure 1.5: Anti-angiogenic mechanism of tocotrienol by downregulation of VEGF receptors and suppression of phospholipase C γ (PLC-γ) and protein kinase C (PKC) in the VEGF signalling pathway *(Modified from Nakagawa et al., 2009).*

1.1.4 Tocotrienol Rich Fraction (TRF)

As shown in table 1.1, palm oil contains as much as 70% tocotrienol in its vitamin E content, one of the richest sources of tocotrienol. Alongside with Japanese researchers, Malaysian Palm Oil Board has patented and commercialised a process for the extraction of palm vitamin E from starting material: palm fatty acid distillate (PFAD) (Nesaretnam *et al.*, 1995; Nesaretnam *et al.*, 2007). PFAD containing 0.4 % vitamin E was first converted to methyl esters by esterification prior to distillation, producing a vitamin E concentrate (Figure 1.6). An ion exchange column was used to concentrate the vitamin E by crystallisation, giving a purity of 60-70 % in the vitamin E concentrate. Further purification process was carried out via molecular distillation in order to improve the vitamin E purity; up to 80-95 % purity was achieved. The vitamin E complex is now known as tocotrienol-rich fraction (TRF). In this study, the composition of TRF used contains 17.6 % α-tocotrienol, 23.1 % γ-tocotrienol, 15.1 % δ-tocotrienol, 15.3 % α-tocopherol and other tocopherol and tocotrienol-related compounds.
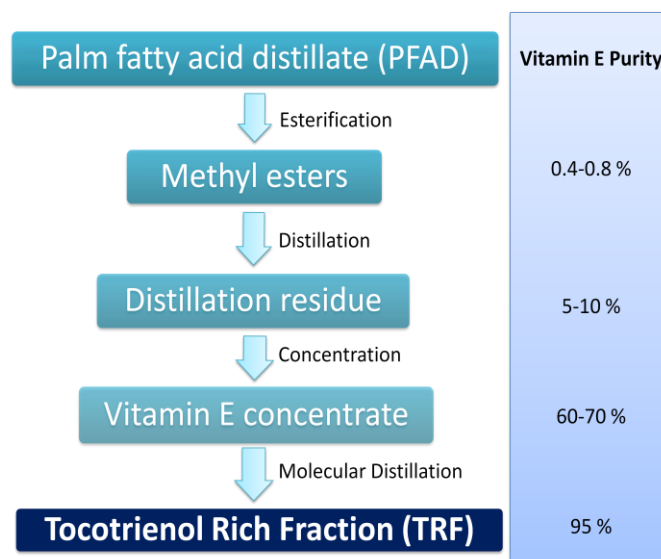
Figure 1.6: Extraction process of tocotrienol-rich fraction (TRF) from palm fatty acid distillate *(Modified from Nesaretnam et al., 2007).*

However, one of the major obstacles in formulating TRF is its high hydrophobicity. Poor aqueous solubility of a drug has often caused significant problems during formulation for clinical applications, limiting its efficacy and utility (Sanghvi *et al.*, 2007; Huh *et al.*, 2008). For hydrophobic compounds, conventional techniques such as the use of organic solvent, surfactants, microemulsions, cyclodextrins and relevant excipients is commonly used to enhance their solubility (Cheng *et al.*, 2006). However, these methods are not always effective, often require excipient to drug ratios of at least 15 : 1 or up to 1000 : 1 (Cheng *et al.*, 2006). For example formulation of paclitaxel in Cremophor EL$^{®}$ (50:50 v/v polyoxyethylated caster oil/ethanol) needs a large volume of solvent to completely solubilise the drug, which frequently causes life-threatening hypersensitivity (Huh *et al.*, 2008). In this context, the introduction of nanotechnology offers an alternative approach to novel formulation of hydrophobic drugs.

1.2 NANOMEDICINE IN CANCER

Cancer remains one of the world's leading cause of mortality, accounted for up to 7 million deaths in 2004 (http://www.who.int/topics/cancer). Surgical intervention, radiation therapy and treatment with chemotherapeutic drugs are among the current treatments for cancer. Despite increasing knowledge about the prevention and treatment of cancer, the number of new cancer cases grows every year and an approximately 50 % rise in new cases was projected over the next 20 years, from 10.9 million in 2002 to 16 million in 2020 (http://www.who.int/topics/cancer). In terms of chemotherapy, its clinical effectiveness requires chemotherapeutic drugs to kill tumour cells at doses that allow enough cells in the patient's critical tissues to survive so that recovery can occur. However, the outcome of conventional chemotherapy remains well below expectations, especially in the cases of breast, pancreatic, ovarian and oesophageal cancers (Baird and Kaye, 2003; Wong *et al.*, 2007). Due to lack of specificity, high doses are often required because the drugs are not targeted to the tumour sites. Even when standard therapeutic doses are administered, poor specificity of chemotherapy drugs often leads to serious systemic toxicity as the drugs are distributed to non-cancerous cells at the same time (Wong *et al.*, 2007). In fact, chemotherapy-induced side effects remain one of the essential challenges to overcome in cancer treatment (Figure 1.7), especially life-threatening symptoms such as cardiac toxicity, renal toxicity, thromboembolism and neuropathy associated with doxorubicin and cisplatin (Longhi *et al.*, 2007; Makrilia *et al.*, 2010), In addition, diagnosis of tumours often occurs in advanced stages when tumours have been widely disseminated as a result of metastases (Gomez-Navarro *et al.*, 1999). This is a major obstacle for cancer treatment because multiple organs are involved,

that the outcome of treatment becomes less predictable. Moreover, due to genomic instability and heterogeneity, development of clinical tumour resistance to chemotherapy, either intrinsic or acquired, is another barrier that needs to be overcome before a treatment can become curative (Gomez-Navarro *et al.*, 1999; Baird and Kaye, 2003).

Treatment agent	Alopecia	Taste changes	Depression/mood changes	Weight changes	Sexual dysfunction	Ototoxicity	Constipation	Fatigue (weakness)	Flu-like syndrome	Peripheral neuropathy	Neutropenia	Anemia	Thrombocytopenia	Diarrhea	Mucositis/stomatitis	Moderate nausea +/− vomiting	Severe nausea +/− vomiting	Hand-Foot syndrome	Headache	Nephrotoxicity	Anorexia	Shortness of breath	Edema	Hot flashes
Carboplatin[b]	—	x	—	—	—	—	—	X	—	x	X	X	X	—	—	X	—	—	—	x	—	—	—	—
Cisplatin[b]	x	x	—	—	—	x	x	x	x	x	X	X	X	—	—	—	X	—	—	X	x	—	—	—
Paclitaxel[b]	X	x	—	—	—	—	—	—	—	X	X	X	X	X	X	X	—	—	—	—	—	—	x	—
Docetaxel	X	—	—	x	—	—	—	X	—	X	X	X	x	X	X	—	—	—	—	—	—	—	X	—
Pegylated liposomal doxorubicin[c]	—	—	—	—	—	—	x	X	—	—	X	X	x	x	X	x	—	X	—	—	x	—	—	—
Topotecan[c]	X	—	—	—	—	—	x	x	—	—	X	X	X	X	x	X	—	—	x	x	x	x	—	—
Altretamine[c]	—	—	x	—	—	—	—	x	—	x	X	X	X	X	—	X	—	—	—	—	X	—	—	—
Gemcitabine	x	—	—	—	—	—	x	X	x	x	X	X	X	x	—	X	—	—	—	—	x	x	x	—
Oral etoposide	X	—	—	—	—	—	—	—	—	—	X	X	X	x	x	X	—	—	—	—	x	—	—	—
Capecitabine	—	—	—	—	—	—	x	X	—	—	x	X	x	X	x	X	—	X	x	x	x	x	—	—
Vinorelbine	x	—	—	—	—	—	X	X	—	x	X	X	—	x	x	X	—	—	—	—	x	—	—	—
Aromatase inhibitors	—	—	x	—	x	—	—	—	—	—	—	—	—	—	—	—	x	—	—	x	—	—	—	X
Tamoxifen	—	—	x	X	X	—	—	—	—	—	—	—	—	—	—	—	x	—	—	x	—	—	X	X
Progestins	—	—	x	x	—	—	x	—	—	—	—	—	—	—	—	—	x	—	—	x	—	—	x	—

Figure 1.7: Side effects associated with chemotherapy treatments currently used in clinical practice *(Adapted from Nature Clinical Practice Oncology, 2007).*

An ideal treatment regime however, would be one that targets cancer cells effectively, hence enabling complete disappearance of tumours without any secondary effects to healthy tissues. Nanotechnology was identified as a promising approach to improve the current status of cancer detection, diagnosis, imaging and therapy (Grobmyer *et al.*, 2010). Nanomedicine is often defined as formulation of materials in the nanometer size range, typically on the scale of 1-100 nm (Moghimi *et al.*, 2005; Peer *et al.*, 2007; Thassu *et al.*, 2007; Alexis *et al.*, 2010; Grobmyer *et al.*, 2010). The potential of nanocarriers in drug delivery lies in their ability to carry therapeutic or diagnostic agents by the virtue of their small size. Peer *et al.* summarized the advantages of nanomedicines over free drugs in a review in 2007, namely a) protection of free drug against premature degradation, b) enhanced drug absorption into a selected tissue, c) controlled pharmacokinetic and biodistribution, and d) improved intracellular penetration (Peer *et al.*, 2007). Furthermore, engineering of nanocarriers offers the opportunity to functionalize their surface characteristics either to control the physicochemical properties or for active targeting. As such, design of nanocarriers often involves steps to improve the integrity of the nanocarrier from biological degradation or to control over drug release as well as the location of drug accumulation (Moghimi *et al.*, 2005). Some examples of functionalized nanocarriers include triggered release formulations sensitive to pH, chemical stimuli, oscillating magnetic field, light or heat sources (Moghimi *et al.*, 2005). One of the most studied approaches for functionalised nanocarriers is active targeting. Active targeting involved the binding of targeting agents on the surface of nanocarriers, for instance ligands that bind to specific receptor such that nanocarriers can be recognized by target cells through ligand-receptor interactions (Peer *et al.*,

2007). Other targeting moieties exploited to date are for example antibodies, peptides or growth factors.

1.2.1 Nanomedicines in clinical practice

Doxil® (Figure 1.8) was the first nanomedicine in the form of liposome to gain US food and drug administration (FDA) approval for the treatment of AIDS associated Karposi's Sarcoma (James, 1995). It is a long-circulating liposome loaded with doxorubicin currently used in clinical practice to treat multiple types of cancer (Alexis *et al.*, 2010). The success of Doxil® and similar products i.e. DaunoXome® and Myocet™ led to enormous progress in the development of nanocarriers and their therapeutic applications. To date, there are 83 clinical trials evaluating nanoparticle carriers, 271 evaluating drug conjugates and 448 evaluating vesicle-based carriers (http://www.clinicaltrial.gov).

Doxorubicin   Liposome   Pegylated Liposome
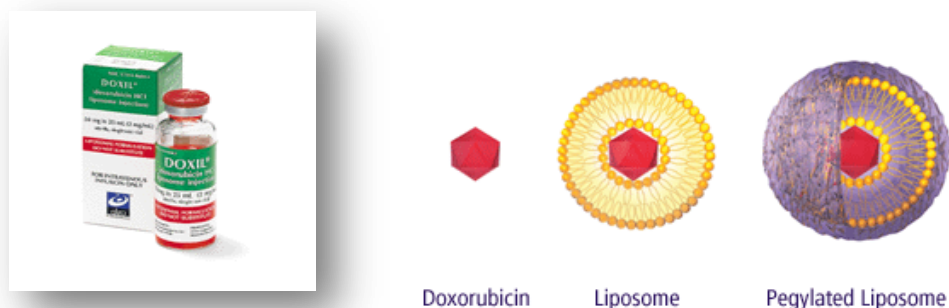
Figure 1.8: Schematic illustration of Doxil® *(Adapted from http://www.doxil.com).*

One major drawback of long-circulating nanocarriers is the side effect named palmar-plantar erythrodysesthesia, also called the hand-foot syndrome, which is commonly induced by the extravasation of nanocarriers in unexpected sites (Peer *et al.*, 2007). Palmar-plantar erythrodysesthesia is a distinctive dermatologic toxic reaction associated with tingling, oedema and erythema of the palms and soles, which has the possibility to progress to crusting, ulceration and epidermal necrosis (Lorusso *et al.*, 2007). To this end, several approaches were investigated such as triggered release, targeted liposomes and multi-drug delivery (Alexis *et al.*, 2010). The main objective is to minimize the distribution of nanocarriers to healthy tissues or managing with the side effects while promoting their accumulation at target site. Polymeric nanoparticles including drug-polymer conjugates, dendrimers and micelles as well as inorganic nanoparticles such as gold and iron oxide nanoparticles are all under rapid progress in clinical trials for treatment of various types of cancer. An array of nanocarrier-based drugs are currently available in the market, for instance Oncaspar®, Neulasta®, Ontak™, Mylotarg®, Zevalin®, Bexxar®, Abraxane® (Peer *et al.*, 2007).

In the context of nanotechnology, new concepts in cancer therapy have been explored over the years in the hope to turn molecular discoveries into benefits for the public. The invention of carbon nanotubes (Figure 1.9) and nanofibres were examples of the latest nanomaterial technologies. In 2007, a breakthrough in nanomedicines was achieved when single-walled carbon nanotubes were able to produce thermal cytotoxicity in malignant cells when subjected to heat release in a radiofrequency field (Gannon *et al.*, 2007). A combination of biological and

chemical intervention created a novel technology able to encapsulate neural progenitor cells in a network of nanofibres formed by the self-assembly of peptide amphiphiles (Silva *et al.*, 2004). This invention was shown to promote cell growth and adhesion in response to the bioactive molecule by forming fibres of diameters 5-10 nm.
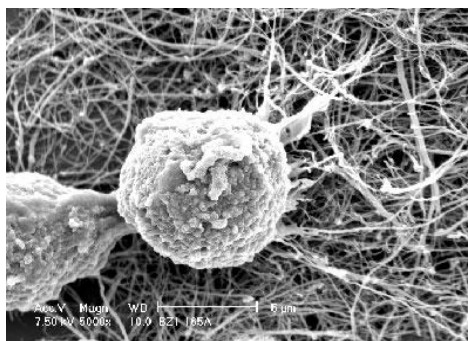
Figure 1.9: A dividing osteoblast grown on multi-walled carbon nanotubes designed for tissue engineering *(adapted from Dr. Laura Zanello from Nano Science and Technology Institute)*.

1.2.2   Challenges in nanomedicine

In spite of the rapid revolution in nanotechnology, there are various challenges to overcome before a safe and effective nanocarrier can be administered for the widespread benefit of patients. Physically, the carrier must have high drug loading capacity and sufficient stability within the vasculature with minimum drug loss (Moghimi *et al.*, 2005). This is especially important in liposomal formulations as they often have low encapsulated load whereas the susceptibility of lipid degradation in bloodstream often leads to burst release of drug (Alexis *et al.*, 2010). Nevertheless, when extravasated from the bloodstream, majority of the nanocarriers do not interact with target cells (Moghimi *et al.*, 2005). While it is essential for nanocarriers to withstand degradation in the bloodstream, the efflux of drug from the carrier when

distributed in target cells is equally important to maintain sufficient drug level in the therapeutic range. Bandak *et al.* showed in 1999 that despite enhanced tumour uptake of a long-circulation formulation of cisplatin liposome, the lack of its anti-tumour activity was attributed to the extremely slow release kinetics (Bandak *et al.*, 1999).

In 2008, FDA in conjunction with the Alliance for NanoHealth (ANH) co-convened a workshop on nanomedical regulatory science in Houston with participants across different disciplines in order to identify the priority areas of concern (Sanhai *et al.*, 2008). One of the top priorities is to determine the distribution of nanocarriers in the body following systemic administration through any route. This is coupled to the second concern, i.e. development of imaging modalities for visualising the biodistribution. *In vivo* biodistribution provide full recognition of the fate of nanocarriers after administration, not only it determines the efficacy of a system but ultimately determines its safety profile as well. The third issue identified was the understanding of mass transport across compartmental boundaries in the body. Compartmental boundaries are essentially the epithelia, vascular endothelium, the reticulo-endothelial system, enzymatic degradation, tumour interstitium, cell membrane as well as subcellular structures (Ferrari, 2010). Generally, the behaviour of nanocarriers in biological microenvironment is strongly influenced by their chemical structure, morphology, sizes and physical characteristics. It was believed that mathematical and computer models play an important role to elucidate the *in vivo* behaviour of nanocarriers by predicting the risk and benefit parameters of nanocarriers (Sanhai *et al.*, 2008). Finally, in order to maintain a healthy growth of the nanomedicine industry, safety is the most crucial factor that should be recognized.

Therefore, it would be essential to develop references and testing protocols, as well as analytical toolkit, to obtain information about the biodistribution, toxicology and safety properties of nanocarriers (Sanhai *et al.*, 2008).

1.2.3 Biological barriers to nanomedicine

Intravenous administration of nanocarriers has proven to provide a new platform in cancer research, not only at the therapeutic level but for diagnosis and imaging purposes as well. Nevertheless, the intrinsic defence mechanism of human body incurs substantial biological barriers for nanocarriers to effectively deliver their bioactive compound. These biological barriers are sequential in nature, therefore an ideal nanocarrier system would be one that has the ability to bypass or alter the molecular mechanisms in such a way that it can cross the barriers without much perturbation to the human system (Figure 1.10).
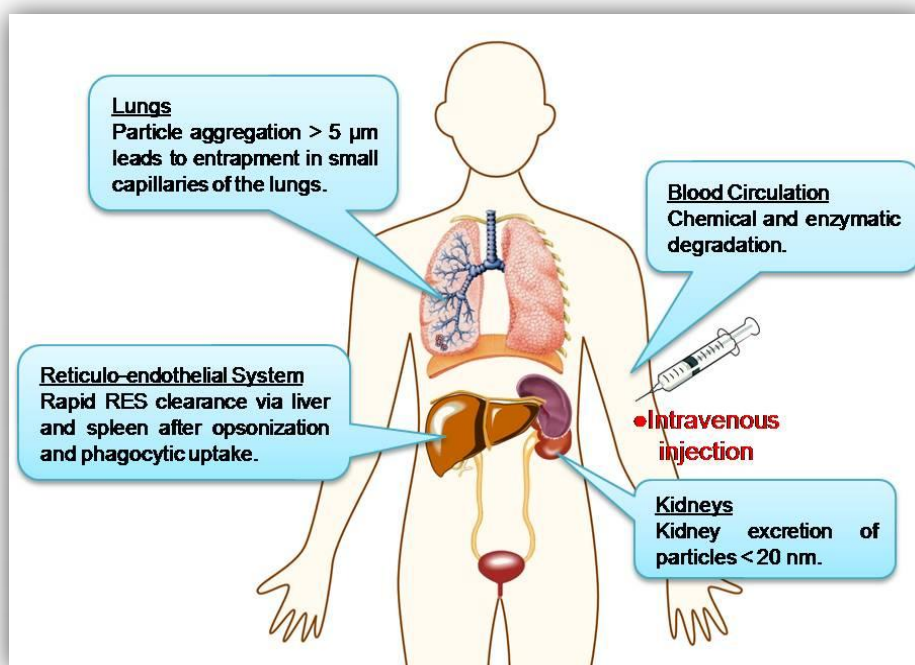
Figure 1.10: Schematic representation of the biological barriers associated with intravenous administration of nanocarriers.

Upon intravenous administration, the stability of nanocarriers is challenged in different aspects: chemical stability, colloidal stability and drug retention (Drummond *et al.*, 1999). The composition of a carrier has a major influence on its chemical stability against enzymatic and chemical degradation, subsequently affecting the amount of drug retained during blood circulation. For example in the case of liposome, hydrolysis and lipid peroxidation are important factors leading to membrane destabilisation. In order to overcome this problem, saturated phospholipids and cholesterol were often used to reduce liposome permeability (Drummond *et al.*, 1999). As far as colloidal stability is concerned, particles in the bloodstream are generally susceptible to rapid aggregation depending on their surface characteristics and geometry. Aggregation of particles is potentially lethal when aggregates (5-7 µm) are entrapped in the small capillaries of the lung, leading to pulmonary embolism (Drummond *et al.*, 2008; Decuzzi *et al.*, 2010).

When nanocarriers are disseminated in the blood circulation, the morphology of blood vessels plays a major role in determining their tissue distribution. Blood vessel endothelium can be classified as continuous (e.g. in the arteries, vessels and the lungs) or discontinuous, fenestrated (Alexis *et al.*, 2008). It is not surprising that particles escaping from the circulation are normally accumulated in the sites where capillaries have open fenestrations such as the bone marrow, liver, spleen and kidney glomerulus (endothelial gaps of up to 50-150 nm), or where the integrity of endothelial barrier is disturbed by inflammatory processes (up to 700 nm) or in tumours (up to 400 nm) (Drummond *et al.*, 1999; Moghimi *et al.*, 2001; Alexis *et al.*, 2008).

Nevertheless, a major drawback of intravenously administered nanocarriers is their rapid clearance from the circulation system by the reticulo-endothelial system (RES), triggered by a phenomenon named opsonization. Opsonization is a process where opsonic factors such as fibronectin, immunoglobulins, the complement proteins, apolipoproteins, thrombospondin or other serum proteins are deposited on the surface of nanocarriers (Moghimi *et al.*, 2005). This process promotes the recognition of nanocarriers by macrophages, which are sequestered in the liver by Kupffer cells and in the spleen, leading to rapid RES clearance (Moghimi *et al.*, 2005; Alexis *et al.*, 2008; Ferrari, 2010). While the opsonisation process and clearance kinetics of nanocarriers are critically influenced by particle physical properties, the effect of size and surface properties will be further discussed in Chapter 2. Small particles of sizes 10-20 nm however, can leave the systemic circulation via the permeable endothelium in lymph nodes or by crossing the tight endothelial junctions in various organs and are rapidly excreted through the glomeruli of the kidneys (Moghimi *et al.*, 2001; Decuzzi *et al.*, 2010). Ideally, the size of a nanoparticle should be relatively small or easily deformable if it is a large particle, in order to avoid the splenic filtration process in sinusoidal spleens, where the slit size are approximately 200-500 nm in width (Moghimi *et al.*, 2001).

Looking at cancer treatment specifically, a solid tumour usually contains well perfused and rapidly growing regions as well as poorly perfused, often necrotic regions where tumour vessels are highly irregular with interrupted endothelium (Moghimi *et al.*, 2001). This "leaky" vasculature in association with impaired lymphatic system gives rise to the phenomenon named enhanced permeability and

retention (EPR) effect, which facilitated the accumulation of macromolecules and nanocarriers in tumours (Maeda, 2000). Nevertheless, as cancer lesions grow, an increase in internal hydrostatic pressure is inevitable due in part to the impaired lymphatic drainage that increases the interstitial pressure (Moghimi *et al.*, 2001; Ferrari, 2005). Thus, the osmotic pressure gradient generated could hamper the uptake of nanocarriers in tumours, as this pressure is countering the extravasation of nanocarriers from the vascular compartment into the tumour.

The above mentioned are some of the key biological barriers before nanocarriers can be successfully delivered to target tissues. However, if they are to accumulate in the tumours effectively, the release kinetics of drugs from their carriers and the ability to undergo intracellular penetration are crucial for therapeutic activity. Intracellular barriers include cell membranes, subcellular structure such as the endosomes and nucleus depending on the mechanism of action of the therapeutic drug, and finally the ability to overcome efflux pumps (Ferrari, 2010).

1.2.4 Types of nanocarriers

Various types of carriers are currently developed for use in cancer therapy, generally tailored according to their functions both for systemic administration or local administration, burst release or controlled release, long circulating or targeted, based on the types of therapeutic compounds to deliver. Materials from lipids, polymers as well as inorganic materials such as gold and iron oxide were used as building material for nanosized drug delivery systems. The most common types of nanocarriers include polymeric nanoparticles, micelles, dendrimers, nanoshells and

liposomes. Every system has its unique physicochemical properties which lead to distinctive *in vitro* and *in vivo* behaviour, as well as individual advantages and disadvantages.

- *Polymeric nanoparticle*

Polymeric nanoparticles are solid colloidal systems ranging in size from 10 nm to 1 μm, normally synthesized using synthetic polymers such as poly(lactic-co-glycolic acid) or poly(lactic acid), polyanhydrides, polystyrene, and polymethylmethacrylate, or natural polymers including cellulose, gelatine, chitosan, alginate and collagen (Kreuter, 1994; Chakravarthi*et al.*, 2007; Peer *et al.*, 2007; Alexis *et al.*, 2010). With precise chemical composition and synthesis process, it is possible to control the physicochemical properties of nanoparticles. Such modification can alter the solubility, permeability and polymer degradation, which ultimately determines the mode of drug release, either via triggered response, erosion, diffusion or swelling of polymers (Chakravarthi*et al.*, 2007; Peer *et al.*, 2007; Alexis *et al.*, 2010). Nanoparticulate formulations are generally categorized as nanospheres or nanocapsules. While nanospheres define solid polymeric matrix in which drugs can be entrapped, dissolved or adsorbed to; nanocapsules (Figure 1.11) compose of a reservoir or a cavity surrounded by a polymer coating (Letchford and Burt, 2007). There are several nanoparticle formulations currently under clinical trials for cancer therapy and other diseases, one of which is polymethacrylate nanoparticles (by Nanolymf Ltd.) (Alexis *et al.*, 2010). Another example of polymeric nanoparticles clinically used to treat breast cancer resistant to conventional cancer therapy is Abraxane[®] (Riehemann *et al.*, 2009). Abraxane is a water-dispersible albumin-based

nanoparticulate system loaded with paclitaxel, shown to increase response rate, longer time to tumour progression and reduced hypersensitivity reactions (Riehemann *et al.*, 2009). However, one of the major drawbacks of polymer-based nanocarriers is the inherent structural heterogeneity of polymers, resulting in high polydispersity index of molecular weight significantly affecting the homogeneity of particle size distribution (Peer *et al.*, 2007; Alexander, 2008).
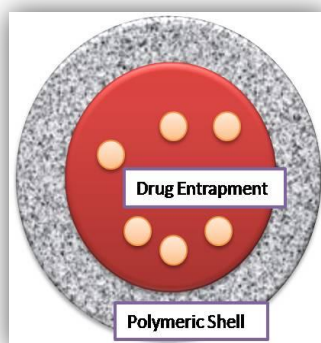
Figure 1.11: Schematic illustration of a polymeric nanocapsule system.

- *Micelles*

Micelles represent colloidal dispersions of particles ranging from 50-100 nm in diameter, commonly prepared from conventional surfactants or amphiphilic co-polymers (Figure 1.12) (Lukyanov and Torchilin, 2004). These amphiphilic molecules aggregates spontaneously to form micelle with hydrophobic core and hydrophilic surface at a certain concentration called the critical micelle concentration (CMC) (Torchilin, 2010). This unique structure allows them to accommodate drugs with varying solubility. In aqueous dispersion, hydrophobic molecules are solubilised within the micelle core; polar molecules will be adsorbed on the micelle surface whereas drugs with intermediate polarity will be distributed along amphiphilic

molecules at intermediate positions (Torchilin, 2010). Due to their smaller size compared to other nanocarrier systems, micelles were shown to enhance intracellular penetration of pharmaceutical agents via passive targeting: extravasation across leaky tumour vasculature through the EPR effect. Its efficiency can be further increased by conjugating hydrophilic polymers such as polyethylene glycol to form long-circulating micelles or by attaching targeting ligands such as antibodies and proteins (Lukyanov and Torchilin, 2004; Peer *et al.*, 2007). The first polymeric micellar formulation to be approved for cancer therapy is Genexol-PM® (Alexis *et al.*, 2010). It is a long circulating formulation loaded with paclitaxel, approved in Korea in 2006 as a first-line therapy for metastatic breast cancer and currently being evaluated in phase 2 clinical trial in the USA for metastatic pancreatic cancer (Zhang *et al.*, 2008; Alexis *et al.*, 2010). When administered to the blood circulation, a practical limitation of micelles is its susceptibility to disintegration as the concentration of amphiphiles is diluted below the required CMC to form micelles by large volume of blood. Nevertheless, polymeric micelles are often more stable than micelles prepared from conventional surfactants owing to their high thermodynamic stability and high kinetic stability (i.e. retarded disintegration at concentrations lower than CMC) (Lukyanov and Torchilin, 2004; Thassu *et al.*, 2007).
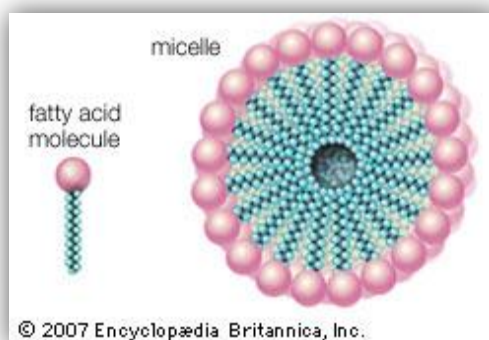
Figure 1.12: Schematic illustration of the formation of micelles from fatty acid molecule *(Adapted from Encyclopaedia Britannica, Inc. 2007).*

- *Dendrimers*

Dendrimers are synthetic polymers composed of multiple branched monomers radiating from central core, forming layered architectures as shown in Figure 1.13 (Lee *et al.*, 2005). Therapeutic drugs or bioactive compounds can be delivered to tumour sites either being encapsulated within the dendritic structure or by interacting with the terminal functional groups at the periphery of dendrimers (Nijlah and D'Emanuele, 2006). The use of dendrimers as drug delivery systems has gained much attention in recent years mainly due to the availability of multiple surface functional groups, which is advantageous for increasing the drug loading capacity and the accessibility of targeting ligands. Polymers widely used to prepare dendrimers include polyamidoamines (PAMAM), polypropyleneimine (PPI), polyamines, poly(acrylethers), etc (Lee *et al.*, 2005). *In vivo* studies showed elevated anti-tumour activity of cisplatin and methotrexate when delivered using PAMAM dendrimer, while enhanced cellular delivery of propranolol and ibuprofen across epithelial cells have been shown *in vitro* (Jevprasesphant *et al.*, 2004; Lee *et al.*,

2005; Alexis *et al.*, 2010). Contrary to polymeric nanocarriers, dendrimers are remarkably monodispersed, essential to minimized therapeutic variability (Lee *et al.*, 2005; Nijlah and D'Emanuele, 2006).
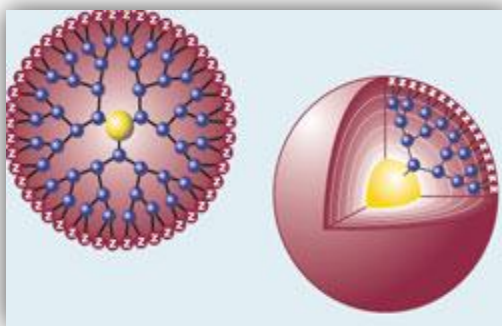
Figure 1.13: Structural illustration of dendrimers (*Adapted from Perkel et al., 2004*).

- *Inorganic nanoparticles*

Inorganic nanoparticles are metal-based particles, primarily used for imaging and diagnosis in previous years but have been extensively explored for therapeutic purposes recently (Alexis *et al.*, 2010). Having the major advantage of near monodispersity, gold or iron nanoparticles and nanoshells are among the most common form of inorganic nanocarriers. Gold nanoparticles (Figure 1.14) were proven effective in hyperthermia-based therapeutics, because of their ability to conduct energy into heat when excited with near-infrared light or magnetic field, leading to irreversible heat damage to cancer cells (Peer *et al.*, 2007). Similar principles were applied to nanoshells, which are composed of a silica core, surrounded by an ultrathin conductive metal layer (Peer *et al.*, 2007; Riehemann *et al.*, 2009). Upon administration, these nanoshells were rapidly distributed due to their small sizes and were able to damage tumour tissues upon application of localised

heating while normal tissues appeared undamaged (Peers *et al.*, 2007). However, the use of high temperature was not necessarily appropriate in some areas, such as the brain, in addition to the risk of damaging adjacent healthy tissues when specific heat was applied.
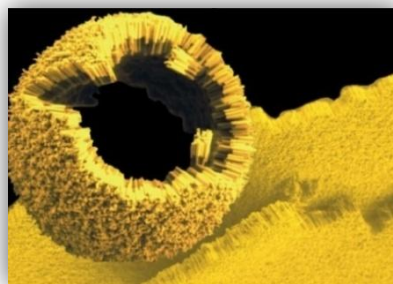
Figure 1.14: A scanning electron microscopy of nanoparticle formed by self assembly of gold amphiphilic rods *(Adapted from Park et al., 2004).*

- *Lipid-based vesicles*

Liposomes have been extensively studied over the past two decades and represent one of the first nanocarriers being approved for clinical use. Generally, liposomes are spherical vesicle systems enclosed by one or several lipid bilayers with an inner aqueous phase as shown in Figure 1.15 (Peer *et al.*, 2007). Therefore, liposomes are able to incorporate hydrophobic compounds in the lipid bilayers and hydrophilic molecules in the inner core, although the loading efficiency and release profile are very much dependent on lipid composition, vesicle size as well as preparation method (Torchilin, 2010). Lipid molecules used to prepare these vesicles can be natural, synthetic or semi-synthetic (Riehemann *et al.*, 2009). The clinical success of liposomes in the case of AmBisome[®]/Amphotec[®]/Abelcet[®] (amphotericin B liposomes), Doxil[®]/Caelyx[®] (doxorubicin liposomes), DaunoXome[®] (daunorubicin liposomes), DepoCyt[®] (cytarabine liposomes), DepoDur[®] (morphine liposomes) and

Visudyne® (verteporfin liposomes) established the lipid vesicles as one of the most biocompatible and robust drug delivery systems (Zhang *et al.*, 2008; Riehemann *et al.*, 2009). Nevertheless, several studies claimed that liposomes are generally sequestered by the reticuloendothelial system within 15-30 minutes upon intravenous administration, subsequently cleared from the circulation system (Torchilin, 2010). In addition, inherent instability of lipid molecules to enzymatic degradation, including the hydrolysis of fatty acid esters and lipid peroxidation of unsaturated lipids, are among the major issues to address in liposomal formulations. To date, several strategies have been developed to modify properties and functionalities of liposomes, for instance long circulating liposomes, targeted liposomes and liposomes sensitive to temperature or pH (Wu *et al.*, 2007). An alternative approach to resolve issues associated with phospholipid instability is to replace the lipid molecule with non-ionic amphiphilic surfactants, forming a new category of vesicles, named niosomes. Among the scores of nanocarriers available in today's pharmaceutical industry, this work is focusing on the use of niosomes as carrier systems to deliver tocotrienol to cancer cells. The main characteristics of niosomes are outlined in the following section.
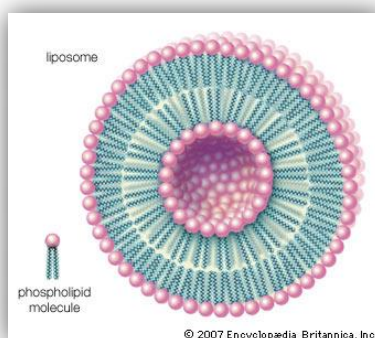
Figure 1.15: Schematic illustration of liposome formed from the self assembly of phospholipid molecules *(Adapted from Encyclopedia Britannica, Inc. 2007).*

1.2.4.1 Non-ionic vesicles (niosomes)

Non-ionic vesicles (niosomes) are vesicular delivery systems first introduced by Handjani-Vila *et al.* in 1979 (Handjani-Vila *et al.*, 1979). Due to the structural resemblance to phospholipid membranes in living cells, vesicular delivery systems have gained much attention as pharmaceutical entities since their discovery. Similar to liposomes, niosomes occupy the general structure of bilayer vesicles, having a hydrophilic core shielded from one or multiple hydrophobic lipid bilayer (Figure 1.16). This unique structure gives rise to one of their major characteristics, i.e. the capacity to accommodate oil-soluble compounds and to encapsulate water-soluble drugs (Malmsten, 2002). While liposomes are formed with phospholipids, niosomes are formed by the self-assembly of non-ionic surfactants. With phospholipids, there have been questions about the physical and chemical stability leading to phospholipid degradation that essentially affects the permeability of liposome (Crommelin and Schreier, 1994). The use of non-ionic surfactants was then proposed as an alternative to phospholipids in the hope that it will offer greater stability and ease of storage (Uchegbu and Vyas, 1998). Previous studies have shown that niosomes were less susceptible to micellar solubilisation and more stable against chemical degradation because of the reduced, if not absence of hydrolysable bonds (Vanlerberghe, 2000).
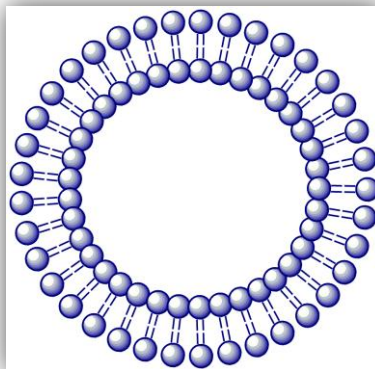
Figure 1.16: Structural illustration of a niosome. ○ Indicates the hydrophilic head group while -- indicates the hydrophobic chain.

1.2.4.2 Principle of vesicle formation

Niosomes can usually be generated using various preparation techniques, as described in table 1.2. Therefore, a large diversity of vesicles with different morphologies and structural properties are available to date, depending on the choice of surfactant and preparation techniques. The most common way of classifying these vesicles is via recognition of their structural properties. Table 1.3 is a summary on types of vesicles commonly found in pharmaceutical preparations.
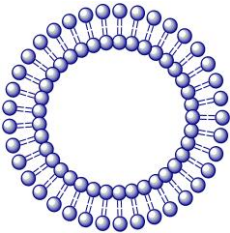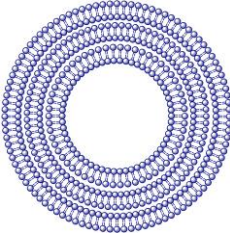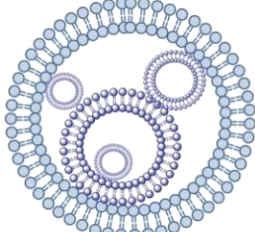
The structure, size, type and stability of vesicular systems can differ widely depending on the preparation technique and composition of surfactants. Over the past four decades, various surfactants have been explored for niosome formulations. The most common ones include polyglycerol alkyl ethers (Handjani-Vila *et al.*, 1979; Uchegbu *et al.*, 1997), polyoxyethylene alkyl ethers (Okahata *et al.*, 1981; Hofland *et al.*, 1992; Arunothayanun *et al.*, 1999) and sorbitan esters (Span surfactants) (Florence and Cable, 1993; Uchegbu *et al.*, 1995; Dimitrijevic *et al.*, 1997).

Table 1.2: Methods applied in the preparation of niosomes.

Methods	Description
Ether Injection Method	Surfactant/cholesterol mixture dissolved in diethyl ether and injected slowly through a needle into the aqueous phase at 60 ^{o}C, ether evaporated.
Hand-shaking (film) method	Surfactant/cholesterol mixture dissolved in diethyl ether in round-bottomed flask, organic solvent evaporated under reduced pressure. Dried surfactant film is hydrated with aqueous phase at 50-60 ^{o}C with gentle agitation.
Sonication	Aqueous phase added to surfactant/cholesterol mixture, probe sonicated.
Reversed phase evaporation	Lipids dissolved in chloroform and ¼ volume of PBS, sonicated and evaporated under reduced pressure. Gel is then hydrated.

(Adapted from Baillie et al., 1985; Bouwstra and Hofland, 1994).

Table 1.3: Classification of vesicles based on structural properties

Small unilamellar vesicles (SUV)	Large unilamellar vesicles (LUV)	Multilamellar large vesicles (MLV)	Multivesicular vesicles (MVV)
20-100 nm	200-800 nm	500 nm -1 µm	> 1 µm

(Adapted from Crommelin and Schreier, 1994; Torchilin, 2010).

One key requirement for a surfactant to form bilayer structure is the amphiphilicity, i.e. contains a polar and a non-polar region. This feature allows them to organize in different structures as hydrophobic regions tend to self aggregate while polar regions tend to be in contact with the aqueous phase (Crommelin and Schreier, 1994). Although the actual process of vesicle formation is not well understood, it is generally accepted that it involves three stages 1) increase in size of mixed micelles, 2) formation of flat lamellae, 3) bilayer bending and closure (Lesieur and Ollivon, 2000). The hydrophilic lipophilic balance (HLB) of an amphiphile was once used as a parameter to indicate the vesicle forming ability of surfactants (Uchegbu and Vyas, 1998). It is an indication of the hydrophilic/lipophilic ratio of an amphiphilic molecule. For example, HLB numbers between 4 to 8 with Span surfactants were found to be within the vesicle formation capacity (Uchegbu and Florence, 1995). However, it was soon realised that prediction based solely on HLB numbers was an underestimated method (Uchegbu and Vyas, 1998). On the basis of molecular shapes, Israelachvili and co-workers (1980) identified a possible measure to predict potential bilayer-forming compounds by defining the critical packing parameter p (Figure 1.17).

$$p = v/a_0 l_c$$
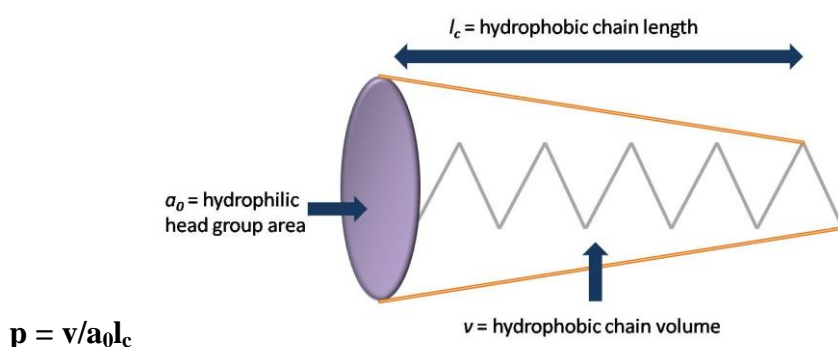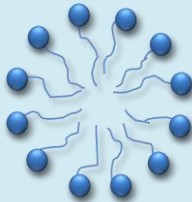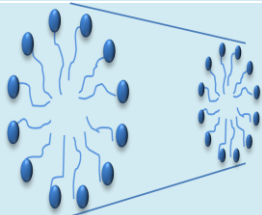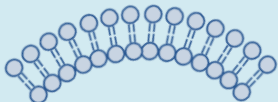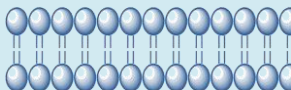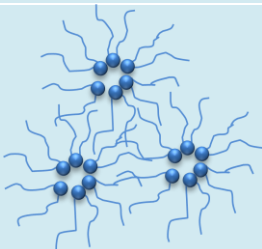
Figure 1.17: The critical packing parameter of an amphiphilic molecule p, where v is the molecular volume of hydrophobic region, a_0 is the hydrophilic head group area and l_c is the length of hydrocarbon tail.

The critical packing parameter defines the molecular shape of an amphiphilic molecule based on the molecule's hydrophilic head group, hydrophobic chain length and hydrophobic chain volume. From the critical packing shape (as illustrated in table 1.4), the resulting shapes of lipid bilayer formed from amphiphiles are elucidated, ranging from spherical micelles to planar bilayers or vesicles. Combining the understanding of HLB and critical packing parameter, it is possible to deduce the likelihood of vesicle formation with a given amphiphilic compound. Nevertheless, it should be noted that this is a simplified approach, in which the effect of additional factors such as pH, temperature and aggregation was excluded.

In general, it is well understood that properties of niosomes, including the release profile, entrapment efficiencies and toxicity, are strongly influenced by the composition, size, number of bilayers and methods of preparation of vesicles. With extensive studies for niosome systems in terms of efficacy, safety and stability as a potential delivery system, they are often referred as an alternative to liposomes. Nevertheless, optimising niosome formulations (i.e. choice of surfactants/adjuvants and respective concentrations) as well as methods of preparation is crucial in determining the system's properties.

Table 1.4: Summary of the influence of the critical packing parameter on the resulting shapes of lipid layers formed from amphiphiles.

Critical Packing Parameter (CPP)	Critical Packing Shapes	Structure formed	Lipid molecules
< 1/3	Cone	Spherical micelles	SDS in low salt
1/3 – 1/2	Truncated cone	Cylindrical micelles	Non-ionic surfactants, SDS and CTAB in high salt
1/2 – 1	Truncated cone	Flexible bilayers, vesicles	PC, PS, PG, PI, sphingomyelin, dihexadecyl phosphate
~ 1	Cylinder	Planar bilayers	PE with saturated chains
> 1	Wedge	Inverted micelles	PE with polyunsaturated chains, cholesterol

SDS: sodium dodecyl sulphate; CTAB: cetrimonium bromide; PC: phosphatidyl choline; PS: phosphatidyl serine; PG: phosphatidyl glycerol; PI: phosphatidyl inositol, PE: phosphatidyl ethanolamine *(Modified from Crommelin and Schreier, 1994)*.

1.2.4.3 Application of niosomes in cancer

Niosomes have been employed as delivery systems for drug (doxorubicin, methothrexate, vincristine, hexadecyl triglycerol sodium stibogluconate, and acetozolamide), vaccine (antigens for herpes simplex virus type 1) and imaging agents (gadolinium salts to target PC3 tumour cells) for applications in cancer, anti-infective, glaucoma, neurological disorders and vaccination (Mullen *et al.*, 1998; Uchegbu and Vyas, 1998; Uchegbu and Schätzlein, 2006). In fact, niosomes were first investigated as an experimental delivery system for the treatment of leishmaniasis (Baillie *et al.*, 1986). It was then reported by William *et al.* (1995) that suppression of parasite burden in liver, spleen and bone marrow was observed upon intravenous administration of niosomes encapsulating anti-leishmaniasis drug. In cancer therapy, niosome formulations of anti-cancer drugs, i.e. methotrexate (Chandraprakash *et al.*, 1993), doxorubicin (Rogerson *et al.*, 1988; Uchegbu *et al.*, 1996) and vincristine (Parthasarathi *et al.*, 1994) showed improved tumoricidal activities and safety profiles *in vivo*. A recent study by Hong *et al.* (2009) also showed that hydroxycamptothecin encapsulated in targeted niosomes demonstrated favourable antitumour effect upon intravenous injection. Other than systemic delivery, oral administration of methotrexate (Azmin *et al.*, 1985) and protein (Yoshida *et al.*, 1992) loaded in niosomes have been widely studied while transdermal delivery of oestradiol (Vanhal *et al.*, 1996) and cyclosporin A (Niemec *et al.*, 1994) niosomes showed enhanced skin penetration upon topical administration. Recent examples of niosome application via the transdermal route include piroxicam (Alsarra, 2008), minoxidil (Balakrishnan *et al.*, 2009) and ammonium glycyrrhizinate (Paolino *et al.*, 2007). In addition, studies were also done to explore the implication

of niosomes in ophthalmic delivery for gentamicin (Abdelbary and El-Gendy, 2008), as nebuliser for asthma (Abd-Elbary *et al.*, 2008) and as carrier for diphtheria toxoid for transcutaneous immunization (Ding *et al.*, 2008). Rapid development in gene therapy has open up another opportunity for the use of niosomes as DNA carriers due to its ability to protect DNA plasmid from enzymatic degradation in biological fluids (Schätzlein, 2003). Recent examples include delivery of oligonucleotides (Huang *et al.*, 2008) and DNA vaccines via the subcutaneous route (Perrier *et al.*, 2004) and topical route (Vyas *et al.*, 2005).

Studies with niosomes to date have well established the role of vesicular delivery systems in the field of cancer. In addition to their capacity to incorporate both hydrophilic and hydrophobic compounds, entrapment of tocotrienol in niosomal system is no doubt a potential approach in an effort to enhance the therapeutic efficacy of tocotrienol. Although we hypothesize a significant improvement in the tumour delivery of tocotrienol with the aid of a delivery system, the lack of specificity and selectivity poses substantial limitation on the system. In this context, targeting of a therapeutic agent is of particular interest, especially in the field of cancer treatment.

1.3 TARGETING

In general, drugs are distributed to the whole body proportional to the regional blow flow, independent of administration route (Torchilin, 2010). This rather even distribution of anticancer drugs have the inherent character to traverse in and out of blood vessels freely, not only imposing the need for higher dose administration to achieve therapeutic concentration, but also causing systemic side effects to healthy tissues. One hundred years ago, Nobel Laureate Paul Ehrlich postulated the concept of "magic bullets", as an entity of chemotherapeutic agent with specific affinity for diseased tissues (Gabizon, 2001; Strebhard and Ullrich, 2008). The idea has since inspired scientists to develop drug targeting for use in the fight against human diseases. Drug targeting can be defined as 'passive targeting' or 'active targeting'. Passive targeting is distinguished by a system's 'intrinsic' properties e.g. physicochemical characteristics while active targeting relies on 'extrinsic' targeting modification, for instance ligand conjugation (Schätzlein, 2003). The ultimate goal of drug targeting is therefore: to reduce the quantity of cytotoxic drugs needed to be administered, by creating a dose differential between healthy and diseased tissues, without negative secondary effects on healthy tissues (Figure 1.18).
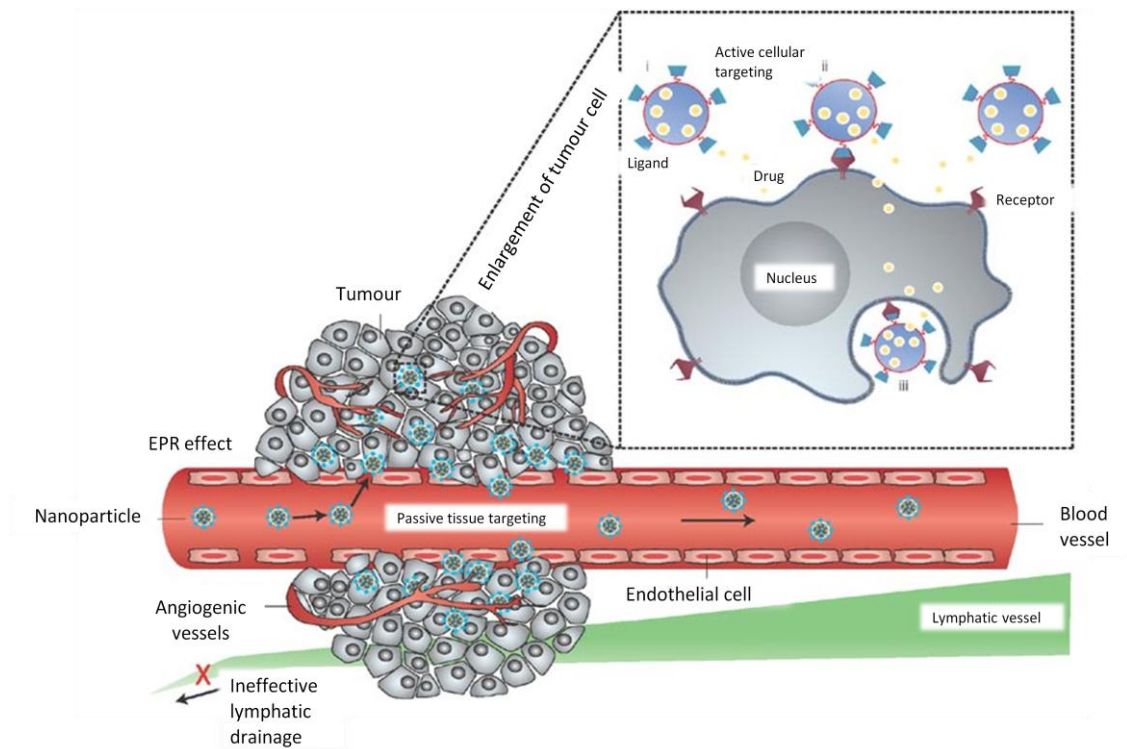
Figure 1.18: Schematic illustration of passive and active targeting in tumour tissues *(Adapted from Peers et al., 2007)*.

1.3.1 Passive Targeting

Passive targeting exploits the microenvironment biology of tumour tissues compared to that of healthy tissues or organs. In most healthy tissues, blood vessels, often non-fenestrated capillaries, are composed of a single layer of endothelial cells with tight junctions, efficiently preventing macromolecules from traversing blood vessels (Maruyama *et al.*, 1999). Small molecular weight compounds however can traverse in and out of blood vessels freely and are rapidly returned to circulating blood by diffusion (Maeda *et al.*, 2000). Tumour vasculature on the other hand, is highly heterogeneous, ranging from areas with vascular necrosis to areas that are densely vascularised in order to supply the growing tumour with adequate oxygen and nutrients (Alexis *et al.*, 2008). These newly sprouting blood vessels have

abnormal vascular architecture with patchy endothelial lining and the lack of smooth-muscle layer. Other abnormal morphology includes large openings and fenestrations in the vasculature network, lack of constant blood flow or direction, lack of pericytes and dilated capillaries (Cassidy and Schätzlein, 2004; Alexis *et al.*, 2008; Maeda *et al.*, 2009). Therefore, as the permeability of tumour blood vessels is increased, the transport of macromolecules across the leaky endothelium is facilitated, which is defined as enhanced permeability and retention (EPR) effect, previously described in section 1.2.3 (Maeda *et al.*, 2000). Concluding remarks from previous studies involving tumour delivery of nanoparticles, polymeric drug conjugates or proteins suggested the pore cut-off size of this transport pathway to be within the 400-500 nm range (Figure 1.19) (Peer *et al.*, 2007; Alexis *et al.*, 2008; Maeda *et al.*, 2009; Torchilin, 2010).
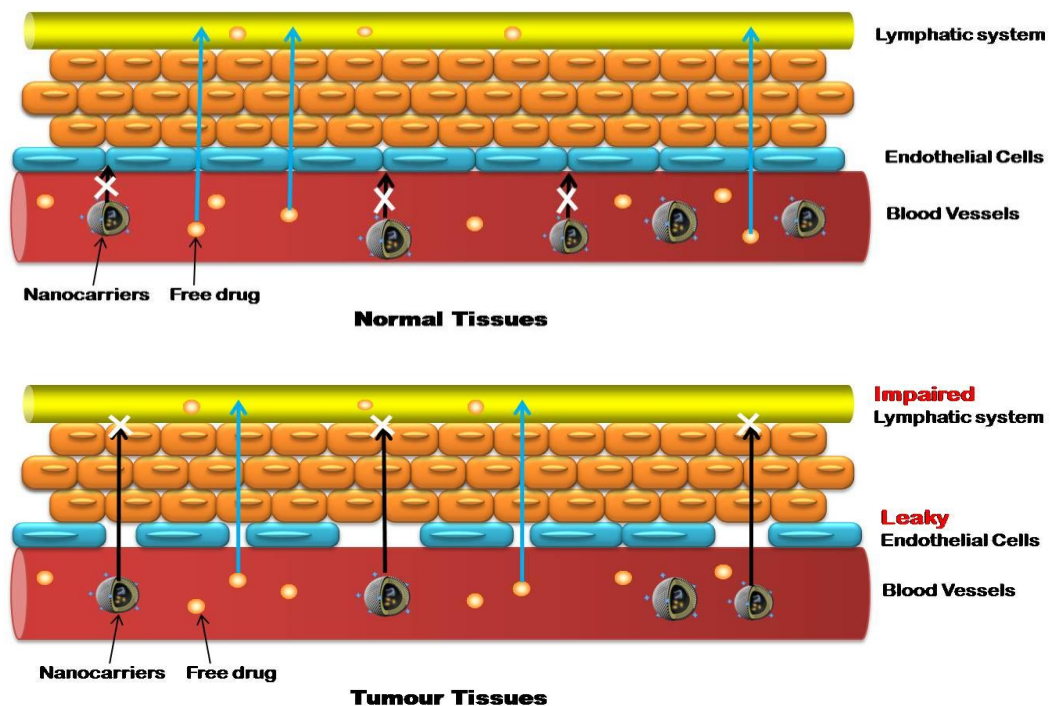
Figure 1.19: The enhanced permeability and retention (EPR) effect for passive targeting of nanocarriers in tumour tissue but not in normal tissues.

In terms of enhanced retention, the growth of tumour in a confined space has a major impact on the lymphatic system. In fact, the tumour lymphatic system is often compromised due to the lack of lymphatic drainage, increased filtration of proteins and fluid retention, resulting in the enhanced retention of macromolecules and nanocarriers (Cassidy and Schätzlein, 2004; Alexis *et al.*, 2008; Torchilin, 2008). The EPR effect forms the basis of passive targeting for nanocarriers, previously shown with liposomes, polymer-drug conjugates and polymeric micelles (Maeda *et al.*, 2000; Torchilin, 2010). The EPR effect is a near universal phenomenon in tumours, including hepatoma, renal cancer, lung cancer, brain tumour and melanoma (Maeda *et al.*, 2000; Maeda *et al.*, 2009). Nevertheless, a prerequisite of passive targeting is to have long-circulating half life, in order to provide sufficient accumulation in the tumours (Torchilin, 2010). Coating nanocarriers with hydrophilic polymers such as polyethylene glycol (PEG) is a measure to protect the nanocarriers from rapid clearance through the reticulo-endothelial system (RES) (further discussed in Chapter 2). Besides, the size and charge of a nanocarrier system play an important role in a system's physicochemistry, thus influencing its tumour accumulation via the EPR effect (Schätzlein, 2003). However, it is well established that the endothelial lining are also more permeable than normal state under certain circumstances, for instance inflammation, hypoxia and infarction (Torchilin, 2010; Maeda *et al.*, 2000). Despite effective EPR effect in tumour sites, there is a possibility for non-specific drug affinity towards tissues with enhanced vascular permeability or high blood flow area such as the RES organs. One approach to overcome this limitation is by active targeting, where specific recognition of a binding site in target tissues can be achieved.

1.3.2   Active Targeting

Active targeting involves coupling of drugs or nanocarriers to a targeting moiety that is capable of recognising cancer cells via specific binding affinity. These targeting moieties, for example antibodies, proteins, hormones, aptamers, polysaccharides and ligands, are high-affinity counterparts of overexpressed surface markers on cancer cells (Alexis *et al.*, 2008; Torchilin, 2010). Upon administration, the targeting agent on nanocarriers will bind with high selectivity to molecules that are uniquely expressed on cancer cell surface. These bound carriers are then internalised to release the drug content inside the cell. Among the various active targeting strategies for nanocarriers, ligand-receptor interactions are most commonly studied. The binding of a ligand to a receptor provides the basis for most specific biological interactions and provides the blueprint for ligand-based targeting strategies, where carriers are effectively internalised via receptor-mediated endocytosis (Schätzlein, 2003).
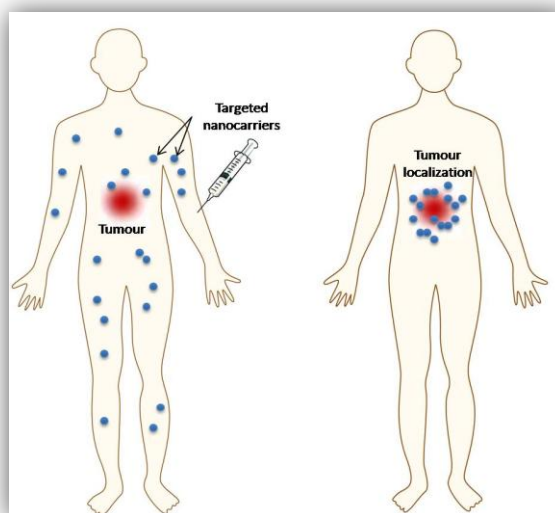
Figure 1.20: Tumour recognition and localization of actively targeted nanocarriers.

In spite of the positive outcome achieved with ligand-receptor-targeted systems, several parameters were acknowledged as the major determinants of drug targeting efficacy. First and foremost, the specificity of the recognition site is crucial (Ferrari, 2005). The most widely used targeting ligands are based on endogenous molecules pre-existing in the body. Hence the concept of targeting is basically built on the differential expression levels of their corresponding receptors between the tumours and normal tissues (Schätzlein, 2003). However, a potential disadvantage of using endogenous ligands is the background expression of their corresponding receptors on healthy tissues, which might give rise to possible interference in their targeting efficacy (Schätzlein, 2003). Secondly, the binding affinity of a ligand to its receptor is directly correlated with its targeting efficacy and promotes specificity (Peer *et al.*, 2007). That being said, there should be a balance of receptor binding affinity, as too high of a binding affinity was found to decrease the penetration of nanocarriers due to a phenomenon called 'binding site barrier' where diffusional transport of targeted material towards the centre of the tumour is prohibited as nanocarriers are bound too strongly to the receptors at the tissue periphery (Cassidy and Schätzlein, 2004; Peer *et al.*, 2007). Last but not least, the number of binding sites is closely associated with the efficacy of an actively targeted system (Torchilin, 2010). A high receptor density on target cells as well as high ligand density on drug carrier system improves drug targeting efficacy via multiple binding sites promoting multipoint interaction between carriers and the target site (Peer *et al.*, 2007; Torchilin, 2010). The array of ligand-receptor targeting approach being investigated to date include the use of transferrin, folic acid, galactose, epidermal growth factor, arginine-glycine-aspartate peptide, vasoactive intestinal peptide (Schätzlein, 2003; Torchilin,

2005; Peer *et al.*, 2007). In this study, transferrin was chosen as the targeting ligand for our niosome systems as it has previously demonstrated excellent targeting ability when combined with liposomes, niosomes as well as polymeric nanocarriers (Dufès *et al.*, 2000; Torchilin, 2005).

1.3.2.1 Transferrin

Transferrin (Tf) is a serum glycoprotein with the capacity to bind and transport iron via interaction with its receptor. Transferrin monomer contains about 700 amino acids with molecular mass of approximately 80 kDa, consisting of two subunits known as the N-lobe and the C-lobe, where each subunit is capable of binding to one iron atom (Figure 1.21) (Qian *et al.*, 2002; Daniels *et al.*, 2006). Therefore each transferrin molecule (apo-Tf) can carry one iron atom (monoferric Tf) or two iron atom (diferric Tf) although the association constant with transferrin receptors for diferric Tf is 30-fold higher than monoferric Tf (Daniels *et al.*, 2006). There are two types of transferrin receptors, namely transferrin receptor 1 (TfR1) and transferrin receptor 2 (TfR2), both are type 2 transmembrane homodimer, consisting of two identical monomers joined by two disulfide bonds (Qian *et al.*, 2002). TfR2 shares similar amino acid sequence and functionality with TfR1 but its affinity for iron-loaded Tf is 25-fold lower than TfR1 (Qian *et al.*, 2002). As iron transporters, the expression of TfR is normally elevated by increased iron requirement for example in maturing erythroid cells that require iron for haem synthesis, placental trophoblasts that are responsible for the delivery of iron to foetus as well as high proliferating cells where there is an increased need for iron as a cofactor of the ribonucleotide reductase enzyme involved in DNA synthesis (Daniels *et al.*, 2006).

Rapidly dividing cells expressing TfR include tissues from bone marrow, intestinal epithelium and basal epidermis (Wagner *et al.*, 1994). In cancer cells, the increased need for iron due to rapid cell growth leads to the overexpression of TfR when compared to their normal counterparts (Daniels *et al.*, 2006; Peers *et al.*, 2007). Up to 5-fold higher of a TfR expression was found in malignant breast cancer cells compared to non-neoplastic breast cells, similar overexpression was also found in pancreatic, colon, lung and bladder cancer cells, as well as in chronic lymphocytic leukaemia and non-Hodgkin's lymphoma (Daniels *et al.*, 2006; Peers *et al.*, 2007). In addition to cells with high proliferation rate, TfR is also present in non-proliferating cells such as brain capillary endothelium and highly overexpressed in brain tumour cells glioblastoma multiforme (Wagner *et al.*, 1994; Beduneau *et al.*, 2007). Elevated expression of TfR in cancer cells has been extensively explored as a targeting strategy in drug delivery systems to enhance the delivery of therapeutic drugs while minimizing drug-induced toxicity. The specific internalization mechanism of Tf via receptor-mediated endocytosis was widely exploited as a site-specific pathway to deliver therapeutic compounds or diagnostic agents.
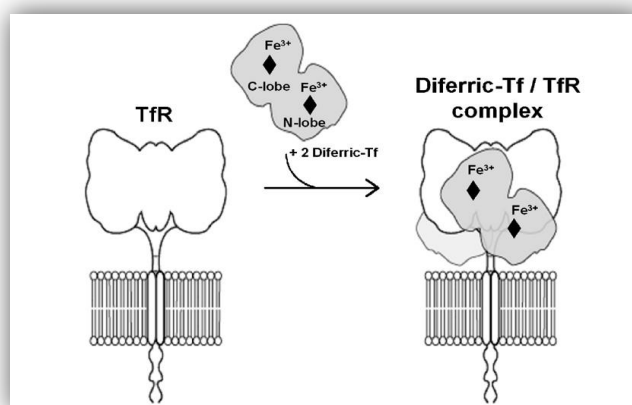
Figure 1.21: The binding mechanism of iron-loaded transferrin to transmembrane transferrin receptor *(Adapted from Daniels et al., 2006).*

The internalization of iron bound Tf via TfR transport (Figure 1.22) is well documented as one of the best characterized processes in cell biology (Li *et al.*, 2002). Upon binding of iron-loaded Tf to TfR at cell surface, Fe_2-Tf-TfR complex is rapidly endocytosed into the endosomal compartment via clathrin-coated pits. Coated pits invaginate and pinch off to form endocytic clathrin transported into the cell (Conner and Schmid, 2003). Upon maturation and the loss of clathrin coat, endosomal lumen is acidified to pH about 5.5 by proton pumps, facilitating a conformational change in Tf where iron is released (Qian *et al.*, 2002; Daniels *et al.*, 2006). Free iron is then reduced and transported from the endosomal membrane to the cytosol by divalent metal transporter DMT1, while apo-Tf-TfR complex is recycled back to the cell surface through exocytic vesicles (Qian *et al.*, 2002). As apo-Tf has about 30-fold lower affinity for TfR at extracellular pH (pH 7.4), apo-Tf will dissociate from its receptor and being released into the circulation for reutilization (Wagner *et al.*, 1994). One major advantage of Tf-TfR internalization pathway is its very high turnover rates, only 4-5 minutes in K562 cells with a mean transit time of about 10 minutes, although its intracellular fate may be influenced when conjugated to therapeutic agents or nanocarriers (Wagner *et al.*, 1994). Studies also showed that compounds transported by this pathway have the ability to avoid the lysosomal compartment, thereby escaping enzyme degradation in the lysosomes (Wagner *et al.*, 1994; Ishida *et al.*, 2001).
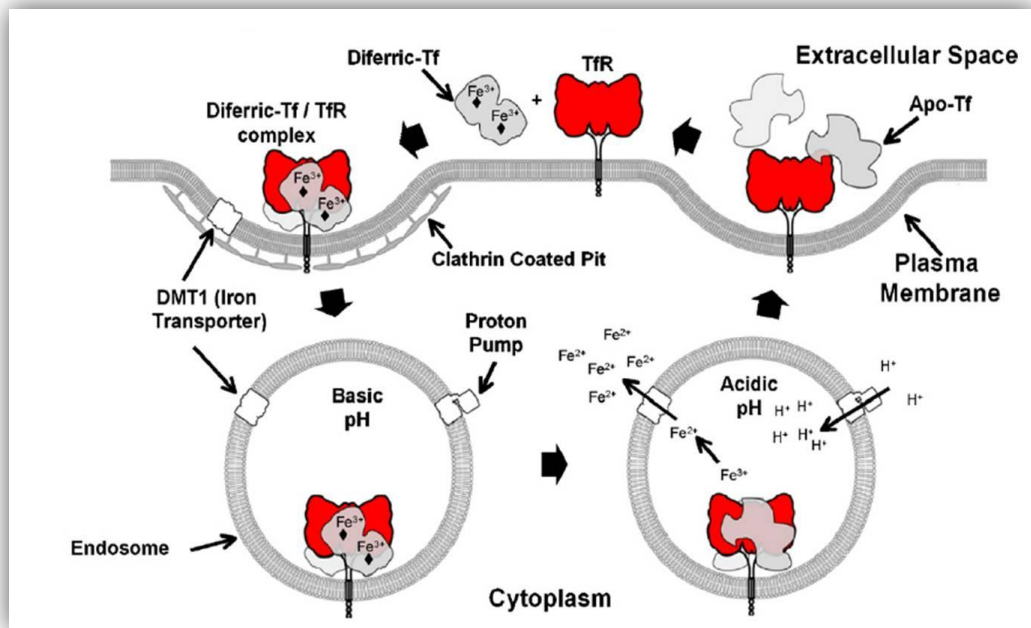
Figure 1.22: Internalization mechanism of iron loaded Tf-TfR complex via clathrin dependent receptor-mediated endocytosis. Irons are release in acidic pH in matured endosomes while transferrin and transferrin receptor are recycled to the plasma membrane. *(Adapted from Daniels et al., 2006).*

1.3.2.2 Transferrin-targeted drug delivery systems in cancer

The coupling of transferrin to drug carriers is no stranger in cancer therapeutics owing to the specific targeting capacity of overexpressed TfR in cancer cells, effectively facilitating the transport of therapeutic drugs into tumour tissues. Significant increase in doxorubicin uptake was achieved by encapsulating doxorubicin in Tf-targeted liposomes when delivered to C6 glioma *in vitro* (Eavarone *et al.*, 2000). Competitive binding studies confirmed the enhanced internalization of doxorubicin was directly correlated with transferrin-dependent receptor-mediated endocytosis. *In vivo*, in mice inoculated with Hep G2 hepatoma cells, intravenous administration of Tf-coupled doxorubicin liposomes demonstrated a favourable doxorubicin tissue distribution where increased tumour accumulation

was observed while concentration in heart and kidney was significantly reduced (Li *et al.*, 2009). Minimizing doxorubicin concentration in heart and kidney is critical to manage drug-induced cardiac toxicity and neuropathy associated with doxorubicin. This was found equally important in cisplatin treatment (Longhi *et al.*, 2007; Cunningham *et al.*, 2008). Iinuma *et al.* found that cisplatin encapsulated in Tf-targeted liposome significantly increased the survival rate of mice inoculated with MKN45P gastric tumour cells, most probably due to the reduced cisplatin accumulation in liver and spleen in addition to higher tumour cisplatin concentration (Iinuma *et al.*, 2002). A novel cisplatin derivative, oxaliplatin, was also found to suppress tumour growth more effectively when encapsulated in Tf-targeted liposomes compared to non-targeted liposomes, correlating with the increase tumour accumulation of oxilaplatin (Suzuki *et al.*, 2008). In the case of niosomes, increased intracellular accumulation in epithelial carcinoma A431 cells was observed when vesicles were targeted with Tf whereas up to 71 % inhibition in tumour growth was observed in mice bearing S180 sarcoma tumours with Tf-targeted niosomes encapsulating hydroxycamptothecin (Dufès *et al.*, 2000; Hong *et al.*, 2009). When Tf was conjugated directly to drug molecule, in the case of artemisinin, the cytotoxicity effect was 34 000 times higher than artemisinin itself (Nakase *et al.*, 2008).

In order to investigate the cellular internalization mechanism, Tf-coupled liposomes were administered *in vitro* and *in vivo* to Colon 26 cells and studied using electron microscopy imaging, where receptor-mediated endocytosis was confirmed as the method of internalization for Tf-targeted liposomes, directly correlated with their increased accumulation in tumour tissues (Ishida *et al.*, 2001). Moreover, when

studied in doxorubicin-resistant leukaemia (K562/DOX) and small cell lung cancer (SBC-3/ADM) cells, 2 to 5-fold improvement in cytotoxicity was observed using Tf-targeted liposome compared to non-targeted doxorubicin, suggesting the role of Tf targeting in combating multidrug resistance (MDR) in cancer cells (Kobayashi *et al.*, 2007; Wu *et al.*, 2007). Further experiments proved that liposomes linked to Tf were able to prevent doxorubicin efflux by P-glycoprotein, effectively circumvented MDR in resistant cell lines, as long as adequate release of the drug was achieved (Kobayashi *et al.*, 2007).

Active targeting via TfR pathway is not only exploited in the field of chemotherapeutics, but also for delivery of bioactive molecules to target sites where TfR are highly expressed. Such area include gene therapy (Kircheis *et al.*, 2001; Chiu *et al.*, 2006; Cardoso *et al.*, 2007; Sakaguchi *et al.*, 2008), delivery of molecules to the brain (Huang *et al.*, 2007; Ying *et al.*, 2009) as well as in boron neutron capture therapy (Maruyama *et al.*, 2004; Doi *et al.*, 2008). Nonetheless, it should be noted that its targeting efficacy might vary according to the degree of Tf modification, the cross-linking method, intrinsic physicochemical properties of nanocarriers and the behaviour of transferrin in different cell lines (Wagner *et al.*, 1994; Kobayashi *et al.*, 2007; Sakaguchi *et al.*, 2008). In summary, the concept of drug targeting involves a coordinated performance of three components: (a) drug; (b) targeting moiety and (c) pharmaceutical carrier (Torchilin *et al.*, 2000) in order to achieve a combined effect of active and passive targeting.

1.4 AIMS AND OBJECTIVES

Tocotrienol, a component in vitamin E, has recently been shown to exhibit impressive tumour suppressive properties on cancer cells. However, despite its superior anti-tumour effect, tocotrienol was never regarded as a therapeutic agent, although it is currently available in the market as supplements, e.g. Tocomin$^{®}$ SupraBio^{TM} by Carotech Inc., NSI Tocomin$^{®}$ SupraBio ^{TM} Palm Tocotrienol Complex by Nutraceutical Sciences Institute and Tocomin$^{®}$ Tocotrienol Vitamin E Complete by Olympian Labs, etc. We believe that the lack of tocotrienol activity is primarily due to poor absorption and tissue distribution after oral administration such that therapeutic doses are not delivered at target tissues. Therefore, this research takes on the challenge to identify a nanocarrier system that can act as a vehicle to deliver tocotrienol at adequate doses specifically to tumour tissues, without compromising safety issues. Precisely, the aims and objectives of this study are outlined in the following:

1. To prepare and characterize transferrin-targeted niosome systems encapsulating tocotrienol

2. To evaluate their therapeutic efficacies on cancer cells *in vitro*

3. To evaluate their therapeutic efficacy on murine xenograft models *in vivo* via intravenous administration

In Chapter 2, we aim to explore two formulations of niosome systems to encapsulate tocotrienol. Both systems were prepared using Span 60, a non-ionic surfactant amphiphile used as the building block for the lipid bilayer. However, these formulations differed by the long chain hydrophilic polymer added to vesicle surface

in order to shield the vesicles from RES clearance, i.e. Span 60/ Solulan C24 vesicles and Span 60/TPGS vesicles. Solulan C24 (cholesteryl poly(24)oxyethylene ether) and TPGS (tocopheryl polyethylene glycol succinate) are polymeric derivatives of cholesterol and α-tocopherol respectively. Similar to PEGylation technique, both hydrophilic long chain polymers will be incorporated in Span 60 vesicles for steric protection against rapid clearance from the circulation system. Therapeutic efficacy of tocotrienol is further enhanced by coupling the vesicles with transferrin, with the aim to promote site specific delivery of tocotrienol to cancer cells that overexpress transferrin receptors (Figure 1.23). To this end, physical characteristics including vesicle morphology, encapsulation efficiency, transferrin conjugation efficiency, size and zeta potential were determined and optimized.
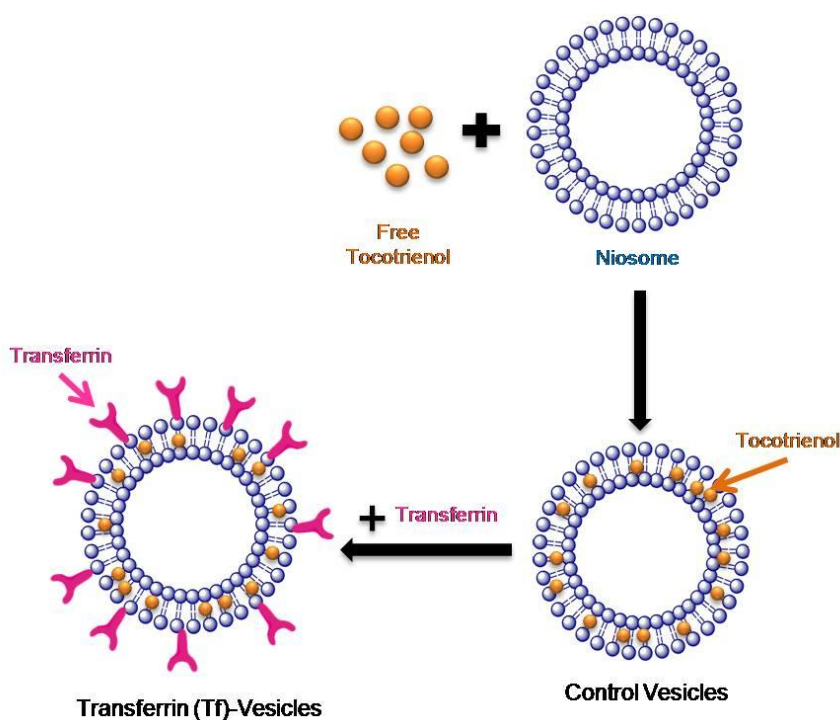
Figure 1.23: Schematic illustration of a tocotrienol entrapped in vesicular formulation as control vesicles and transferrin (Tf)-vesicles.

Chapters 3 and 4 describe the *in vitro* and *in vivo* evaluations of the targeting and therapeutic efficacies of these tocotrienol-loaded therapeutic systems. *In vitro*, two major aspects were studied, i.e. intracellular accumulation and anti-proliferative effect. The concentration of tocotrienol accumulated in cancer cells was quantified and visualised using various microscopy techniques when tocotrienol was encapsulated in targeted and non-targeted niosomes or as free tocotrienol. Anti-proliferative effect was subsequently assessed using a standard anti-proliferative assay. The objective of *in vivo* evaluation is to determine the tumour suppressing effect of tocotrienol when delivered using different therapeutic systems. Mice bearing subcutaneous tumours were treated with tocotrienol delivery systems intravenously via tail vein injections and monitored daily for tumour growth, animal weight and general well being.

Chapter 2

Preparation and Characterization

2.1. INTRODUCTION

2.1.1 Span 60 Niosomes

As mentioned in Chapter 1, niosomes are vesicular systems formed from the self-assembly of non-ionic surfactants. In a review by Uchegbu and Florence (1995), vesicle-forming non-ionic surfactants include alkyl ethers, alkyl esters, amides, fatty acids and amino acid compounds. Among all, alkyl ethers are the most widely studied surfactants, classified according to the nature of their hydrophilic head groups, i.e. glycerol subunits or ethylene oxide subunits (Uchegbu and Florence, 1995).

On the other hand, alkyl esters of sorbitan headgroups have been explored as potential drug carriers due to their common use as emulsifiers in food and pharmaceuticals (Yoshioka *et al.*, 1994). Some examples include the Span series (20, 40, 60, 80) and Tween series (20, 60, 80). In general, these surfactants contain alkyl chain length of C12 to C18 (Figure 2.1). Among the above mentioned surfactants, Span 60 was chosen as the main focus in this study due to its previous success in the field of cancer chemotherapy for doxorubicin (Uchegbu *et al.*, 1995), paclitaxel (Bayindir and Yuksel, 2010), cisplatin (Gude *et al.*, 2002) and cytarabine (Ruckmani *et al.*, 2000). Yoshioka *et al.* (1994) did an extensive review on the variation in vesicle properties in terms of vesicle size, drug entrapment and drug release with niosomes prepared from Span 20, 40, 60, 80 and 85 (Yoshioka *et al.*, 1994). In the study, a general trend of decreasing vesicle size with increasing surfactant alkyl chain was observed. Hydrophile-lipophile balance, HLB (Span 20: 8.6, Span 40: 6.7, Span 60: 4.7, Span 80: 4.3, Span 85: 1.8) was used as an indication for size as a

decrease in surface energy is often associated with increasing hydrophobicity (Yoshioka *et al.*, 1994). As such, the longer the hydrophobic chain, surface energy of vesicles appeared to be lower, resulting in the formation of smaller vesicles. In the same study, using water soluble carboxyfluorescein, Span 40 and Span 60 were shown to have the highest encapsulation efficiency due to their higher phase transition temperature. The bilayer membrane is an ordered structure that may exist in the gel state or the liquid crystalline state. While bilayers in the liquid crystal state are usually less ordered, the arrangement of bilayers are mostly ordered when in gel state (Uchegbu and Vyas, 1998). By increasing the temperature, the gel state bilayer "melts" at phase transition temperature and is converted from the gel into a liquid-crystalline state (Crommelin and Schreier, 1994). At room temperature 25°C, Span 20, Span 80 and Span 85 were in disordered liquid-crystalline state while Span 40 and 60 were in ordered gel state (Yoshioka *et al.*, 1994). This resulted in a less fluid membrane bilayer in Span 40 and Span 60 vesicles, thus elevating the amount of encapsulated hydrophilic and hydrophobic drug. For hydrophobic drugs, although longer alkyl chain length was said to give better encapsulation efficiency due to enhanced hydrophobic interaction within the lipid bilayer, encapsulation efficiency of paclitaxel in Span 80 and Span 85 vesicles were relatively low compared to Span 60 vesicles (Bayindir and Yuksel, 2010). The relationship between a lipophilic drug and niosome properties is of very high importance in our study because it correlates with the lipophilicity of TRF (log P: approximately 7.5-9.9). The fact that both Span 80 and Span 85 have unsaturated alkyl chain increased the chain fluidity, leading to a marked enhancement in the bilayer permeability of vesicles (Uchegbu and Florence, 1995). Similar trend was observed with hydrophilic molecules, studies using

doxorubicin and carboxyfluorescein in Span 80 and Span 85 vesicles showed inefficient encapsulation in addition to increased release rates owing to the unsaturated alkyl chain (Uchegbu and Florence 1995; Yoshioka *et al.*, 1995).
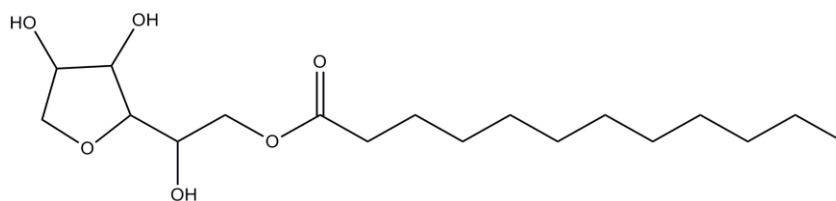
Span 20
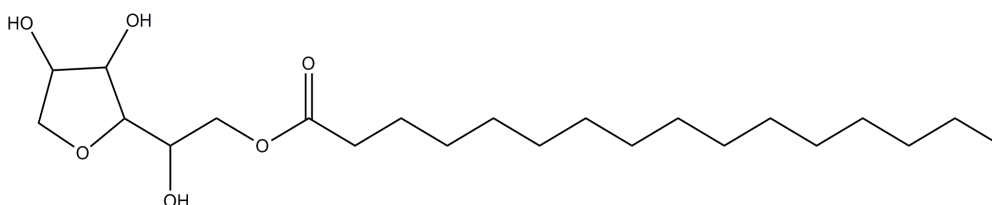
Span 40
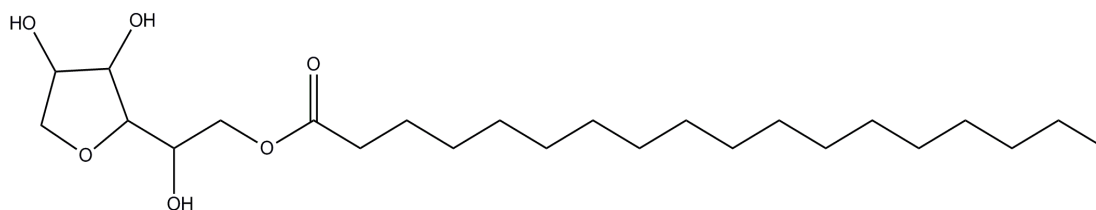
Span 60
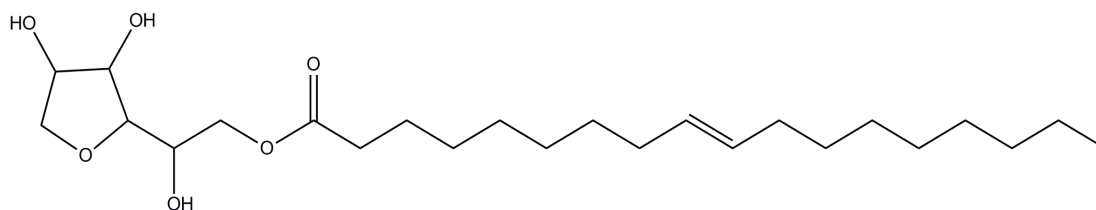
Span 80

Figure 2.1: Chemical structure of non-ionic surfactants from the Span series.

Besides the main vesicle forming surfactants, physical properties of a vesicle are often altered by membrane additives, for instance cholesterol (Figure 2.2). Inclusion of cholesterol was very common in vesicular formulations, mainly because of its ability to alter the fluidity of bilayer membrane. In a study done by Arunothayanum *et al.* (1999), addition of cholesterol increased the curvature of bilayer membranes, leading to the formation of spherical vesicles instead of polyhedral vesicles. The capacity to control membrane fluidity also helped in preventing drug leakage from vesicles. Cholesterol acts as a space filling material when surfactant assembles into vesicles (Uchegbu and Florence, 1995; Bayindir and Yuksel, 2010). By increasing the orientational order of bilayers, permeability of vesicles is reduced. Thus, incorporation of cholesterol in vesicles often helps to minimize both hydrophilic and hydrophobic drug leakage from vesicles. Reduced bilayer permeability was also attributed to the ability of cholesterol to abolish the gel to liquid phase transition (Crommelin and Schreier, 1994). While lipid bilayers can be in a liquid-crystalline phase or in a gel phase, in which gel phase is more rigid and less permeable than liquid crystalline phase, elimination of phase transition locks the bilayer membrane in a gel state, resulting in membrane stabilization. In niosome formulations, gel to liquid transition was abolished with inclusion of 30-50 mole% cholesterol (Cable, 1989), effectively preventing drug leakage (Uchegbu and Vyas, 1998). This feature may contribute to the enhanced encapsulation efficiency as well. Yoshioka *et al.* (1994) and Hao *et al.* (2002) showed that the quantity of water-soluble carboxyfluorescein and colchicine encapsulated in niosomes increased with increasing cholesterol. Surfactant cholesterol molar ratio of 1:1 is most beneficial

while extra cholesterol was found to be unfavourable (Yoshioka *et al.*, 1994; Uchegbu and Vyas, 1998; Hao *et al.*, 2002).
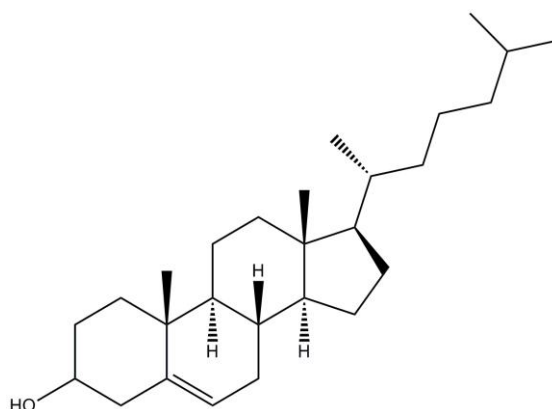
Figure 2.2: Chemical structure of cholesterol.

In applications where colloidal nanocarriers are administered intravenously, rapid clearance of nanocarriers from the circulation by cells of the reticulo-endothelial system (RES) in the liver, lung and spleen is inevitable (Crommelin and Schreier, 1994). The uptake of colloidal drug carriers by the RES is initiated by adsorption of serum proteins at the carrier surface, followed by phagocytosis in macrophages of the RES (Malstem, 2002). It was found that the amount of drug carrier taken up by macrophages increases with increasing particle size, hydrophobicity and charge (Malstem, 2002). Therefore, the crucial property of any multifunctional nanocarrier is its longevity, in order to maintain a required level of pharmaceutical agent in the blood circulation prior to clearance from the RES (Torchilin, 2006). Surface hydration of vesicles with hydrophilic polymers is a common method to prolong vesicle circulation in the blood. Modification of vesicle surfaces with long chain polymers helps to enhance the steric hindrance between vesicles. In addition to protect individual vesicles from aggregation, the repulsive

steric force effectively prevents the adsorption of serum proteins to modified vesicles (Malstem, 2002; Uchegbu and Schätzlein, 2006). In general, the adsorption of serum proteins to any surface is mainly driven by electrostatic forces, hydrophobicity and van der Waals interactions (Malstem, 2002). Hence, surface coating of vesicle with hydrophilic polymers combines the benefits of an uncharged, hydrophilic and steric stabilized drug carrier, leading to sufficiently long-circulating drug carriers. Practically, adsorption of all serum proteins will be dramatically reduced provided that the polymer coating is sufficiently thick and dense, generally requiring the polymer molecular weight at the order of 1000-2000 Da (Malstem, 2002). In such case, polyethylene glycol (PEG) has been widely used as polymeric steric stabilizer (Immordino *et al.*, 2006).

PEG is a long chain hydrophilic polymer having numerous useful properties such as biocompatibility, solubility in aqueous and organic solution, lack of toxicity and good excretion kinetics (Immordino *et al.*, 2006). PEGylation of nanocarriers has demonstrated various biological advantages, especially in increasing the longevity of nanocarriers in blood circulation. In biological environment, coating of nanocarriers with PEG sterically suppressed the interactions of blood components with their surface, subsequently reducing the binding of plasma proteins (Torchilin, 2007). As a result, opsonisation of PEGylated nanocarriers was minimized, effectively protecting the nanocarriers from RES clearance. Several mechanisms by which PEG exert its steric stabilization effect has been proposed, including shielding of surface charge, increased surface hydrophilicity, enhanced repulsive forces between nanocarriers and

blood components and formation of a polymeric layer over particle surface, which renders impermeable for large molecules such as opsonins (Torchilin, 2007).

In this study, two long circulating hydrophilic polymers were chosen as protective polymer coatings on vesicles in order to withstand clearance from the blood circulation. These polymers were namely cholesteryl poly(24)oxyethylene ether (Solulan C24) and tocopheryl polyethylene glycol succinate (TPGS). Solulan C24 is a polyoxyethylene-modified derivative of cholesterol (Figure 2.3). When incorporated in niosome formulations, it has been found to increase and prolong the plasma levels of doxorubicin (Florence and Cable, 1993; Uchegbu and Vyas, 1998). However a concentration higher than 30 mole % forms mixed micelles system as Solulan C24 itself forms micellar solutions at high concentrations (Florence and Cable, 1993). Similar observation was reported in a study by Uchegbu *et al.* in 1997, where high concentrations of Solulan C24 induced vesicle aggregation whereas Solulan C24 at mol % of 9 was found to give the best encapsulation efficiency (Uchegbu and Duncan, 1997).
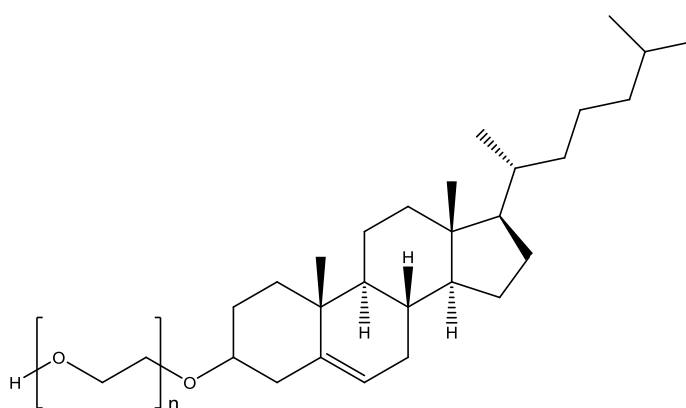
Figure 2.3: Chemical structure of cholesteryl poly-24-oxyethylene ether (Solulan C24).

Span 60/Cholesterol/Solulan C24 niosomes have been previously studied for intravenous administration of doxorubicin and doxorubicin-polymer conjugate (Uchegbu *et al.*, 1995; Gianasi *et al.*, 1997). *In vitro*, Gianasi *et al.* (1997) indicated a reasonable stability of this niosome formulation for long circulation in the bloodstream based on an experiment by incubating the niosomes with plasma. Storage stability against pH and temperature was also established in the study in which doxorubicin release was not affected by both factors. *In vivo*, plasma level of doxorubicin was increased by 6-fold when encapsulated in Span 60/Cholesterol/Solulan C24 niosomes (Uchegbu *et al.*, 1995). Furthermore, encapsulation of doxorubicin reduced its clearance significantly compared to doxorubicin solution. In the same study, the efficacy of doxorubicin in suppressing tumour growth on mice MAC 15A tumour model was twice higher when encapsulated in niosomes compared to drug in solution.

TPGS, on the other hand, is a hydrophilic derivative of vitamin E formed via the esterification of α-tocopherol with polyethylene glycol (PEG molecular weight 1000) through succinate diester linker (Figure 2.4). Not only it has been approved in Japan as a pharmaceutical excipient for oral administration, TPGS is also an FDA approved drug solubiliser for oral, parenteral, topical and nasal therapies (Yan *et al.*, 2007). TPGS is a valuable excipient or carrier in drug delivery systems widely used to enhance the solubility and bioavailability of poorly absorbed drugs. Its emulsifying and solubilising properties are attributed to the amphiphilic structure: having a hydrophilic PEG chain and a lipophilic tocopherol which gives a HLB of about 13 (Constantinides *et al.*, 2006). Before the synthesis of water soluble vitamin

E, severe vitamin E deficiency was previously treated with painful intramuscular injections of vitamin E. Water soluble TPGS was one of the vitamin E derivatives developed as a potential source of vitamin E for oral administration in patients with severe fat malabsorption and vitamin E deficiency secondary to short-bowel syndrome (Eastman Chemical Company, 2005).

Figure 2.4: Chemical structure of d-α-tocopheryl polyethylene glycol 1000 succinate (TPGS).

TPGS has been extensively used to improve the absorption of poorly soluble drug including cyclosporine (Wacher *et al.*, 2002), amprenavir (Yu *et al.*, 1999), paclitaxel (Varma *et al.*, 2005), vancomycin (Prasad *et al.*, 2003), camptothecin (Mu *et al.*, 2005) and oestradiol (Sheu *et al.*, 2003). In addition to its emulsifying and solubilising abilities, P-glycoprotein (P-gp) inhibition was also proposed as a mechanism of action for the improved absorption of drugs when administered with TPGS. P-glycoprotein is a membrane-bound transporter that mediates "efflux" of drugs and toxins out of the cells by active transport, protecting cells against toxins (Constantinides and Wasan, 2007). Due to their expression in the entire length of the gut, liver, kidney, blood-brain barrier and tumour, not only do they drive the efflux of toxic substrates out of the cells, P-glycoprotein is also responsible for drug elimination in multi-drug resistance (Constantinides and Wasan, 2007). Multi-drug

resistance has a great impact in infectious diseases and cancer as P-gp-mediated efflux mechanisms are the rate limiting factors in the absorption and accumulation of effective therapeutics in the cells (Chan *et al.*, 2004). TPGS was among the polymer excipients/ surfactants shown to inhibit P-gp efflux via the interaction with lipid membrane (Constantinides and Wasan, 2007). TPGS exhibited most potent inhibition on P-gp efflux among 4 other surfactants investigated, including Pluronic PE6100, Pluronic PE8100, Cremophor EL, and Tween 80 (Bogman *et al.*, 2003). Enhanced drug permeability induced by inhibition of P-gp efflux due to the presence of TPGS has previously been shown with paclitaxel (Varma *et al.*, 2005), HIV protease inhibitor amprenavir (Yu *et al.*, 1999), celiprolol and digoxin (Cornaire *et al.*, 2004). The ability of TPGS to inhibit the function of P-gp was also believed to have contributed to the intrinsic anti-tumour effect of TPGS in conjunction with its apoptosis-inducing properties (Youk *et al.*, 2005).

In pharmaceutical formulations, TPGS was previously incorporated in nanoparticles composed of poly(lactide-co-glycolide) (PLGA) and poly(lactide) (PLA) in order to deliver small molecule chemotherapy, for instance paclitaxel. When loaded in TPGS nanoparticles, paclitaxel retained a prolonged half-life of 4 to 27 times higher than Taxol[®] (a commercial form of paclitaxel formulated in Cremophor EL) (Win and Feng, 2006; Zhang *et al.*, 2008). Significant advantage of paclitaxel-TPGS nanoparticles in suppressing mice tumour model was observed, up to 2 times more effective compared to Taxol[®] (Zhang *et al.*, 2008). The use of TPGS in mixed micelle formulations was also investigated as a nanocarrier for camptothecin and doxorubicin (Mu *et al.*, 2005; Yi *et al.*, 2005; Gao *et al.*, 2008;

Zhao *et al.*, 2008). Besides, a recent work by Yan *et al.* has also demonstrated the potential of TPGS used as a safe surfactant for "green processing" of carbon nanotubes (Yan *et al.*, 2007).

For parenteral delivery, numerous injectable emulsion systems containing TPGS were developed, such as TOCOSOL®-paclitaxel. Using B16 mouse melanoma model, TOCOSOL®-paclitaxel exhibited superior antitumour activity in a dose-dependent manner when compared to Taxol® (Constantinides *et al.*, 2000). Parenteral emulsions using TPGS for the delivery of amiodarone, estradiol, vincristine and aclacinomycin are currently under vast development in the hope to replace clinical formulations which contain mildly toxic polysorbate 80 (Constantinides *et al.*, 2006). Emulsions of carmofur, fluorouracil, mitomycin C and cyclocytidine have also been formulated using TPGS (Eastman Chemical Company, 2005).

2.1.2 Fluorescence Spectrophotometry

One of the most valuable analytical techniques in pharmaceutics is absorption spectroscopy, owing to its speed, simplicity, specificity and sensitivity (Connors, 2002). A molecule can be excited from its ground electronic state to an excited electronic state by absorbing energy in the form of visible or ultraviolet light. Many molecules are capable of emitting this energy as radiation, thus returning to ground state. The emitted radiation is called fluorescence (Connors, 2002). A schematic illustration of a spectrofluorometer is shown in Figure 2.5. An essential condition for fluorescence is strong light absorption by the molecule, for instance molecules with

aromatic, heterocyclic and highly conjugated structures. Most aromatic and phenolic compounds fluoresce under many conditions (Connors, 2002).
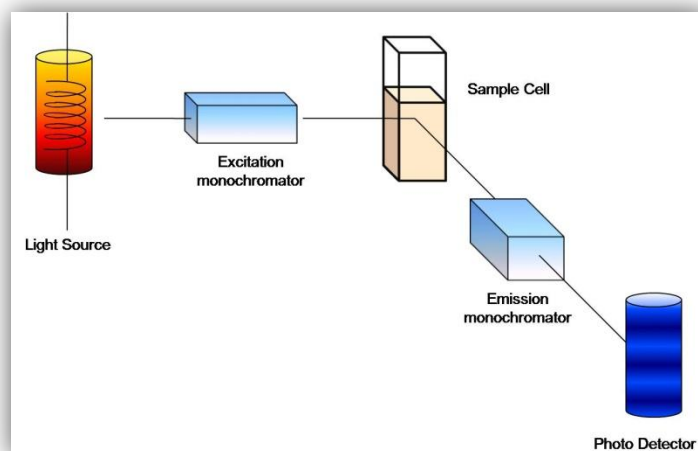
Figure 2.5: Schematic illustration of a fluorescence spectrophotometer.

In previous studies, analysis of Vitamin E was performed using high performance liquid chromatography (HPLC) method to separate the eight components in vitamin E, namely tocopherol and tocotrienol in the form of α-, β-, γ-, δ-. Most of these systems were connected to a fluorescence detector to operate at an excitation wavelength in the range of 292-296 nm and emission wavelength ranging from 325-330 nm (Katsanidis and Addis, 1999; Yap *et al.*, 1999; Nesaretnam *et al.*, 2004; Puah *et al.*, 2006; Nesaretnam *et al.*, 2007). In our study, while tocotrienol was administered as a mixture of tocopherol and tocotrienol, fluorescence spectrofluorimetry offers quick and accurate quantification method to identify TRF. Maximum excitation and emission wavelengths will be identified prior to construction of TRF calibration curves, subsequently used for TRF measurements.

2.1.3 Protein quantification

Lowry assay was first described in 1951 by Lowry *et al.* as a colorimetric assay for protein determination (Lowry *et al.*, 1951). It has been widely used since then as a protein assay for cell fractions, enzyme preparations and chromatography fractions (Stoscheck, 1990). In our study, we aim to graft transferrin onto TRF-loaded vesicles for targeted delivery of TRF to tumour cells. As described by Dufès *et al.* (2000), Lowry assay is a reliable method used to quantify the amount of transferrin conjugated to vesicles, hence the conjugation efficiency of transferrin.

The first reaction of Lowry assay was the Biuret reaction, based on the interaction between divalent copper ions with protein amide bonds in alkaline solutions. In the second reaction, Folin Ciocalteu reagent (a mixture of phosphomolybdate and phosphotungstate) was added to resultant monovalent copper ions, the copper-amide bond complex and radical groups in protein amino acids, subsequently reduced to a tungsten blue that could be detected colorimetrically by UV absorbance at 500-750 nm (Olson and Markwell, 2007). Addition of Folin Ciocalteu reagent increases the sensitivity of the Biuret reaction to about 100 times (Lowry *et al.*, 1951). A major disadvantage of the Lowry assay is its susceptibility to interfering compounds and variation of colour with different proteins. These interferences include detergents, carbohydrates, glycerol, phenols, potassium compounds, disulfide compounds, etc (Olson and Markwell, 2007). Nevertheless, the assay is linear at 1 to 100 µg protein and various precipitation techniques have been proven useful to eliminate contaminations (Olson and Markwell, 2007).

2.1.4 Transmission electron microscopy

Transmission electron microscopy (TEM) is a powerful technique for structure characterization, especially in nanostructures. It has the ability to give atomic-resolution for nanoparticles from less than 1 nm to 100 nm (Williams and Carter, 1996). Due to limited resolution in images produced by light microscopes, electron microscopes were developed in the 1950s (Williams and Carter, 1996). In fact, TEM is a direct derivative of light microscope, which uses electron illumination instead of visible light (Watt, 1997). When a beam of electrons are transmitted across specimens, images are constructed based on the interaction between electrons and the specimen. A schematic illustration of TEM imaging process is depicted in Figure 2.6. Briefly, a well-defined beam of electrons is generated from a heated tungsten filament contained in the electron gun, with a typical accelerating voltage of 20-200 kV. A condenser lens is in place to focus the electron source. The electron beam is then passed through the specimen stage, in which samples are supported on a thin circular metallic mesh or specimen grid usually 3 mm in diameter. The objective lens is the most important lens in a TEM which focuses and constructs the images. Before collecting the images from a photographic recording camera, a projector lens is usually in place to reduce or magnify the images (Watt, 1997). There are currently more than a dozen of different models of TEM developed for various purposes. They are operating over a range of magnification between $\times$ 500 up to $\times$ 500 000 enlargement.
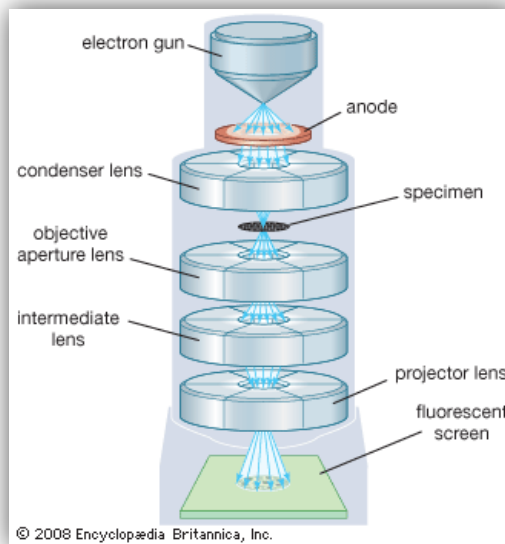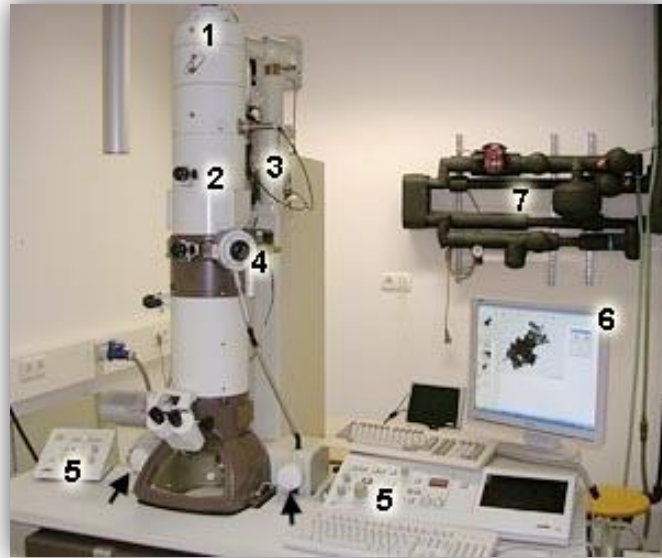
Figure 2.6: A brief illustration of a transmission electron microscope. (1) Electron gun, (2) Condenser lens to focus the electron beam, (3) Vacuum pumps, (4) Specimen, (5) Operation panels, (6) Image display, (7) Cooling system. *(Adapted from Encyclopedia Britannica, Inc.)*

2.1.5 Photon correlation spectroscopy

In colloidal drug delivery systems, size distribution and zeta potentials are two very important factors dictating the intracellular and *in vivo* fates of delivery systems. They are generally measured using Photon Correlation Spectroscopy, also referred to as Dynamic Light Scattering or Quasi-Elastic Light Scattering technique (Figure 2.7) (Malvern Instruments Ltd., 2005).

Particle size, typically in the sub micron region was measured by correlating to the speed at which the particles are diffusing due to Brownian motion. The Brownian motion is the random movement of particles due to the interaction with solvent molecules that surround them. Photon Correlation Spectroscopy calculates the diameter of particles from the velocity of Brownian motion (also known as the translational diffusion coefficient) under controlled temperature and viscosity. As the diameter obtained by this technique refers to how a particle diffuses within a fluid, measurements were referred to as hydrodynamic diameter (d (H)).

$$d\,(H) = (\kappa T)/(3\pi\eta D)$$

where d (H) = hydrodynamic diameter, κ = Boltzmann's constant, T = absolute temperature, η = viscosity, D = translational diffusion coefficient
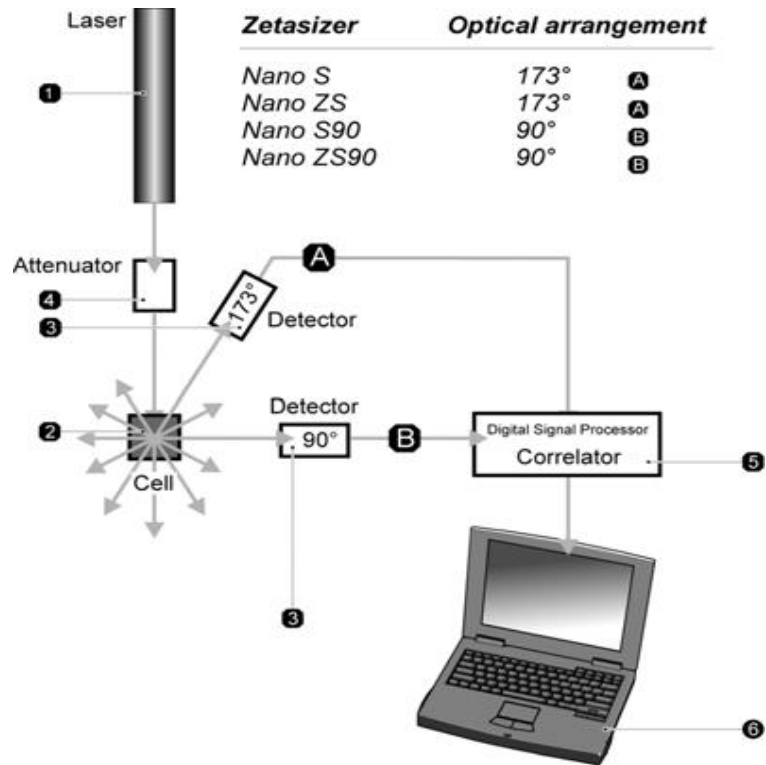
Figure 2.7: Schematic illustration of dynamic light scattering measurements. Briefly, a laser (1) provides a light source to illuminate the sample in a cell (2). The laser beam passes through the sample with some light source scattered by the particles at all angles, which will be measured with a detector (3). An attenuator (4) is in place to adjust the intensity of the laser source for the intensity of the scattered light to be measurable with the detector. The scattering intensity is passed to a correlator (5) to derive the rate at which the intensity is varying. Information from the correlator is passed to a computer (6) for data analysis *(Adapted from Malvern Instruments Ltd., 2004).*

Surface interaction forces of particles are the key to understanding dispersion stability and aggregation. Zeta potential is a useful indicator of particle surface charge. Almost all particles in contact with liquid acquire an electric charge on their surface (Heurtault *et al.*, 2003). An electrical double layer exists round each particle, consisting of a Stern layer denoting the inner region where ions are strongly bound to the particle; and a diffuse layer where ions and particles form a stable entity (Malvern Instruments Ltd., 2004). A notional boundary exists in the diffuse layer where ions within the boundary move when a particle moves, whereas ions beyond the boundary do not travel with the particle. Zeta potential measures the potential at this boundary (Figure 2.8) (Malvern Instrument Ltd., 2004). Measurement of zeta potential exploits the colloidal stability of particle dispersion as it is directly correlated with the interaction forces between the particles as well as potential interactions in biological systems (further discussed in Discussion).
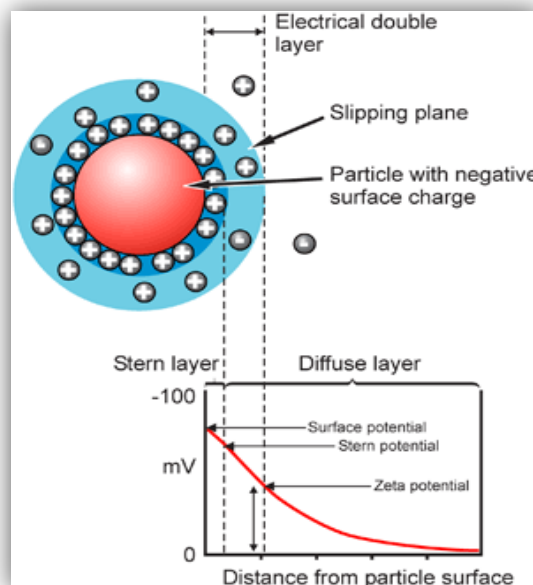
Figure 2.8: Illustration of the electrical double of a particle and the measurement of zeta potential using photon correlation spectroscopy *(Adapted from Malvern Instruments Ltd., 2004).*

2.1.6 Aims and Objectives

In summary, the aim of this Chapter is to synthesize a niosomal vesicular system suitable for effective delivery of tocotrienol via entrapment in the lipid bilayer. Based on literature reviews establishing Span 60/Cholesterol/Solulan C24 niosome system as a versatile and robust delivery system for cancer therapeutics, this formulation was chosen as our first attempt to formulate tocotrienol in a nanocarrier delivery system for intravenous administration. In an attempt to imply active targeting for tumour-delivery of tocotrienol, tocotrienol-loaded vesicles were then linked to an iron transporter: transferrin. In 2000, Dufès *et al.* reported a very positive outcome with transferrin targeted vesicular formulation using palmitoyl glycol chitosan vesicles (Dufès *et al.*, 2000). Successful conjugation of transferrin to the vesicles showed an enhanced uptake of encapsulated fluorescein in A431 human epidermoid carcinoma cells. Although fluorescein is hydrophilic while tocotrienol is highly lipophilic, transferrin-targeted niosome system encapsulating hydrophobic drugs, as in hydroxycamptothecin, showed consistent results with enhanced *in vitro* and *in vivo* therapeutic efficacy (Hong *et al.*, 2009). In this work, using the strategy reported by Dufès *et al.*, we aim to prepare a transferrin-bearing Span 60/Solulan C24 niosome system able to encapsulate tocotrienol.

This system will give us a platform as a proof of concept on the applicability of tocotrienol when encapsulated in tumour-targeted vesicles. In addition to Span 60/Solulan C24 niosomal systems, we are interested to further improve the vesicle formulation by replacing Solulan C24 with TPGS, a vitamin E derivative conjugated with long chain polyethylene glycol. While Solulan C24 and TPGS shared

substantial similarities in their chemical properties, we intend to investigate their ability to form vesicles with tocotrienol as well as their targeting and therapeutic efficacies. Prior to biological studies, this Chapter will be focusing on the preparation and physical characterizations of Span 60/Solulan C24 and Span 60/TPGS vesicular systems. In the presence or absence of transferrin as a targeting moiety, the respective physical properties of these systems including vesicle morphology, size and zeta potential, encapsulation efficiency as well as transferrin conjugation efficiency were discussed. Based on their physical characteristics, the systems were then optimized to be at close proximity to the parameters of an ideal system for cancer therapy.

2.2 MATERIALS AND METHODS

2.2.1 Materials

Materials	Supplier
Tocotrienol Rich Fraction (TRF)	Dr. Abdul Gapor from the Malaysian Palm Oil Board (MPOB), Malaysia
Palm Oil	Dr. Nor Aini Idris from MPOB, Malaysia
Sorbitan monostearate (Span 60)	Sigma-Aldrich, UK
Cholesterol	Sigma-Aldrich, UK
Cholesteryl poly-24-oxyethylene ether (Solulan C24)	D.R. Anstead, USA
D-α-tocopheryl polyethylene glycol 1000 succinate (TPGS)	Eastman Chemical Company, USA
Dioleoyl-phosphatidylethanolamine (DOPE)	Sigma-Aldrich, UK
Dimethylsuberimidate dihydrochloride (DMSI)	Sigma-Aldrich, UK
Human holo-transferrin	Sigma-Aldrich, UK
Triethanolamine	Sigma-Aldrich, UK
Folin Ciocalteu reagent	Sigma-Aldrich, UK
Potassium tartrate	Sigma-Aldrich, UK
Cupric sulphate	Sigma-Aldrich, UK
Sodium carbonate	Sigma-Aldrich, UK

Sodium hydroxide	Sigma-Aldrich, UK
Hydrochloric acid	Sigma-Aldrich, UK
Dimethyl sulfoxide (DMSO)	Sigma-Aldrich, UK
Isopropanol	Sigma-Aldrich, UK

2.2.2 Determination of optimum λ_{ex} and λ_{em} for TRF

In order to identify the specific wavelength associated with TRF, a fluorescence scan was carried out to pre-determine the excitation and emission wavelength at which TRF emits highest fluorescence absorption. TRF stock solution of 5 mg/mL was first prepared in dimethyl sulfoxide (DMSO). As vesicle encapsulation efficiency was quantified using isopropanol, TRF was further diluted in isopropanol to give a final TRF concentration of 20 μg/mL. TRF was then subjected to fluorescence scan (from λ 295 to 400 nm at λ_{ex} 295 nm) where specific wavelengths obtained were then used to construct a standard calibration curve with TRF concentration ranging from 0 to 25 μg/mL (Cary eclipse spectrofluorometer, Varian).

2.2.3 Preparation of targeted Span 60/Solulan C24 vesicles

Due to solubility constrains associated with TRF (Log P ~ 7.5 to 9.9 depending on isoforms), different methods were attempted to encapsulate TRF in vesicles. In order to limit the amount of DMSO (at 0.05 % v/v) to be added to vesicle formulation, highly concentrated TRF stock solution of 100 mg/mL was prepared in palm oil and DMSO. To prepare control vesicles, Span 60 (65 mg): cholesterol (58 mg): Solulan C24 (54 mg) at molar ratios of 1:1:0.22 with a mixture of TRF and distilled water (2 mL) was stirred at 60 °C for 1 hour. Three types of control vesicles were prepared, i.e. using TRF without solvent (10 mg) or 0.1 mL of TRF stock solution (100 mg/mL) in palm oil and DMSO, respectively. TRF-loaded control vesicles were then subjected to probe sonication for 2 × 2 minutes (Sonics Vibracell^{TM}).

Similar to procedures described in Dufès *et al.* (2000), transferrin was conjugated to control vesicles using an imidoester crosslinker, dimethylsuberimidate (DMSI). To 2 mL control vesicles, human holo-transferrin (3 mg/mL) and DMSI (6 mg/mL) was incubated with triethanolamine hydrochloride buffer pH 7.4 (2 mL) at room temperature for 2 hours.

Transferrin-bearing vesicles (Tf-vesicles) and control vesicles were then subjected to two cycles of ultracentrifugation to remove excess materials. Each centrifuge cycle was run at 40 000 rpm for 2 hours (Optima^{TM} L-100 XP Ultracentrifuge, Beckman Coulter UK Ltd.). Vesicles were dispersed in 2 mL phosphate-buffered saline (PBS) pH 7.4 for *in vitro* experiments or 5 % glucose solution for *in vivo* experiments.

2.2.4   Preparation of Targeted Span 60/TPGS Vesicles

2.2.4.1 Determination of maximum solubilisation of TRF in TPGS

TPGS solution was prepared in distilled water at concentrations of 1 mg/mL, 5 mg/mL and 100 mg/mL. TRF at various concentrations (1, 2, 3, 4, 5, 10 mg/mL) were added to TPGS solutions (1 mL) and probe sonicated for 2 minutes. The amount of TRF emulsified by TPGS solution was quantified with fluorescence measurement of TRF at $\lambda_{excitation}$ 295 nm and $\lambda_{emission}$ 325 nm upon dilution $\times$ 100 in distilled water.

2.2.4.2 Vesicle Preparation

Span 60/TPGS vesicles were prepared from a composition of Span 60, cholesterol, TPGS and dioleoyl-phophatidylethanolamine (DOPE). DOPE is an unsaturated phospholipid molecule having a terminal primary amine functional group. It was added to Span 60/TPGS formulation in order to facilitate the coupling of transferrin to vesicles via conjugation of terminal amine group with the imidoester group in DMSI. The molar ratio of Span 60, cholesterol and TPGS was maintained in a similar proportion as in Span 60/Solulan C24 vesicles, i.e. at molar ratio of 1:1:0.22. DOPE was then added at two molar ratios (0.1 and 0.05). Control vesicles encapsulating TRF were prepared by shaking Span 60, cholesterol, DOPE and TRF (emulsified at 5 mg/mL in TPGS solution containing 57 mg TPGS in 2 mL distilled water) for 1 hour at 60°C. Vesicles were formed upon probe sonication (Sonics Vibracell^{TM}) for 2×2 minutes with instrument set at 75% of its maximal capacity. Decoration of vesicles with transferrin was done with coupling method similar to Span 60/Solulan C24 vesicles, previously described by Dufès *et al.* (Dufès *et al.*, 2000). A volume of vesicles (2 mL) were mixed with cross-linker dimethylsuberimidate (DMSI) and holo-transferrin in 0.2 M triethanolamine buffer (2 mL), pH 7.4 for 2 hours at room temperature. All vesicles were purified with 2 cycles of ultracentrifugation (40 000 rpm $\times$ 2 hours), and dispersed in 2 mL PBS (pH 7.4) for *in vitro* experiments or 5 % glucose solution for *in vivo* experiments.

2.2.5 Transmission Electron Microscopy

Tf-vesicles and control vesicles were visualized under transmission electron microscopy (TEM) to confirm the formation of vesicles. Vesicles were diluted to

1:100 in PBS before imaging. A drop of each sample was applied to a pre-coated (carbon support film) copper grid. Excess liquid was blotted off with filter paper prior to negative staining using 1 % w/v uranylformate. TEM images were then captured with LEO 912 energy filtering electron microscope at voltage 80 kV.

2.2.6 Encapsulation Efficiency

The amount of TRF entrapped in Tf-vesicles and control vesicles was quantified upon vesicle disruption with isopropanol. Vesicles were then diluted to 1:100 in isopropanol for measurement. TRF-derived fluorescence was measured in triplicates at excitation wavelength of 295 nm and emission wavelength of 325 nm. Fluorescence intensity obtained was subsequently correlated with TRF calibration curve acquired in section 2.2.2. Encapsulation efficiency was calculated as the percentage of TRF encapsulated in vesicles compared to the initial amount of TRF added:

$$\rule{3cm}{0.4pt}$$

2.2.7 Transferrin Conjugation Efficiency

The amount of transferrin grafted to vesicles was determined by Lowry Assay as previously described (Dufès *et al.*, 2000). Span 60/Solulan C24 and Span 60/TPGS vesicles were prepared as described in section 2.2.3 and section 2.2.4.2 respectively. In order to avoid possible interference from TRF, blank vesicles were used in this assay. As such, TRF was replaced with distilled water for both vesicle formulations.

For Lowry assay, 50 mL of 2 % w/v sodium carbonate solution was first prepared in 0.1 M sodium hydroxide. To this sodium carbonate solution, 1 mL of sodium potassium tartrate 2 % w/v and 1 mL cupric sulphate 1 % w/v was added to make up solution A. Two solutions were prepared, a 100 µL of vesicle suspension (diluted 1:100 in PBS) as well as a transferrin standard solution (concentration ranging from 0 to 500 µg/mL) to which 1 mL of solution A was added to both of them. After 10 minutes incubation, 100 µL of diluted Folin Ciocalteu's reagent (1:1 in distilled water) was added to each sample and incubated for another 30 minutes. The UV absorbance of each sample was determined at a wavelength of 750 nm (50 Bio UV-Visible Spectrophotometer), using blank vesicles as zero reference. The amount of transferrin conjugated to vesicle surface was calculated by correlation using the transferrin standard curve. The measurements were determined in triplicate. The coupling efficiency of transferrin was calculated as the percentage of transferrin conjugated to vesicles compared to the initial amount of transferrin added:

2.2.8 Stability of TRF encapsulation after storage at 4 ^{o}C

At days 0, 4, 7, 14, 21 and 30, Span 60/TPGS vesicles stored at 4 ^{o}C were centrifuged at 40 000 rpm for 2 hours. Vesicles pellet were redispersed in PBS where TRF-derived fluorescence was measured at $\lambda_{excitation}$ 295 nm and $\lambda_{emission}$ 325 nm upon vesicle disruption with isopropanol at dilution 1:100. The amount of TRF in vesicles was correlated against TRF standard curve obtained in section 2.2.2.

2.2.9 Size and Zeta Potential Measurement

Using photon correlation spectroscopy, vesicle samples were first prepared at dilution 1:100 in distilled water (3 mL). Samples were then transferred to a capillary cell and measurements were performed using a Malvern Zetasizer Nano series Nano-ZS (Malvern Instruments, Malvern UK) equilibrated at room temperature (25 ^{o}C).

2.2.10 Statistical Analysis

All values were expressed as means ± standard error. Statistical significance was determined by one-way ANOVA or Student's *t*-test as appropriate (GraphPad Prism Software). A difference of *p*-values < 0.05 was considered statistically significant.

2.3 RESULTS

2.3.1 TRF Quantification

In previous reports, tocotrienol was shown to fluoresce with excitation peak occurring at wavelengths within the range of 295-297 nm; emission wavelengths within the range of 325-330 nm (Katsanidis and Addis, 1999; Yap *et al.*, 1999; Nesaretnam *et al.*, 2004; Puah *et al.*, 2006; Nesaretnam *et al.*, 2007). The peak of fluorescence scan with TRF showed close agreement with previous literature findings, with excitation wavelength occurring at 295-297 nm (Figure 2.9A) and emission wavelength occurring at 325-330 nm (Figure 2.9B). Therefore, further quantification of TRF was performed at $\lambda_{excitation}$ 295 nm and $\lambda_{emission}$ 325 nm.

2.3.2 Vesicle Preparation

For Span 60/Solulan C24 vesicles, TRF-loaded vesicles were successfully prepared using a molar ratio of 1:1:0.22 for Span 60: Cholesterol: Solulan C24 as previous described (Uchegbu *et al.*, 1995). Formation of vesicles was confirmed using transmission electron microscopy (Figure 2.10). Small unilamellar vesicles within submicron range were observed for both control vesicles and Tf-vesicles. The morphology of Tf-vesicles was not significantly different from control vesicles despite the presence of transferrin, although negative staining at the periphery of vesicles was seen more intense in transferrin-bearing vesicles.
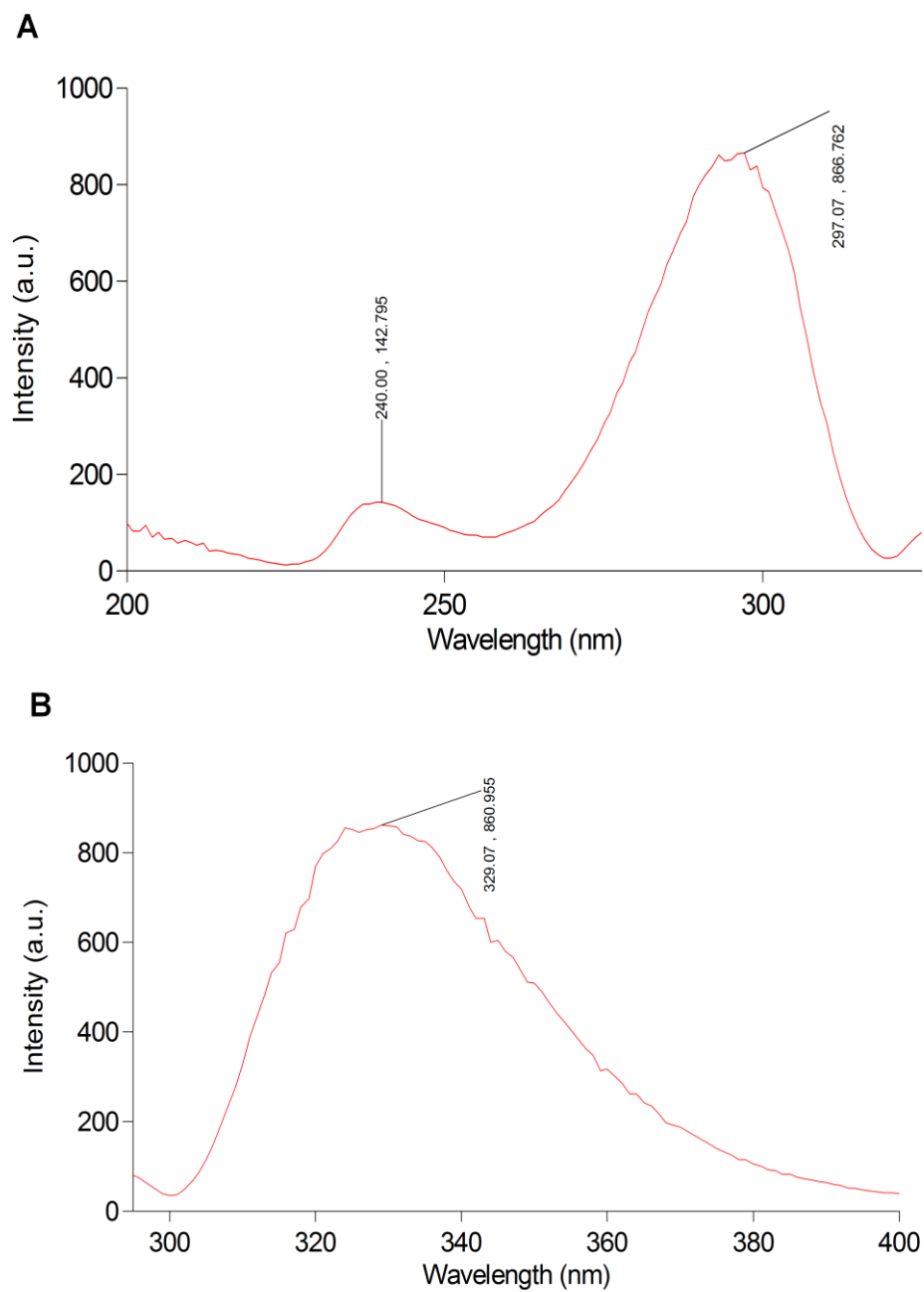
Figure 2.9: Excitation wavelength (A) and emission wavelength (B) obtained using fluorescence scan with TRF solution, prepared at 20 µg/mL using DMSO solvent.

A
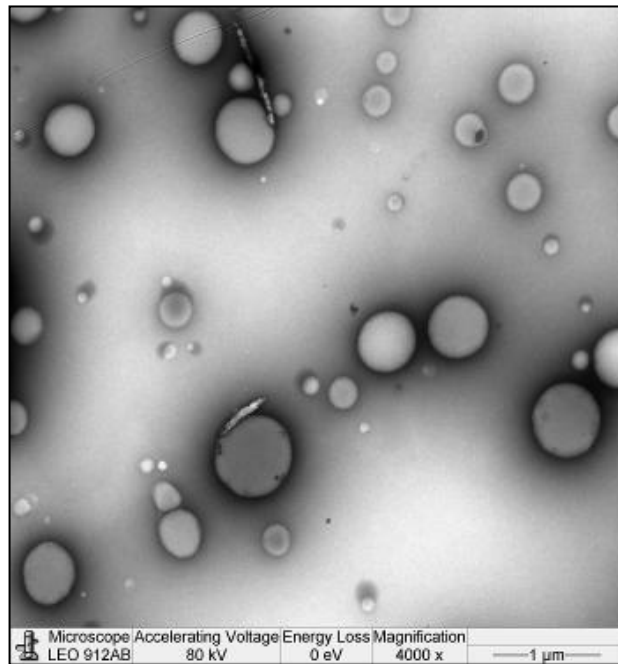
B
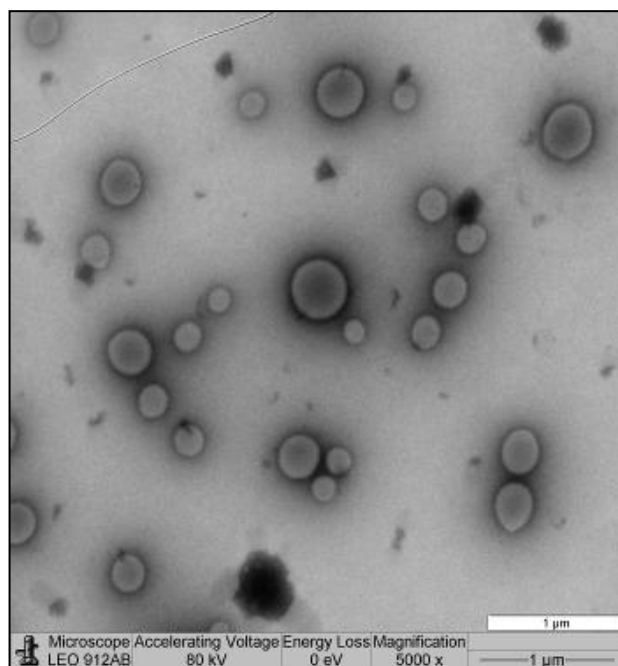
Figure 2.10: Transmission electron micrographs confirming the formation of Span 60/Solulan C24 vesicles. A: Tf-vesicles, B: Control vesicles. (Bar: 1 μm)

For Span 60/TPGS vesicles, the capacity of TPGS to emulsify TRF was first determined. Upon sonication, TRF formed stable emulsions in TPGS solutions of 1, 5 and 100 mg/mL. The amount of TRF-derived fluorescence increased with increasing TRF until a point where the fluorescence absorbance started to plateau at 4 mg/mL TRF (Figure 2.11). Further increase in TRF concentration above 5 mg/mL did not incur significant changes in fluorescence absorbance. These data suggested an optimal TRF concentration of 5 mg/mL for preparation of Span 60/TPGS vesicles in order to achieve optimum encapsulation of TRF. Upon successful preparation, TEM images in Figure 2.12 revealed a homogenous distribution of Span 60/TPGS vesicles, conferring to a spherical multilamellar structure.
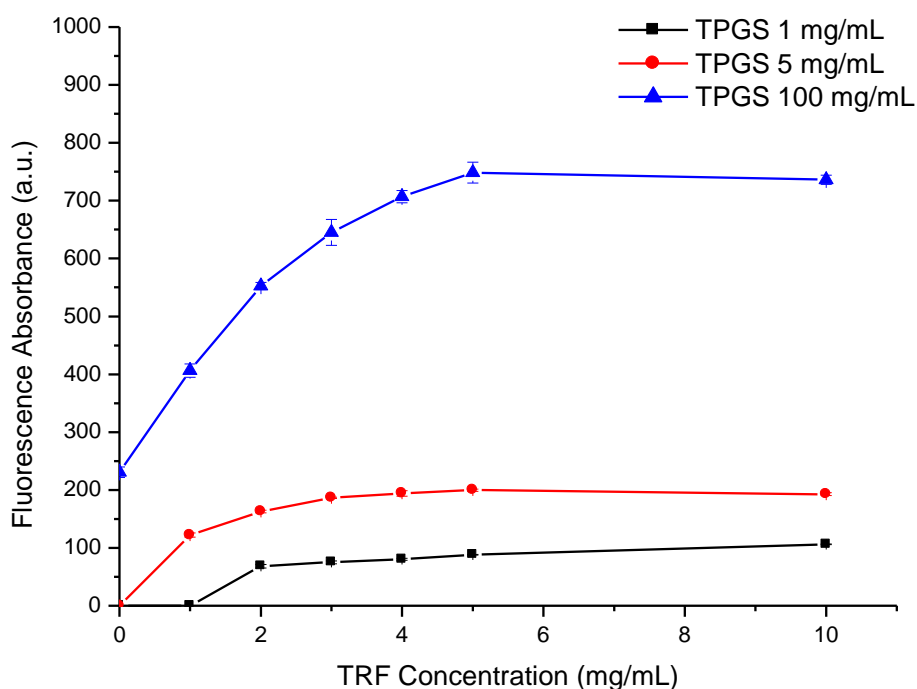
Figure 2.11: Concentration curve of TRF emulsified in TPGS solutions at 1, 5 and 100 mg/mL (n = 3).

A
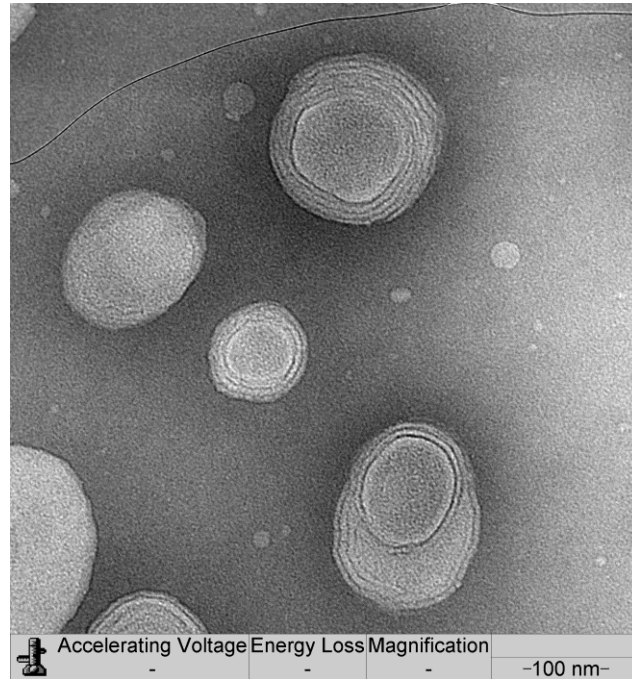
B
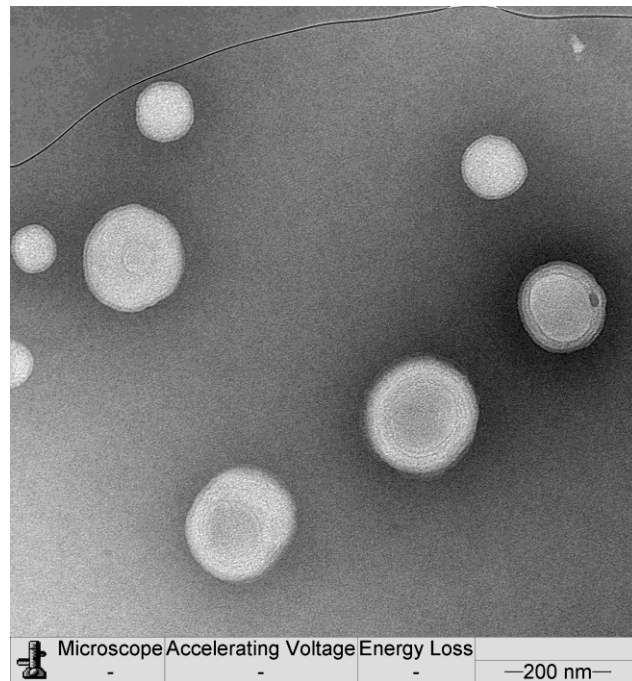
Figure 2.12: Transmission electron micrograph of Span 60/TPGS vesicles prepared from a composition of Span 60, cholesterol and TPGS at molar ratios 1 : 1 : 0.22. A: Tf-vesicles, B: Control vesicles.

2.3.3 Conjugation of Transferrin

For Span 60/Solulan C24 vesicles, the amount of transferrin remained with Tf-vesicles after centrifugation was determined from the transferrin standard curve obtained using Lowry assay. From the transferrin standard curve ranging from 0-500 µg/mL (R value: 0.994), the coupling efficiency of transferrin with Span 60/Solulan C24 vesicles was determined to be at a rate of 89 ± 5 %.

However, when similar technique was applied to prepare transferrin-bearing Span 60/TPGS vesicles, a mere coupling efficiency of 3.2 ± 0.5 % was obtained. Both TPGS and Solulan C24 are long chain hydrophilic polymers used to coat the surface of vesicles to prevent rapid clearance from the RES. As shown in TEM images, preparation of vesicles using TPGS instead of Solulan C24 imparted a significant impact on the vesicle morphology. Hence, we hypothesize that the decrease in transferrin conjugation in Span 60/TPGS vesicles was most probably due to excessive shielding of vesicle functional group by TPGS for transferrin attachment. Subsequently, a decrease in available functional group might have contributed to the lower transferrin conjugation efficiency in Span 60/TPGS vesicles compared to that of Span 60/Solulan C24 vesicles. Therefore, dioleoyl-phosphatidylethanolamine (DOPE) as a lipid molecule bearing terminal amine functional group was incorporated to the formulation in the hope to facilitate transferrin attachment. A DOPE/Span 60 molar ratio of 0.05 or 0.1 was investigated. At a molar ratio of 0.05 DOPE, transferrin coupling efficiency was increased from 3.2 ± 0.5 % to 47.5 ± 2.5 %. Following a 15-fold improvement in transferrin conjugation via addition of DOPE, enhanced transferrin conjugation would be anticipated with increasing DOPE

(from 0.05 to 0.1 molar ratios) but it was proven otherwise. In fact, addition of 0.1 molar ratio DOPE led to an ineffective 8.3 ± 2.2 % transferrin coupling efficiency. A possible reason might be the perturbation of hydrophilic-lipophilic balance or the critical packing parameter (described in Chapter 1) of vesicles forming surfactants, induced by the addition of DOPE at high concentration. This might have led to early deformation of vesicles, or a disruption of vesicle integrity, causing a drastic drop in the amount of transferrin able to be linked to the vesicle periphery. In such case, we conclude that further preparation of Span 60/TPGS vesicles will be formulated according to the composition of molar ratios of 1:1:0.22:0.05 for Span 60/cholesterol/TPGS/DOPE respectively. When examined under the microscope, incorporation of DOPE in Span 60/TPGS vesicles did not change the vesicle morphology (Figure 2.13).

A

Accelerating Voltage | Energy Loss | Magnification
- | - | -
—100 nm—

B

Accelerating Voltage | Energy Loss | Magnification
- | - | -
—100 nm—
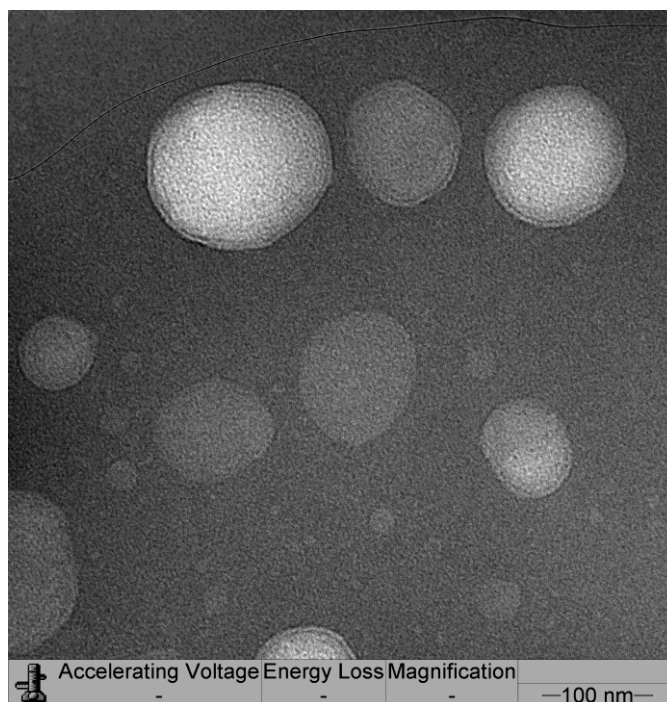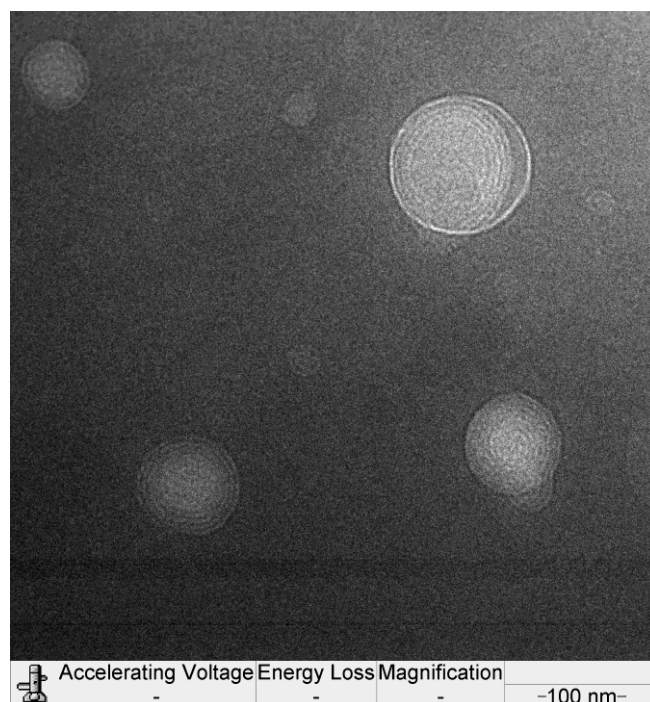
Figure 2.13: Transmission electron micrograph of Span 60/TPGS vesicles prepared from a composition of Span 60, cholesterol, TPGS and DOPE at molar ratios 1 : 1 : 0.22 : 0.05. A: Tf-vesicles, B: Control vesicles.

To further improve the transferrin coupling efficiency, increasing amount of transferrin and DMSI was investigated in the coupling process. Table 2.1 is a summary of the obtained coupling efficiency. Increasing transferrin concentration to vesicle formulation led to a decrease in conjugation efficiency. This is not surprising as the initial amount of transferrin has varied from previous method. Here, expressing transferrin conjugation in relation to coupling efficiency was no longer an accurate parameter to justify the targeting efficiency of these formulations. Instead, the total amount of transferrin attached to vesicles at mg/mL was used as a measurement. When equal amount of transferrin was added (F3 and F4), increasing DMSI did not lead to a significant difference in the total amount of transferrin attached. According to manufacturer's instruction, the concentration of DMSI was suggested to be 10-fold molar in excess to protein at protein concentration above 5 mg/mL and 20- to 30-fold molar excess at protein concentration below 5 mg/mL (Thermo Fisher Scientific Inc., 2009). Therefore, in our case, as DMSI was added at molar excess at least 30-fold to transferrin, increasing its concentration above 12 mg/mL was rather excessive. However, at constant amount of DMSI, increasing transferrin concentration led to a proportional increase in the total amount of transferrin grafted on vesicles. Summarizing from table 2.1, Formulations 3 and 5 which demonstrated most favourable transferrin-vesicle coupling efficacy, were chosen for further investigation.

Table 2.1: Transferrin conjugation efficiency in Span 60/TPGS vesicles obtained using various combinations of transferrin and DMSI concentration.

Formulation	Transferrin Concentration (mg/mL)	DMSI Concentration (mg/mL)	Conjugation Efficiency (%)	Amount of transferrin attached to vesicles (mg/mL)
F1	3	6	47.5 ± 2.5	1.41 ± 0.15
F2	6	6	30.5 ± 2.9	1.83 ± 0.17
F3	**12**	**6**	**25.7 ± 2.5**	**3.08 ± 0.30**
F4	12	12	25.3 ± 1.3	3.03 ± 0.15
F5	**24**	**12**	**16.8 ± 0.5**	**4.04 ± 0.11**

2.3.4 Encapsulation Efficiency

To measure the encapsulation efficiency, vesicles were first disrupted with isopropanol followed by fluorescence quantification using wavelength specified in section 2.3.1. The actual amount of TRF encapsulated in vesicles was calculataed by correlating to TRF standard curves. Figure 2.14 was the TRF standard curve obtained using TRF/DMSO stock solution diluted in isopropanol to a final TRF concentration between 0-25 µg/mL. Fluorescence intensity was linearly correlated with TRF concentration with an R value of 0.993. TRF standard curve for Span 60/TPGS was also shown in Figure 2.15 using TRF/TPGS stock solution diluted in isopropanol to a final TRF concentration ranging from 0 to 20 µg/mL. A linear correlation between fluorescence intensity and TRF concentration was demonstrated with an R value of 0.999.
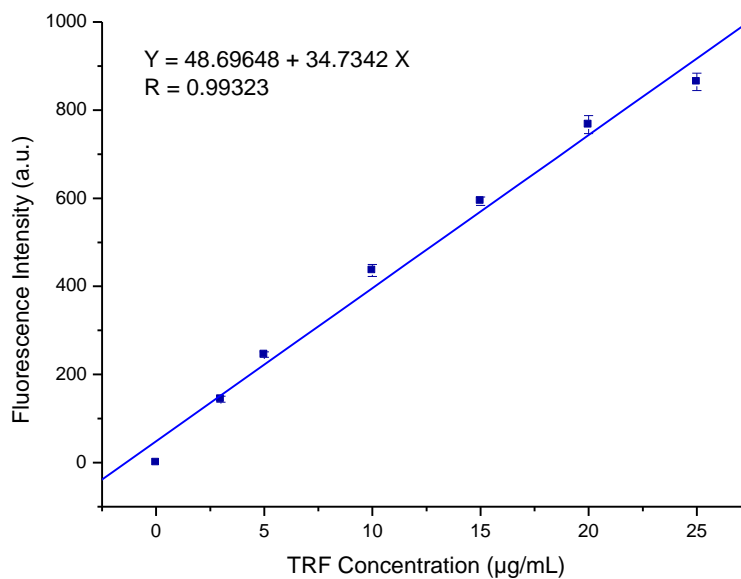
Figure 2.14: Standard curve of TRF for quantitative measurements of Span 60/Solulan C24 vesicles. Fluorescence intensity in arbitrary unit (a.u.) was obtained upon serial dilution of TRF stock solution (100 mg/mL) in isopropanol which was done in triplicate.
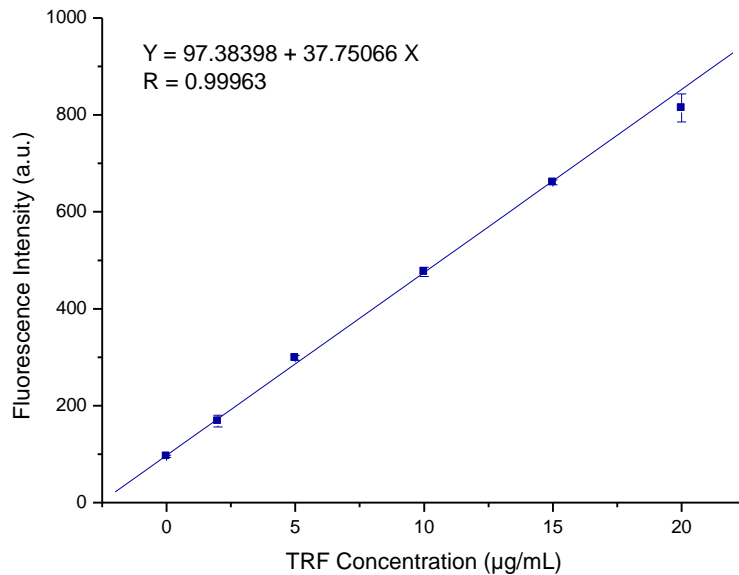
Figure 2.15: Standard curve of TRF for quantitative measurements of Span 60/TPGS vesicles. Fluorescence intensity in arbitrary unit (a.u.) was obtained upon serial dilution of TRF stock solution (5 mg/mL) in isopropanol which was done in triplicate.

For tocotrienol-loaded vesicles, encapsulation efficiency of the vesicles was determined using fluorescence spectrophotometry by correlating to the standard calibration curve obtained from Figure 2.14 for Span 60/Solulan C24 vesicles and Figure 2.15 for Span 60/TPGS vesicles. For Span 60/Solulan C24 formulation, three types of vesicles were prepared, i.e. using TRF only or using stock solutions of TRF dissolved in palm oil and DMSO. As shown in Figure 2.16, the encapsulation efficiency of vesicles prepared using TRF/DMSO was significantly higher (31.5 ± 0.9 %) compared to TRF/Palm oil (23.4 ± 0.5 %) and TRF only (9.4 ± 0.8 %). Therefore, among the three types of Span 60/Solulan C24 vesicles prepared, TRF/DMSO vesicle formulation was chosen as the focus of our study, which will be further investigated *in vitro* and *in vivo*.
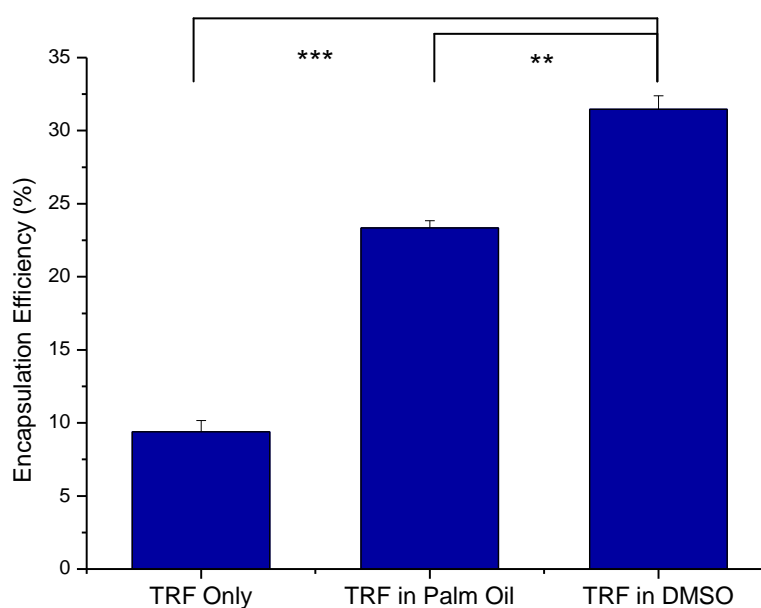
Figure 2.16: Encapsulation efficiency of Span 60/Solulan C24 vesicles prepared using TRF only, TRF dissolved in palm oil and TRF dissolved in DMSO (**: $p < 0.01$, ***: $p < 0.001$).

As for Span 60/TPGS vesicles, Formulations 3 and 5 were prepared with 5 mg/mL TRF solution, according to the preliminary data obtained from transferrin conjugation study. The encapsulation efficiencies of Formulations 3 and 5 were measured at a level of 48.6 ± 1.7 % and 19.8 ± 1.4 % respectively (Figure 2.17). Surprisingly, while conjugated to transferrin with highest efficiency, the encapsulation efficiency of Formulation 5 was 2.5-fold lower compared to Formulation 3. As Formulation 5 was prepared with a very high concentration of transferrin (24 mg/mL) with a conjugated efficiency of about 4 mg transferrin per mL vesicles, its low encapsulation efficiency was most probably closely related to the vesicle permeability. High protein concentration might have incurred substantial perturbation to vesicle bilayer, thus disrupting the vesicle's bilayer integrity which affects the bilayer permeability. Therefore, due to low TRF encapsulation associated with Formulation 5, the focus of study in Span 60/TPGS vesicles were shifted towards Formulation 3, which demonstrated optimum physicochemical properties among the vesicle formulations. Collectively, Span 60/TPGS vesicles prepared for further biological studies were composed of Span 60/cholesterol/TPGS/DOPE with molar ratio 1:1:0.22:0.05 at TRF concentration 5 mg/mL. Transferrin-bearing vesicles will be synthesized at transferrin concentration 12 mg/mL associated with DMSI as a linker at a concentration of 6 mg/mL.
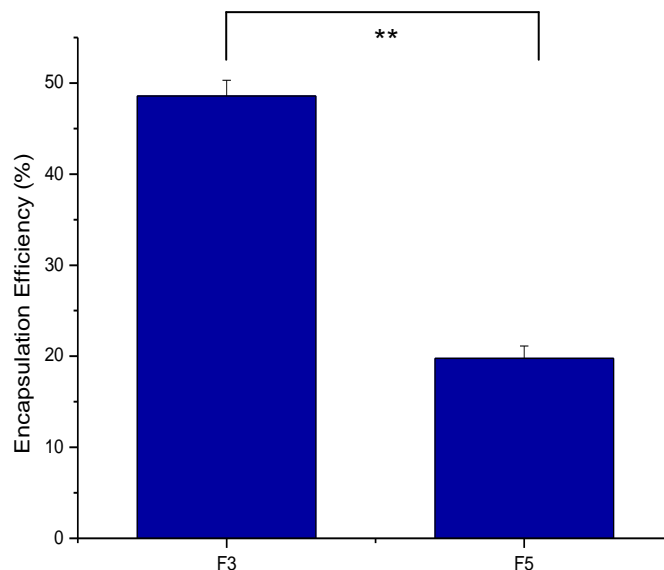
Figure 2.17: Encapsulation efficiency of Formulation 3 and Formulation 5 of Span 60/TPGS vesicles, prepared with 5 mg/mL TRF *(**: p < 0.01)*

2.3.5 Stability of TRF encapsulation after storage at 4 $^{\circ}$C

The stability of TRF encapsulation in Span 60/TPGS vesicles was quantified in order to give a general idea of possible TRF leakage during vesicle storage at 4 $^{\circ}$C (Figure 2.18). At day 7, about 10 to 15 % of TRF was release from Tf-vesicles and control vesicles. Apart from the burst release within the first 7 days, a sustained release was observed over the next 3 weeks. An average release rate of less than 1 % per day was recorded for both Tf-vesicles and control vesicles. At day 30, the amount of TRF retained in the vesicles was not significantly different (*p*-value = 0.2287) between control and Tf-vesicles: up to 33.3 ± 4.9 % and 23.8 ± 4.5 % of TRF was released from control vesicles and Tf-vesicles respectively.
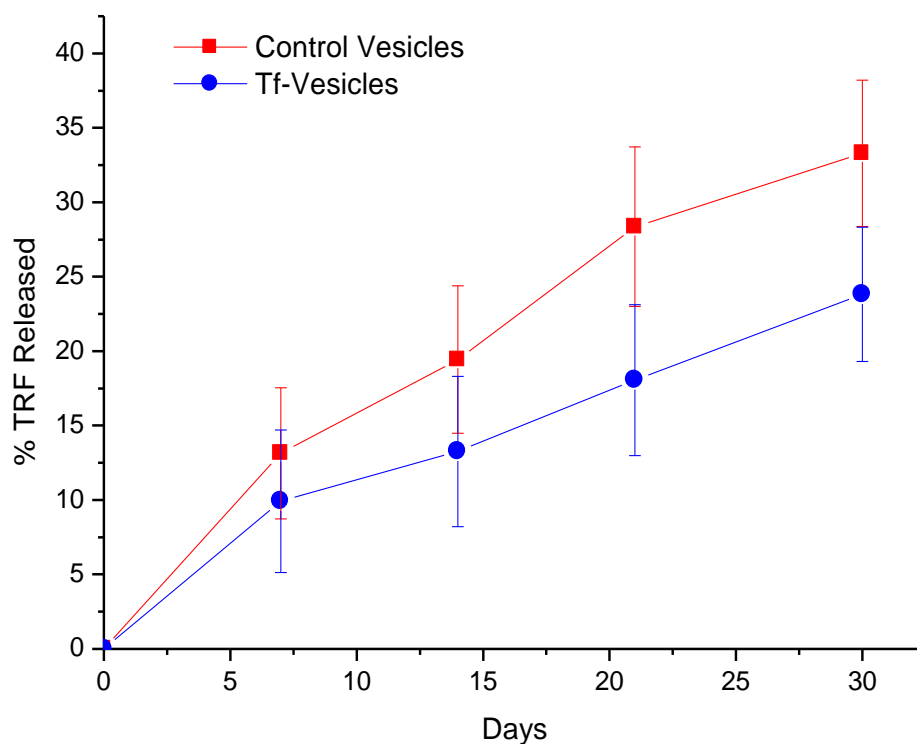
Figure 2.18: Percentage of TRF released from Span 60/TPGS vesicles stored at 4 $^{\circ}$C over 30 days which was measured in triplicate.

2.3.6 Size and Zeta Potential

Photon correlation spectroscopy is the most common and accurate technique to measure size and zeta potential of colloidal drug delivery systems to date. The average sizes measured for Span 60/Solulan C24 and Span 60/TPGS vesicles were within the range of 100 to 200 nm, except for Tf-vesicles of Span 60/TPGS vesicles. Tables 2.2 summarized the parameters associated with size and zeta potential measured using photon correlation spectroscopy Nanosizer system. Despite the difference in average diameter between the control and Tf-vesicles of Span 60/TPGS formulations, their maximum peaks were found to be similar at 160 nm. Polydispersity index (PDI) is an estimate of the width of size distribution (Malvern

Instruments Ltd., 2005). It was found to be less than 0.4 for all formulations prepared. As for their respective surface charges, all vesicles were shown to be negatively charged with zeta potential measured at a magnitude higher than -30 mV.

Table 2.2: Size and zeta potential measurements for Span 60/Solulan C24 and Span 60/TPGS vesicles.

	Average Diameter (nm)	Maximum Peak (nm)	Polydispersity Index	Zeta Potential (mV)
Span 60/Solulan C24 Vesicles				
Control Vesicles	154 ± 30	128 ± 13	0.285 ± 0.13	-40.1 ± 0.7
Tf-Vesicles	147 ± 9	144 ± 9	0.276 ± 0.11	-43.3 ± 0.9
Span 60/TPGS Vesicles				
Control Vesicles	184 ± 7	163 ± 7	0.368 ± 0.04	-48.9 ± 0.03
Tf-Vesicles	341 ± 11	160 ± 2	0.377 ± 0.01	-50.4 ± 0.88

2.4   DISCUSSION

Over the past decade, increasing interest in tocotrienol research helped to clarify the traditional understanding of vitamin E. Instead of directly correlating vitamin E to α-tocopherol, it is now widely accepted that vitamin E is a mixture of four tocopherol isoforms and four tocotrienol isoforms. Tocotrienol, although proven to have significant potential as an anti-cancer therapeutic, administration via the oral route has been the only route of administration studied to date. However, the efficacy of tocotrienol by oral administration is drastically hampered by its poor absorption. It has been shown that the absorption of tocotrienol via the gastrointestinal tract is generally incomplete and highly dependent on food intake (Cohn *et al.*, 2010). The absorption of vitamin E from the intestine is similar to mechanisms involved in the transport of other lipid molecules *in vivo*, essentially depending on emulsification (Iqbal and Hussain, 2009). Emulsification of lipids is crucial for lipid absorption because only very small particles are able to diffuse in substantial amount across the mucosa layer in order to reach the enterocytes (Cohn *et al.*, 1991). As illustrated in Figure 2.19, bile salts and pancreatic enzymes are the rate limiting substances in the process of emulsification. They have the ability to form micelles with large fat droplets, breaking the lipids into smaller micelles that are more readily absorbed through the enterocytes (Bjorneboe *et al.*, 1990; Cohn *et al.*, 1991). Micellar solubilisation by bile salts increases the lipid solubility and surface area, leading to enhanced rate of lipid dissolution thus improving lipid absorption (Charman *et al.*, 1997). Nevertheless, the production and secretion of bile salts are often very much dependant on food intake (Lindholm *et al.*, 1990). Previous studies suggested that the bile micelle concentration is 5-fold higher in the fed state than the fasted state

(Sugano *et al.*, 2010). In addition, bile secretion varies in response to food matrix as the presence of lipid and lipid digestion products helps to stimulate the secretion of bile salts (Charman *et al.*, 1997). It follows, therefore that vitamin E absorption is dependent on the amount and composition of fats eaten concurrently (Cohn *et al.*, 1992). Using R-tocopheryl nicotinate as a model for vitamin E, its bioavailability was improved by 28-fold when administered in the fed state compared to the fasted state (Charman *et al.*, 1997). Roxborough *et al* also reported in 2000 that a significant inter-individual variation in vitamin E absorption was observed, ranging from 20% to 80% (Roxborough *et al.*, 2000). Such poor and erratic bioavailability suggested that a controlled delivery system is needed to improve the efficacy of tocotrienol, for it to be delivered to the tumours at substantial amount. Here, we hypothesize that administration of tocotrienol via intravenous route should effectively bypass the problems associated with bioavailability. In addition, intravenous administration of tocotrienol also helps to increase the plasma concentration of tocotrienol available for tissue distribution upon sufficient circumvention from the intestinal absorption factor. However, due to its highly lipophilic characteristics, intravenous administration of tocotrienol would not be possible without a suitable delivery system that could accommodate lipophilic tocotrienol and yet dispersible or soluble in aqueous media.
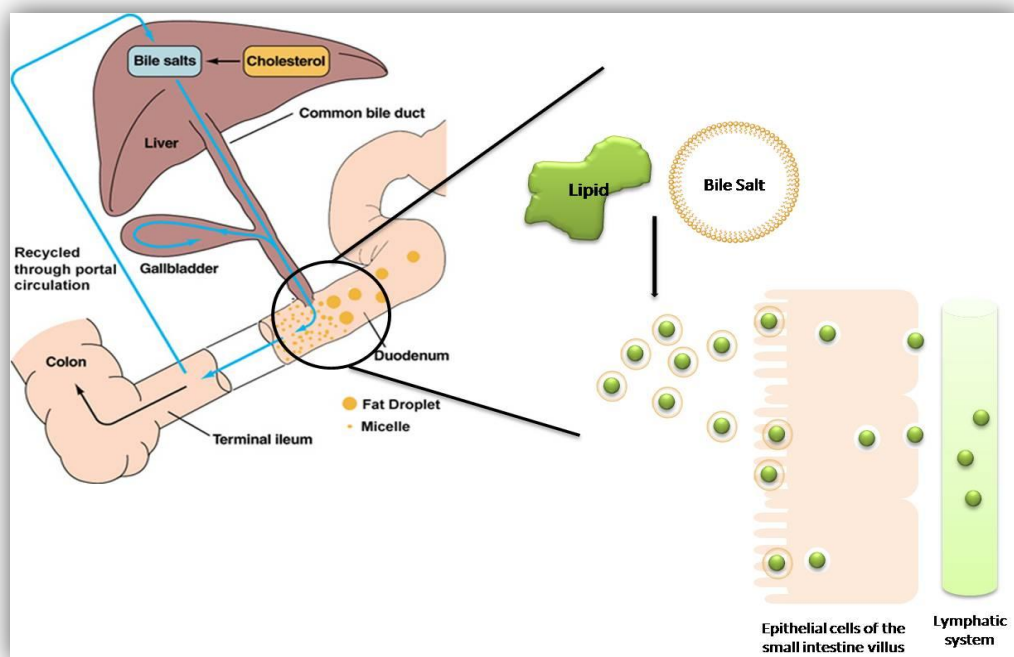
Figure 2.19: Lipid transport in the villus of the small intestine and the role of bile salts in lipid absorption *(Modified from http://www.colorado.edu)*.

In aqueous media, Span 60 amphiphiles are prone to form vesicular systems in order to reduce the high energy interaction between the hydrophobic portion while maximizing the interaction between the hydrophilic head group and the aqueous disperse phase (Uchegbu and Schätzlein, 2006). Figure 2.20 is the schematic illustration of vesicle formation for Span 60/Solulan C24 vesicles and Span 60/TPGS vesicles. Upon heating above the phase transition temperature, Span 60 forms bilayer in the liquid crystalline state incorporating TRF in the hydrophobic portion. As lipid bilayer self assembly is rarely spontaneous, input of energy is often required (Lasic, 1991). In this regard, probe sonication is a good source of energy in addition to the advantage of controlling vesicle size distribution. The sonication method for preparation of niosomes was first introduced by Baillie *et al.* (1985) and has been used as a delivery system for the anti-leishmanial drug, sodium stiobogluconate. In

this study, a fairly homogeneous suspension of vesicles was formed. Upon purification using ultracentrifugation to remove excess raw materials, Span 60/Solulan C24 vesicles measured a size distribution of approximately 150 nm while Span 60/TPGS vesicles measured a size distribution of approximately 160 nm.
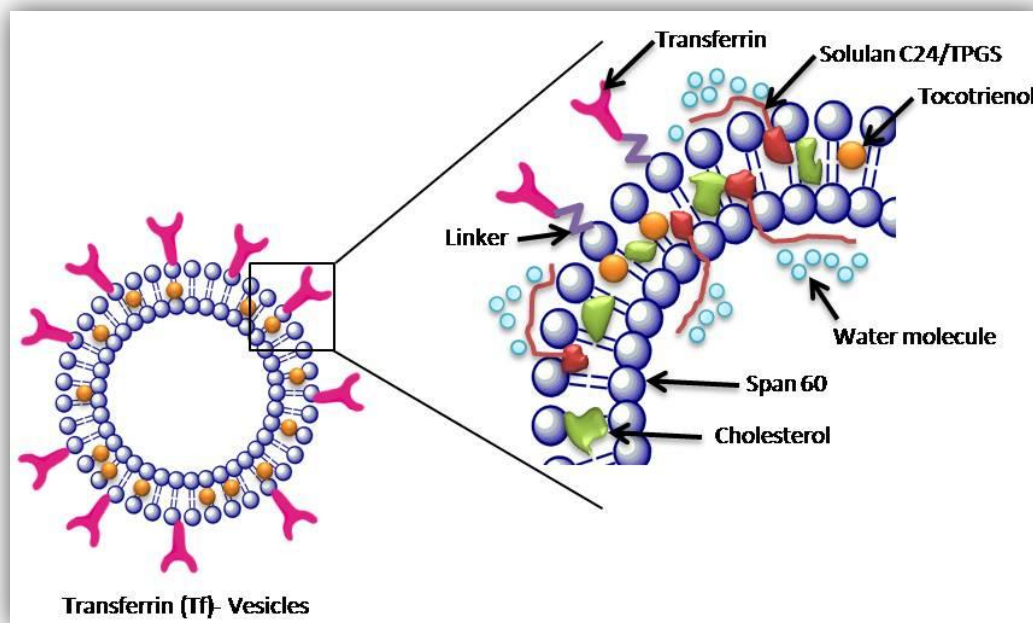
Figure 2.20: Schematic representation of Span 60/Solulan C24 vesicles and Span 60/TPGS vesicles.

In close agreement to the ternary phase diagram proposed by Uchegbu and Vyas (1998) using hexadecyl diglycerol-cholesterol-Solulan C24 vesicle system, at hexadecyl diglycerol/cholesterol/Solulan C24 molar ratio of 45:45:10, spherical niosomes within 10 μm were formed (Figure 2.21). Due to the lipophilicity and viscosity of TRF, TRF alone formed unstable emulsions when mixed in aqueous phase during vesicle preparation. This has vast consequences on the preparation process which contributed to the low encapsulation efficiency. On the other hand, palm oil was previously used as a media for oral delivery of TRF to tumour-bearing mice models (Nesaretnam *et al.*, 2004) while DMSO was used to dissolve TRF prior

to *in vitro* assays (Srivastava and Gupta, 2006). During vesicle preparation, both palm oil and DMSO enhanced the encapsulation efficiency of TRF to at least 2-fold compared to using TRF alone. Of the three types of control vesicles prepared, DMSO was found to be the best solvent to dissolve TRF in order to prepare vesicles with high encapsulation efficiencies. Compared to TRF without solvent or dissolved in palm oil, TRF dissolved in DMSO enabled high accuracy for volume measurement while demonstrating the highest encapsulation efficiency for TRF. Therefore, subsequent study on Span 60/Solulan C24 vesicles was focused on formulations prepared with stock solution of TRF dissolved in DMSO. After successful preparation of TRF-loaded control vesicles, transferrin-bearing vesicles (Tf-vesicles) were synthesized using method adopted from Dufès *et al.* in 2000. At a conjugation efficiency of 89 ± 5 %, it corresponds to an improvement compared to the previously reported 50 % (Dufès *et al.*, 2000).
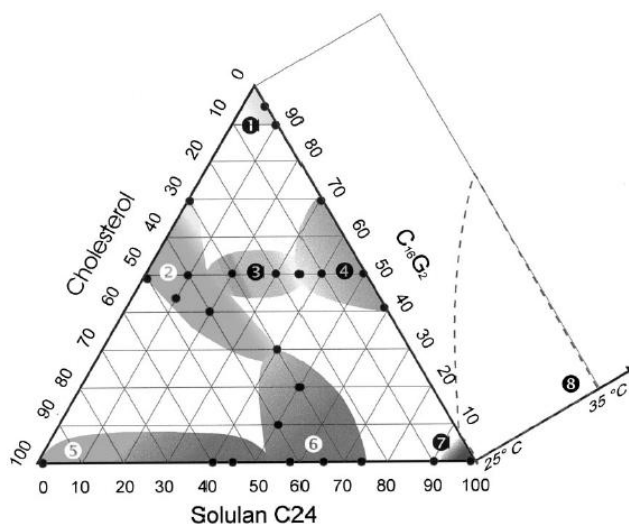
Figure 2.21: Ternary phase diagram in molar ratios of hexadecyl diglycerol:cholesterol:Solulan C24. Region (1): polyhedral niosome, region (2): spherical, helical and tubular niosomes, region (3): discomes, large niosomes, region (4): discomes and mixed micelles, region (5): cholesterol crystals, region (6) spherical niosomes, region (7): clear liquid possibly mixed micelles, (8) mixed micelles formed on elevation of temperature *(Adapted from Uchegbu and Vyas, 1998).*

For Span 60/TPGS vesicle formulation, spherical multilamellar vesicles (MLV) within a size range of 100-200 nm were formed. The multilamellar structure has several advantages: 1) enhanced encapsulation efficiency of hydrophobic drug due to the increase in number of lipid bilayer; 2) a controlled release of drugs encapsulated in the vesicles depending on the microstructure of lamellar layers; 3) improved structural rigidity of the vesicles due to the densely packed multiple layer structure, hence more stable against vesicle deformation. While hydrophilic drugs are most efficiently loaded in small unilamellar vesicles due to the large enclosed aqueous compartment, multilamellar vesicles are more capable of loading a hydrophobic drug. This has been shown previously with steroids and acetazolamide that hydrophobic molecules are readily incorporated in the multiple bilayers of lipid membranes in multilamellar vesicles (Brown *et al.*, 1995; Guinedi *et al.*, 2005). Therefore in Span 60/TPGS vesicles, encapsulation efficiency was more than 15 % higher than the amount of TRF entrapped in Span 60/Solulan C24 vesicles. In terms of vesicle stability, Span 60/Solulan C24 vesicles have been subjected to stability test with previous study using model drug doxorubicin-polymer conjugate, quantified over 28 days of storage at 4 ^{o}C (Gianasi *et al.*, 1997). Therefore results from Gianasi *et al.* were adopted to compare against the storage stability of Span 60/TPGS vesicles. In fact, Span 60/Solulan C24 vesicle has a fairly different release profile compared to Span 60/TPGS vesicles. With Span 60/Solulan C24 vesicles, an initial 25 % drop in the level of drug entrapped was observed within the first 24 hours (Gianasi *et al.*, 1997). On the contrary, the initial burst release was significantly lower in vesicles prepared from TPGS (less than 5 %). Although the amount of drug retained at Day 28 was approximately 75 % for both Span 60/Solulan C24 (Gianasi *et al.*, 1997) and

Span 60/TPGS vesicles (Figure 2.18), the release profile of Span 60/TPGS occupied a sustained release model, i.e. at a rate of less than 1 % TRF released per day. The closest explanation for the variation in release pattern could be attributed the structural resemblance of Span 60/TPGS vesicles to multilamellar vesicles whereas small unilamellar vesicles were obtained with Span 60/Solulan C24 vesicles. In unilamellar vesicles, the rate of tocotrienol release was largely dependent on the permeability of lipid bilayers; whereas in Span 60/TPGS vesicles, a sustained release of tocotrienol from the multiple bilayers was observed. As tocotrienol was most likely to be incorporated in the multiple bilayers in Span 60/TPGS vesicles, leakage of tocotrienol from inner bilayers was effectively protected from outer bilayers. Upon sequential destabilization of outer bilayers, the contents of inner bilayers were released in a controlled rate. Hence, a sustained release profile with Span 60/TPGS vesicles would be exceptionally advantageous in cases where adequate therapeutic doses are required for extended duration in order to achieve optimum therapeutic activity.

Multilamellar vesicles are usually prepared using film hydration method (Crommelin and Schreier, 1994) or a sheer induced transition method (Medronho *et al.*, 2008). With hydration method, multilamellar vesicles were produced upon hydration of thin lipid films deposited from an organic solvent (Crommelin and Schreier, 1994). Sheer induced transition method on the other hand, was used to produce multilamellar vesicles by applying a sheer flow at a certain sheer rate on stacks of long-range bilayers (Medronho *et al.*, 2008). In our study, it was unclear how Span 60/TPGS vesicles formed vesicles of multiple bilayers as they were

prepared using a similar method to Span 60/Solulan C24 vesicles. In the study of Zou *et al.* (2007), bilayers in a multilamellar system were usually formed as a result of balanced attractive forces and long-ranged repulsive forces between the surfactants to stabilize against vesicle deformation. To this end, many have used polyelectrolytes (charged polymers) to induce bilayer attractive forces in order to form stable MLVs (Robertson *et al.*, 2004; Vivares *et al.*, 2005). In a recent study, Kepczynski *et al.* (2010) attached fatty acid esters (that were subsequently hydrolyzed to cationic carboxyl groups) to anionic surfactant vesicles and successfully synthesized densely packed MLVs with reasonable stability. This phenomenon was most probably occurring in Span 60/TPGS vesicles as well. Ester groups in TPGS might have been hydrolysed via a similar mechanism, resulting in an elevated attractive force between Span 60 headgroups and TPGS. As a consequence, resultant attractive forces increased the interaction between Span 60 bilayers, leading to spontaneous assembly of a multilamellar vesicle. Nevertheless, it should be noted that the lamellarity of a vesicular structure was also dependant on temperature and the concentration of surfactants used (Pozo Navas *et al.*, 2005).

It is generally accepted that the particle size of drug carriers can determine the circulation half-life, delivery volume, release characteristics and accumulation site in the body, ultimately affecting the treatment efficacy (Kong *et al.*, 2000). In tumour microenvironment, the cut-off size for extravasation was found to be at the range of 400-600 nm (Yuan *et al.*, 1995). Although some reports suggested that sizes between 200 nm up to 2 μm were acceptable in certain conditions (Dufès *et al.*, 2004), it should be noted that particles greater than 1 μm which increases over time

can be an indicator of physical instability and particles above 5 μm might be lethal due to the possibility of embolism (Heurtault *et al.*, 2003). However, tumour accumulation for liposome with size 60 nm was very limited, owing to the ability of small particles to traverse in and out of blood vessels freely via diffusion (Ishida *et al.*, 1999). This has not only reduced the efficiency of the carrier but also increased the risk of systemic side effects in healthy tissues due to non-selective accumulation. Collectively, the optimum size for selective tumour delivery with colloidal system is ideally between 60 nm to 500 nm. In this study, Tf-vesicles (136 nm) and control vesicles (115 nm) prepared from Span 60/Solulan C24 formulations were both within the reasonable size range for tumour targeting. In fact, results from Ishida's study in 1999 mentioned that particles of diameter 120 nm was most favourable for prolonged circulation and optimum accumulation in solid tumours (Ishida *et al.*, 1999). Nevertheless, mutations in cancer cells are no doubt a common issue contributed to the inherent heterogeneity in tumour microenvironment (Maeda *et al.*, 2009). Therefore, one should note the significance of inter-tumour variation in terms of tumour accumulation despite having particles within a similar size range. As for Span 60/TPGS vesicles, although the average diameter of Tf-vesicles was 341 ± 11 nm, the highest peak of vesicle diameter occurred at 160 ± 2 nm, which was much similar to the maximum peak obtained with control vesicles (163 ± 7 nm). This could be an indication of possible aggregation in Tf-vesicles, possibly close to the μm range, leading to a dramatic increase in the measurements obtained for the average diameter. In this case, it would be worth investigating the distribution of vesicle dispersion by looking at two factors: individual peak intensity and polydispersity index. Indeed, the only peak detected for Tf-vesicles occurred at about 160 nm with

100 % peak intensity, indicating the absence of significant aggregation. In addition, a polydispersity index of approximately 0.377 would suggest a rather narrow size distribution of vesicles, similar to that observed with control vesicles. Collectively, although an average diameter larger than 200 nm might render unfavourable for tumour accumulation, several evidence showed that the actual distribution of Tf-vesicles was in fact similar to control vesicles in close proximity to a size range within 160 nm. Nevertheless, in case of possible aggregation, suitable filters can be used to control the vesicle size.

In general, the zeta potential is often used as an indication on the storage stability of a colloidal particulate system. The stability of colloids depends on the forces of interaction between them. The Derjaguin-Landau-Verwey-Overbeek (DLVO) theory is one of the most commonly used principle for quantification of forces in colloidal sciences (Sabin *et al.*, 2010). The DLVO theory is built on the assumption that the forces between two surfaces are determined by the sum of two forces: the London-van der Waals attractive force and the electrical double layer repulsive force (Figure 2.22) (Liang *et al.*, 2007). In aqueous electrolyte solutions, most colloidal dispersions carry an electric charge due to ionization of surface group and adsorption of ions from surrounding medium. As the particles approach each other due to Brownian motion, an energy barrier resulting from the electrical repulsive forces prevents two particles from adhering together. However if the particles collide with sufficient energy to overcome that barrier, the attractive forces will pull them into contact where flocculation takes place (Malvern Instruments Ltd., 2004). In colloidal systems, vesicle aggregation can be effectively prevented by the

sufficient repulsive forces brought about from electrostatic, steric and hydration forces (Cevc and Richardsen, 1999). It was suggested that zeta potentials of more than |30| mV, (optimum |60| mV) are required for full electrostatic stabilization, whereas potentials between |5| and |15| mV are prone to limited flocculation while potentials between |3| and |5| mV tend to have maximum flocculation (Heurtault *et al.*, 2003). At least -40 mV, up to -50 mV of a zeta potential were measured for control and Tf-vesicles prepared using Span 60/Solulan C24 and Span 60/TPGS formulations. This is a fair indication that all vesicles should have reasonable colloidal stability in aqueous solution. Moreover, measurement of zeta potential also facilitated the understanding of vesicles-cell interactions *in vitro*. Although reports suggested that particles bearing positive charges have enhanced interaction with negatively charged cell membrane, the major drawback for these systems is their non-specificity, i.e. widespread internalization of drugs in both diseased and healthy tissues (Torchilin, 2006). Therefore, the net negative charge on Span 60/Solulan C24 and Span 60/TPGS vesicles would have facilitated a selective delivery of tocotrienol to tumour cells, while minimizing non-specific cellular uptake in healthy tissues. However, the lower zeta potential recorded for Tf-vesicles was most probably due to the grafting of transferrin, a serum glycoprotein that gives a negative charge in solution with pH 7.4 because of its isoelectric point of 5.5 (Ying *et al.*, 2010). Similar reduction of zeta potential upon transferrin grafting to polymeric vesicles was observed in studies by Simoes *et al.*, (1998) and Kircheis *et al.*, (2001).
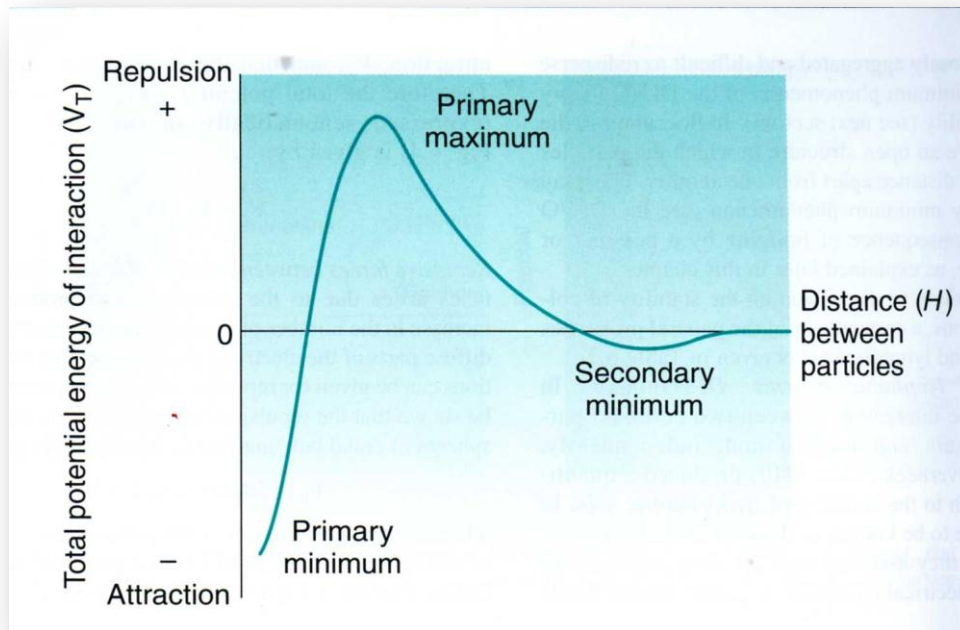
Figure 2.22: The interaction forces involved in a colloidal particulate system as stated by the DLVO theory. Schematic curve of total potential energy of interaction V_T versus distance of separation, H, for two particles. V_T is the sum of van der Waals attractive forces V_A and electrical repulsion V_R ($V_T = V_A + V_R$) (Adapted from Aulton, 2007).

In summary, two formulations of Span 60 vesicles encapsulating tocotrienol were prepared: 1) Span 60/Cholesterol/Solulan C24 vesicles with molar ratio 1: 1: 0.22 and 2) Span 60/Cholesterol/TPGS/DOPE with molar ratio 1: 1: 0.22: 0.05. In both formulations, control vesicles were prepared using TRF in 5 mg/mL either dissolved in DMSO (for Span 60/Solulan C24 vesicles) or emulsified in TPGS solutions (for Span 60/TPGS vesicles). Transferrin was then grafted to tocotrienol-loaded control vesicles as previously described (Dufès *et al.*, 2000) to synthesize transferrin-targeted vesicles (Tf-vesicles). Successful preparation of vesicles was first confirmed using transmission electron microscopy. Each carrier was found to have its unique properties upon physical characterizations in terms of encapsulation efficiency, transferrin conjugation efficiency, release profile as well as size and zeta

potential. Span 60/Solulan C24 and Span 60/TPGS vesicles shared similarities in terms of size, zeta potential and encapsulation efficiency while transferrin conjugation and vesicle morphology were considerably different from one vesicle formulation to another.

It is generally accepted that physicochemical properties of a delivery system are crucial determinants of their cellular fate in biological systems. This Chapter provides fundamental understanding on tocotrienol-loaded vesicular system, either targeted or non-targeted, as well as their potential as chemotherapeutic agents. As such, the next step of this study involves detailed investigation into their intracellular fate in cancer cell culture *in vitro*, further discussed in Chapter 3.

Chapter 3

In vitro Evaluation

3.1   INTRODUCTION

The introduction of cell culture more than a century ago created enormous opportunities in the study of human and animal behaviour (Freshney, 2000). While it is not possible to conduct animal studies at all instances, development of cell culture has made most cellular studies accessible, including intracellular activity, protein synthesis, membrane trafficking, receptor interactions, cell adhesion, genetic recombination techniques and immunology (Freshney, 2000). The major advantage of tissue culture is the control of the physicochemical environment (i.e. pH, temperature, carbon dioxide), often essential for precise and consistent experimental studies. In the field of cancer research, cell proliferation, drug-cell interaction, mechanism of action, screening of new therapeutics and drug metabolism have well progressed under the knowledge of *in vitro* cell culture techniques.

The formation of a cell line is usually derived from a primary explant, which disperses into cell suspensions upon mechanical or enzymatic digestion (Freshney, 2000). Cell suspension is then propagated into adherent monolayer cultures or as suspensions under controlled physiochemical environment. When confluence is reached (when all available growth area is utilized and cells make close contact with one another), cells are subcultured, or "passaged", to ensure continuity of growth (Freshney, 2000). Cells in culture usually develop a standard pattern of growth. After seeding, a lag phase followed by the log phase (a period of exponential growth) is observed (Freshney, 2000). When the cell density reaches a stage where all the available substrate is occupied, or when the cell concentration exceeds the capacity of the medium, cell growth is greatly reduced (Freshney, 2000). In such case,

dividing of cell culture (i.e. subculture) is recommended. For an adherent cell line, the standard procedure usually involves removal of medium and dissociation of cells with trypsin. Cell suspension, diluted to an appropriate split ratios, are re-seeded into new vessels for propagation. Subcultures are usually performed when the density of culture reaches confluence as cells often withdraw from cell cycle progression without adequate re-seeding. It is also performed when large amount of cells are needed for experimental purposes as well as in routine subculture schedule to maintain reproducible cellular behaviour (Freshney, 2000).

3.1.1   Cell culture

For *in vitro* studies, four cell lines were used to investigate the activity of tocotrienol, either entrapped in targeted and non-targeted vesicles or as free drug. Human squamous carcinoma, A431 cell line, is an epithelial carcinoma derived from the skin tissue of an 85 year old female (ECACC). A431 cells were previously found to carry large number of transferrin receptors (Dufès *et al.*, 2000). Thus, this cell line can be exploited as an indicator cell for the targeting efficacy of transferrin-targeted systems. Another strain of epithelial carcinoma, A2780 cell line, was also investigated. A2780 cells are human ovarian carcinoma derived from the tumour tissue from the ovary of an untreated patient (ECACC). On the other hand, a strain of glioblastoma, T98G cell line, was included in our study as glioblastoma was known to be one of the most effective cell lines from the brain for transferrin targeting (Beduneau *et al.*, 2007). T98G cells are derived from glioblastoma multiform tumour from a 61 year old Caucasian male (ECACC). Last but not least, a mice strain of melanoma was used for *in vitro* and *in vivo* studies. In 1997, He and colleagues

showed an increased in survival rate after oral supplementation with tocotrienol in mice bearing B16F10 melanoma tumours (He *et al.*, 1997). Following the study, we aim to further investigate B16F10 cells in our work in order to reflect on the therapeutic efficacy of tocotrienol when encapsulated in targeted vesicles. Besides, these vesicles will be administered via intravenous injection instead of oral supplementation. B16F10 cell line origins from mouse melanoma, derived from the skin of mice strain C57BL/6J (ATCC).

3.1.2 Confocal Laser Scanning Microscopy (CLSM)

A conventional light microscope is very limited in biological applications because of its relatively low resolution (up to 0.2 µm). Although transmission electron microscopy offers outstanding resolution, high electron energy beam is often damaging to biological specimens (Wright and Wright, 2002). The concept of confocal microscopy was first patented in 1957 by Marvin Minsky, suggesting a better performance using point-by-point image construction while focusing a point of light sequentially across a specimen and then collecting the returning rays out of a pinhole aperture (Semwogerere and Weeks, 2005). Modern confocal microscopy provides improvements on speed, image quality and data storage (Semwogerere and Weeks, 2005). The most widely used design in biological analysis is fluorescence confocal microscope. Briefly, a fluorescence confocal imaging works by first exciting the fluorescence compounds by a point source of laser beam. This light source is reflected by the dichroic mirror and directed to the objective lens, creating an incident beam on the focal plane of the specimen. Fluorescence emission from the specimen returns via the objective lens whereby lights with longer wavelengths pass

through the dichroic mirror and a pinhole-like filter. Lights that make it through the pinhole is measured by a photomultiplier detector (Figure 3.1) (Wright and Wright, 2002; Semwogerere and Weeks, 2005).
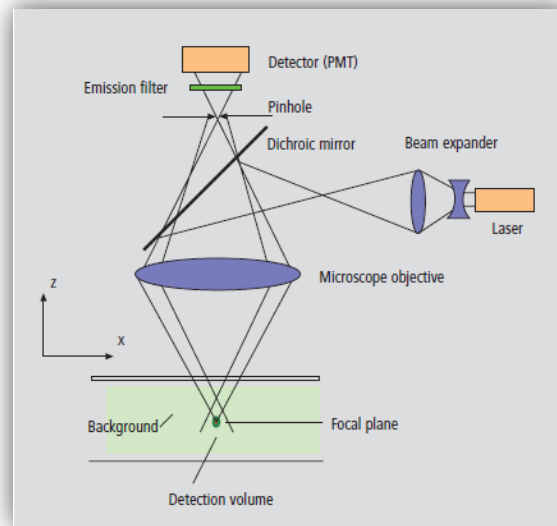
Figure 3.1: Schematic illustration of image construction using Confocal Laser Scanning Microscope (CLSM) *(Adapted from Carl Zeiss, Inc.)*.

Successful elimination of out-of-focus lights remains one of the major advantages of CLSM over conventional light microscope, for sharper and thinner optical section images can now be achieved (Inoue, 1995). Besides, different optical sections i.e. the *xy* plane, *xz* plane and *yz* planes can now be obtained; especially the z-axis which gives substantial information along the depth of a cell or tissue (Wright and Wright, 2002). These series of optical sections can also be reconstructed to build a three dimensional rendition of the specimen (Semwogerere and Weeks, 2005). Moreover, the CLSM offers the advantage of multiple-labelled imaging with the technology to detect more than one fluorophore in a specimen where images can then be merged to show relationships between different cell structures (Wright and Wright,

2002). Yet, a major limitation of confocal microscopy lies in specimen preparation where fluorescent labelling and cell fixation processes are known to incur perturbations to biological environments. Therefore, in this study, an introduction to a new chemical imaging protocol (discussed below) was proposed, effectively avoiding additional photo-bleaching problems associated with fluorescent labelling.

3.1.3   Coherent Anti-Stokes Raman Scattering (CARS) Microscopy

Chemical imaging based on intrinsic vibrational fingerprints of molecules offers an alternative approach in imaging studies for accurate identification of cellular drug uptake and location of drug accumulation. When photons from a laser light source interact with a molecule, the scattering event by molecular bonds in the molecule forms a characteristic vibrational energy (Wachsmann-Hogiu *et al.*, 2009). Although conventional vibrational microscopy based on infrared absorption and spontaneous Raman scattering offers the possibility of direct chemical imaging, the use of long wavelength infrared (IR) are limited in live cell imaging because of the IR absorption incurred by water molecule (Humecki, 1995). In Raman spectroscopy, incident laser light momentarily promotes the system into a "virtual" state (Matthaus *et al.*, 2008). Upon energy dissipation, the energy difference between vibrational state and ground state is defined as the Stokes shift. If the molecule is initially in the vibrational state but emits light at higher energy, it is defined as an anti-Stokes shift (Rodriguez *et al.*, 2006). Spontaneous Raman microscopy provides good spatial resolution by using visible lasers but requires a high average power and a long exposure time because of the small cross section of Raman scattering (Shafer-Peltier *et al.*, 2002). Besides, Raman scattering of a molecule is at least six times lower than

fluorescence and was not able to be observed microscopically until recently (Matthaus *et al.*, 2008). These shortcoming can be circumvented by coherent anti-Stokes Raman Scattering (CARS) microscopy, where CARS signals are more than a thousand times stronger than the original Raman signals (Cheng and Xie, 2004; Evans and Xie, 2008; Matthaus *et al.*, 2008). In a CARS system, molecules are stimulated to generate an anti-Stokes shift emission using two frequencies: a pump photon and a "Stokes" photon (Rodriguez *et al.*, 2006). When these two populations of coherent photons are combined and tuned to match the frequency of a Raman active molecular vibration, resonant molecules are coherently driven with the excitation fields, resulting in the generation of a strong coherent anti-Stokes signal, or known as the CARS signal (Potma *et al.*, 2008).
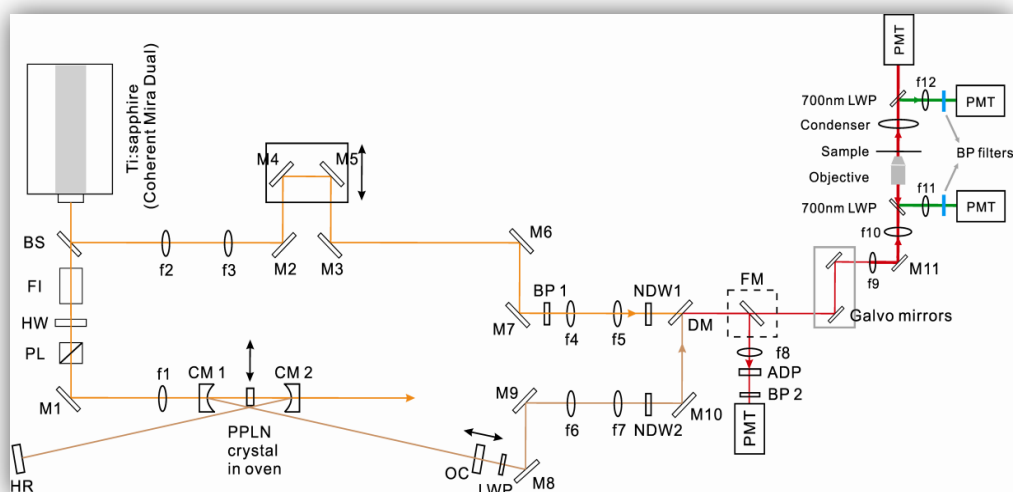
Figure 3.2: Schematic setup of the CARS microscope. FI: Faraday isolater; HW: half wave plate; PL: polarizer; M1-M11: high reflective mirrors for near infrared region; CM1, CM2, OPO: cavity concave mirrors with a radius of curvature 100 mm; PPLN: periodically pole lithium niobate crystal for parametric generation; OC: output coupling mirror; f1-f12: lenses; NDW1-2: neutral density wheels; DM: dichroic mirror; FM: flip mirror; ADP: sum-frequency missing crystal; BP: bandpass filters; LWP: long wavelength pass filters; PMT: photomultiplier tube.

As a two-beam modality, CARS microscopes are mostly operated with picoseconds (ps) pulses, either from two synchronized titanium-sapphire lasers or from a synchronously pumped optical parametric oscillator (OPO) (Le *et al.*, 2010). Figure 3.2 is a schematic diagram of a CARS microscopy system currently used in our study. Detailed arrangement on the setup and technical specification of individual components of the system has been published by Zhang and colleagues in the Centre of Biophotonics, University of Strathclyde (Zhang *et al.*, 2010). Briefly, a home-built synchronously pumped optical parametric oscillator (OPO) based laser system was developed to provide pump and Stokes beams required in CARS process. The pump laser generated a 1 ps 76 MHz pulse train with over 1.2 W of output power. Combining the signal output of the OPO (~180 mW) with a fraction of the titanium-sapphire laser (~120 mW), a total Raman range from 1900 cm^{-1} to approximately 5700 cm^{-1} was accessible. Spectral resolution of the laser system in this configuration was estimated to be 21 cm^{-1}. This CARS microscope was in fact modified from an infrared corrected Olympus FV300/IX71 laser scanning confocal microscope. The internal photomultiplier detector tubes (PMTs) in the scanhead were used for forward and epidetection. The temporal and spatial pulse trains from the overlapping of titanium-sapphire and OPO were coupled collinearly into the scanhead and focused on the same spot of the sample with water-immersion objective (Olympus, UPLSAPO 60X, NA 1.2). A 700 nm long wave pass chromatic reflector was placed above the condenser lens to separate the CARS signal from the fundamental excitation sources. The CARS signal was then guided through a stack of band pass filters and focused into the photomultiplier detector tubes.

3.1.4 Anti-proliferative Assay: MTT Assay

Cytotoxicity assays are widely used in drug-screening program for new drug development. Tetrazolium salts are part of the group of heterocyclic organic compounds readily reduced to formazan by viable cells (Liu *et al.*, 1997). [MTT 3-(4,5-dimethylthiazol-2-yl)-2,5-diphenyltetrazolium bromide] assay is among the most common studies for indication of cell viability. In fact, it was evaluated by the American National Cancer Institute as a possible endpoint in rapid *in vitro* screening assay for antitumor drug (Alley *et al.*, 1988). In a homogeneous cell population, cells are exposed to several drug dilutions for certain duration. MTT solution is a water soluble yellow tetrazolium dye that is reduced by live but not dead cells to a purple formazan product insoluble in aqueous solutions (Plumb, 2004). The amount of formazan are then colorimetrically determined after being solubilised in an organic solvent (dimethylsulfoxide). Under optimized conditions, the MTT formazan production demonstrates a linear relationship with viable cell number, on the assumption that only viable cells are able to reduce tetrazolium salts to formazan derivatives (Plumb *et al.*, 1989; Vistica *et al.*, 1991). The reduction of MTT was taking place presumably in the mitochondria by active mitochondrial reductase enzymes, however it was later shown by Liu *et al.* (1997) that many cellular components such as endosomes and lysosomes also participate in formazan production via MTT reduction. In a study correlating protein production and two different cytotoxicity assays, i.e. the MTT assay and Alamar Blue assay, MTT was found to be a more robust technique with better correlation against protein analysis (Holst and Oredsson, 2005). Nevertheless, a major drawback of MTT assay is that it does not distinguish between cytotoxic effect (killing of cells) versus cytostatic effect

(inhibition of cell growth), although cytostatic effects are not common among most cytotoxic drugs (Plumb, 2004).

3.1.5 Aims and Objectives

From Chapter 2, Span 60/Solulan C24 and Span 60/TPGS vesicles were successfully prepared and characterized. Briefly, tocotrienol was entrapped in non-targeted vesicles (control vesicles) and transferrin-bearing vesicles (Tf-vesicles). In this Chapter, the therapeutic efficacy of tocotrienol in these vesicular formulations will be compared against the free drug form. With the implication of passive targeting and active targeting, we hypothesize that tocotrienol, when formulated in transferrin-targeted niosomes would exhibit enhanced therapeutic efficacy facilitated by improved delivery of tocotrienol to cancer cells. *In vitro* study forms the basis for evaluation of these formulations in biological system, as it provides vital information before a therapeutic system can be taken on *in vivo* studies. In this Chapter, two major aspects of cellular interaction were investigated: the intracellular accumulation and therapeutic efficacies of tocotrienol. These experiments will be done on four different neoplastic cell lines overexpressing transferrin receptors, namely skin epithelial carcinoma A431 cells, ovarian epithelial carcinoma A2780 cells, glioblastoma T98G cells and mouse melanoma cells B16F10.

3.2 MATERIALS AND METHODS

3.2.1 Materials

Materials	Supplier
Span 60/Solulan C24 vesicles	Prepared as described in Chapter 2
Span 60/TPGS vesicles	Prepared as described in Chapter 2
Dulbecco's Modified Eagle Medium (DMEM)	Invitrogen, UK
Roswell Park Memorial Institute (RPMI)-1640 medium	Invitrogen, UK
Foetal Calf Serum (FCS)	Invitrogen, UK
L-Glutamine	Invitrogen, UK
Penicillin-Streptomycin	Invitrogen, UK
Trypsin	Invitrogen, UK
Triton-X	Sigma-Aldrich, UK
FluoroNunc® fluorescence 96-well Plates	Sigma-Aldrich, UK
3-(4,5-dimethylthiazol-2-yl)-2,5-diphenyl-tetrazolium bromide (MTT)	Sigma-Aldrich, UK
Vectashield® mounting medium with propidium iodide	Vector Laboratories, CA, USA
Lab-Tek™ Chamber Slide (4 wells)	Thermo Scientific Nunc, UK
Methanol	Sigma-Aldrich, UK
Phosphate-Buffered Saline pH 7.4 (PBS)	Sigma-Aldrich, UK

Sodium chloride	Sigma-Aldrich, UK
Sodium hydroxide	Sigma-Aldrich, UK
Dimethyl sulfoxide (DMSO)	Sigma-Aldrich, UK
Glycine	Sigma-Aldrich, UK

3.2.2 Cell Culture

Human tumour cell lines epidermoid carcinoma A431 and glioblastoma T98G, were grown as monolayer cultures in Dulbecco's Modified Eagle Medium (DMEM) supplemented with 10 % v/v foetal bovine serum, 1 % v/v L-glutamine and 0.5 % v/v penicillin-streptomycin. Ovarian carcinoma (A2780) and mouse melanoma (B16F10) were maintained in RPMI 1640 medium. All cells were cultured in an atmosphere of 37 ^{o}C, 5 % carbon dioxide.

3.2.3 Quantification of TRF cellular accumulation

To measure the efficacy of TRF cellular uptake, cells (A431, T98G and A2780) were seeded at 2000 cells/ well in 96-well plates for 72 hours. Medium was removed and replaced with medium containing TRF formulated as transferrin vesicles (Tf-vesicles), control vesicles or as free TRF at 10 µg/well. Free TRF was prepared in DMSO at 5 mg/mL. Treatments were incubated for 24 hours. After incubation, cells were washed with PBS three times followed by cell lysis with 100 µL/well trypsin and 100 µL 10 % Triton X per well. Cell lysate were transferred to opaque FluoroNunc$^{®}$ 96-well plates for fluorescence quantification. TRF accumulation in the cells was then quantified using a fluorescence plate reader at λ_{ex} = 295 nm and λ_{em} = 325 nm (SpectraMax, Molecular Devices).

3.2.4 Confocal Microscopy

TRF cellular uptake was visualized using confocal laser scanning microscopy (CLSM). Cells were seeded on cover slips in 6-well plates at 1×10^{5} cells/ well. After 72 hours incubation, growing medium was replaced with medium containing

TRF formulated as Tf-vesicles, control vesicles or free TRF at 20 µg/mL. Free TRF was prepared in DMSO at 5 mg/mL. Treatments were incubated for 24 hours. Cells were washed with PBS for three times at the end of incubation and fixed in methanol for 10 minutes. Cover slips were then rested on microscope slides with a drop of Vectashield® mounting medium containing nuclei stain propidium iodide. A Leica SP-5 confocal laser scanning microscope was used to generate images from the slides at λ_{ex} = 535 nm, λ_{em} = 615 nm for propidium iodide and λ_{ex} = 295 nm, λ_{em} = 325 nm for TRF.

3.2.5   Coherent Anti-Stokes Raman Scattering (CARS) Microscopy

Raman spectra of TRF, transferrin-bearing blank vesicles and blank vesicles were identified using a micro-Raman spectroscopy system (inVia, Renishaw, UK). Spectra were collected using long working distance air objective at 20 × magnification (LWD C A20 PL, NA 0.4, Olympus). A 632 nm HeNe laser provided approximately 5.7 mW of power at laser focus. The spectra of the samples were collected using a 300 s integration time.

Cells were seeded in 4-well chamber slides (Lab-Tek^{TM} Chamber Slide, Thermo Scientific, UK) at a density of 1× 10^4 cells /well for 72 hours. Growing medium was replaced with medium containing 20 µg/mL TRF formulated as Tf-bearing vesicles, control vesicles or free TRF. Treatments were incubated for 24 hours. Cells were washed three times with PBS at the end of incubation and fixed in methanol for 10 minutes. Slides were then rinsed with distilled water prior to imaging in order to remove traces of methanol.

3.2.6 Anti-proliferative assay

The efficacy of TRF to inhibit cancer cell proliferation either as a free drug or encapsulated in tumour-targeted vesicles were evaluated using a standard MTT assay. Cells were seeded at 2000 cells/well in 96-well plates for 72 hours. Growth medium was then replaced with medium containing Tf-vesicles, control vesicles and free TRF at TRF concentration ranging from 1×10^{-7} to 1×10^{3} μg/mL. Treatments were incubated for a further 72 hours. At the end of incubation, the medium was aspirated from all treatment wells and replaced with fresh medium. MTT solution at 0.5 % w/v (prepared in PBS) was added to the wells at 50 μL/well. Upon 4 hours exposure, the MTT solutions was aspirated from the wells and the cells resuspended with DMSO at 200 μL/well. Glycine buffer was added (25 μL/well) prior to measurement of absorbance at 570 nm (Thermo Labsystems, Multiskan Ascent). Dose-response curves were fitted to percentage UV absorbance values to obtain growth inhibitory concentration for 50% of cell population (IC_{50}).

3.2.7 Statistical analysis

All values were expressed as means ± standard error. Statistical significance was determined by one-way ANOVA or Student's t-test as appropriate (GraphPad Prism Software). Difference of p-values < 0.05 were considered statistically significant.

3.3   RESULTS

In this Chapter, extensive cellular studies were carried out in order to investigate the efficacy of the two delivery systems tailored for tocotrienol as described in Chapter 2. Before its anti-proliferative activity can be accurately assessed, cellular association of tocotrienol should be investigated in order to distinguish the uptake efficiency of tocotrienol, when entrapped in vesicular formulations or as free drug. Not only will it provide supporting data on the targeting efficacy of transferrin in recognizing its receptor counterpart, but also provide insight information regarding the intracellular characteristics of tocotrienol when accumulated in cancer cells. Having said that, while anti-proliferative activity was mainly evaluated using MTT cell proliferation assay, cellular uptake was assessed qualitatively and quantitatively using confocal microscopy, CARS microscopy and conventional uptake analysis.

3.3.1   Span 60/Solulan C24 Vesicles

To demonstrate the cellular binding affinity of transferrin-targeted vesicles, cells of epithelial carcinoma (A431), glioblastoma (T98G) and ovarian carcinoma (A2780) origin were incubated with tocotrienol formulations for 24 hours. Figure 3.3 depicts the confocal microscopy images obtained using Span 60/Solulan C24 vesicles as a delivery system for tocotrienol. Cell nuclei were fluorescing in red upon propidium iodide staining whereas the intrinsic fluorescence of tocotrienol appeared in blue. Co-localization of tocotrienol in the nuclei was clearly visible in the three cell lines treated with Tf-vesicles, with some accumulation in the central compartment, possibly the nucleolus. In A431 cells, tocotrienol-derived fluorescence

was also disseminated in the cytoplasm after treatment with Tf-vesicles. By contrast, cells treated with control vesicles or free tocotrienol showed no tocotrienol-derived fluorescence, except after treatment of A2780 cells with free tocotrienol. In this case, a faint tocotrienol-derived fluorescence was observed in the cytoplasm.
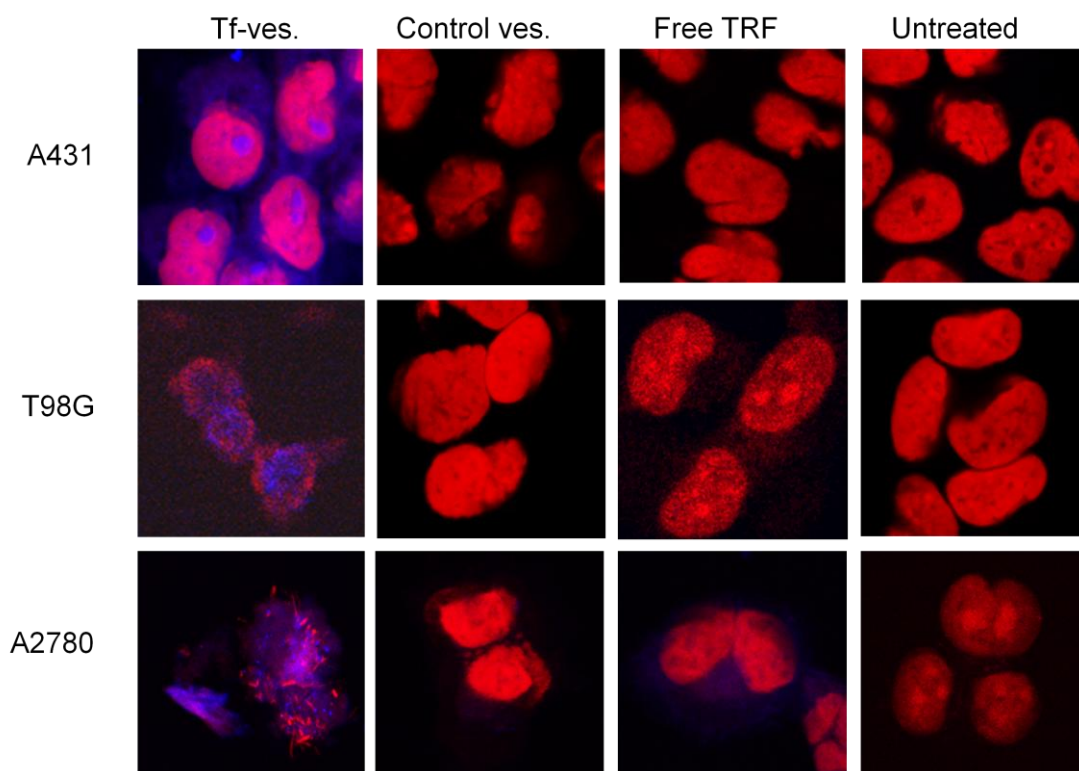
Figure 3.3: Confocal laser scanning microscopy imaging of the cellular uptake of TRF either entrapped in Tf-vesicles, control vesicles or as free TRF, after incubation of 4 hours in A431, T98G and A2780 cells (Red: Nuclei stained with propidium iodide, Blue: TRF) (Magnification × 40).

Although confocal microscopy remains one of the most widely used method to elucidate the intracellular accumulation of nanocarriers, it has several limitations in the case of tocotrienol. First being the weak quenching capacity of tocotrienol-derived fluorescence, which is dependent on the intrinsic property of tocotrienol. Thus, when images were superimposed with a strong fluorophore such as propidium

iodide, distribution of tocotrienol-derived fluorescence became diffused and pale. Although not visible in Figure 3.3, autofluorescence from cellular molecules, arising from endogenous fluorophores such as pyridinic (NADPH) and flavin coenzymes could be a possible interference in fluorescence imaging (Monici, 2005). Therefore, the most common way of cellular trafficking for drugs or nanocarriers is to label the subject of interest with an exogenous fluorophore in order to distinguish themselves from cellular autofluorescence. However, with the advancement of technology in molecular imaging, we have explored a novel microscopy technique, operating without the need of an exogenous fluorescence label. Coherent anti-Stokes Raman scattering (CARS) microscopy, as mentioned in section 3.1.3, has the major advantage to accurately detect molecules based on their intrinsic vibrational signals. Thus when applied in TRF, intracellular accumulation of TRF is readily detected by tuning the laser system to match the vibrational spectrum distinguishable to TRF, successfully avoiding photo-bleaching and perturbations to biological environments induced by fluorescence labelling. It is therefore an excellent tool for precise detection of the amount of drug accumulated in cells as well as the location of which the drug has resided. Figure 3.4 showed the Raman spectra of TRF, blank vesicles and transferrin-grafted blank vesicles, where the specific wavelength used to identify TRF in cell samples was determined to be 2916 cm^{-1}.
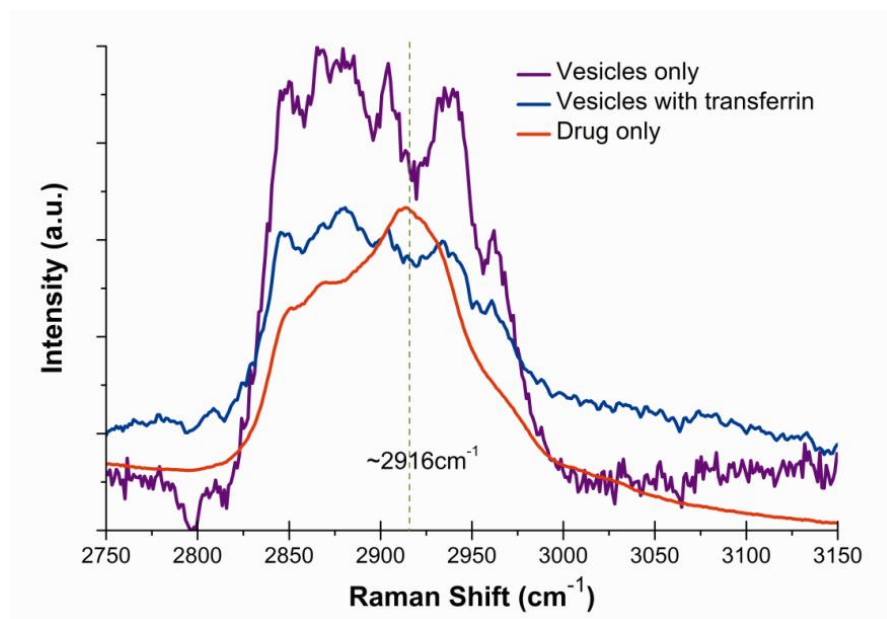
Figure 3.4: Raman spectra of TRF (red) and plain vesicles with (blue) or without transferrin conjugation (violet).

The full width half maximum bandwidth of TRF spectrum (~120 cm^{-1}) was slightly narrower than that of the vesicles (~133 cm^{-1}). Conjugation with transferrin did not affect of the Raman spectrum of vesicles in the range of 2750 to 3050 cm^{-1}. A strong Raman peak at 2916 cm^{-1} was used to distinguish free TRF from that entrapped in the vesicles with/without transferrin as it corresponded to a dip (with a width of ~19 cm^{-1}) in the spectrum of the vesicles. We note that this strong Raman peak correlates with the Raman peak reported by Beattie *et al* (2007) for detection of vitamin E in cellular structures. Figure 3.5 showed the images obtained with cells A431, T98G and B16F10 after treatment of Tf-vesicles, control vesicles, blank vesicles, free TRF and untreated cells.

A431
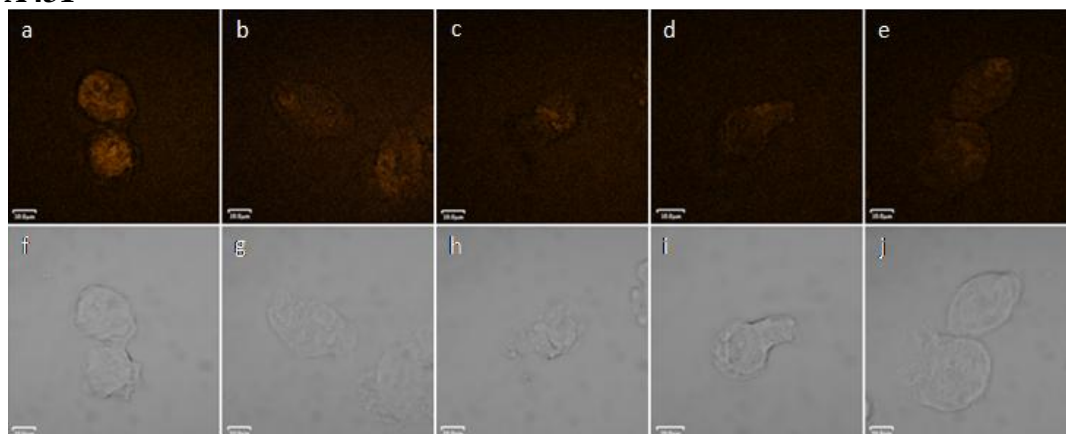
B16F10
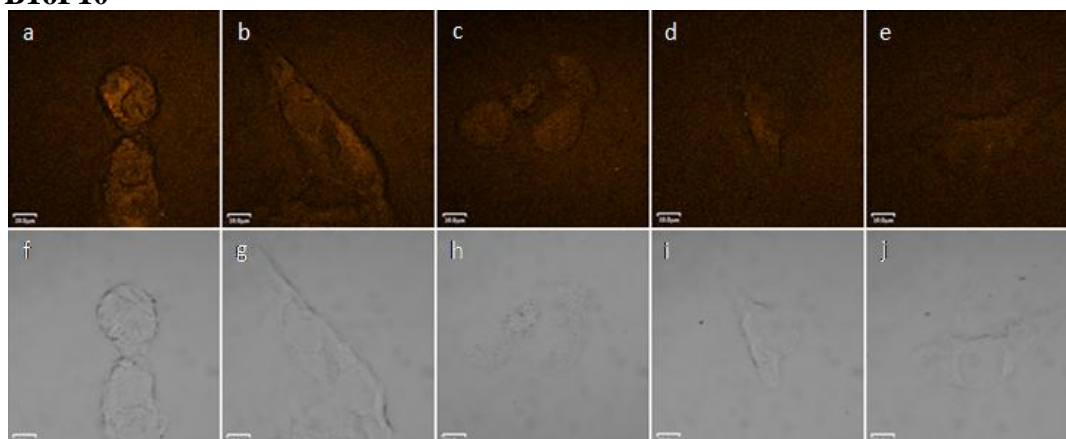
T98G
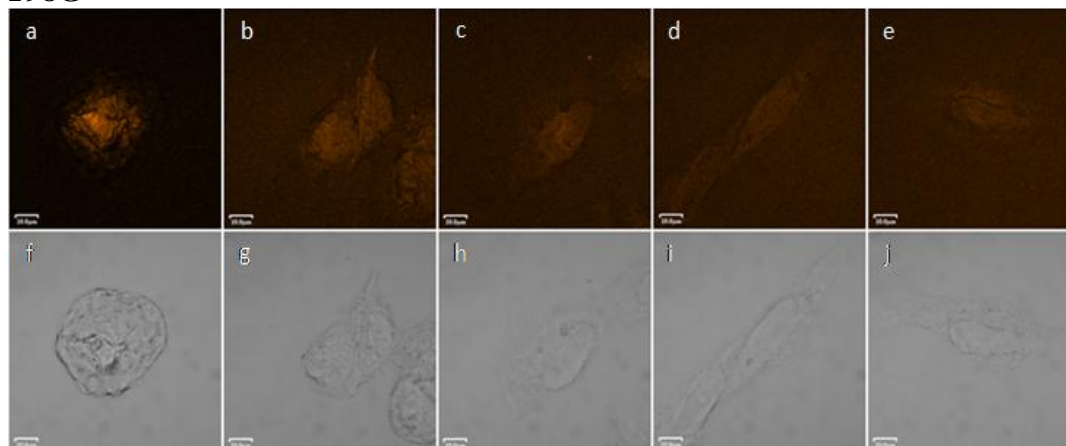
Figure 3.5: Optically-sectioned CARS images in the x-y lateral plane (a-e) and transmission images (f-j) of three cancer cell lines A431, B16F10 and T98G after treatment with (a/f) Tf-vesicles, (b/g) control vesicles, (c/h) plain vesicles, (d/i) free TRF and (e/j) untreated cells. All images were taken in the size of 512 pixels × 512 pixels and were averaged over 5 frames with a frame capture rate of 1.68 s. Scale bar represents 10 μm while pump and Stokes wavelengths were tuned to 752.1 nm and 963.4 nm respectively, corresponding to a Raman shift of 2916 cm^{-1}.

These images were produced by tuning the laser system to match the 2916 cm^{-1} symmetric C-H stretching mode where the drug was expected to give the strongest CARS signals. The average powers of the pump wavelength at 752.1 nm and the Stokes beam wavelength at 963.4 nm at the sample were around 20 mW and 40 mW, respectively. From Figure 3.5, signals generated from cells treated with plain vesicles and free TRF resembled intensity similar to that observed with untreated cells. In agreement with images obtained using confocal microscopy, highest TRF-derived CARS signals were observed in cells treated with Tf-vesicles, while other treatments generated signals insignificantly different from untreated cells. While TRF was generally dispersed in the cell cytoplasm when treated with control vesicles, treatment with Tf-vesicles on the other hand resulted in a concentrated accumulation of TRF within the central compartment. Localized nucleus distribution of TRF upon incubation with Tf-vesicles was most evident in T98G cells, compared to A431 and B16F10 cell lines. For quantification purpose, comparison of the intensities (in arbitrary unit, a.u.) of CARS signals generated in relative to each treatment was measured. Figure 3.6 is a quantification of average CARS signals detected over 10 μm × 10 μm square areas in the cells from each CARS images.
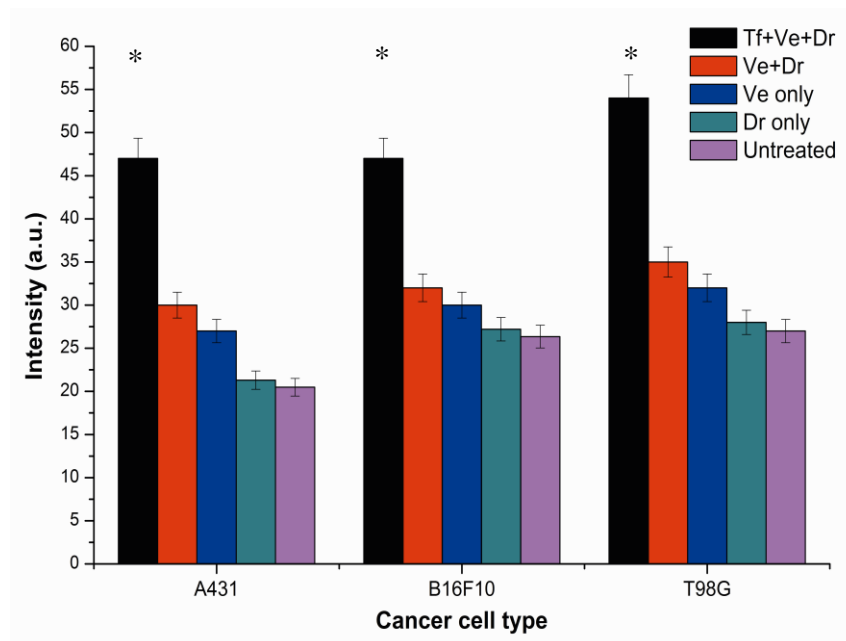
Figure 3.6: Qualitative analysis of TRF cellular uptake in cells treated with Tf-vesicles (black), control vesicles (red), plain vesicles (blue), free TRF (green) and untreated cells (violet) by CARS ($n=10$) (*: $p < 0.05$ against other treatment groups). Measurements were obtained by quantifying the average intensity of a 10 μm × 10 μm square area at the brightest position in the cell in each CARS image.

For all cell lines, the signal level intensities of the cells treated with TRF solution were similar to that of the untreated cells, indicating the low drug uptake with free TRF, i.e. about 20 a.u. for A431 cells, 25 a.u. for B16F10 and T98G cells, which is about 1 a.u. higher than baseline untreated cells. Taking the signal intensity generated from untreated cells as a base line, entrapment of TRF in Span 60/Solulan C24 vesicles enhanced its cellular uptake by at least 5-fold, about 10 a.u. higher than that obtained from free TRF. The CARS signal intensity after treatment with control vesicles was respectively 7 a.u., 5 a.u. and 10 a.u. higher than the untreated cells for A431, B16F10 and T98G cells. It is important to note that the vesicles without drug can be detected by CARS microscopy in a non-specific way, but with very low signal intensities that they became insignificant compared to signals obtained with

untreated cells. The grafting of transferrin on these vesicles further improved TRF uptake compared to control vesicles. The CARS signal intensity after treatment with Tf-bearing vesicles was 25 a.u., 20 a.u. and 25 a.u. higher than baseline signals from untreated cells for A431, B16F10 and T98G cells respectively. More than twice the amount of TRF was taken up by the three cancer cell lines when treated with Tf-vesicles compared to control vesicles. These findings were similar to that observed during the quantification of TRF uptake using conventional quantitative analysis, based on the intrinsic fluorescence property of TRF (Figure 3.7).

Using conventional quantification technique, cellular concentration of TRF was significantly increased when delivered to cancer cells via Span 60/Solulan C24 vesicles. Cells treated with control vesicles measured a cellular TRF concentration at least twice higher than that observed with cells treated with free TRF in the case of T98G and A2780 cell lines. The grafting of transferrin on the vesicles further improved TRF uptake compared to control vesicles: more than twice the amount of TRF was taken up by A431 cells when treated with Tf-vesicles compared to control vesicles. The highest amount of cell-associated fluorescence was found in A431 cells incubated with Tf-vesicles. The close correlation of CARS data to quantitative analysis proved that CARS could be a reliable and robust method for intracellular uptake analysis, offering the possibility of direct chemical imaging on samples without fluorescent staining.
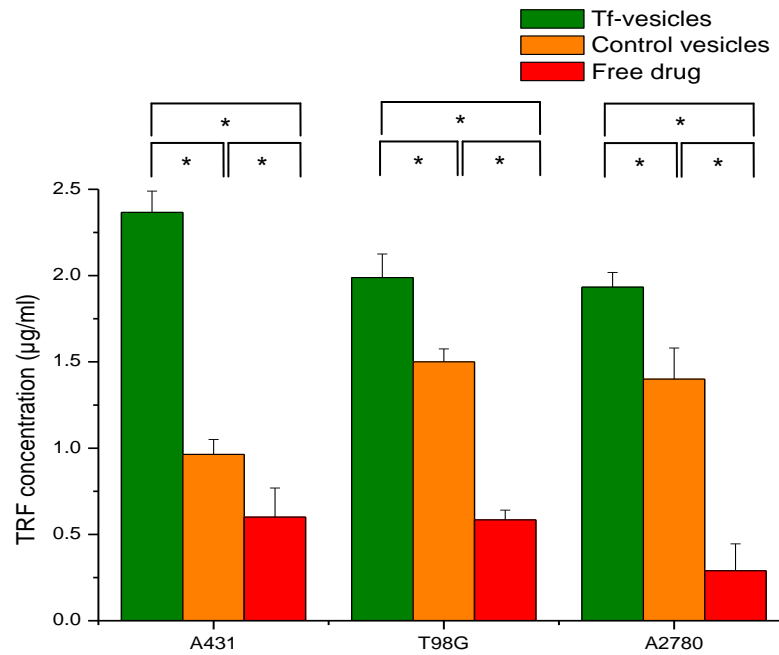
Figure 3.7: Spectrofluorimetric quantification of the cellular uptake of TRF formulated as Tf-vesicles (green), control vesicles (orange) or as free TRF (red) in A431, T98G and A2780 cells ($n = 15$) (*: $p < 0.05$).

The increased uptake of TRF when entrapped in Tf-vesicles led to a corresponded improvement in its anti-proliferative effect, when assessed using MTT cell proliferation assay. Figure 3.8 is a collection of dose response curves constructed by colorimetric assay of % cell survival against increasing doses of TRF. The growth inhibitory concentrations (IC_{50}) of respective treatments in each cell line were stratified against the concentrations of TRF needed to inhibit cell growth in 50 % of the population.
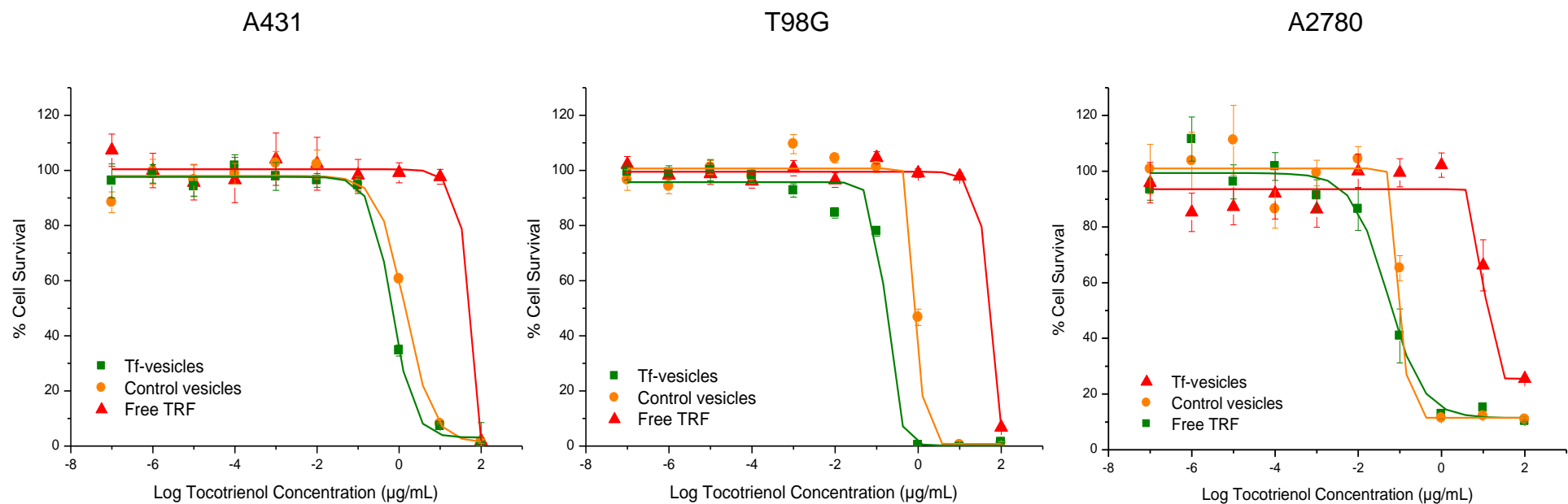
Figure 3.8: Anti-proliferative activity of TRF delivered as free TRF (red) or entrapped in Span 60/Solulan C24 vesicles. Treatment with Tf-vesicles was represented in green and control vesicles in orange against A431, T98G and A2780 cells (*n* = 15).

Table 3.1: Anti-proliferative activity of free TRF or TRF formulated in Tf-vesicles or control vesicles in A431, T98G and A2780 cells, expressed as IC_{50} values ($n = 15$).

Cell lines	IC_{50} (µg/mL) (mean ± S.E.M.)		
	Tf-vesicles	Control vesicles	Free TRF
A431	0.66 ± 0.08	1.42 ± 0.30	131.06 ± 1.94
T98G	0.17 ± 0.14	0.97 ± 0.48	79.49 ± 0.16
A2780	0.05 ± 0.02	0.11 ± 0.10	10.73 ± 4.36

After 72 hours incubation, the growth inhibitory concentration of TRF was significantly lower when encapsulated in vesicles compared to free TRF. At least 80-fold improvement was observed in control vesicles compared to free TRF. IC_{50} was measured between 0.11 ± 0.10 to 1.42 ± 0.30 µg/mL with control vesicles in contrast to IC_{50} values between 10.73 ± 4.36 to 131.06 ± 1.94 µg/mL when treated with free TRF. Grafting of transferrin to the vesicles further improved the therapeutic efficacy of TRF by 2-fold in A431 and A2780 cells. The targeting efficacy of transferrin was most pronounced in T98G cells, whereby the IC_{50} obtained with Tf-vesicles was 5-fold lower compared to control vesicles. Empty vesicles of Span 60/Solulan C24 were found to be non-toxic *in vitro* and *in vivo* (data not shown).

3.3.2 Span 60/TPGS Vesicles

As mentioned in the above section, Span 60/Solulan C24 vesicles revealed at least 80-fold improvement in tocotrienol therapeutic efficacy compared to free tocotrienol. It is not surprising to observe similar trends in Span 60/TPGS vesicles as they shared similar physical properties despite different stearic coating with two types of long-chain polymers. As size and zeta potential are primarily manifesting the cellular association of a nanocarrier, they were correlated with the *in vitro* characteristics of the vesicles. Both Span 60/Solulan C24 and Span 60/TPGS vesicles measured sizes between 100-200 nm and zeta potentials between -40 to -50 mV. It is thus fair to anticipate little discrepancy between the intracellular characteristics of Span 60/TPGS vesicles compared to what has been observed for Span 60/Solulan C24 vesicles. Nevertheless, it should be noted that multivesicular systems as seen with Span 60/TPGS might behave otherwise compared to small unilamellar vesicles. Figure 3.9 showed the CARS images obtained with A431, T98G and B16F10 cells after treatment with free TRF as well as TRF-loaded vesicles. Non-specific uptake of free tocotrienol and control vesicles showed little or no penetration of tocotrienol after 24 hours incubation, except in A431 cells. A431 cells incubated with control vesicles showed substantial increase in TRF signals in the nucleus and cytoplasm compared to free TRF. Nevertheless when TRF was delivered using Tf-targeted vesicles, cellular accumulation of TRF was significantly higher in all cell lines compared to free TRF or control vesicles. In terms of intracellular distribution, while treatment with control vesicles and free TRF resulted in a disseminated distribution of TRF in the cytosolic compound, cells treated with Tf-vesicles showed a much localized accumulation of TRF in the nuclei. Especially in Tf-vesicles-treated A431

and B16F10 cells, perinuclear localization of TRF was clearly visible. For enhanced nucleus penetration, perinuclear localization of TRF was believed to facilitate the delivery of TRF to the cell nucleus (Torchilin, 2005b). Besides, as opposed to the non-specific uptake observed with control vesicles and free TRF, uptake mechanism via the endocytotic pathway often leads to vesicular accumulation in the perinuclear region, further supporting the fact that Tf-vesicles were most probably transported into the cells via endocytosis-mediated pathway (Torchilin, 2005b).

A431
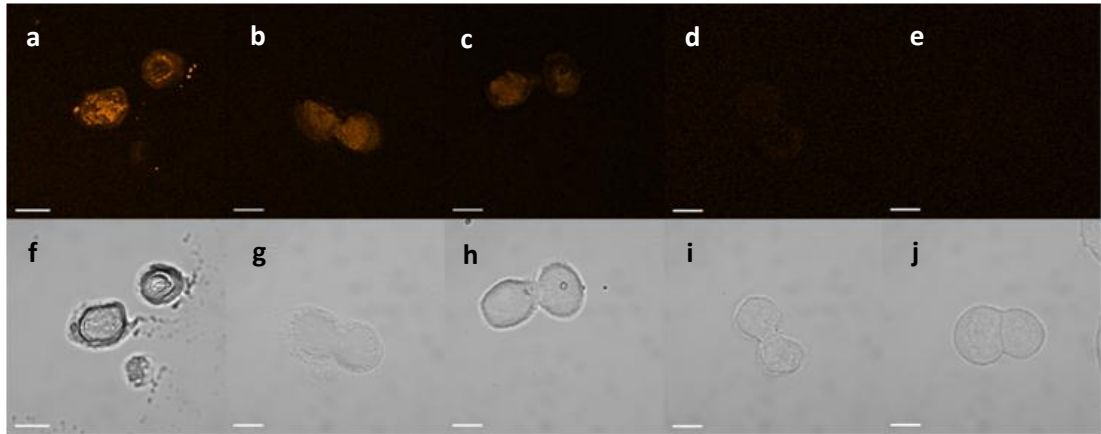
B16F10
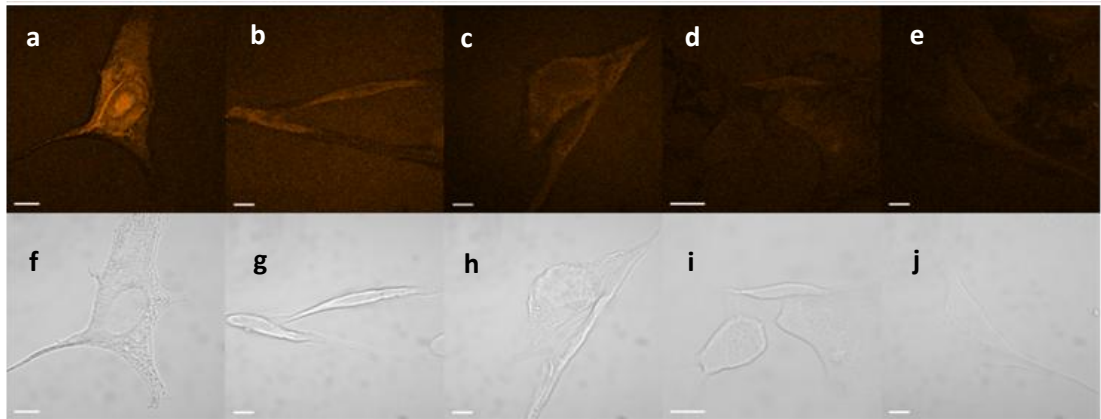
T98G
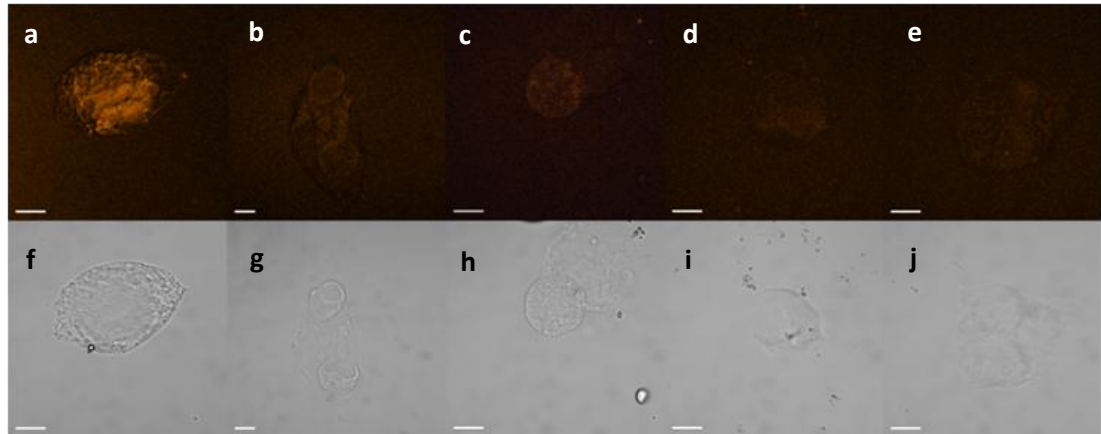
Figure 3.9: Optically-sectioned CARS images in the x-y lateral plane (a-e) and transmission images (f-j) of three cancer cell lines A431, B16F10 and T98G after treatment with (a/f) Tf-vesicles, (b/g) control vesicles, (c/h) plain vesicles, (d/i) free TRF and (e/j) untreated cells. Microscope settings identical to Figure 3.5.
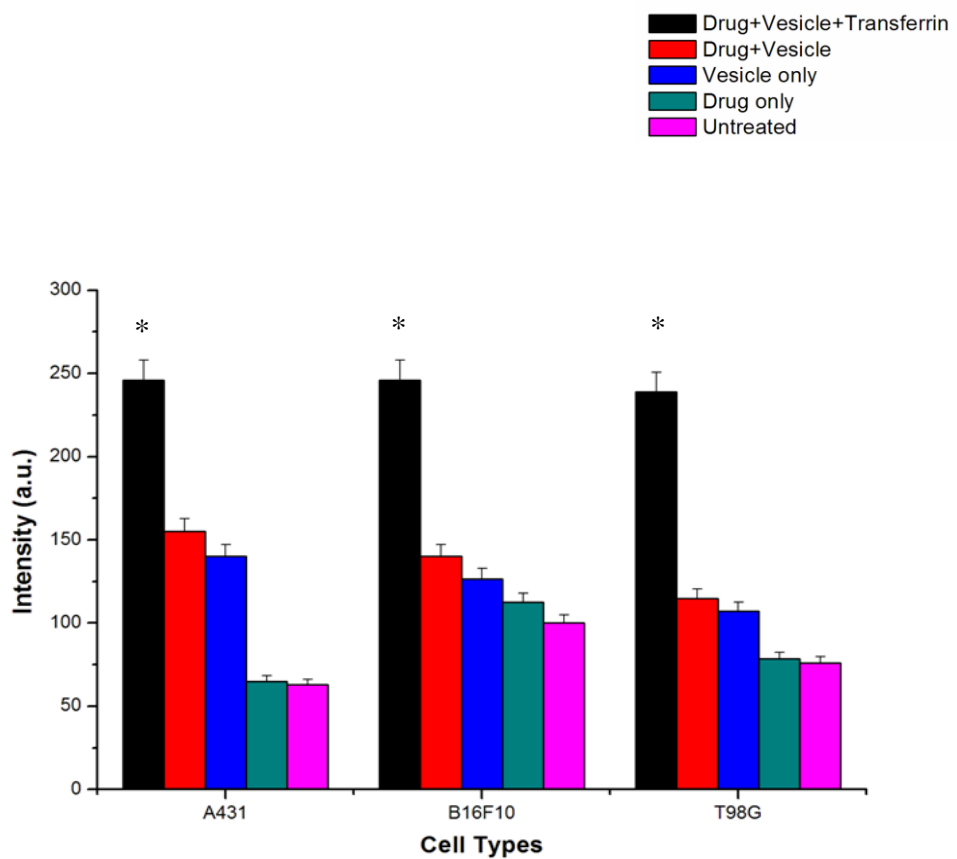
Figure 3.10: Qualitative analysis of TRF cellular uptake in cells treated with Tf-vesicles (black), control vesicles (red), plain vesicles (blue), free TRF (green) and untreated cells (violet) by CARS (*n*=10) (*: $p < 0.05$ against other treatment groups). Measurements obtained as in Figure 3.6.

CARS signals in Figure 3.10 were quantified using the average intensity of a 10 μm x 10 μm square area at the brightest position in the cell. A baseline intensity of 50-100 a.u. was detected in the untreated cells of all three cancer cell lines. Minimal penetration of tocotrienol was observed in cells treated with free tocotrienol recording CARS signals indifferent from untreated cells. When normalised against baseline untreated cells, at least 2-fold increase in TRF-associated CARS signal (except for B16F10 cells) was observed in control vesicles-treated cells compared to cells treated with free tocotrienol. A further 2-fold increase (in T98G and B16F10

cell lines) was measured when vesicles were targeted with transferrin. A431 cells recorded the highest improvement with control vesicles whereas T98G cells showed highest targeting efficacy with transferrin vesicles compared to non-targeted vesicles. Nevertheless, it should be noted that plain vesicles recorded a slightly higher CARS signal compared to baseline untreated cells. This is not surprising as TPGS is a derivative of α-tocopherol, thus its association in the cells might have been readily detected by the Raman laser distinguishable for TRF.
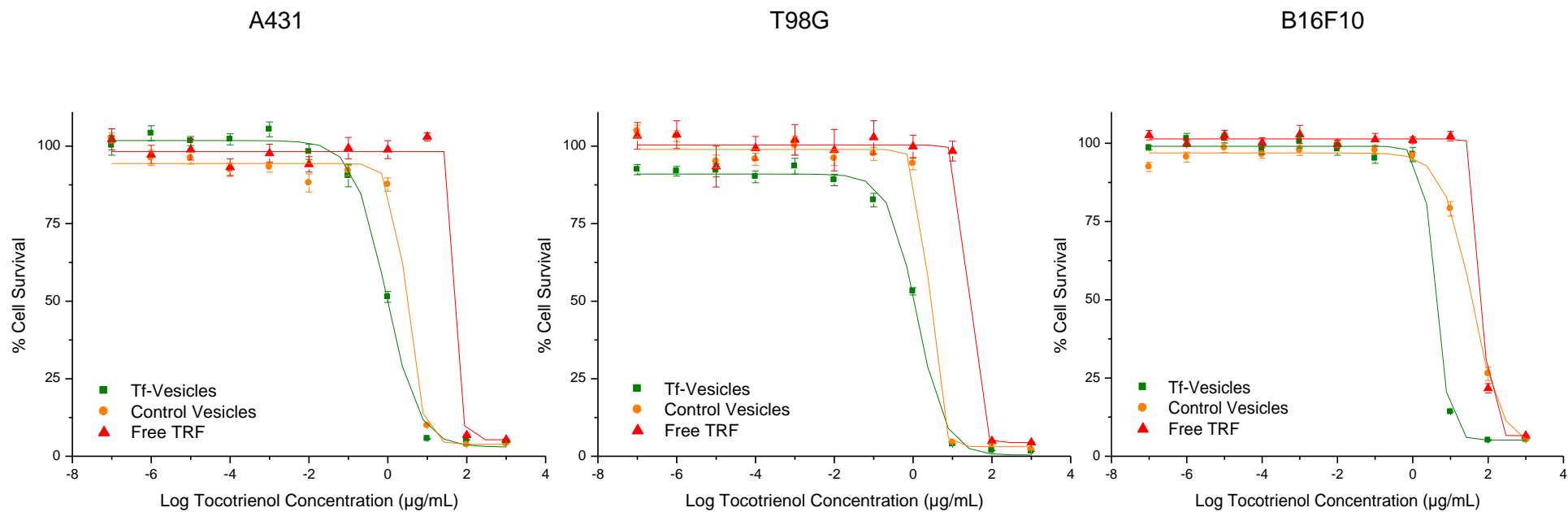
Figure 3.11: Anti-proliferative activity of TRF delivered as free TRF (red) or entrapped in Span 60/TPGS vesicles. Treatment with Tf-vesicles was represented in green and control vesicles in orange against A431, T98G and B16F10 cells ($n = 15$).

Table 3.2: Anti-proliferative activity of free TRF or TRF formulated in Tf-vesicles or control vesicles in A431, T98G and B16F10 cells expressed as IC_{50} values ($n = 15$).

Cell lines	IC_{50} (µg/mL) (mean ± S.E.M.)		
	Tf-vesicles	Control vesicles	Free TRF
A431	0.89 ± 0.11	3.07 ± 0.79	64.72 ± 2.47
T98G	1.24 ± 0.13	2.58 ± 1.23	26.48 ± 2.86
B16F10	4.09 ± 0.65	36.98 ± 4.52	71.86 ± 6.01

Concentration curves for TRF entrapped in Span 60/TPGS vesicles (as shown in Figure 3.11) showed a typical increase in TRF anti-proliferative effect with increasing TRF concentration. Sigmoidal fittings were subsequently done to elucidate the IC_{50} values for each treatment after 72 hours incubation with the cells. In A431 cells, TRF was found to be at least 20-fold more potent when encapsulated in control vesicles, while a further 3-fold improvement was obtained when vesicles were targeted with transferrin. On the other hand, IC_{50} obtained in T98G cells treated with control vesicles and Tf-vesicles were 10-fold and 20-fold lower compared to IC_{50} of free TRF. For B16F10 cells, although a mere 2-fold improvement was observed when encapsulating TRF in control vesicles, Tf-targeted vesicles generated the highest transferrin targeting efficacy of up to 9-fold improvement in relative to non-targeted vesicles. In consistent with results obtained using Span 60/Solulan C24 vesicles, the therapeutic efficacy of TRF was substantially improved when formulated in vesicles, ranging from 2-fold to 80-fold improvement depending on cell lines. Targeting of vesicles with transferrin further improved TRF therapeutic efficacy by at least 2-fold with IC_{50} ranging from 0.05 ± 0.02 to 4.09 ± 0.65 µg/mL.

Similar to Span 60/Solulan C24 vesicles, Span 60/TPGS vesicles were found non-toxic *in vitro* and *in vivo* (data not shown). However, comparing table 3.2 and table 3.1, a significant difference (p-value = 0.2041) in IC_{50} values was observed in cells treated with free TRF (between Span 60/Solulan C24 and Span 60/TPGS vesicles) although studies were done on the same cell lines (A431 and T98G). This discrepancy might be attributed to the batch-to-batch variation of TRF extract. As the source of TRF was obtained from the extraction of palm oil, it is not possible to produce identical composition of individual tocotrienol isoforms at each extraction, depending on the condition of palm oil produced. These variations may be due to the time of collection and geographical source (i.e. altitude) from which the palm oil was collected. Nevertheless, the tocotrienol content should not be significantly different between batches, although the amount of impurities might vary. Collectively, elevated cellular accumulation of tocotrienol correlated well with its therapeutic efficacy, i.e. significantly higher when entrapped in transferrin-targeted vesicles, followed by control vesicles when compared against free tocotrienol.

3.4   DISCUSSION

Despite established data confirming the anti-proliferative activity of tocotrienol on cancer cells, efficient delivery of tocotrienol to target cells is still a major concern. When incubated as a free drug in cell culture growth medium, less than 50 nM tocotrienol was taken up by the cells at various time points, which is equivalent to about 1 % uptake of the total tocotrienol added (Sylvester, 2009). Two mechanism of *in vitro* vitamin E uptake in the free drug form was proposed. First being the lipophilic interaction between tocotrienol and cell membrane (Simone and Palozza, 2009). Many have shown that tocotrienol has superior biological effect compared to tocopherol, attributed to its higher cellular accumulation. Having an unsaturated polyenoic chain, tocotrienols possess higher mobility and flexibility in their interaction with membrane lipids, thus are more readily incorporated into the bilayers of cellular membrane (Simone and Palozza, 2009). Membrane fusion, is a transport process for vesicles or virus particles to gain entry into cells. It is a common process where two lipid entities fuse into one membrane, spilling the contents of the entity into cellular cytoplasm (Ware *et al.*, 2004). On the other hand, Negis *et al.* (2007) proposed that an active transport pathway was involved when intracellular mechanism of α-tocopheryl-phosphate uptake was studied. According to this paper, loss of tocopherol activity was observed in the presence of active transport inhibitors, blocking tocopherol penetration into cells. Although it signified the role of active transport involved in vitamin E cellular internalization, no experimental data has yet confirm which protein or pathways are responsible in the mechanism.

A study by the group of Noguchi reported a detail account of the uptake and distribution of tocotrienols in cultured cells (Noguchi *et al.*, 2009). As cells were treated with 1 μM of α-tocotrienol and α-tocopherol, the cellular content of tocotrienol was increasing linearly with increasing incubation time and reaches a plateau after 6 hours incubation. Consistent results were obtained from Sylvester's analysis when cells treated with tocotrienol at 5 μM concentration showed a linear uptake profile and start to plateau after 6 hours incubation (Sylvester, 2009). For tocopherol however, an increase in cellular uptake was observed with increasing incubation time up to 72 hours, yet cellular level of tocopherol was more than 6 times lower than that of tocotrienol (Noguchi *et al.*, 2009). In addition, treatment with up to 120 μM tocopherols was needed to obtain cellular concentration similar to those obtained with 5 μM tocotrienols (Sylvester, 2009). It was then concluded that the cellular uptake between tocopherol and tocotrienol could be considerably different despite similar chemical properties, that tocotrienol was more readily taken up by the cells at a faster rate.

Cellular distribution of tocotrienol as free drug has also been quantified by fractionation method using differential centrifugation. Both α-tocopherol and α-tocotrienol were found to accumulate most profoundly in mitochondrial fraction, followed by microsomal fraction, nuclear fraction and less apparent in the cytosolic fraction (Noguchi *et al.*, 2009). In consistent to this notion, cellular distribution of α-tocopherol showed a similar trend when incubated with rat pheochromocytoma PC12 cells (Saito *et al.*, 2009). Nevertheless, contradictory findings were revealed in a report published in 2006. When analyzed using human colorectal adenocarcinoma

Caco-2 cells, Anwar and colleague found that the microsomal fraction contained the highest amount of α-tocopherol (up to 39 %) contrary to mitochondrial fraction as reported earlier (Anwar *et al.*, 2006). Second to microsomal fraction was cytosolic fraction, followed by mitochondria fraction, while very little tocopherol was detected in the nuclear fraction (Anwar *et al.*, 2006).

Nevertheless, using appropriate nanocarriers, the *in vitro* behaviour of tocotrienol encapsulated in niosomes was altered dramatically. With non-targeted control vesicles, approximately 10-15 % of tocotrienol has penetrated into A431, T98G and A2780 cells at the time of analysis (Figure 3.7). This is a significant increase compared to the reported 1-6 % incorporation when treated with free tocotrienol (Sylvester, 2009). With regard to improved tocotrienol delivery, the portals of entry into the cells are crucial. Transport of molecules across the cells occurs via two broad categories, phagocytosis and pinocytosis. While phagocytosis are conducted primarily in specialized cells such as macrophages, monocytes, and neutrophils, pinocytosis is the most common mechanism for the uptake of fluid and solutes, generally occurring via four basic mechanism: macropinocytosis, clathrin-mediated endocytosis, caveolae-mediated endocytosis as well as clathrin- and caveolae- independent endocytosis (Figure 3.12) (Conner and Schmid, 2003). In cancer cells, the intracellular fate of non-specific nanocarriers, depending on their physicochemical characteristics, is dominated by endocytosis (Kelf *et al.*, 2010). This was proven in cellular studies when energy-dependent endocytosis was abolished (at 4°C), significant inhibition of nanoparticle uptake was observed (Chiu *et al.*, 2010; Kelf *et al.*, 2010). For example, detailed cellular trafficking experiments

using specific pathway inhibitors showed that clathrin-mediated endocytosis was the predominant internalization method for quantum dot nanoparticles (Kelf *et al.*, 2010). With hydrophobically modified chitosan nanoparticles, the internalization route was clearly related to lipid raft-mediated endocytosis and caveolae-mediated endocytosis (Chiu *et al.*, 2010).

Clathrin-mediated endocytosis (CME) is generally a rapid internalization process occurring constitutively in all mammalian cells for uptake of nutrients, macromolecules and plasma membrane constituent (Conner and Schmid, 2003). It was previously referred to as receptor-mediated endocytosis because it involves the concentration of high-affinity transmembrane receptors and their bound ligands into clathrin coated pits, subsequently pinching off the pit to form early endosomes (Conner and Schmid, 2003). Examples of receptor-mediated CME include LDL receptor and transferrin receptor. However, it has been clarified that non-specific CME also exists via non-specific electrostatic and hydrophobic interactions with cell membrane (Hillaireau and Couvreur, 2009). Caveolae-mediated endocytosis (CvME) are characteristics flask-shaped membrane invaginations, generated from the ruffling of the cell membrane to form large troughs (Kelf *et al.*, 2010). It is a genuinely non-specific process, essentially slower than that of the clathrin internalization, hence lower efficiency (Kelf *et al.*, 2010). Macropinocytosis on the other hand is a process similar to phagocytosis but their protusions do not zipper up along the ligand-coated particle, instead they collapse and fuse with plasma membrane (Conner and Schmid, 2003). Little is known about this pathway as it does not seem to display any selectivity, but it is clearly involved in the uptake of drug nanocarriers (Hillaireau

and Couvreur, 2009). Clathrin- and caveolin-independent endocytosis involves lipid rafts, where unique lipid compositions forms the physical basis for specific sorting of membrane proteins (Conner and Schmid, 2003). These lipid rafts are cholesterol- and sphingolipid-enriched microdomains, presumably able to be captured by, and internalized within any endocytic vesicle (Conner and Schmid, 2003; Chiu *et al.*, 2010).
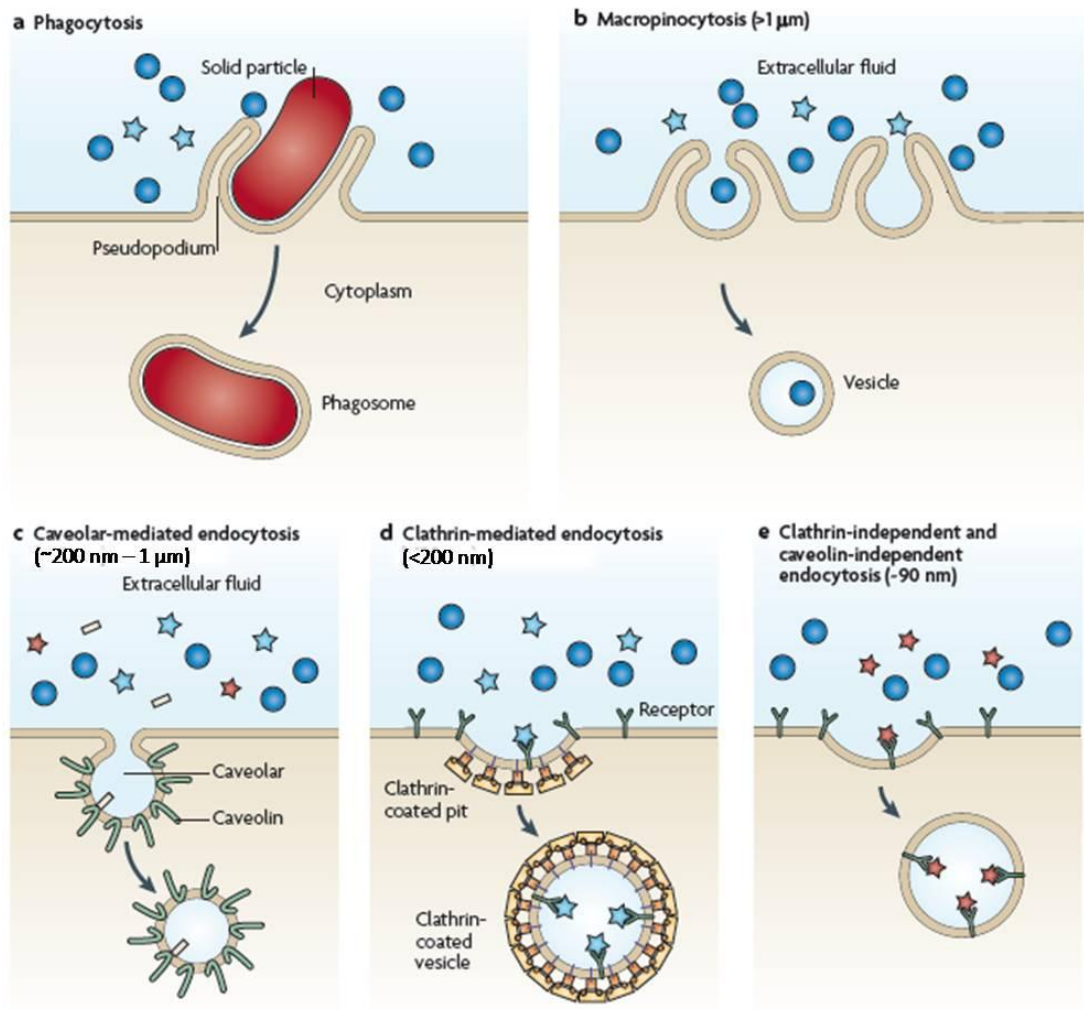
Figure 3.12: Modes of cellular internalization of nanocarriers. Internalization of large particles is facilitated by phagocytosis (a). Nonspecific internalization of particles > 1 μm might occur via micropinocytosis (b). Smaller nanocarriers can be internalized through several pathways, including caveolar-mediated endocytosis (c) clathrin-mediated endocytosis (d) and clathrin- and caveolin-independent endocytosis (e) *(Modified from Petros et al., 2010).*

Many physicochemical and environmental factors can influence the cellular uptake of nanocarriers, as to which cargo or trafficking pathway was chosen to import the particles. In general, particle size, charge and surface properties of non-specific nanocarriers are crucial determinants. For example in particle size, macromolecules of 200 nm to 1 μm are most likely to be transported via caveolae-mediated endocytosis, whereas clathrin-mediated endocytosis is typically associated with particles with a size limit of around 200 nm (Decuzzi and Ferrari, 2008; Hillaireau and Couvreur, 2009; Kelf *et al.*, 2010). For particles over 1 μm in size, macropinocytosis becomes a major mechanism of internalization, although the uptake rate starts to drop dramatically for particles above 1 μm due to the difficulty of forming large vesicles (Kelf *et al.*, 2010). Besides, phagocytosis and subsequent clearance from the reticular-endothelial system (RES) are more prone to particles of sizes 250nm to 3 μm (Hillaireau and Couvreur, 2009).

The role of surface charge in the uptake rate of a nanocarrier relies on its interaction with the cell membrane. As mentioned in Chapter 2, positively charged nanocarriers display better association and internalization rates as a result of attractive interaction with negatively charged cell membrane (Hillaireau and Couvreur, 2009). However, as far as surface charge is modified to increase cellular uptake, care is taken not to compromise the specificity of nanocarriers to cancer cells. Another surface property that greatly influences a nanocarrier's cellular uptake is the surface coating. During preparation of nanocarriers, long chain hydrophilic polymers (e.g. PEG) are often incorporated in order to create high steric stabilization while preventing the particles from rapid clearance by the RES. These coatings however

were reported to impose controversial effects on cellular uptake efficiency. *In vitro*, a decrease in cellular accumulation of PEG-derivatized nanoparticles compared to their uncoated counterparts was observed (Kelf *et al.*, 2010). Surface shielding from PEG polymers is believed to attenuate the electrostatic interaction between positively charged particles and cell membrane in addition to a shielding effect on the terminal groups of particle surface, leading to a decrease in non-specific internalization (Kelf *et al.*, 2010). However when administered *in vivo*, elevated accumulation of nanocarriers in cancer cells can be achieved via PEG coating, most probably due to prolonged blood circulation time (Hillaireau and Couvreur, 2009). Other than the above mentioned factors that influence the efficiency of internalization of a nanocarrier, surface decoration of nanocarriers with targeting ligands is responsible to promote specific delivery of the nanocarriers. Such specific ligand-receptor internalization mechanism was exploited in our study using transferrin as a targeting moiety.

In addition to the superior cellular uptake using niosome as a carrier system for tocotrienol, active targeting using transferrin as a binding ligand further enhanced its cellular penetration via specific recognition to the overexpressed transferrin receptors on cancer cells. Compared to the 10-15 % tocotrienol accumulation using non-targeted niosomes, transferrin-bearing vesicles were able to deliver as much as 23 % of the total tocotrienol added (Figure 3.7). As for Span 60/TPGS vesicles, when quantified using CARS microscope, at least 2-fold higher of a tocotrienol accumulation was observed in T98G and B16F10 cells (Figure 3.10). From a chemistry point of view, this is an indication that transferrin molecules attached to

the vesicle surface were accessible to transferrin receptors for specific recognition, thus facilitating the transport of tocotrienol across cellular barriers. Presumably , if conjugation of transferrin to drug molecules or drug carriers does not affect the binding and dissociation properties of transferrin, which has been proven with transferrin-doxorubicin conjugate, the internalization of transferrin-targeted niosome should be similar to the mechanism of transferrin internalization described earlier (Chapter 1) (Qian *et al.*, 2002). Receptor-mediated endocytosis is the most versatile type of cellular transport, involving a high degree of recognition and specificity (Ware *et al.*, 2004). Briefly, upon receptor binding, ligand bound receptor complex undergoes endocytosis forming early endosomes. In most cases, these early endosomes mature into late endosomes containing hydrolases, then become lyososomes containing more digestive enzymes that act to degrade their contents (Ware *et al.*, 2004). Transferrin receptor-mediated endocytosis however differs from them, i.e. having the ability to avoid the lysosomal compartment (Wagner *et al.*, 1994; Ishida *et al.*, 2001). After iron is released at low endosomal pH, transferrin-bound receptors are usually being sorted into exocytic vesicles to be recycled to cell surface (Iinuma *et al.*, 2002). Thus combining the effect of specific uptake and lysosomal bypass, cellular accumulation of tocotrienol was significantly elevated using transferrin-targeted niosomes. Assuming that therapeutic efficacy is principally depending on the amount of tocotrienol being delivered into cells, anti-proliferative studies (MTT assays) were conducted to prove the point.

Indeed, with a 2-fold increase in cellular tocotrienol concentration, IC_{50} was improved by at least 80-fold when treated with control vesicles. As for transferrin targeted vesicles, a further 2-fold increase in cellular accumulation subsequently led to another 2 to 5-fold improvement of IC_{50} concentrations, i.e. as much as 200-fold improvement compared to free tocotrienol. For many years, lack of activity of tocotrienol has been associated with inefficient cellular delivery, mostly owing to the hydrophobic nature of tocotrienol. Here, the crucial correlation between cellular delivery and biological activity was further emphasized. In fact we managed to prove that tocotrienol, when delivered efficiently to cancer cells can exert potent anti-proliferative effect. In addition to the efficiency of tocotrienol delivery, the intracellular location at which tocotrienol was accumulated in the cells is equally important. Both confocal microscopy and CARS microscopy demonstrated a different location of accumulation among tocotrienol administered as free drug or when encapsulated in targeted and non-targeted vesicles.

As mentioned earlier in this discussion, tocotrienol administered as free drug is mostly accumulated in the microsomal or mitochondrial fractions, but little was detected in the cytosol and nucleus fraction. Correlating with its mechanism of action (discussed in Introduction), lack of cytosol and nucleus penetration might hamper the activity of tocotrienol to a great extent. Cytosolic proteins from the TRAIL receptor cascade, DR-4, DR-5; NF-κB proteins from TNF receptor pathway and Raf-1 protein from the GF receptor pathway are located in cellular cytosol, while tumour suppressor gene p53 is located in the nucleus. With transferrin-targeted niosomes, tocotrienol was internalized via a different mechanism. Profound co-localization of

tocotrienol in cell nucleus upon treatment with Tf-vesicles was a favourable outcome, as shown in confocal microscopy images (Figure 3.3). Instead of being directed towards the microscomal organelles, tocotrienol entrapped in Tf-targeted vesicles can now be transported towards cell nucleus, where it is most likely to be exerting its anti-proliferative activity. Enhanced distribution of tocotrienol to the nucleus with Tf-vesicles was further confirmed using CARS microscopy. Using chemical imaging techniques in CARS microscope, detection of tocotrienol was more accurate because it was based on the intrinsic vibrational signal generated from tocotrienol molecules. For example with transferrin-targeted Span 60/TPGS vesicles (Figure 3.9), profound accumulation of tocotrienol in the perinuclear region and cell nucleus was observed. Especially in the case of A431 and B16F10 cells, a clear indication of endocytotic transport mechanism was portrayed. A review written by Torchilin reported similar observations with vitamin K3 nanoparticles and peptide-targeted liposomes (Torchilin, 2005b). A typical pattern of intracellular localization of liposome coupled with targeting peptide was depicted. Diffused localization in the cytoplasm was observed after 1 hour incubation, followed by perinuclear accumulation after 2-4 hours, after which the total contents of the liposomes were entirely released at 9 hours post-incubation. It was believed that gradual perinuclear localization of liposomes was directly correlated with the release of liposome contents to the nucleus (Torchilin, 2005b).

In summary, enhanced cellular uptake and anti-proliferative effect of tocotrienol by encapsulation in transferrin-targeted niosomes were in agreement to our hypothesis. Despite the presence of some cell line variation, the overall positive

outcome obtained was most probably attributed to the following factors. Firstly, the role of niosome as a drug carrier system increased the amount of tocotrienol that can be administered in a controllable fashion, due to the solubilising effect of surfactants. Furthermore, being a highly hydrophobic molecule, the stability of tocotrienol in aqueous dispersion was significantly improved when encapsulated in vesicles because it is shielded from an aqueous environment, yet were able to be administered in aqueous colloidal suspension. Finally, active targeting using transferrin as a targeting ligand facilitated the internalization of tocotrienol in a specific manner. Unlike sparse diffusional accumulation observed with free tocotrienol, uptake of transferrin-targeted tocotrienol via receptor-mediated endocytosis resulted in a relatively high accumulation of tocotrienol in the cell nucleus and cytosol, rather essential for its anti-proliferative activity.

No doubt, in-depth cellular studies were able to provide an overall representation of the *in vitro* behaviour of tocotrienol, either administered as a free drug or encapsulated in targeted or non-targeted vesicles. Nevertheless, *in vitro* / *in vivo* correlation is not always a direct relationship. In all cases, *in vitro* studies offer basic knowledge of dosage adjustment, biological stability and potency of a therapeutic system before it can be carried forward for *in vivo* experiments.

Chapter 4

In vivo Evaluation

4.1   INTRODUCTION

Although cell culture experiments and biochemical studies have contributed to many recent advances in molecular physiology and drug discovery, *in vivo* study remains essential in drug development due to the complexity of biological processes (Kelland, 2004). A series of carefully constructed testing protocols are often applied for rapid and efficient evaluation of pharmaceutically active molecules prior to Phase I and II clinical trials (Kelland, 2004). In general, there are 4 phases of clinical trials. While Phase I trials investigate the best dose and the safety of a trial treatment, Phase II trials are usually focused on the therapeutic efficacy of treatment. Treatments gone through Phase II trials go into Phase III trials where a new treatment is tested against the existing standard treatment to investigate whether it gives better results. Finally, Phase IV trials are carried out with licensed drug to collect information about side effects, safety and long term risks and benefits of a drug (Cancer Research UK). Preclinical testing (Figure 4.1), when integrated with pharmacology studies, are believed to provide realistic predictive values for translation in clinical settings (Peterson *et al.*, 2004). As such, *in vivo* models are one of the most crucial studies prior to clinical trials in a drug evaluation cascade.
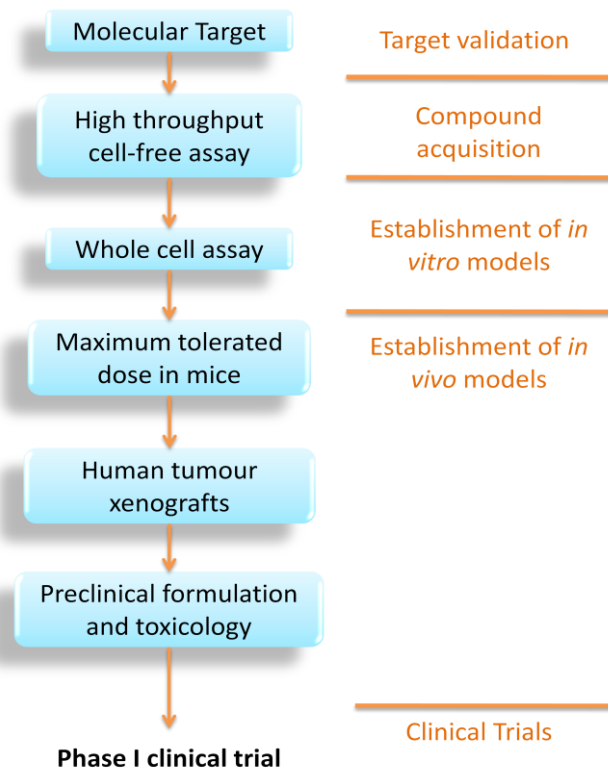
Figure 4.1: Procedures involved in preclinical testing for novel drug evaluation (*Modified from Kelland, 2004*).

4.1.1 Animal studies

Ethics in medical studies apply both to standards of professional competence and conduct and to dilemmas encountered in practice, such that the ultimate objective for maintenance and/or enhancement of human health can be achieved (ScotPIL Training manual, 2006). In laboratory animal studies, the moral balance is supported by researcher's duties and the Animals (Scientific Procedures) Act 1986. A researcher's duties, as mentioned in the following, are outlined to diminish society conflicts, including: 1) using non-animal procedure wherever possible, 2) reducing the number of animals used, 3) refining the procedures to minimize harm, 4) weighing the harms against the benefits, thus proceeding only when there is a favourable balance, 5) ensuring good communication between members of the

research community and the society (ScotPIL Training Manual, 2006). The Animals (Scientific Procedures) Act 1986, on the other hand, covers regulated procedures and aims to ensure that any research using animals is regulated and justified, and has no alternative (Wolfensohn *et al.*, 1998). This Act regulates the designated establishments where scientific procedures are to be performed in addition to ensure procedures carried out by authorized personal and project licences are appropriately justified, trained and supervised (Wolfensohn *et al.*, 1998).

For the past two decades, transplantation of human cancer cells or tumour biopsies into immunodeficient rodents (xenograft models) has constituted the major preclinical screen for development of novel cancer therapeutics (Morton and Houghton, 2007). Historically, cancer drug screening relied on inoculation of murine cancer cells on mouse models (Sausville *et al.*, 2006). From mid-1980s, the discovery of nude anythmic (nu/nu) mice that are T-cell deficient and subsequently B-cell and T-cell-deficient severe combined immunodeficient (scid/scid) mice allowed propagation of established *in vitro* human cancer cells in mouse model (Morton and Houghton, 2007). Since then, formation of solid tumours in mouse model was feasible, providing a platform for studies on tumour biology, disease progression and evaluation of therapeutic agents. While orthotopic transplantation is technically difficult, subcutaneous xenograft models are mostly selected due to the ease of tumour assessment (Sausville *et al.*, 2006). In fact, orthotopic tumour models are often limited by technical skills in order to produce vascularised tumours, hence more time-consuming and expensive (Bibby, 2004). By contrast, subcutaneous xenografts readily produce vascularised palpable tumours and are technically

straightforward where substantial data can be generated within a limited time frame (Bibby, 2004). The major challenge of these models is their practical applicability as their predictive value has been debated extensively when extrapolating the results to clinic (Peterson *et al.*, 2004; Morton and Houghton, 2007). Nevertheless, the National Cancer Institute revealed that more than 30 % of the therapeutic activity in subcutaneous xenograft models was well correlated with their respective clinical performance (Morton and Houghton, 2007).

It is generally accepted that the most reliable results are likely to be obtained when healthy animals are used. To this end, animal housing and environmental conditions are playing crucial roles (ScotPIL Training Manual, 2006). For optimum adaptation, mice are housed in groups of 5-6 with temperatures between 19 to 23 $^{\circ}$C, humidity of 40-70 %, 12-15 air changes per hour, and 12 hour daylight cycle for circadian rhythm regulation (Wolfensohn *et al.*, 1998). Light intensity should be 350-400 lx and less than 60 lx for albino mice to prevent retina damaging, while noise level should be kept minimal as mice are very sensitive to ultrasound (Wolfensohn *et al.*, 1998). The normal fed for adult mice (weight 20-40 g) is about 3-5 g of pelleted mouse diet daily and about 6-7 mL water daily (Wolfensohn *et al.*, 1998). As the consumption of food and water may vary drastically during the course of study, the experimentalist or carer ought to make sure the animals have enough supply throughout the experiment.

4.1.2 Bioluminescence imaging

In accordance to the three 'Rs' in animal studies, i.e. reduce, replace, refine, bioluminescence imaging offers a powerful imaging methodology that is more sensitive, non-invasive and less toxic. This imaging system is a versatile and sensitive tool based on the detection of light emission from cells or tissues (Sato *et al.*, 2004). In the assessment of tumour load, genetically engineered cancer cells carrying the luciferase gene are inoculated (Klerk *et al.*, 2007). The most common luciferase genes (*Fluc*) are extracted from North American firefly *Photinus pyralis*, other examples of bioluminescence include Renilla luciferase gene (*Rluc*) from sea pansy, as well as luciferases cloned from corals, click beetle and several bacterial species (Sadikot *et al.*, 2005). Production of luciferase enzyme from *luc* genes is able to catalyse the oxidation of substrate D-luciferin to non-reactive oxyluciferin, meanwhile emitting photons of light at 562 nm (Sato *et al.*, 2004). The intensity of emitted light can be converted into a pseudocolour graphic which then provides a visual interpretation of tumour growth, regression, metastases and to monitor the efficacy of a therapeutic intervention (Sato *et al.*, 2004; Welsh and Kay, 2005). In particular, detection of the photon flux by a sensitive optical imaging system, such as the IVIS spectrum, an absolute quantification of the bioluminescent signal can be performed and displayed as an intensity map (Lim *et al.*, 2009). It was previously proven that the bioluminescence profile of a tumour growth was synchronized with the results obtained using calliper measurements (Sato *et al.*, 2004).

A major advantage of bioluminescence imaging is the ability to construct longitudinal studies in living organisms where multiple measurements can be made in the same animal over time, thus providing information on the various stages of tumour development (Sadikot *et al.*, 2005; Klerk *et al.*, 2007). This will potentially reduce the number of animals required for experimentation while minimizing the effects of biological variation (Sadikot *et al.*, 2005). The depth of light emission is able to penetrate tissues of several millimeters to centimeters, allowing organ-level resolution (Sato *et al.*, 2004; Sadikot *et al.*, 2005). Compared with fluorescence imaging where quenching of autofluorescence by tissue components causes significant interference at wavelengths below 600 nm, high signal-to-noise ratios can be achieved with bioluminescence imaging because mammalian tissues do not naturally emit bioluminescence (Klerk *et al.*, 2007). Therefore bioluminescence images can often be generated with very little background signals. In addition, the need for exogenous illumination such as fluorescence labelling is known to bleach the reporter, perturb physiology in light-sensitive tissues and cause phototoxic damage to cells (Welsh and Kay, 2005). Bioluminescence imaging potentially avoids these problem, hence is an ideal system for long term studies in living organisms (Welsh and Kay, 2005). However, as luciferase reaction is ATP-dependent, only metabolically active cancer cells contribute to bioluminescence signals (Klerk *et al.*, 2007). Therefore, necrotic areas in the tumour are usually correlated with reduced bioluminescence, even if the tumour mass remained unchanged (Lim *et al.*, 2009).

When changes in tumour mass was correlated in relative to the initial bioluminescence signal of animals, a good indication of the actual tumour mass and its bioluminescence signal can be achieved, providing accurate quantification of tumour growth (Klerk *et al.*, 2007). Consequently, the number of animals needed in order to produce robust scientific data can be significantly reduced (Sato *et al.*, 2004). Besides, the pathophysiology of diseases may be better understood using bioluminescence imaging, or a combined approach with ultrasound or magnetic resonance imaging (Sato *et al.*, 2004; Klerk *et al.*, 2007).

4.1.3   Aims and Objectives

From *in vitro* evaluations reported in Chapter 3, therapeutic efficacy of tocotrienol, when entrapped in transferrin-targeted niosome was rather positive, compared to free tocotrienol. Following the paradigm of drug evaluation, human tumour xenografts are no doubt one of the most common animal models used to obtain preclinical data prior to clinical trials. In this chapter, murine models of transplanted human epithelial carcinoma A431 cells were used to assess the therapeutic efficacy of tocotrienol, when administered intravenously as free drug or when entrapped in transferrin-targeted and non-targeted niosomes. Assessment of antitumour activity is based on relative tumour growth, tumour response, animal survival and general toxicity based on animal weight. Similar experiments were carried out using murine melanoma cells modified with luciferase gene (B16-F10-luc), to be implanted in mice models for bioluminescence imaging.

4.2 MATERIALS AND METHODS

4.2.1 Materials

Materials	Supplier
Span 60/Solulan C24 vesicles	Prepared as described in Chapter 2
Span 60/TPGS vesicles	Prepared as described in Chapter 2
Dulbecco's Modified Eagle Medium (DMEM)	Invitrogen, UK
Roswell Park Memorial Institute (RPMI)-1640 medium	Invitrogen, UK
L-Glutamine	Invitrogen, UK
Penicillin-Streptomycin	Invitrogen, UK
Trypsin	Invitrogen, UK
Dimethyl sulfoxide (DMSO)	Sigma-Aldrich, UK
D-glucose	Sigma-Aldrich, UK

4.2.2 Cell culture

A431 and B16-F10-luc-G5 cell lines were grown as monolayers in DMEM and RPMI-1640 medium respectively. Growth medium were supplemented with 10 % v/v foetal calf serum, 1 % v/v L-glutamine and 0.5 % v/v penicillin-streptomycin. Cells were cultured at 37 ^{o}C in a humid atmosphere of 5 % CO_2.

4.2.3 Animals

Female immunodeficient BALB/c mice (initial mean weight 20 g) housed in groups of five at 19 ^{o}C to 23 ^{o}C with a 12-hour light-dark cycle were fed a conventional diet (Rat and Mouse Standard Expanded, B&K Universal, Grimston, UK) with mains water *ad libitum*. Experimental work was carried out in accordance with UK Home Office regulations and approved by local ethics committee.

4.2.4 Antitumour activity

Tumours were palpable (typical diameter 5 mm) 6 days after subcutaneous implantation of A431 and B16-F10-luc-G5 cancer cells in exponential growth (1×10^6 cells per flank). TRF entrapped in Tf-vesicles, control vesicles or as free drug was administered by intravenous tail vein injections (10 μg TRF per injection). Free TRF was prepared in DMSO at 5 mg/mL. Once a day of daily injections were scheduled for 10 days for the preliminary experiments. The experiment was repeated on a another set of animals and extended to 20 days. Animals were weighed daily and tumour volume was determined by calliper measurements calculated as follows:

$$\text{Tumour volume} = d^3 \times \pi/6$$

Where d: tumour diameter measured using callipers

Results were expressed as relative tumour volume:

$$\text{Rel. Vol}_{tx} = \text{Vol}_{tx} / \text{Vol}_{t0}$$

Where Rel. Vol_{tx}: relative tumour volume; Vol_{tx}: tumour volume on the day of treatment; Vol_{t0}: initial tumour volume on the first day of experiment.

Tumour response was classified analogous to Response Evaluation Criteria in Solid Tumours (RECIST) guidelines (Eisenhauer *et al.*, 2009). Progressive disease is defined as an increase in relative tumour volume of higher than 1.2-fold, stable disease as a relative volume between 0.7 and 1.2 of starting volume, partial response as measureable tumour with a reduction of more than 30 % (0 to 0.7-fold) and complete response as the absence of any tumour.

4.2.5   Bioluminescence imaging

Bioluminescence imaging of treatment-induced antitumour effect was visualized using an IVIS® Spectrum (Caliper Life Sciences, USA). Mice bearing subcutaneous B16-F10-luc-G5 tumours were treated intravenously as described above on a daily injection for 10 days. On alternate days (i.e. days 1, 3, 5, 7, 9, 11), imaging procedures were carried out after intraperitoneal injection of luciferase substrate D-luciferin solution (150 mg/kg body weight) and anaesthetized by isoflurane inhalation. Light emission was measured 10 minutes after injection of D-luciferin using Living Image software. Resulting pseudocolour images represented the spatial distribution of photon counts within the tumour. Identical illumination settings were synchronized for all images acquired.

4.3 RESULTS

4.3.1 Antitumour activity

Following the positive results obtained for Span 60/Solulan C24 and Span 60/TPGS vesicles from *in vitro* experiments, the *in vivo* therapeutic efficacy of both formulations were examined in mice bearing A431 tumour xenografts. In addition, with the aid of an IVIS system, tumour progression of murine B16-F10-luc tumours was evaluated using conventional quantification method as well as bioluminescence imaging system.

4.3.1.1 Span 60/Solulan C24 Vesicles

In A431 tumour xenograft, tocotrienol entrapped in Tf-targeted vesicles induced a measurable reduction in tumour volume within the first 24 hours post-injection (Figure 4.2A). Daily injections for 10 days with Tf-vesicles led to a marked tumour regression in mice bearing A431 tumours, in fact the antitumour effect of Tf-vesicles was at its maximum efficacy at Day 10 where tumour growth was reduced by more than 30-fold compared to untreated tumours. On the contrary, no significant advantage was observed in mice treated with control vesicles and free tocotrienol, albeit a slight decrease in tumour growth during the course of treatment. However upon treatment cessation, the relative growth rate of tumours treated with control vesicles and free tocotrienol was no different than that of untreated tumours, whereas Tf-vesicles-treated tumours were re-growing at a much slower rate than the other treatment groups. According to the RECIST guidelines, 40 % of tumours treated with Tf-vesicles were stable on the last day of injections while the remaining 60 %

showed a partial response (Figure 4.3B). By contrast, 100 % of tumours treated with control vesicles and free tocotrienol were progressive.

The overall effect of Tf-vesicles led to an extended survival of tumour-bearing mice for 19 days compared to untreated mice, while 12 days and 2 days extended survival was observed in mice treated with control vesicles and free tocotrienol (Figure 4.3A). Systemic use of tocotrienol, when administered as free drug or entrapped in vesicles was well tolerated in tumour-bearing mice, without apparent signs of toxicity. From daily measurements of relative animal weight, accumulating data showed no significant weight loss, that the variations in animal weights were less than 10 % for all treatment groups (Figure 4.2B). Due to tumour regrowth observed after cessation of treatment, the scope of improvement was focused on two major factors: extending the length of treatment and using a higher dose of tocotrienol.
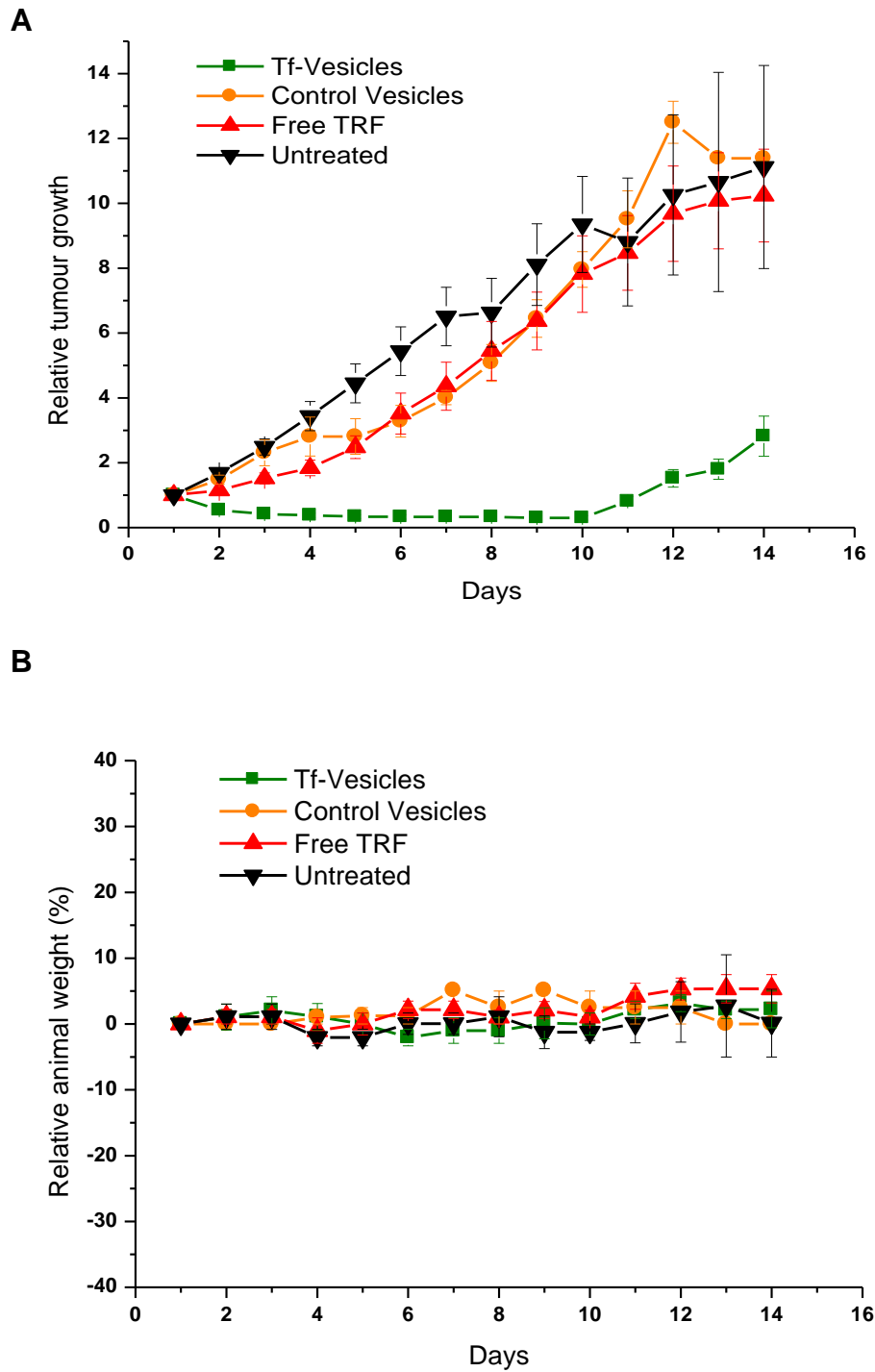
Figure 4.2: Antitumour studies in a mouse A431 xenograft after intravenous administration of tocotrienol entrapped in Span 60/Solulan C24 vesicles. (A) Relative tumour growth upon 10 injections of Tf-vesicles (green), control vesicles (orange), free tocotrienol (red) and untreated tumours (black) *(n=5)*. (B) Variations of the animal body weight throughout treatment regime *(n=5)*.
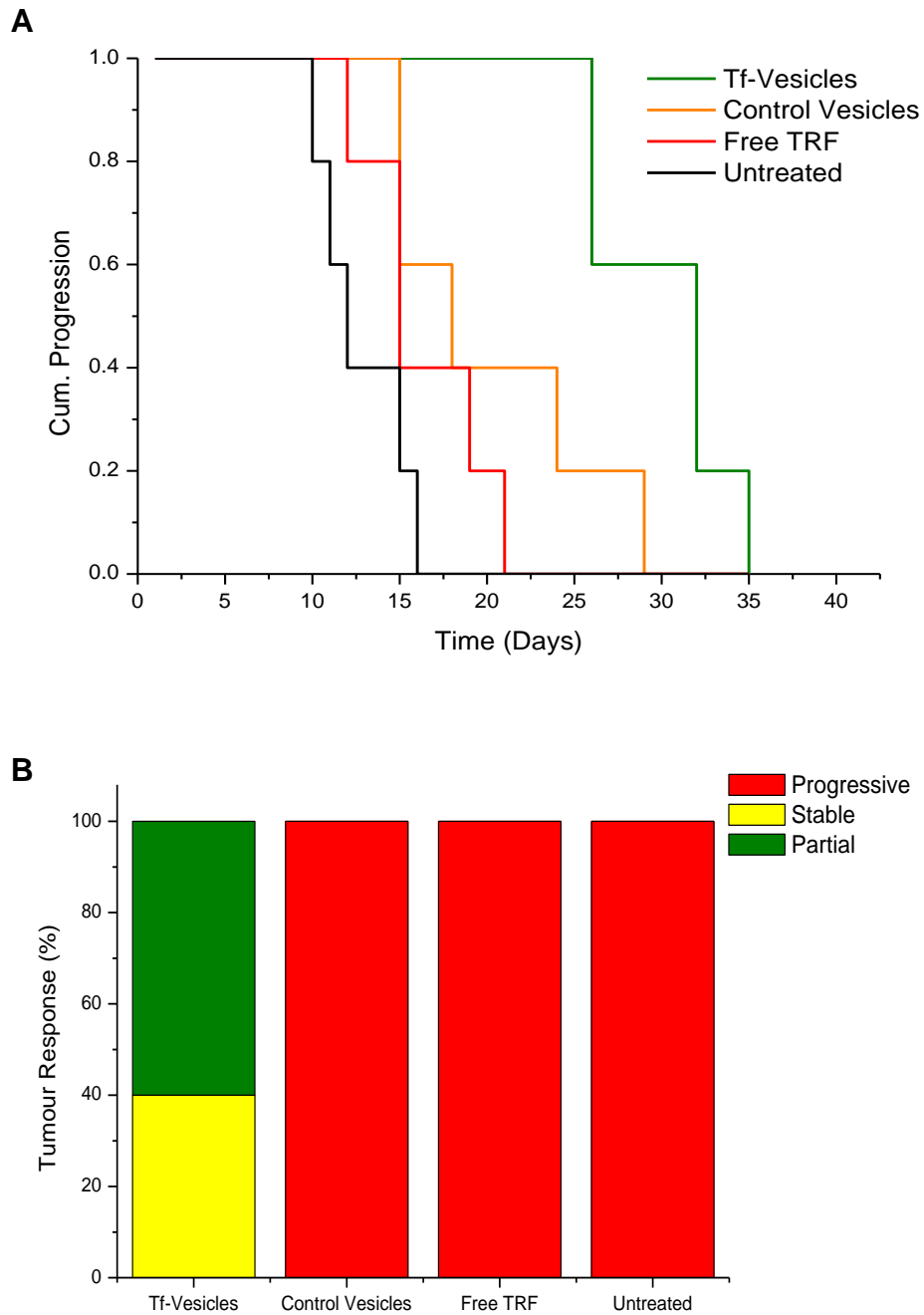
Figure 4.3: Antitumour studies in a mouse A431 xenograft after intravenous administration of tocotrienol entrapped in Span 60/Solulan C24 vesicles. (A) Time to disease progression where animals were removed from the study once their tumour reached 12 mm diameter. Tf-vesicles (green), control vesicles (orange), free tocotrienol (red) and untreated tumours (black). (B) Overall tumour response to treatments, stratified according to change in tumour volume.

When duration of treatment was extended from 10 injections to 20 injections, all mice treated with Tf-vesicles survived for at least 24 days, whereas mice in the other treatment groups had been sacrificed before Day 15 due to tumour growth reaching 12 mm diameter. The maximum tumour size allowed by our Project Licence was 12 mm in diameter as tumour beyond this diameter might cause considerable discomfort to animals. Consistent to previous observation with 10 injections, treatments with control vesicles and free tocotrienol did not initiate measureable tumour regression, although the tumour growth rate was slower than that observed with untreated mice. With Tf-vesicles however, the antitumour effects induced by tocotrienol were prominent, including significant tumour regression and prolonged absence of tumour regrowth (Figure 4.4A). From Day 15 onwards, 60 % of tumours started showing signs of regrowth while 40 % of tumours remained regressed. With continued observation, one animal (20 %) from the Tf-vesicles group was tumour-free, while 20 % of tumours showing partial response to treatment and the remaining 60 % was defined as progressive tumours (Figure 4.5B). Treatment with control vesicles was less successful (10 % partial response, 10 % stable response, 80 % progressive) whereas tumours receiving free tocotrienol were 100 % progressive. Therefore when disease progression was analysed against time, treatment with free tocotrienol did not prolong the survival of animals compared to untreated mice (Figure 4.5A). On the contrary, mice receiving Tf-vesicles and control vesicles showed an extended survival of 23 days and 8 days respectively, compared to untreated mice. Again, no apparent signs of toxicity or significant weight loss were observed in all treatment groups (Figure 4.4B).
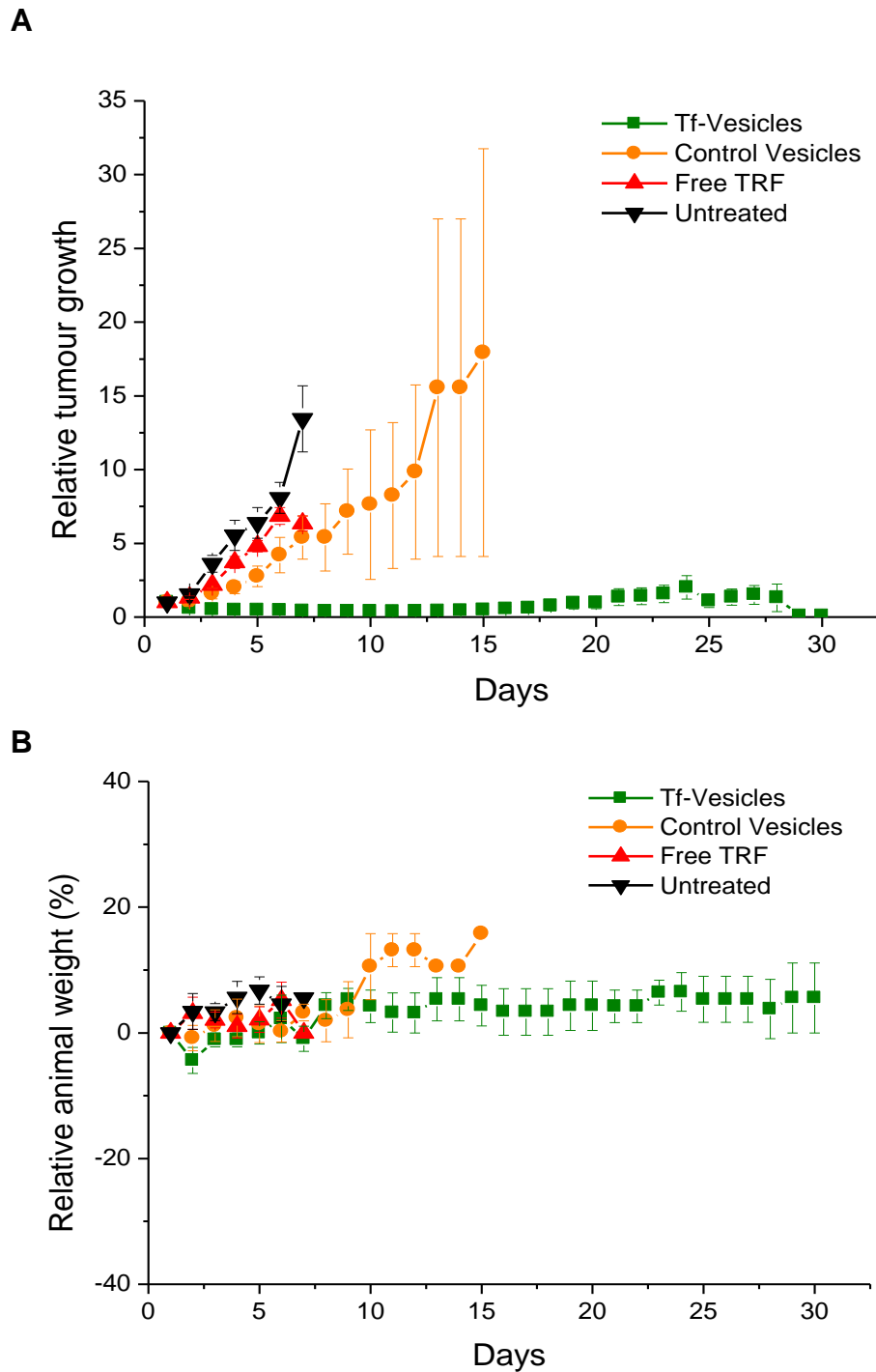
Figure 4.4: Antitumour studies in a mouse A431 xenograft with extended treatment duration (20 injections) of tocotrienol entrapped in Span 60/Solulan C24 vesicles. (A) Relative tumour growth upon intravenous injection of Tf-vesicles (green), control vesicles (orange), free tocotrienol (red) and untreated tumours (black) *(n=5)*. (B) Variations of the animal body weight throughout treatment regime *(n=5)*.
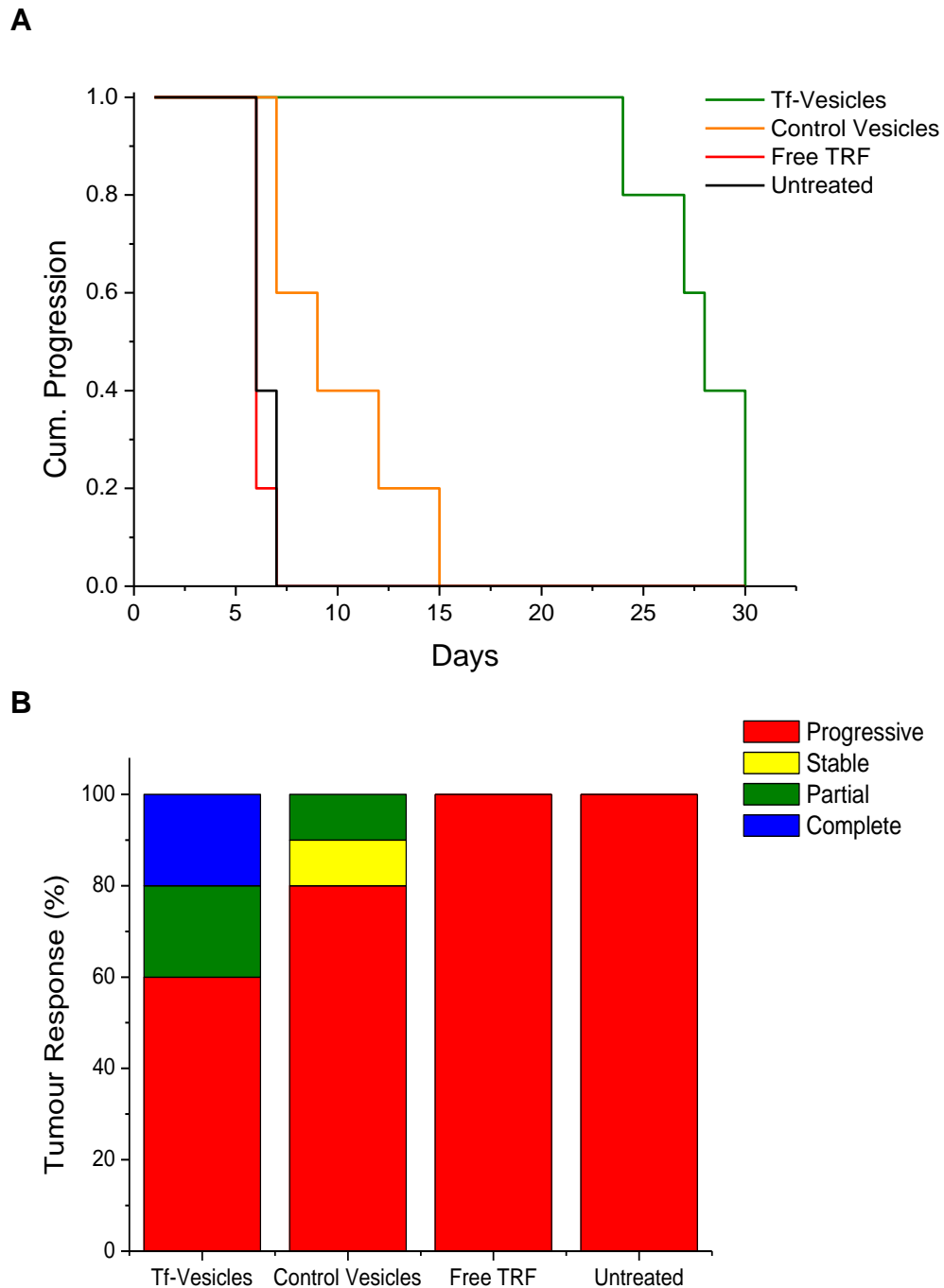
Figure 4.5: Antitumour studies in a mouse A431 xenograft with extended treatment duration (20 injections) of tocotrienol entrapped in Span 60/Solulan C24 vesicles. (A) Time to disease progression where animals were removed from the study once their tumour reached 12 mm diameter. Tf-vesicles (green), control vesicles (orange), free tocotrienol (red) and untreated tumours (black). (B) Overall tumour response to treatments, stratified according to change in tumour volume.

In mice bearing murine B16-F10-luc tumours, tumour progression was slightly different from what has been observed in A431 xenografts, most probably due to their characteristic rapid growth rate. In mice receiving Tf-vesicles, despite initial tumour regression during the first 3 days post-injection, two of the mice showed eventual regrowth at Day 4 (Figure 4.6A). However, the remaining mice receiving Tf-vesicles showed prolonged suppression of tumour growth. Only one animal from the group was showing signs of regrowth at Day 25 (5 days after halting the treatment) while two of the mice remained tumour-free. Thus the overall tumour response for Tf-vesicles group was quantified as 50 % complete absence of tumours, 10 % partial response and 40 % progressive (Figure 4.7B). On the other hand, no significant superiority was observed in mice treated with free tocotrienol and control vesicles compared to untreated control, where tumours were categorized as 100 % progressive. Compared to untreated mice, treatment with Tf-vesicles led to an extended survival of 26 days, a significant advantage compared to the 3 days extended survival observed with control vesicles (Figure 4.7A). Furthermore, assessment of animal weights showed no signs of toxicity or weight loss in all treatment groups (Figure 4.6B).
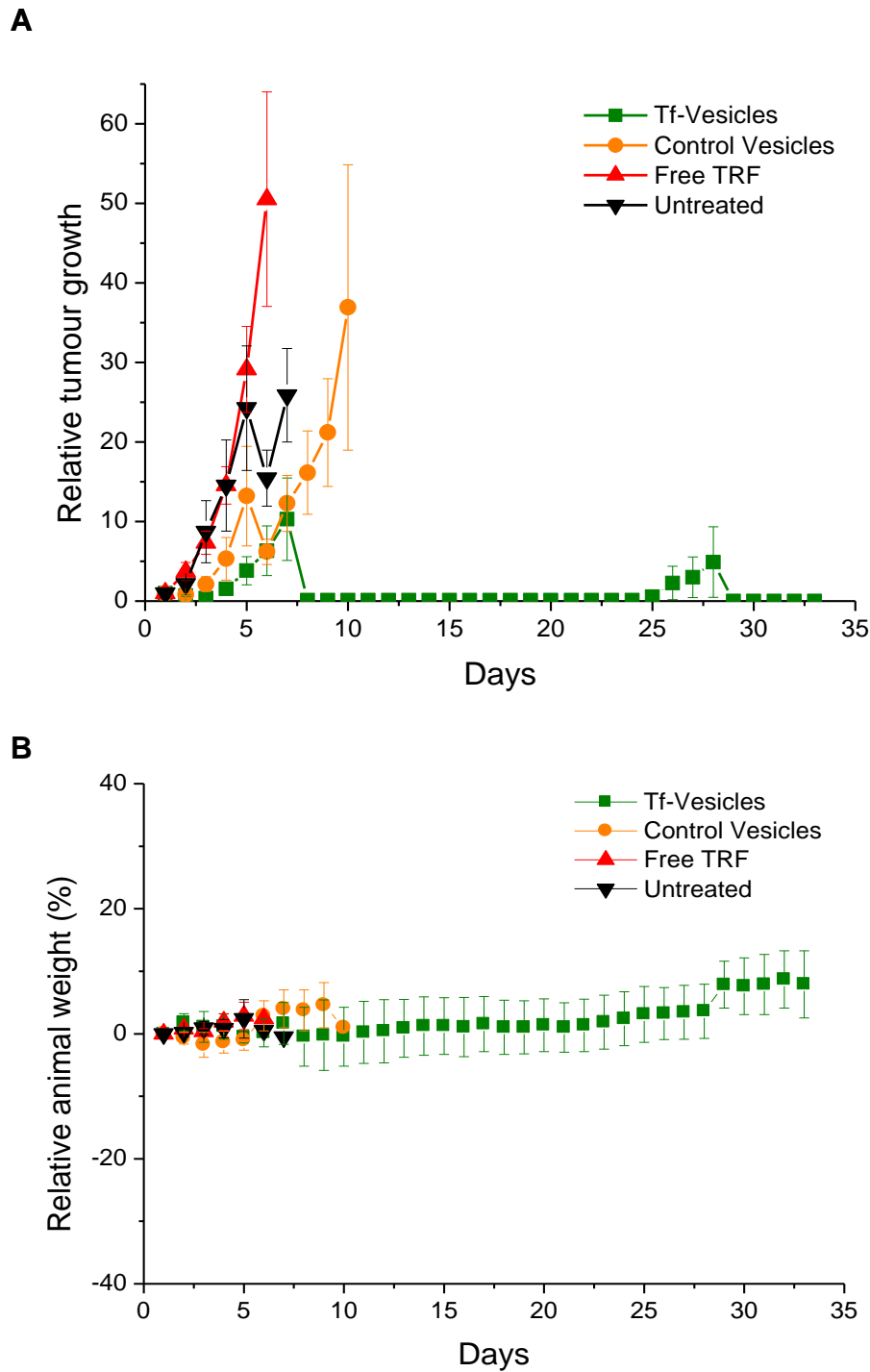
Figure 4.6: Antitumour studies in a murine B16-F10-luc tumour model after intravenous administration of tocotrienol entrapped in Span 60/Solulan C24 vesicles. (A) Relative tumour growth upon 20 injections of Tf-vesicles (green), control vesicles (orange), free tocotrienol (red) and untreated tumours (black) *(n=5)*. (B) Variations of the animal body weight throughout treatment regime *(n=5)*.
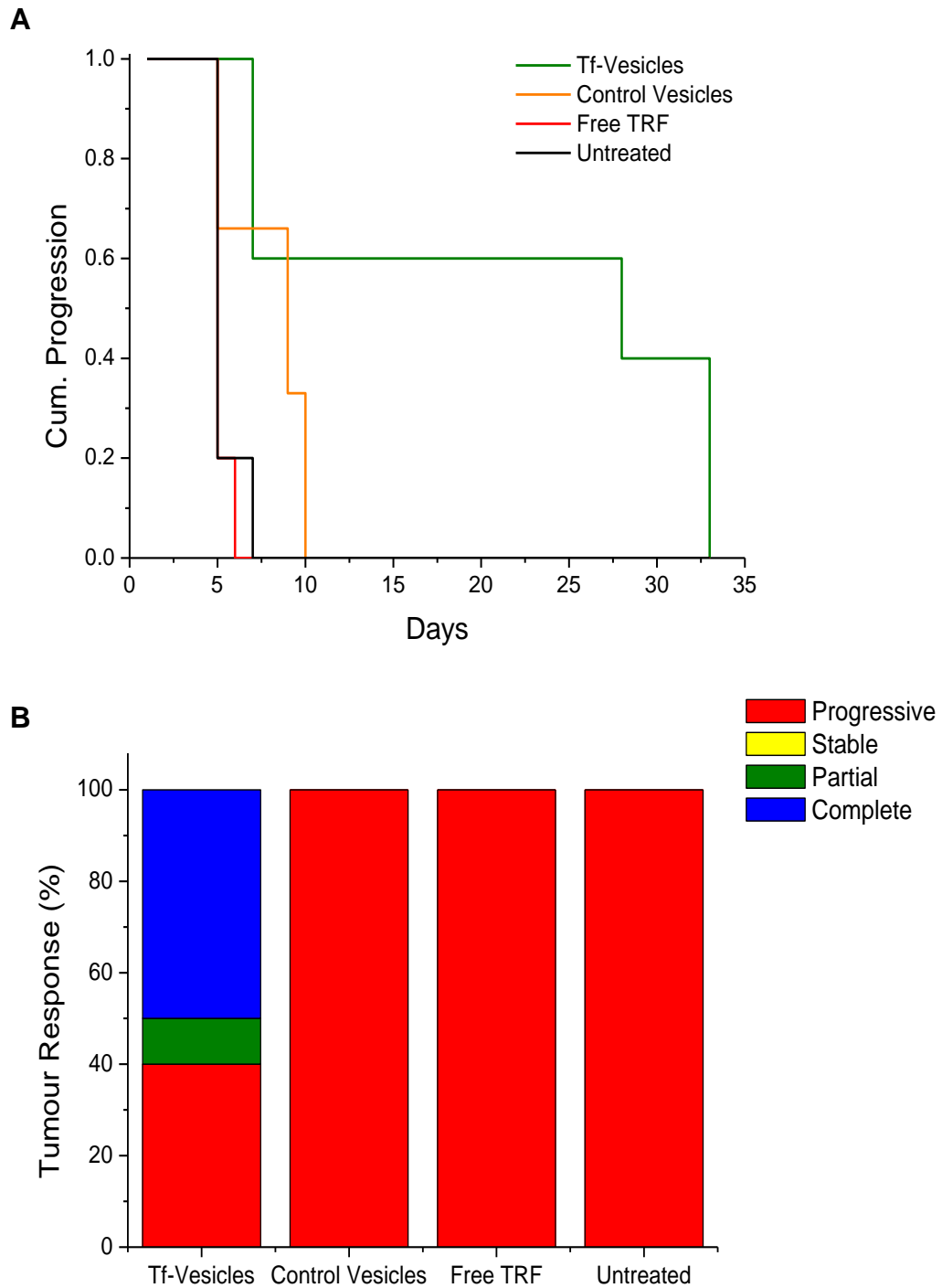
Figure 4.7: Antitumour studies in a murine B16-F10-luc tumour model after intravenous administration of tocotrienol entrapped in Span 60/Solulan C24 vesicles. (A) Time to disease progression where animals were removed from the study once their tumour reached 12 mm diameter. Tf-vesicles (green), control vesicles (orange), free tocotrienol (red) and untreated tumours (black). (B) Overall tumour response to treatments, stratified according to change in tumour volume.

To conclude, it was evident in murine models of implanted A431 and B16-F10-luc tumours that tumour-targeted delivery of tocotrienol significantly enhanced its tumour suppressive effect when administered via intravenous injection. With 10 injections, relative tumour growth was suppressed to a factor of 10 in Tf-vesicles-treated tumours compared to untreated tumours despite an eventual tumour regrowth upon cessation of treatment. When treatment duration was extended to 20 injections, as much as 20-50 % of mice remained tumour-free at study end point. Hence, this is a proof of concept in relative to the importance of an efficient delivery system for tocotrienol to exert its utmost tumour suppressive properties. According to the results obtained from Span 60/Solulan C24 vesicles, tumour suppressive effect of tocotrienol was enhanced by Tf-vesicles > control vesicles > free tocotrienol. In some cases free tocotrienol showed limited superiority compared to untreated tumours. Murine models of A431 and B16F10 tumours were also studied using Span 60/TPGS vesicle formulations with 20 daily injections of equivalent doses of tocotrienol (discussed below).

4.3.1.2 Span 60/TPGS Vesicles

Contrary to Span 60/Solulan C24 vesicles, tumours treated with Span 60/TPGS vesicles started showing signs of tumour regrowth by Day 5 despite continuous treatment with Tf-vesicles (Figure 4.8A). Within 24 hours post injection, relative tumour growth of tumours receiving Tf-vesicles was reduced by 30 %, whereas tumours in other treatment groups were demonstrating an exponential growth. At Day 7, while all mice in the group of free tocotrienol and untreated tumours had to be sacrificed as a consequence of tumour growing over the limit of 12

mm, tumours treated with Tf-vesicles remained regressed with a growth rate 14-fold lower than untreated tumours. In the group of animals receiving Tf-vesicles, 40 % of tumours showed a considerable increase in growth rate from Day 10 onwards while the remaining tumours remained regressed. Prolonged regression in tumours receiving Tf-vesicles led to complete disappearance of tumours in 20 % of the animals. Although no significant tumour regression was observed in tumours treated with control vesicles, the relative tumour growth rate was much lower than that observed in untreated tumours as well as in tumours treated with free tocotrienol. In Figure 4.9B, 20 % of Tf-vesicles-treated mice remained tumour free while 10 % of tumours were partially responding to treatment. By contrast, treatment with control vesicles resulted in 10 % stable tumours and 90 % progressive tumours, whereas tumours treated with free tocotrienol were 100 % progressive. In regard to animal survival rate (Figure 4.9A), passive targeting of tocotrienol in control vesicles extended the survival of mice by 4 days while tumour-targeted delivery with Tf-vesicles resulted in an extended animal survival of at least 23 days. Free tocotrienol however, did not show any superiority compared to untreated tumours. Quantification of relative animal weight (Figure 4.8B) showed little variation of animal weight and the absence of significant weight loss. Continuous observation did not reveal any apparent signs of treatment-induced side effects or toxicity.
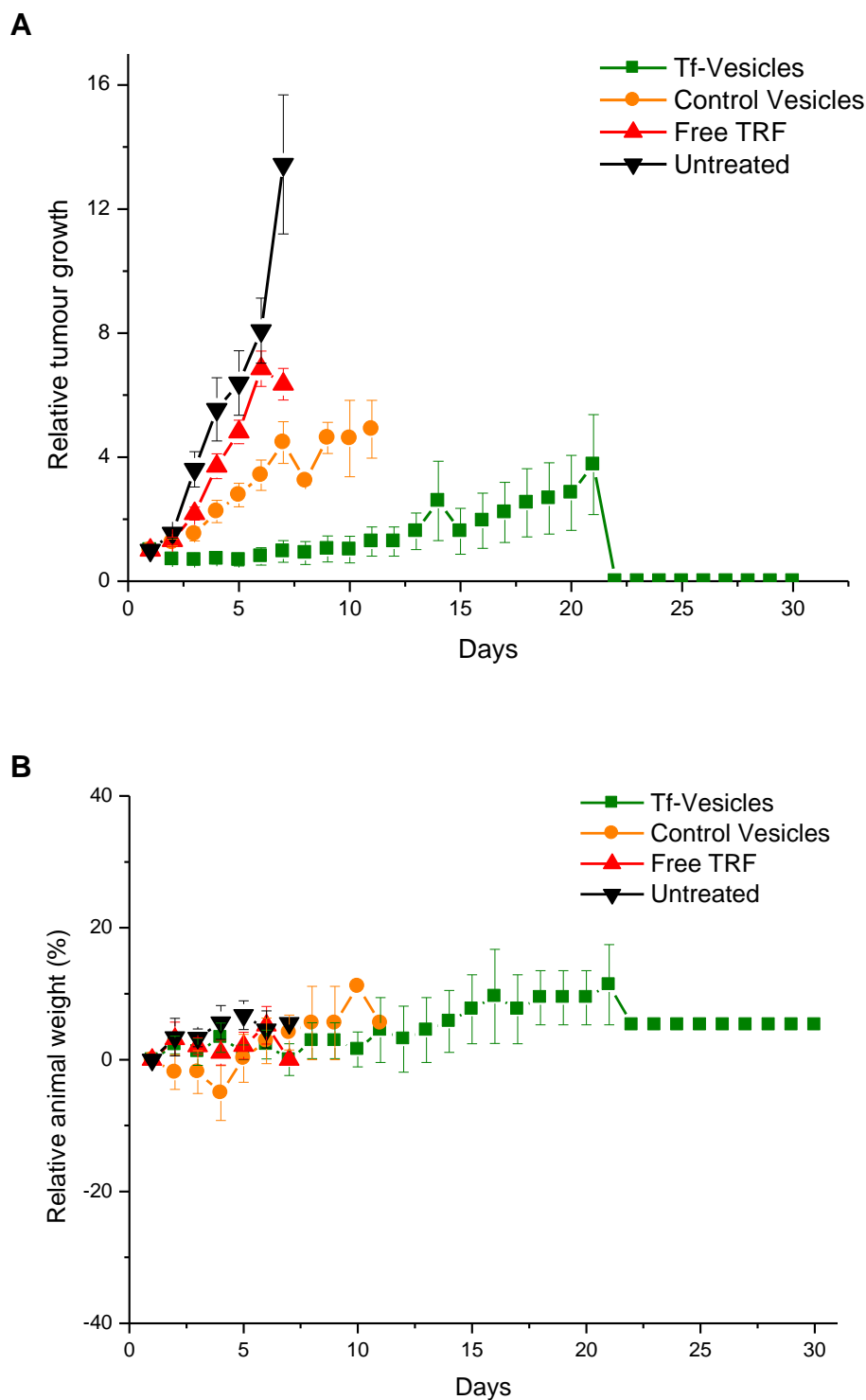
Figure 4.8: Antitumour studies in a mouse A431 xenograft after intravenous administration of tocotrienol entrapped in Span 60/TPGS vesicles. (A) Relative tumour growth upon 20 injections of Tf-vesicles (green), control vesicles (orange), free tocotrienol (red) and untreated tumours (black) *(n=5)*. (B) Variations of the animal body weight throughout treatment regime *(n=5)*.
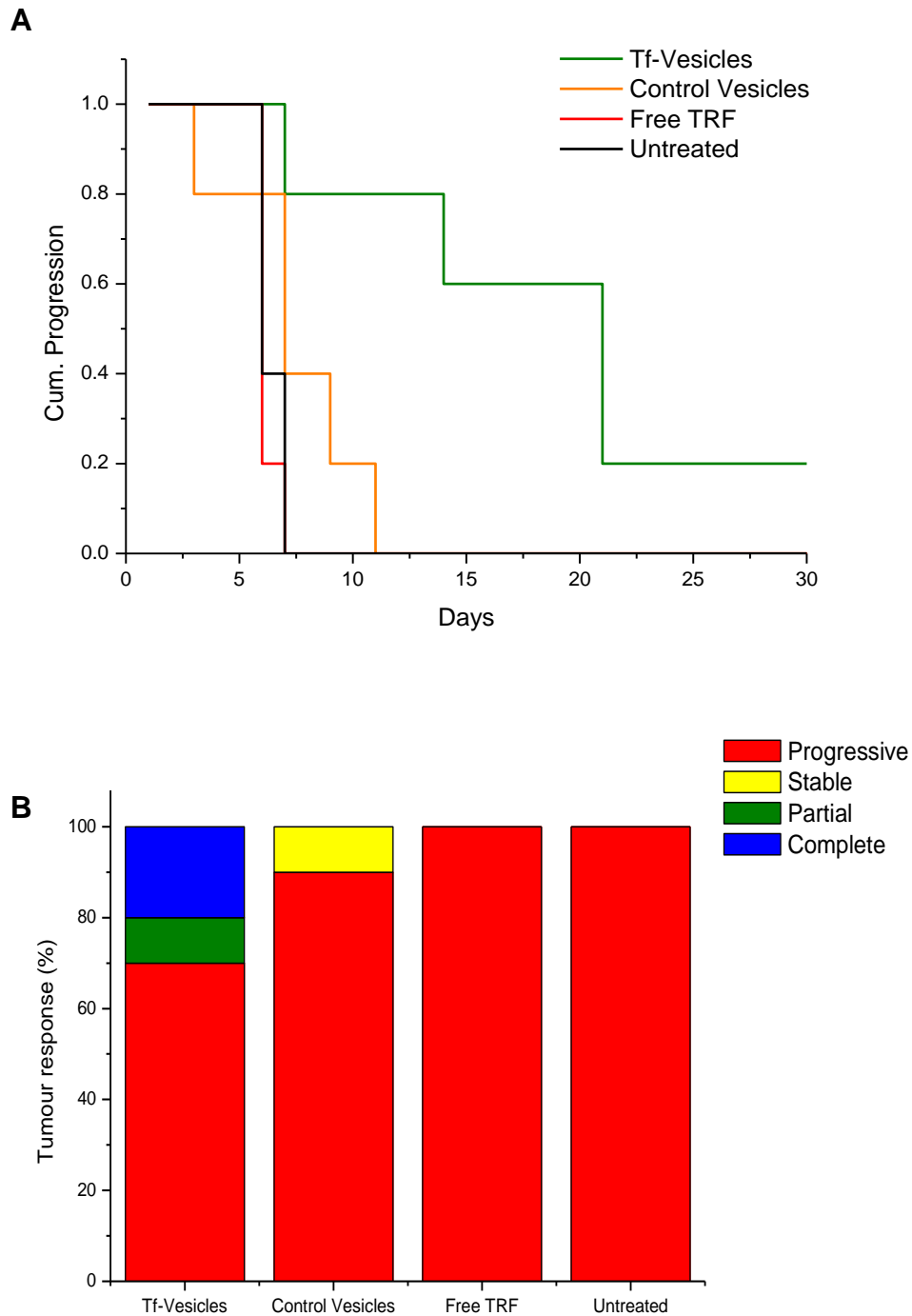
Figure 4.9: Antitumour studies in a mouse A431 xenograft after intravenous administration of tocotrienol entrapped in Span 60/TPGS vesicles. (A) Time to disease progression where animals were removed from the study once their tumour reached 12 mm diameter. Tf-vesicles (green), control vesicles (orange), free tocotrienol (red) and untreated tumours (black). (B) Overall tumour response to treatments, stratified according to change in tumour volume.

In B16-F10-luc murine tumour model, tumour suppressive property of tocotrienol when entrapped in Span 60/TPGS vesicles was similar to that observed with Span 60/Solulan C24 vesicles. When treated with Span 60/Solulan C24 Tf-vesicles, measureable tumour volume reduction was prominent for the first 3 days of treatment, followed by eventual tumour regrowth from Day 4 onwards. In Figure 4.10A, treatment of B16-F10-luc tumours with tocotrienol entrapped in Span 60/TPGS vesicles revealed a similar trend. With Tf-vesicles, substantial tumour regression was observed upon initiation of treatment. However at Day 3 to 4, tumours started growing at an elevated rate, albeit significantly slower compared to other treatment groups. From Day 5 onwards, 60 % of tumours were showing signs of rapid growth whereas 40 % of the remaining tumours remained regressed. Over continuous treatment of a total of 20 injections, regressing tumours had been completely eradicated in 40 % of the mice. On the other hand, tumours treated with control vesicles showed a trend of tumour growth similar to that observed with Tf-vesicles in the first 3 days. After which, tumours were growing at an exponential rate despite constant treatment. All mice from treatment groups of control vesicles, free tocotrienol and untreated mice had to be sacrificed before Day 10 of experiment due to tumours growing beyond a diameter of 12 mm, whereas at least 23 days extended survival was observed in mice treated with Tf-vesicles (Figure 4.11A). Treatment with control vesicles showed an extended survival of 2 days compared to untreated mice while no superiority was found in mice treated with free tocotrienol. At study end point, treatment with Tf-vesicles led to complete tumour eradication in 40 % of the animals and 10 % of tumours showing partial response towards treatment (Figure 4.11B). Ten percent of the tumours treated with control vesicles were partially

responding to treatment (90 % progressive) while tumours in free tocotrienol group were 100 % progressive. Assessment of relative animal weights was in consistent with previous experiments, showing no significant weight loss without apparent signs of treatment-induced toxicity (Figure 4.10B).
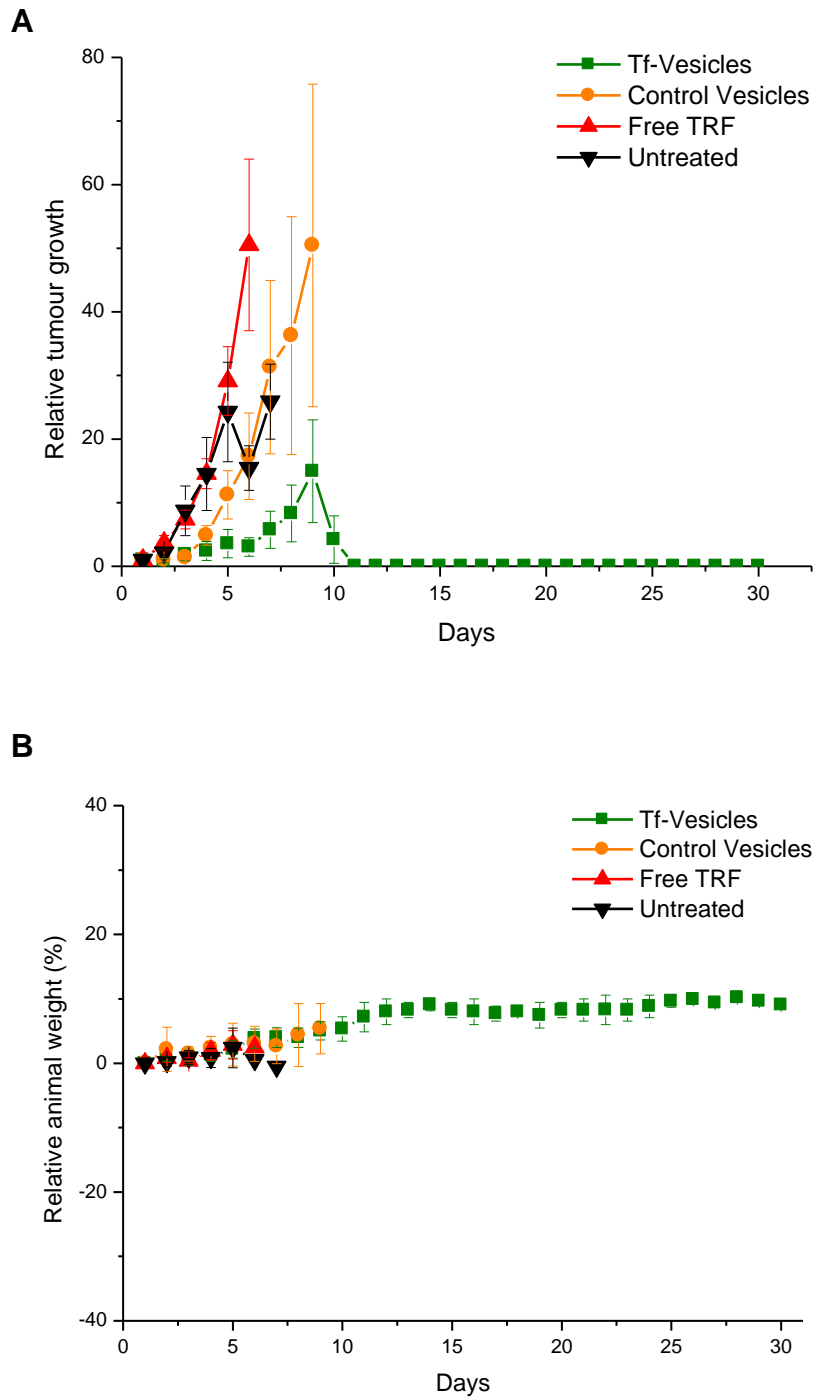
Figure 4.10: Antitumour studies in a murine B16-F10-luc tumour model after intravenous administration of tocotrienol entrapped in Span 60/TPGS vesicles. (A) Relative tumour growth upon 20 injections of Tf-vesicles (green), control vesicles (orange), free tocotrienol (red) and untreated tumours (black) *(n=5)*. (B) Variations of the animal body weight throughout treatment regime *(n=5)*.
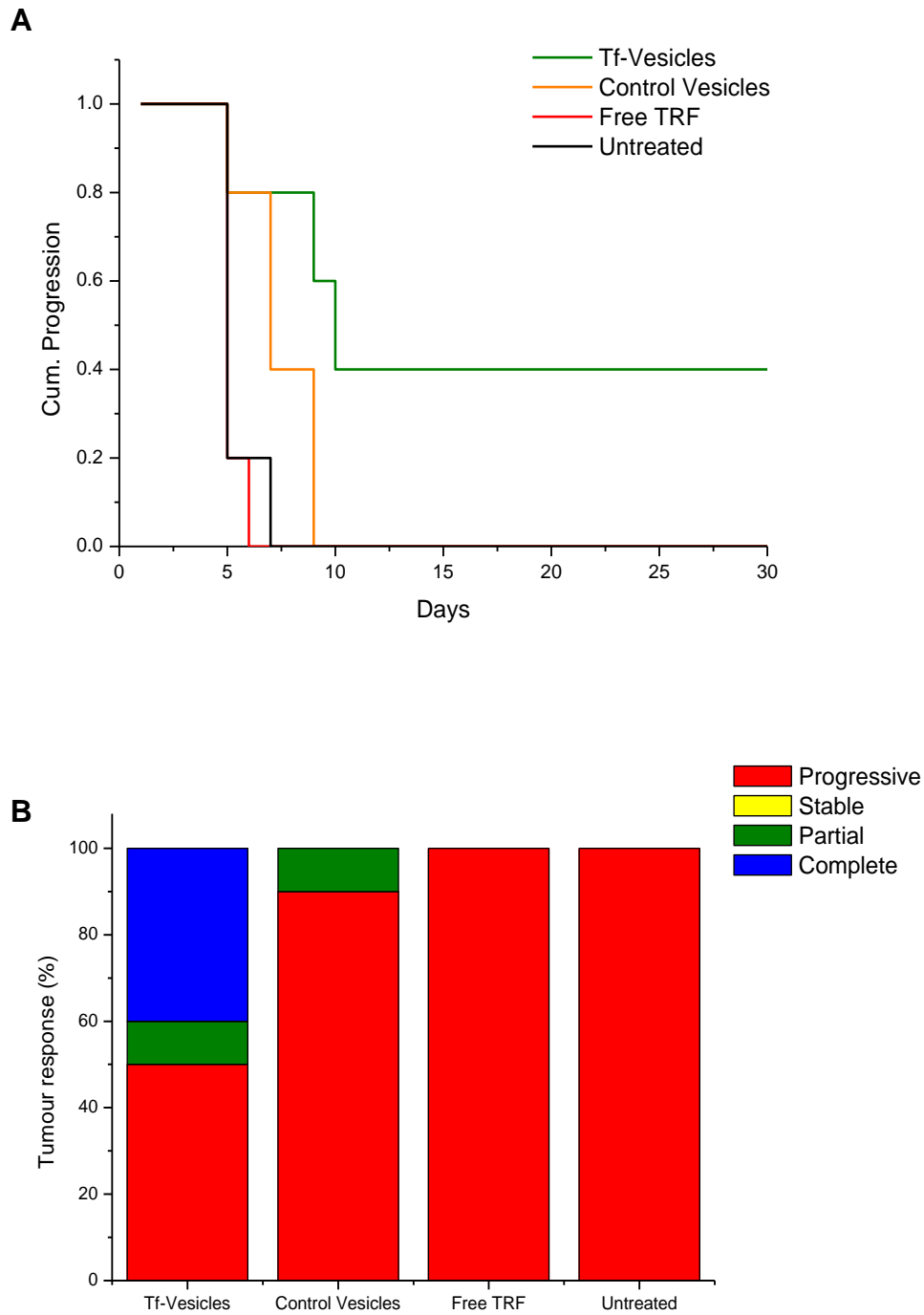
Figure 4.11: Antitumour studies in a murine B16-F10-luc tumour model after intravenous administration of tocotrienol entrapped in Span 60/TPGS vesicles. (A) Time to disease progression where animals were removed from the study once their tumour reached 12 mm diameter. Tf-vesicles (green), control vesicles (orange), free tocotrienol (red) and untreated tumours (black). (B) Overall tumour response to treatments, stratified according to change in tumour volume.

4.3.2 Bioluminescence imaging

4.3.2.1 Span 60/Solulan C24 Vesicles

The antitumour effect of tocotrienol, when encapsulated in vesicles (Span 60/Solulan C24) or administered as free drug, was validated using non-invasive bioluminescence imaging system. In treatment groups of control vesicles and free vesicles, the increase in bioluminescence signal correlated with the increase in tumour size over time (Figure 4.12). As for Tf-vesicles, although tumour growth in this treatment group was highly variable, serial imaging of the same animal allowed accurate assessment of tumour progression. In agreement with calliper measurements, the emitted bioluminescence signal started decreasing significantly at Day 5 mainly in the viable periphery of the tumour, and was undetected thereafter. Correlating with tumour response data, up to 50% of mice treated with Tf-vesicles remained tumour-free throughout the study.

4.3.2.2 Span 60/TPGS Vesicles

In accordance with the results obtained with calliper measurements, the therapeutic efficacy of tocotrienol was significantly enhanced when encapsulated in Tf-vesicles (Span 60/TPGS vesicles). Mice administered with Tf-vesicles showed a considerable reduction in tumour volume from Day 3 (Figure 4.13). While therapeutic effect was sustained throughout treatment duration, only traces of cancer cells were detected from Days 7 and 9, leading to a complete eradication of tumours in Day 11. In mice treated with control vesicles, tumour volume did not change in Day 3 but has considerably enlarged from Day 5 and 7. On the contrary, tumours

treated with free tocotrienol were growing at a constant rate, similarly to that observed with untreated tumours.
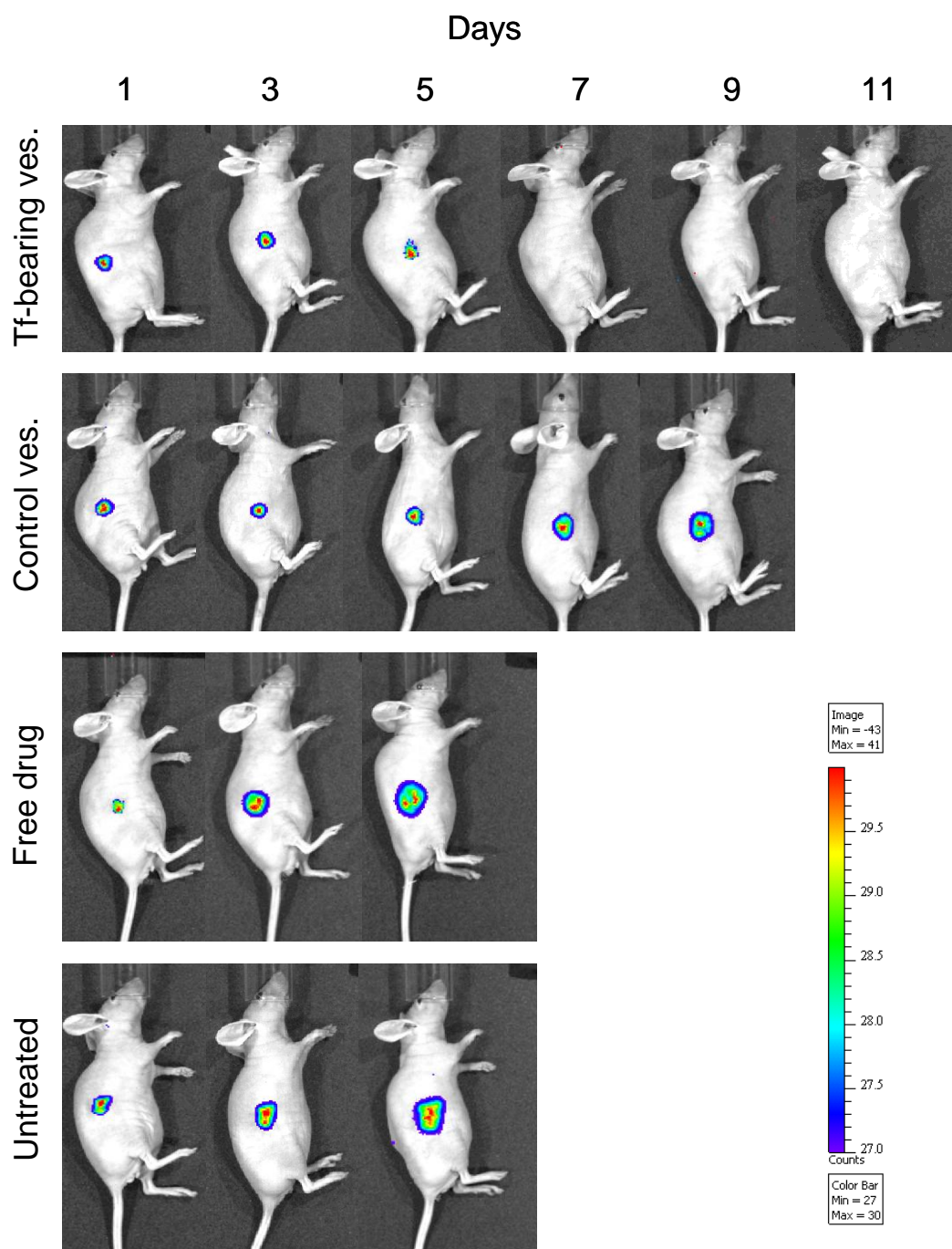
Figure 4.12: Bioluminescence imaging of the antitumour activity of TRF entrapped in Span 60/Solulan C24 vesicles in a mouse B16-F10-luc tumour model. Treatment was administered intravenously once daily on 10 occasions. The mice were imaged using the IVIS Spectrum every other day. The scale indicates surface radiance (photons/s/cm^2/steradian).
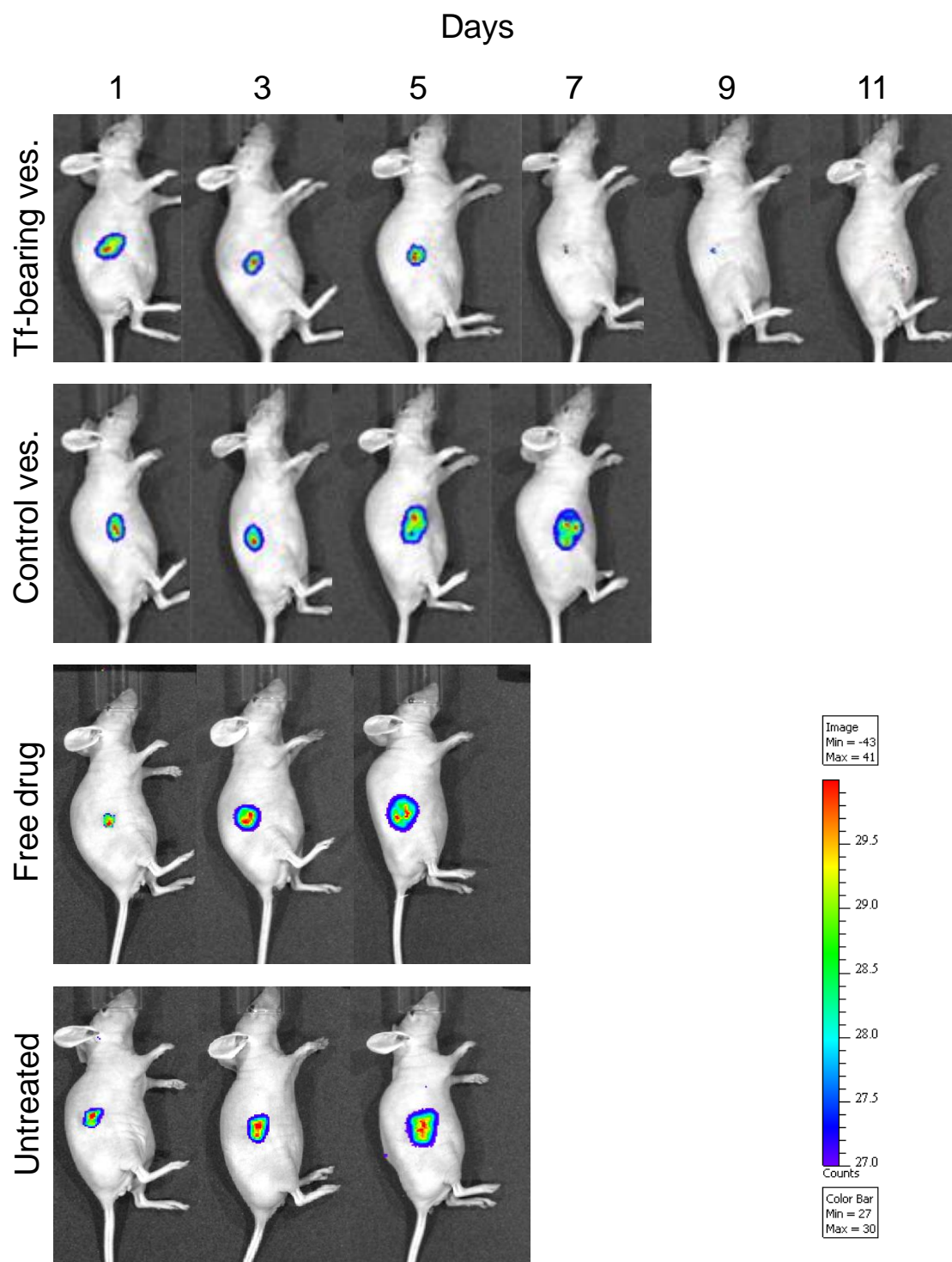
Figure 4.13: Bioluminescence imaging of the antitumour activity of TRF entrapped in Span 60/TPGS vesicles in a mouse B16-F10-luc tumour model. Treatment was administered intravenously once daily on 10 occasions. The mice were imaged using the IVIS Spectrum every other day. The scale indicates surface radiance (photons/s/cm^2/steradian).

4.4   DISCUSSION

Similar to fat-soluble vitamins (vitamin A, D, E and K), tocotrienol extracted from palm oil vitamin E exists as an oily liquid. Due to poor aqueous solubility and miscibility, the major limitations of its biological activity are closely related to its absorption and bioavailability, depending on the route of administration. When administered as an oily mixture via intraperitoneal and intramuscular routes in rats, α-, γ-, and δ-tocotrienol was found to be negligibly absorbed, with tocotrienol levels essentially similar to baseline concentrations (Yap *et al.*, 2003). Among the various routes of administration, oral route appeared to be a better option compared with intraperitoneal and intramuscular routes, however many disregarded intravenous route as an option when it comes to lipophilic molecules due to poor aqueous solubility. In a study by Yap *et al.* (2003), intravenous administration of tocotrienols in an emulsion form yielded a classic two-compartment pharmacokinetic model, with plasma concentration less than 1 % of the total administered dose. Nevertheless, as with lipophilic drugs such as paclitaxel and campthothecin, intravenous administration is possible with the aid of a suitable delivery system.

In our study, entrapping tocotrienol in transferrin-targeted niosomes presented several advantages. First is the opportunity to exploit intravenous administration with tocotrienol, dispersed as niosomes in aqueous suspension, essentially avoiding the variability that might have been implicated by administration via the oral route. Besides, higher doses can be administered as a result of increased drug payload when encapsulated in delivery systems, subsequently improving the dosing regimen and therapeutic index. In addition to elevated tumour accumulation

via the EPR effect, active targeting with transferrin helps to facilitate intracellular accumulation of tocotrienol via receptor-mediated endocytosis. We aim to promote an efficient delivery of tocotrienol to the tumours while shielding tocotrienol from degradation and metabolism, which are equally important to ensure adequate circulating tocotrienol available for tissue distribution.

In fact, previous studies involving tocotrienol were conducted using dosing regimen between 1 mg to 10 mg tocotrienol per kg animal weight per day (Nesaretnam *et al.*, 2004; Khanna *et al.*, 2005; Hiura *et al.*, 2009). Most of these studies were focusing on the chemopreventive effect of tocotrienol after oral supplementation with tocotrienol-rich diets. For example, a study by Nesaretnam *et al.* (2004) showed that high vitamin E diets containing 1 mg TRF per day delayed the development of tumour growth upon breast cancer cell inoculation. Similar studies were done in mice fed with a high γ- and δ-tocotrienol diet prior to tumour inoculation, whereby significant delay in tumour growth was observed compared to the control group (He *et al.*, 1997; Hiura *et al.*, 2008). Unlike the other studies, Wada *et al.* (2005) conducted several experiments to demonstrate the tumour suppressive effects of tocotrienol *in vivo*. In his report, liver and lung carcinogenesis was induced before oral supplementation of tocotrienol mixture and the amount of tumours developed were quantified. Interestingly, the average number of tumours per mouse was 4 to 7-fold lower in mice receiving tocotrienol mixture compared to control group. Hence, it is fair to say that oral supplementation of tocotrienol has potential chemopreventive effect, successfully delaying the time to tumour growth while increasing the duration of animal survival.

In this study, we aim to investigate the antitumour effect of tocotrienol using a different approach. Instead of pre-supplementing the mice with tocotrienol, cancer cells were inoculated subcutaneously until they reach a palpable size of a solid tumour, a similar approach as any other chemotherapeutic agents would have been evaluated. Subsequent administration of tocotrienol either as free drug or formulated in vesicles allowed practical assessment of the extent of treatment-induced tumour regression or tumour response. Indeed, we found that when entrapped in transferrin-targeted niosomes, tocotrienol was most efficacious for its antitumour activity, with an impressive tumour eradication effect within 20 injections in 20-50 % of mice. Probably one of the most understandable explanations for the superior therapeutic efficacy associated with transferrin-bearing vesicles is due to the increased delivery of tocotrienol to the tumours via a combined effect from passive and active targeting. Although biodistribution analysis is yet to be done to confirm the claim, similar observations have been reported by Shah *et al.* (2009) and Jiang *et al.* (2007). Direct correlation was obtained between antitumour activity and tumour accumulation of various therapeutic agents, usually highest when delivered using transferrin-targeted delivery systems compared to non-targeted systems.

Nevertheless, it is not surprising to find little therapeutic effect with passively-targeted therapeutic systems, despite increased tumour accumulation via the EPR effect, as seen with control vesicles. This is most probably because of the absence of a ligand-receptor interaction, substantially limiting the rate of internalization of control vesicles into tumour cells. Therefore, although enhanced extravasation from tumour blood vessels can be achieved via passive targeting,

control vesicles were most probably retained in the tumour interstitium. In such case, the delivery of tocotrienol was rather ineffective.

On the other hand, when administered as free drug, the distribution of tocotrienol was expected to resemble a profile similar to what has been observed with oral supplementation. Dietary vitamin E undergoes intestinal absorption, cellular uptake and metabolism pathways closely related to overall lipid and lipoprotein homeostasis due to its lipophilic nature (Rigotti, 2007). When taken orally, vitamin E appears to be similarly taken up along dietary fats by the intestine and secreted in chylomicron particles together with triacylglycerol and cholesterol (Figure 4.14) (Jiang, 2009). Upon lipoprotein lipase catabolism of chylomicron particles, some of the chylomicron-bound vitamin E is transported to peripheral tissues via circulating lipoproteins (Jiang, 2009). Lipoproteins are the major, if not the only, carriers of plasma lipid-soluble molecules (Khanna *et al.*, 2005; Rigotti *et al.*, 2007). Among them, vitamin E is mostly associated in low-density-lipoprotein (LDL) and high-density-lipoprotein (HDL), with less than 20 % distributed in very low-density-lipoprotein (VLDL) and other lipoproteins (Perugini *et al.*, 2000). The remaining chylomicron remnants are subsequently taken up by the liver. In the liver, α-tocopherol transfer protein (α-TTP) is the major intracellular transport protein that binds selectively to α-tocopherol (Khanna *et al.*, 2005). Most of the vitamin E is then incorporated into nascent VLDL by α-TTP, and re-secreted as plasma vitamin E in LDL and HDL available for tissue uptake (Khanna *et al.*, 2005; Jiang, 2009). No doubt α-TTP is playing a crucial role in the plasma concentration of tocopherol, however it has been estimated that α-TTP has 8.5-fold lower binding affinity towards

α-tocotrienol compared to α-tocopherol, and its role in the absorption and distribution of tocotrienol and other isoforms remains unclear (Hosomi *et al.*, 1997; Yuen *et al.*, 2009). In a study with α-TTP knockout mice, supplementation of α-tocotrienol was able to restore their reproductive dysfunction, suggesting successful delivery of tocotrienol to relevant tissues despite the absence of α-TTP (Khanna *et al.*, 2005). It was thus proposed that tocotrienol transport might not be entirely dependent on α-TTP.
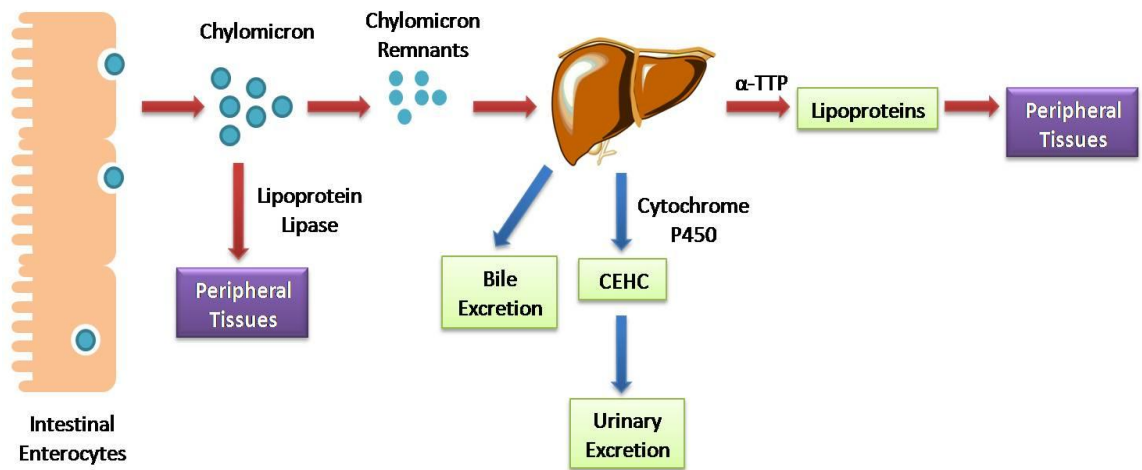
Figure 4.14: Schematic illustration of the absorption, transport, metabolism and excretion of vitamin E upon oral administration *(Modified from Jiang, 2009).*

Various studies suggested that the distribution of tocotrienols via oral administration was tissue-specific albeit some inconsistency observed among the few published studies (Yuen *et al.*, 2009). A study by Cheng *et al.* (2005) suggested highest tocotrienol accumulation in the heart, followed by skin, liver, muscle and least in the brain of Sprague-Dawley rats. On the contrary, another study in rats reported a primary accumulation of palm tocotrienol in the adipose tissue and skin, while little was detected in the brain, liver, kidney and plasma (Ikeda *et al.*, 2001). Predominant accumulation in the adipose tissue and skin was further established in studies by Podda *et al.* (1996) and Hayes *et al.* (1993) carried out in mice and hamsters, whereas tocotrienol distribution in the heart, liver, spleen, kidney, pancreas, muscle and testes were negligible. The mechanism underlying its tissue-dependent distribution is believed to be associated with two receptor pathways, the LDL receptor superfamily and the lipoprotein receptor SR-BI (scavenger receptor class B type I) (Rigotti *et al.*, 2007). The LDL receptor was the first lipoprotein receptor reported to be involved in vitamin E uptake via cell surface receptor-mediated lipoprotein endocytosis (Traber and Kayden, 1984). However, some evidence suggested that the LDL receptor pathway might not be the only route for the maintenance of normal tissue vitamin E levels because sufficient vitamin E accumulation was observed in mice with impaired LDL receptor activity (Mardones *et al.*, 2002). While HDL is another major carrier of vitamin E, a selective lipid uptake mediated by lipoprotein receptor SR-BI was involved, especially in the central nervous system, lungs and gonads (Mardones *et al.*, 2002).

Therefore free tocotrienol, when administered via intravenous injection is most probably associated with LDL, either incorporated in circulating LDL or resecreted from the liver. Due to its non-specific tissue distribution, it is not surprising to find little or no antitumour activity of free tocotrienol on subcutaneous xenografts, as shown with both A431 epithelial carcinoma and murine B16-F10-luc melanoma cancer cell lines. Besides, due to the absence of a protective layer as with vesicles encapsulation, free tocotrienol is more susceptible to enzymatic metabolism or degradation. Many researchers have studied the metabolism of vitamin E, showing a plasma half-life of α-, γ-, δ-tocotrienol being 7.5, 7.0 and 7.4 hours in rats and 4.4, 4.3 and 2.3 hours in human volunteers (Yuen *et al.*, 2009). In the liver, metabolism of tocopherol and tocotrienol to respective metabolites carboxyethylhydrochroman (CEHC) are mediated by a cytochrome P450-dependent process (Khanna *et al.*, 2005; Hiura *et al.*, 2008). Among cytochrome P450 family, CYP3A4 and CYP4F2 play important roles in catabolism of vitamin E via ω-hydroxylation and by β-oxidation, primarily excreting CEHC into the urine (Khanna *et al.*, 2005). Excess hepatic vitamin E is also excreted into the bile via ABC transporter P-glycoprotein, schematically depicted in Figure 4.14 (Jiang, 2009).

Despite the fact that vitamin E compounds are extremely well tolerated in humans, minor side effects were reported in a subset of subjects including gastrointestinal symptoms, generalized dermatitis and fatigue (Lawson *et al.*, 2004). During the course of study in our *in vivo* experiment, animals were closely observed for signs of toxicity or discomfort. However, to date, no visible signs of toxicity especially weight loss or behavioural changes were observed in our study. In

agreement with previous *in vivo* studies involving oral supplementation of tocotrienol, either administered alone or in food matrix, tocotrienol was proven nontoxic to normal tissues (Lawson *et al.*, 2004; Wada *et al.*, 2005; Hiura *et al.*, 2008). In the case of TPGS, the National Cancer Institute (NCI) has identified TPGS being a safe excipient for oral consumption of up to 1 g/kg/day in rats and dogs, as well as in commercial human doses for paediatric vitamin E deficiency, protease inhibitor, cyclosporine and in dietary supplements (Eastman Chemical Company, 2005).

Comparing the therapeutic efficacy of Span 60/Solulan C24 and Span 60/TPGS vesicles as carriers for tumour delivery of tocotrienol, both vesicle formulations exhibited a similar therapeutic potential *in vivo*. Tf-bearing vesicles were most efficient in tumour regression, followed by control vesicles, whereas free tocotrienol did not show significant superiority from untreated tumours. In terms of relative tumour growth, treatment of Tf-vesicles suppressed tumour growth to a greater extent in A431 tumours compared to B16-F10-luc tumours, most probably due to the higher growth rate in B16-F10-luc tumours. However, continuous observation suggested a better tumour response and prolonged animal survival in mice bearing B16-F10-luc tumours, in addition to the complete tumour eradication of at least 40 % of the tumours. The unique biology of melanoma (B16-F10-luc) might have contributed to the enhanced therapeutic efficacy observed. The tumour environment of melanomas is often characterized by high reactive oxygen species (ROS) levels, either produced from exogenous sources or within melanoma cells (Joosse *et al.*, 2010). In melanosomes, the balance between production and

scavenging of ROS are in equilibrium under normal cellular processes (Wittgen and van Kempen, 2007). Disturbance of this equilibrium in tumour cells leads to excessive production of free radicals (e.g. hydrogen peroxide), resulting in DNA damage, resistance to chemotherapy as well as metastasis (Fruehauf and Trapp, 2008; Joosse *et al.*, 2010). Moreover, ROS are also generated as a result of increased metabolism of cancer cells, immune reaction against developing tumour, ultraviolet radiation, melanin production and altered antioxidant system (Wittgen and van Kempen, 2007). Therefore, using agents that reverse or block the production of ROS has been a promising strategy. Tocotrienol, as a potent antioxidant, might have the ability to target the excess free radicals in melanomas. The enhanced sensitivity of tocotrienol towards B16-F10-luc tumours was most probably attributed to a combined effect of antioxidant activity and anti-proliferative properties in tocotrienol. However, it should be noted that tumour-targeting and entrapment of tocotrienol in niosomes were crucial for their optimum efficacy.

The most striking effect of tocotrienol, when entrapped in transferrin-targeted vesicles was the induction of tumour regression within 24-hours post treatment, without apparent toxicity. This work corresponds to the first preparation of a tumour-targeted delivery system for tocotrienol, not only allowing intravenous administration of tocotrienol but also able to exert its antitumour effect on subcutaneously implanted tumours. Within 20 days, as much as 50 % of animals were tumour free. This research is a breakthrough in cancer therapy because conventional chemotherapy generally takes months for sufficient tumour shrinkage whereas in this study, the trend of possible tumour eradication was observed within

20 days by intravenous administration of tumour-targeted tocotrienol. Although a high inter-tumour variation was observed, this study provide a proof of concept for the entrapment of vitamin E component tocotrienol in a targeted delivery system. Combining the delivery approach of passive and active targeting, both Span 60/Solulan C24 and Span 60/TPGS demonstrated excellent delivery of tocotrienol, leading to a significant therapeutic effect on tumour cells with lowest possible secondary effects on normal tissues after systemic administration.

Chapter 5

Conclusion and Future Works

5.1   CONCLUSION

Cancer remains one of the leading causes of mortality worldwide. It has accounted for 7.9 million deaths in 2007 while an estimated 20 million new cancer cases was projected to occur by year 2020 (Aggarwal, 2010; http://www.who.int/topics/cancer/). Despite its major impact, oncology has one of the poorest records for investigational drugs in clinical development, with success rates more than three times lower than that for cardiovascular disease (Kamb *et al.*, 2007). Cancer drug development is generally hampered by numerous obstacles, including selection of drug target, variation in tumour biology, regulatory environment and pricing, all of which contributed to the main challenges in cancer drug discovery (Kamb *et al.*, 2007; Hait, 2010). Natural product, as a source of remedies to treat human diseases, was established since the dawn of medicine. Drugs derived from natural sources are still making an enormous contribution to drug discovery today, especially in cancer chemotherapy and chemoprevention (da Rocha *et al.*, 2001; Reddy *et al.*, 2003). In anticancer therapy, plant-derived agents currently in clinical use include vincristine, etoposide, paclitaxel, flavopiridol, camptothecin and homoharringtonine (Slichenmyer and Von Hoff, 1990; da Rocha *et al.*, 2001). Paclitaxel for example, is used as a standard therapy for ovarian, breast, non-small cell lung cancer and several other malignancies (Sparreboom *et al.*, 2005). However, commercial formulation of paclitaxel (Taxol®) is emulsified in Cremophor and dehydrated ethanol, which often leads to serious toxicity, including severe, sometimes fatal hypersensitivity reactions (Sparreboom *et al.*, 2005). With the advancement of drug delivery technologies, Abraxane®, an albumin-bound nanoparticle of paclitaxel was developed by Abraxis Bioscience/AstraZeneca in

order to retain the therapeutic benefits of paclitaxel but eliminate the toxicities associated with Taxol[®] (Sparreboom *et al.*, 2005; Davis *et al.*, 2008). In addition to higher response rate, the maximum tolerated dose of Abraxane[®] was approximately 70-80 % higher than that reported for Taxol[®] (Sparreboom *et al.*, 2005).

In the case of tocotrienol, although it has recently been shown to exhibit impressive chemoprevention properties *in vitro* and *in vivo*, its therapeutic index was not sufficient to induce considerable tumour regression when administered via oral supplementation. Besides, tocotrienol shared a similar problem encountered in paclitaxel formulation, i.e. high lipophilicity. For paclitaxel, steps taken to formulate highly lipophilic paclitaxel included the use of organic solvent (Taxol[®]) and encapsulation of paclitaxel into nanoparticles (Abraxane[®]). Hence in this study, we aim to formulate tocotrienol in transferrin-targeted niosomes (non-ionic vesicles) for optimum delivery to cancer cells. Following extensive literature reviews on niosomes, Span 60 was chosen as the main vesicle forming surfactant for our system, owing to its enhanced drug encapsulation capacity and stability. In order to provide sufficient shielding of the Span 60 niosomes from rapid reticular-endothelial clearance, two types of polymers (i.e. polyethylene oxide derivatives of cholesterol and α-tocopherol) were incorporated to form a protective layer on the surface of the niosomes.

Preparation and Characterization. Vesicles incorporated with Solulan C24 (cholesteryl poly(24)oxyethylene ether) formed a distribution of small unilamellar vesicles at diameters approximately 150 nm, while vesicles incorporated with TPGS

(tocopheryl polyethylene glycol succinate) formed multilamellar vesicles at diameters close to 160 nm. Although passively targeted therapeutic agents were previously shown to be efficacious under certain circumstances, we hypothesize that a combined approach of active targeting and passive targeting would maximize the therapeutic activity of tocotrienol at its target site. At a tocotrienol loading capacity of approximately 30 to 50 %, the therapeutic efficacy and targeting efficacy of these vesicles were evaluated *in vitro* and *in vivo*.

In vitro evaluation. In cellular studies, the therapeutic efficacy of tocotrienol has correlated well with the intracellular accumulation of tocotrienol, when delivered either as a free drug or entrapped in transferrin-targeted vesicles (Tf-vesicles) and non-targeted vesicles (control vesicles). As transferrin receptors are over-expressed on cancer cells, vesicles targeted with transferrin were most probably taken up by the cells via transferrin receptor-mediated endocytosis. The specific uptake of Tf-vesicles was confirmed by an enhanced intracellular tocotrienol accumulation of more than 4-fold higher in cells treated with Tf-vesicles compared to free tocotrienol. This led to a significant improvement in the therapeutic efficacy of tocotrienol, elevated by an order of up to 400-fold in cells treated with Tf-vesicles versus free tocotrienol. Although non-targeted vesicles were presumably taken up by the cells via non-specific internalization mechanisms, the therapeutic efficacy of control vesicles were considerably better than that observed with free tocotrienol (up to 90-fold improvement in IC_{50} values). Moreover, the enhanced therapeutic effect of tocotrienol delivered using transferrin-targeted vesicles was notably translated into *in*

vivo results obtained with mice bearing subcutaneous A431 and B16-F10-luc tumours.

In vivo evaluation. Significant tumour regression was observed in A431 and B16-F10-luc tumours upon intravenous administration of transferrin-targeted vesicles. The most prominent effect was observed in mice bearing B16-F10-luc tumours as treatment with Tf-vesicles was able to completely eradicate up to 50 % of tumours in the treatment group. Despite successful eradication of tumours in B16-F10-luc tumour bearing mice, large inter-tumour variation was observed. Looking at cancer at the molecular level, it is likely that no two cancers are identical due to exceptional heterogeneity and adaptability of cancers (Kamb *et al.*, 2007). Inevitably, physical manifestation of tumour heterogeneity is often reflected in observed differences in drug responses, and is the probable cause of acquired resistance (Kamb *et al.*, 2007). Nevertheless, one major advantage of tocotrienol was its ability to induce measureable tumour regression with an exceptional safety profile: no significant weight loss or signs of toxicity were observed in all treatment groups despite intensive treatment regime. This is very rare in anticancer drugs given their cytotoxic properties and potency.

In conclusion, the development of nanocarrier drug delivery systems is expected to have great impact for cancer therapy. By rationally designing nanocarriers based on better knowledge of cancer biology and tumour microenvironment, improved therapeutic index in the treatment of cancer is achievable. Summarizing the study, an ideal delivery system for cancer treatment

should be one that: (1) facilitates fast and effective accumulation of therapeutic agent in the tumours, (2) delivers a higher amount of drug to tumours to create a dose differential between tumour tissues and healthy tissues, (3) efficiently taken up by tumour cells upon extravasation, (4) potentially non-toxic to healthy tissues. In our study, successful preparation of transferrin-targeted niosomes entrapping tocotrienol has led to a significant advantage in therapeutic efficacy of tocotrienol compared to non-targeted niosomes and free tocotrienol. A combined approach with active targeting (transferrin) and passive targeting (entrapment in niosomes) demonstrated a significant tumour regression upon intravenous administration of tocotrienol, in addition to prolonged animal survival as well as improved tumour response. The potential of this therapeutic system was further supported by the lack of visible toxicities and side effects associated with the treatment regime. Therefore, this is a proof of principle that the entrapment of the vitamin E component, tocotrienol, in a targeted delivery system can be a promising strategy for anti-cancer treatment, demonstrating enhanced therapeutic efficacy in conjunction with minimal side effects on normal tissues.

5.2   FUTURE WORKS

With the aid of advances in nanotechnology, development of drug delivery systems in nanoscale provide opportunities for designing properties that are not possible with other types of therapeutics. Upon extensive elucidation of the optimal characteristics for cancer therapeutics, newer, personalised and more sophisticated multifunctional nanocarriers are reaching the clinic. Unfortunately, although intravenous administration of tocotrienol entrapped in transferrin-targeted niosomes was able to induce significant tumour regression, eventual tumour regrowth was observed. In regard to this shortcoming, we believe that optimization of tocotrienol formulation is a crucial factor. With liposomes, drug molecules are kinetically trapped in the vesicles but there is no way to modify the amount that gets trapped unless changes are made on the lipid composition or preparation process (Jones, 2007). This is a major disadvantage in all vesicular formulations. While encapsulation efficiency of a system is directly correlated with the administered dose, modification of the delivery system which enables higher loading of tocotrienol is an elemental step in enhancing its therapeutic efficacy. An ideal delivery system however, would be one that is able to load therapeutic agents at any amount depending on the treatment purpose. In addition to optimizing the vesicle formulation, optimization of dosing regime is crucial for future work as well. Varying concentrations of tocotrienol are to be administered in order to determine the maximum tolerated dose, which might indicate the possibility to administer a higher dose of tocotrienol. Also, by increasing the dose of TRF, the schedule or number of injections can be reduced as daily injections are rather intensive for clinical settings.

Quoting from *The Art of War* "So it is said that if you know your enemies and know yourself, you will not be imperilled in a hundred battles; if you do not know your enemies but do know yourself, you will win one and lose one; if you do not know your enemies nor yourself, you will be imperilled in every single battle. ~ Sun Tzu". In order to fully functionalise the potential of tocotrienol, we need to first understand the precise behaviour of tocotrienol in the biological system, from the interaction with blood components and its affinity for specific tissue distribution to intracellular transport mechanisms. Therefore, our main focus in the future research is to involve cellular trafficking studies similar to works done by Torchilin (2005) and Matthaus *et al.* (2008). In addition to robust microscopy methods, cellular internalization of these systems can be elucidated using competitive binding assays by blocking specific transport pathways. This is potentially valuable in assessing the targeting efficiency of targeting moieties, in our case is the transferrin-transferrin receptor interaction. For example, energy-dependant endocytosis can be inhibited by treating cells in 4°C while pre-incubation of cells with excess transferrin blocks the transferrin receptor pathway. To further elucidate the cellular uptake pathway, specific inhibitors such as chlorpromazine can be used to inhibit clathrin-mediated uptake as it causes clathrin to accumulate in late endosomes (Chiu *et al.*, 2010). Wortmannin and cytochalasin D are commonly used to block macropinocytosis while genistein are used to inhibit caveolar-mediated endocytosis (Chiu *et al.*, 2010). Besides, the transport and release of bioactive compounds from nanocarriers are often concentration and time dependent. Thus, a time course study will be essential to determine the optimum condition for tocotrienol to reach cancer cells specifically to exert its anti-proliferative effect. Collectively, in-depth cellular studies in

combination with *in vivo* biodistribution assessment and pharmacokinetic/pharmacodyanamic studies will hopefully provide a comprehensive overview of the biological properties of the system when administered intravenously. From these findings, synthesis of the delivery system can be modified accordingly in order to correlate with the specific requirements for optimal accumulation in the tumour, a prerequisite for enhanced therapeutic efficacy.

One of the common obstacles for effective delivery of chemotherapeutic agents to tumours is the lack of release kinetic from the nanocarriers albeit efficient extravasation from tumour vasculature. In an attempt to increase the cellular internalization of therapeutic molecules, liposomes with fusogenic properties were developed (Simoes *et al.*, 2004). The fusogenic liposomes were prepared by incorporating lipids that are able to undergo a phase transition under acidic conditions, promoting the fusion or destabilization of target membranes (including plasma membrane and endosomal membrane), effectively increasing the amount of drug released. Phosphatidylethanolamine (PE) and its derivatives are well known to have such properties. While at physiological pH, stable liposomes are formed. A drop in pH however triggers the protonation of carboxylic groups of the amphiphiles, reducing their stabilizing effect (Simoes *et al.*, 2004). As such, PE molecules revert into their inverted hexagonal phase leading to liposomal destabilization (Simoes *et al.*, 2004). In one of our vesicular systems, i.e. Span 60/TPGS vesicles, dioleoylphosphatidylethanolamine (DOPE) was used as a helper lipid to improve the grafting of transferrin onto the surface of vesicles. It was anticipated that DOPE was capable of performing dual functions: not only in enhancing transferrin conjugation,

but also facilitating the endosomal escape of tocotrienol from niosomes as previously shown with DOPE liposomes encapsulating fluorescence probe and DNA (Bellavance *et al.*, 2010; Candiani *et al.*, 2010). However, Span 60/TPGS failed to show significant advantage over Span 60/Solulan C24 vesicles in terms of *in vitro* and *in vivo* therapeutic efficacy. We hypothesize that the concentration of DOPE might be a major limitation for its functionality. In this context, it is strongly suggested a future study be undertaken to investigate the role of DOPE in formulating a pH-sensitive niosome encapsulating tocotrienol.

No doubt tocotrienol-rich fraction (TRF) has demonstrated impressive antitumour effect upon intravenous administration when entrapped in transferrin-targeted vesicles. However, there is scope for improvement for TRF by implementing the knowledge of separation technique. As a mixture containing α-tocopherol, α-tocotrienol, γ-tocotrienol and δ-tocotrienol, TRF might not be at its best therapeutic efficacy due to the possible countering effect from α-tocopherol. It was previously shown that supplementation with α-tocopherol depressed the absorption level of γ-tocotrienol, subsequently attenuating its biological effect (Levin and Clouatre, 2009). Additionally, high dose supplementation with α-tocopherol was also reported to deplete plasma and tissue concentration of γ-tocotrienol (Kosowski *et al.*, 2009). A possible way to resolve this dilemma is by identifying a fraction of tocotrienol devoid of α-tocopherol. An example of such attempt was accomplished by Gapor *et al.* (2005) where tocotrienol-enriched fraction (TEF) was successfully extracted from palm oil. TEF, a mixture of vitamin E containing only the fractions

from tocotrienol, would be a promising anti-cancer agent exhibiting higher therapeutic activity than that observed with TRF.

Tumor regression after systemic administration of tocotrienol entrapped in tumor-targeted vesicles

Ju Yen Fu [a], David R. Blatchford [a], Laurence Tetley [b], Christine Dufès [a,*]

[a] Strathclyde Institute of Pharmacy and Biomedical Sciences, University of Strathclyde, 27 Taylor Street, Glasgow G4 0NR, United Kingdom
[b] Faculty of Biomedical and Life Sciences, University of Glasgow, Glasgow G12 8QQ, United Kingdom

ARTICLE INFO

ABSTRACT

The therapeutic potential of tocotrienol, an extract of vitamin E with anti-cancer properties, is hampered by its failure to specifically reach tumors after intravenous administration, without secondary effects on normal tissues. We hypothesize that the encapsulation of tocotrienol-rich fraction (TRF) within vesicles bearing transferrin, whose receptors are overexpressed on many cancer cells, could result in a selective delivery to tumors after intravenous administration. The objectives of this study are therefore to prepare and characterize transferrin-targeted vesicles encapsulating TRF, and to evaluate their therapeutic efficacy in vitro and in vivo.

The entrapment of TRF in transferrin-bearing vesicles led to a 3-fold higher TRF uptake and more than 100-fold improved cytotoxicity in A431 (epidermoid carcinoma), T98G (glioblastoma) and A2780 (ovarian carcinoma) cell lines compared to TRF solution. The intravenous administration of TRF encapsulated in transferrin-bearing vesicles led to tumor regression and improvement of animal survival in a murine xenograft model, contrary to that observed with controls. The treatment was well tolerated by the animals.

This work corresponds to the first preparation of a tumor-targeted delivery system able to encapsulate tocotrienol. Our findings show that TRF encapsulated in transferrin-bearing vesicles is a highly promising therapeutic system, leading to tumor regression after intravenous administration without visible toxicity.

© 2009 Elsevier B.V. All rights reserved.

1. Introduction

An extract of vitamin E, tocotrienol, has recently gained considerable attention for its tumor suppressive effects on many cancers, including prostate, breast, liver and lung cancers [1]. Tocotrienol has been reported to exert its anti-cancer effect through mechanisms such as decrease of oxidative stress, activation of p53, modulation of Bax/Bcl-2 ratio and induction of apoptosis. It also inhibits several enzymes related to cancer cell proliferation, such as DNA polymerase and telomerase, and NF-κB activation pathway, leading to potentiation of apoptosis. Tocotrienol was also able to downregulate the expression of the vascular endothelial growth factor (VEGF) receptor and to block intracellular VEGF signaling, thus resulting in the inhibition of angiogenesis [2–4].

However, its therapeutic potential is currently limited by its failure to reach tumors at high concentrations without secondary effects on normal tissues. Given the anti-proliferative properties of tocotrienol, it is crucial to deliver the therapeutic drug specifically to its site of action.

As iron is essential for tumor cell growth and can be effectively carried to tumors by using transferrin receptors, we hypothesize that the encapsulation of tocotrienol within vesicles bearing transferrin could result in a selective delivery of tocotrienol to tumors after intravenous administration, leading to an improved therapeutic efficacy. Transferrin receptor is an attractive target for selective receptor-mediated gene delivery to tumors because it is overexpressed in a high percentage of human cancers, including ovarian, breast, colon cancers and glioblastoma cell lines [5,6]. Although transferrin receptors are also expressed in some rapidly dividing healthy tissues, the combination of active targeting, based on the use of ligands, and passive targeting, based on the accumulation of particulate delivery systems due to enhanced permeability and retention [7], should provide a tumor-selective targeting strategy. Transferrin (Tf) has previously been used successfully as a tumor-targeting ligand for several drug delivery systems [5,8–10].

The objectives of this study are therefore to prepare and characterize transferrin-bearing vesicles encapsulating TRF and to evaluate their therapeutic efficacy in vitro and in vivo.

2. Materials and methods

2.1. Cell lines and reagents

Palm oil and Tocotrienol Rich Fraction (TRF), a mixture of 17.6% α-tocotrienol, 23.1% γ-tocotrienol, 15.1% δ-tocotrienol, 15.3% α-tocopherol, and other tocotrienol-related compounds, were kindly donated by Dr. Nor Aini Idris and Dr. Abdul Gapor from the Malaysian Palm Oil Board (Kuala Lumpur, Malaysia). Solulan C24 was purchased from Amerchol

* Corresponding author. Tel.: +44 141 548 3796; fax: +44 141 552 2562.
E-mail address: C.Dufes@strath.ac.uk (C. Dufès).

(Edison, NJ). Vectashield® mounting medium with propidium iodide was obtained from Vector Laboratories (Peterborough, UK). Isopropanol and dimethylsulfoxide were purchased from Merck (Nottingham, UK). A431 epidermoid carcinoma, T98G glioblastoma and A2780 ovarian carcinoma were obtained from the European Collection of Cell Cultures. Tissue culture media were purchased from Invitrogen (Paisley, UK). All other chemicals came from Sigma (Poole, UK).

2.2. Preparation and characterization of transferrin-bearing vesicles encapsulating TRF

Transferrin (Tf)-bearing vesicles encapsulating TRF were prepared by modification of a previously described method [9,10]. Control vesicles encapsulating TRF were prepared by shaking a mixture of Span 60 (65 mg), cholesterol (58 mg), Solulan C24 (54 mg) in TRF solution (0.5 mg/mL, 2 mL, prepared in PBS, palm oil or dimethylsulfoxide) at 60 °C for 1 h, followed by probe sonication (Soniprep 150, Fisher Scientific) for 4 min with the instrument set at 75% of its maximal capacity. Transferrin (6 mg) was linked to the vesicles (2 mL) by cross-linking with dimethylsuberimidate as previously described [9]. Free drug was removed by ultracentrifugation as described [9]. Vesicles were visualized by transmission electron microscopy on a LEO 912 energy filtering electron microscope as described [9]. TRF loading of the vesicles was measured spectrofluorometrically (λ_{ex} 295 nm, λ_{em} 325 nm, using a Cary eclipse spectrofluorometer, Varian) after disruption of vesicles with isopropanol. The amount of conjugated transferrin was determined using the Lowry method as described [9]. Vesicle size and zeta potential were respectively measured by photon correlation spectroscopy and laser Doppler electrophoresis on a Zetasizer Nano-ZS (Malvern Instruments, Malvern, UK).

2.3. In vitro biological characterization

2.3.1. Cell culture
A431, T98G and A2780 cell lines were grown as monolayers in DMEM (A431 and T98G) or RPMI (A2780) medium supplemented with 10% (v/v) fetal bovine serum, 1% (v/v) L-glutamine and 0.5% (v/v) penicillin–streptomycin. Cells were cultured at 37 °C in a humid atmosphere of 5% CO_2.

2.3.2. Cellular uptake of TRF entrapped in Tf-bearing vesicles
A431, T98G and A2780 cells (4×10^3 cells/well in 96-well plates seeded 72 h prior treatment) were incubated for 96 h with TRF (10 µg/well) formulated as Tf-vesicles, control vesicles or as free drug. After the incubation, cells were washed twice with PBS and lysed. The amount of TRF in the cell lysate was assessed by fluorescence spectrophotometry ($\lambda_{ex} = 295$ nm, $\lambda_{em} = 325$ nm).

Imaging of TRF cellular uptake was carried out using confocal microscopy. A431, T98G and A2780 cells were grown on microscope slides (0.6×10^6 cells/90-mm Petri dish) for 24 h. The cells were then treated for 4 h with 50 µg TRF either entrapped in Tf-vesicles, control vesicles or in solution. They were then washed with PBS and fixed in methanol for 10 min. Upon staining of the nuclei with propidium iodide, cells were examined using a Leica SP-5 confocal laser scanning microscope ($\lambda_{ex} = 535$ nm and $\lambda_{em} = 615$ nm for stained nuclei, $\lambda_{ex} = 295$ nm and $\lambda_{em} = 325$ nm for TRF).

2.3.3. Cytotoxicity assay
Anti-proliferative activity of transferrin- and control vesicles entrapping TRF was compared with TRF solution in A431, T98G and A2780 cell lines. Cells (2×10^3 cells per well in 96-well plates seeded 72 h prior treatment) were incubated for 72 h with TRF formulations at final concentrations of 1×10^{-7} to 1×10^2 µg/mL. Cytotoxicity was evaluated by measurement of the growth inhibitory concentration for 50% of the cell population (IC_{50}) in a standard MTT [3-(4,5-dimethylthiazol-2-yl)-2,5-diphenyl-tetrazolium bromide] assay [11].

Dose–response curves were fitted to percentage absorbance values to obtain IC_{50} values (three independent experiments with $n = 5$ for each concentration level).

2.4. In vivo study

2.4.1. Animals
Female immunodeficient BALB/c mice (initial mean weight 20 g) housed in groups of five at 19 °C to 23 °C with a 12-hour light–dark cycle were fed a conventional diet (Rat and Mouse Standard Expanded, B&K Universal, Grimston, United Kingdom) with mains water *ad libitum*. Experimental work was carried out in accordance with UK Home Office regulations and approved by the local ethics committee.

2.4.2. In vivo tumoricidal activity
Tumors (typical diameter 5 mm) were palpable 6 days after subcutaneous implantation of A431 cancer cells in exponential growth (1×10^6 cells per flank). TRF entrapped in Tf-vesicles, control vesicles or in solution was administered by intravenous tail vein injection (10 µg TRF per injection) once daily for 10 days. Animals were weighed daily and tumor volume was determined by caliper measurements (volume $= d^3 \times \pi/6$). Results were expressed as relative tumor volume (rel. $Vol_{tx} = Vol_{tx}/Vol_{t0}$) and responses classified analogous to Response Evaluation Criteria in Solid Tumors (RECIST, [12]). Progressive disease is defined as an increase in relative tumor volume higher than 1.2-fold, stable disease as a relative volume between 0.7 and 1.2 of starting volume, partial response as measurable tumor with a reduction of more than 30% (0–0.7) and complete response as the absence of any tumor.

2.5. Statistical analysis

Results were expressed as means ± S.E.M. Statistical significance was determined by one-way ANOVA followed by the Bonferroni post-test (GraphPad Prism software). Differences were considered as significant when $P < 0.05$.

3. Results and discussion

3.1. Preparation and characterization of transferrin-bearing vesicles encapsulating TRF

The formation of vesicles encapsulating TRF and bearing transferrin (Tf-vesicles) was confirmed by TEM (Fig. 1A). TRF loading within the vesicles was 28.5 ± 1.9% of the initial TRF. However the solubilization of TRF in palm oil or dimethylsulfoxide led to an improved TRF loading of 30.8 ± 0.6% and 44.1 ± 0.6% respectively. TRF will therefore be solubilized in dimethylsulfoxide prior further preparations of vesicles. Transferrin was conjugated to the vesicles at a level of 89 ± 5% of the initial transferrin added, which corresponds to an improvement compared to our previous conjugation rate of around 50% [9,10]. Loaded Tf- and control vesicles respectively had a z-average mean diameter of 137 nm (polydispersity: 0.169) and 188 nm (polydispersity: 0.154). As the cut-off size for extravasation has been found to be 400 nm [13–15] for most tumors, this delivery system has the required properties to access the receptor-expressing tumor cells and specifically deliver TRF. Tf- and control vesicles were bearing negative surface charges, slightly higher after conjugation of the iron-saturated holo-transferrin (respectively − 36 mV and − 40 mV for Tf-vesicles and control vesicles). These net negative charges would reduce non-specific cellular uptake of the vesicles due to a decrease of electrostatic interactions with the negatively charged cellular membrane [16]. To our knowledge, this is the first formulation of tocotrienol entrapped in a targeted delivery system. The combination of active targeting (based on the use of Tf ligands) and passive
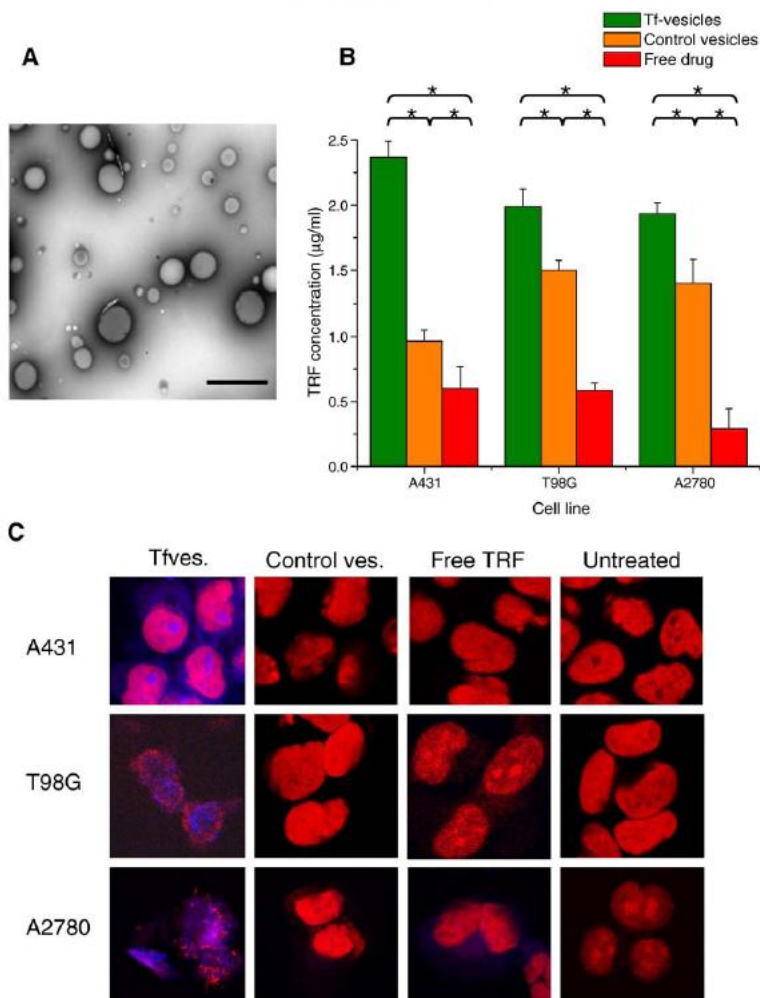
Fig. 1. Preparation and characterization of transferrin-vesicles entrapping TRF. A) Transmission electron micrographs confirming the formation of vesicles entrapping TRF and bearing Tf (Bar: 1 μm). B) Spectrofluorimetric quantification of the cellular uptake of TRF (10 μg/well) formulated as Tf-vesicles (green), control vesicles (orange) or as free drug (red), in A431, T98G and A2780 cell lines ($n=15$)(*: $p<0.05$). C) Confocal laser scanning microscopy imaging of the cellular uptake of TRF (50 μg/dish) either entrapped in Tf-vesicles, control vesicles or free in solution, after incubation for 4 h in A431, T98G and A2780 cells (red: nuclei stained with propidium iodide, blue: TRF) (magnification×40).

targeting (based on the accumulation of particulate delivery systems due to the enhanced permeability and retention) should provide a tumor-selective targeting strategy.

3.2. Cellular uptake of TRF entrapped in Tf-bearing vesicles

The entrapment of TRF in the vesicles significantly improved TRF uptake by the three cell lines compared to TRF solution (Fig. 1B): TRF uptake after treatment with control vesicles was at least twice higher than that of TRF solution for T98G and A2780 cell lines. The grafting of transferrin on the vesicles further improved TRF uptake compared to control vesicles: more than twice the amount of TRF was taken up by A431 cells when treated with Tf-vesicles compared to control vesicles.

The highest amount of cell-associated fluorescence was found in A431 cells incubated with Tf-vesicles. TRF uptake was also qualitatively confirmed using confocal microscopy in the three cell lines. Co-

Table 1
Cytotoxicity of TRF, free or formulated as Tf-vesicles or control vesicles, in A431, T98G and A2780 cells expressed as IC$_{50}$ values ($n=15$).

Cell lines	IC$_{50}$ (μg/mL) (mean ± S.E.M.)		
	Tf-vesicles	Control vesicles	Free TRF
A431	0.66 ± 0.08	1.42 ± 0.30	131.06 ± 1.94
T98G	0.17 ± 0.14	0.97 ± 0.48	79.49 ± 0.16
A2780	0.05 ± 0.02	0.11 ± 0.10	10.73 ± 4.36

220
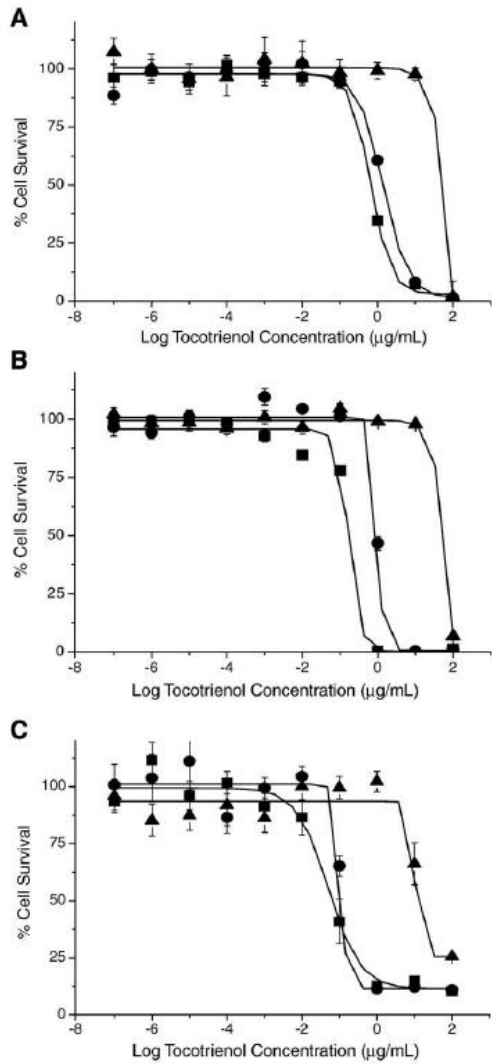
Fig. 2. Cytotoxicity of TRF delivered as free drug (▲), entrapped in Tf-vesicles (■) or in control vesicles (●), against (A) A431, (B) T98G and (C) A2780 cells (*n* = 15).

localization of TRF in the nuclei was clearly visible in the three cell lines treated with Tf-vesicles, with some accumulation in a central compartment, possibly the nucleolus. The repartition of TRF within the nuclei was particularly heterogeneous in A2780 cells. In A431 cells, TRF-derived fluorescence was also disseminated in the

Fig. 3. A) Tumor growth studies in a mouse A431 xenograft model after intravenous administration of transferrin-vesicles encapsulating TRF (10 μg/injection) (green) (controls: control vesicles encapsulating TRF (orange), TRF solution (red), untreated tumors (black). Treatment was administered intravenously once daily on ten occasions. Results were expressed as relative tumor volume (rel. Vol$_{EX}$ = Vol$_{EX}$/Vol$_{t0}$) (*n* = 5). B) Variations of the animal body weight throughout the treatment regime (*n* = 5). C) Overall tumor response to treatments on the last injection day, stratified according to change in tumor volume. D) Time to disease progression. Animals were removed from the study once their tumor reached 12 mm diameter. (Color coding as in A).
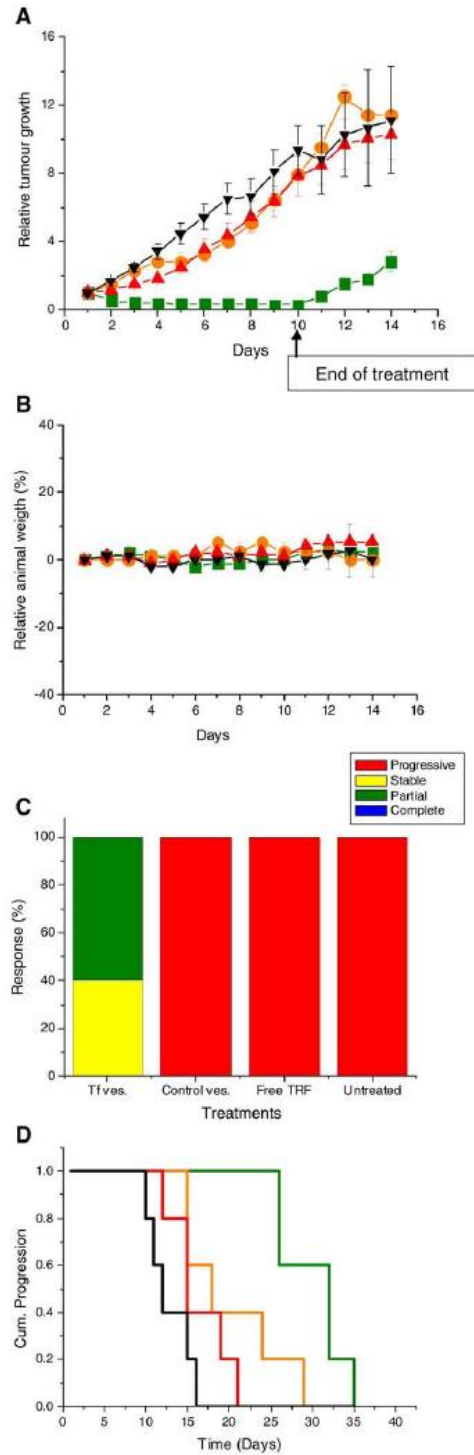
221

cytoplasm after treatment with Tf-vesicles. By contrast, cells treated with control vesicles or free TRF showed no TRF-derived fluorescence, except after treatment of A2780 cells with free TRF. In this case, a faint TRF-derived fluorescence was observed in the cytoplasm, probably due to the non-specific diffusion of the drug. These data demonstrated that the entrapment of TRF in Tf-vesicles led to a significant improvement of TRF uptake by the tested cell lines overexpressing Tf receptors. Free TRF enters the cell by diffusion, while the vesicular formulations are taken up by endocytosis, a comparatively slower but highly specific process.

3.3. Cytotoxicity assay

The improvement of TRF uptake when administered in Tf-vesicles led to similar improvement in the level of cytotoxicity of the various formulations. The vesicle formulations of TRF were all significantly more efficacious than the free drug by at least 80 times, with IC_{50} ranging from 0.05 ± 0.02 to 1.42 ± 0.30 μg/mL (Table 1, Fig. 2). The grafting of transferrin to the vesicles further improved the therapeutic efficacy of the vesicles entrapping TRF, by 5-fold for T98G cells and 2-fold for A2780 and A431 cells. Although the highest TRF uptake was found in A431 cells after treatment with Tf-vesicles, improved cytotoxic activities were found in A2780 and T98G, probably because A431 cells are more resistant than the two other cell lines. As mentioned above, TRF consists of a mixture of tocotrienols and tocopherols, but previous studies have demonstrated that its anti-proliferative effects are mediated by tocotrienols only [17].

3.4. In vivo tumoricidal activity

In vivo, TRF entrapped in Tf-vesicles induced a measurable tumor volume reduction within 24 h. Over the following 10 days, this led to a marked regression of the tumors and improvement of the animal survival, whereas none of the other treatments led to any tumor regression. On the day of the last injection, 40% of tumors treated with Tf-vesicles entrapping TRF were stable, while the remaining 60% showed a partial response. By contrast, 100% of the tumors treated with control vesicles or free TRF were progressive (Fig. 3). Although the tumor grew after cessation of treatment, the rate of re-growth in mice treated with Tf-vesicles was significantly lower than all other treatment groups. As a result, the extended survival of the mice treated with targeted vesicles, control vesicles and free TRF was respectively 19 days, 12 days and 2 days compared to untreated mice. Although a further extension of the number of injections to the animals was currently not allowed, the extended survival results obtained after 10 injections still demonstrated the superiority of Tf-vesicles over the other formulations. The systemic use of TRF entrapped in vesicles or administered as a solution was well tolerated and no apparent signs of toxicity or significant weight loss were observed (Fig. 3B).

The most striking effects of TRF entrapped in targeted vesicles was the induction of tumor regression within one day of treatment and the near disappearance of the tumors for many animals of this treatment group within 10 days of treatment, a duration generally acknowledged as sufficient for treating minor ailments but not a cancer, even with traditional chemotherapy. This therapeutic system was able to act on subcutaneous implanted tumors after systemic administration and should therefore have the potential to target multiple metastasic nodules disseminated throughout the body. There may be scope to further improve on the *in vivo* activity of these extremely safe delivery systems, by using a higher dose, reducing the size of the vesicles and extending the length of the treatment, hopefully leading to an optimized therapeutic effect.

In conclusion, this work corresponds to the first preparation of a tumor-targeted delivery system able to encapsulate tocotrienol. Transferrin-conjugated vesicles showed a statistically significant uptake advantage when compared to the non-targeted vesicles. The vesicle formulations of tocotrienol significantly improved the therapeutic efficacy of tocotrienol *in vitro* by at least 80 times compared to the drug solution. The grafting of transferrin to the vesicles further improved their therapeutic efficacy by at least 2-fold compared to control vesicles. Our findings show that TRF encapsulated in transferrin-bearing vesicles is a promising therapeutic system, leading to tumor regression after intravenous administration without visible toxicity.

These studies provide a proof of principle that the entrapment of vitamin E extract tocotrienol in a targeted delivery system may be an attractive strategy for anti-tumor therapy, combining efficacy against the tumor with the lowest possible effects on normal tissues and organs after systemic administration.

References

[1] C. Constantinou, A. Papas, A.I. Constantinou, Vitamin E and cancer: an insight into the anticancer activities of vitamin E isomers and analogs, Int. J. Cancer 123 (2008) 739–752.
[2] K. Nesaretnam, Multitargeted therapy of cancer by tocotrienol, Cancer Lett. 269 (2008) 88–395.
[3] S. Wada, Y. Satomi, M. Murakoshi, N. Noguchi, T. Yoshikawa, H. Nishino, Tumor suppressive effects of tocotrienol in vivo and in vitro, Cancer Lett. 229 (2005) 181–191.
[4] T. Miyazawa, A. Shibata, P. Sookwong, Y. Kawakami, T. Eitsuka, A. Asai, S. Oikawa, K. Nakagawa, Antiangiogenic and anticancer potential of unsaturated vitamin E (tocotrienol), J. Nutr. Biochem. 20 (2009) 79–86.
[5] T.R. Daniels, T. Delgado, G. Helguera, M.L. Penichet, The transferrin receptor part II: targeted delivery of therapeutic agents into cancer cells, Clin. Immunol. 121 (2006) 159–176.
[6] A. Calzolari, I. Oliviero, S. Deaglio, G. Mariani, M. Biffoni, N.M. Sposi, F. Malavasi, C. Peschle, U. Testa, Transferrin receptor 2 is frequently expressed in human cancer cell lines, Blood Cells Mol. Diseases 39 (2007) 82–91.
[7] H. Maeda, The tumor blood vessel as an ideal target for macromolecular anticancer agents, J. Control. Release 19 (1992) 315–324.
[8] Z.M. Qian, H. Li, H. Sun, K. Ho, Targeted drug delivery via the transferrin receptor-mediated endocytosis pathway, Pharmacol. Rev. 54 (2002) 561–587.
[9] C. Dufès, A.G. Schätzlein, L. Tetley, A.I. Gray, D.G. Watson, J.C. Olivier, W. Couet, I.F. Uchegbu, Niosomes and polymeric chitosan based vesicles bearing transferrin and glucose ligands for drug targeting, Pharm. Res. 17 (2000) 1250–1258.
[10] C. Dufès, J.M. Muller, W. Couet, J.C. Olivier, I.F. Uchegbu, A.G. Schätzlein, Anticancer drug delivery with transferrin targeted polymeric chitosan vesicles, Pharm. Res. 21 (2004) 101–107.
[11] J.A. Plumb, R. Milroy, S.B. Kaye, Effects of the pH dependence of 3-(4,5-dimethylthiazol-2-yl)-2,5-diphenyltetrazolium bromide-formazan absorption on chemosensitivity determined by a novel tetrazolium-based assay, Cancer Res. 49 (1989) 4435–4440.
[12] P. Therasse, S.G. Arbuck, E.A. Eisenhauer, J. Wanders, R.S. Kaplan, L. Rubinstein, J. Verweij, M. Van Glabbeke, A.T. Van Oosterom, M.C. Christian, S.G. Gwyther, New guidelines to evaluate the response to treatment in solid tumors, European Organization for Research and Treatment of Cancer, National Cancer Institute of the United States, National Cancer Institute of Canada, J. Natl. Cancer Inst. 92 (2000) 205–216.
[13] F. Yuan, M. Dellian, D. Fukumura, M. Leunig, D.A. Berk, V.P. Torchilin, R.K. Jain, Vascular permeability in a human tumor xenograft: molecular size dependence and cutoff size, Cancer Res. 55 (1995) 3752–3756.
[14] O. Ishida, K. Maruyama, K. Sasaki, M. Iwatsuru, Size-dependent extravasation and interstitial localization of polyethyleneglycol liposomes in solid tumor-bearing mice, Int. J. Pharm. 193 (1999) 49–56.
[15] G. Kong, R.D. Braun, M.W. Dewhirst, Hyperthermia enables tumor-specific nanoparticle delivery: effect of particle size, Cancer Res. 60 (2000) 4440–4445.
[16] R.I. Mahato, L.C. Smith, A. Rolland, Pharmaceutical perspectives of nonviral gene therapy, Adv. Genet. 41 (1999) 95–156.
[17] B.S. McIntyre, K.P. Briski, A. Gapor, P.W. Sylvester, Antiproliferative and apoptotic effects of tocopherols and tocotrienols on preneoplastic and neoplastic mouse mammary epithelial cells, Proc. Soc. Exp. Biol. Med. 224 (2000) 292–301.

British Pharmaceutical Conference 2009

Tumour regression after systemic administration of a novel targeted vitamin E therapeutic system

J.Y. Fu[a], L. Tetley[b], D. Blatchford[a] and C. Dufès[a]
[a]University of Strathclyde, Glasgow and [b]University of Glasgow, Glasgow, UK.

Objectives

Tocotrienol, an extract of vitamin E, has been shown to exert anti-proliferative and tumour suppressive effects on cancer cells (Nesaretnam *et al.*, 2008). However, its therapeutic potential is currently limited by its failure to reach tumours after intravenous administration, without secondary effects on normal tissues. The objectives of this study are 1) to prepare and characterize novel transferrin-targeted vesicles encapsulating tocotrienol, able to recognize transferrin receptors overexpressed on many cancer cell lines and 2) to evaluate *in vitro* and *in vivo* the therapeutic and targeting efficacies of this therapeutic system.

Methods

Tocotrienol was encapsulated in Span 60 vesicles upon heating and probe sonication, prior to transferrin conjugation by cross-linking. Upon purification by ultracentrifugation, vesicles were visualized by transmission electron microscopy and have their size and zeta potential measured by photon correlation spectroscopy. Transferrin conjugation was assessed by a Lowry protein quantification assay. Tocotrienol encapsulation was quantified by spectrofluorimetry. Tocotrienol uptake by cancer cells was assessed quantitatively by spectrofluorimetry and qualitatively by confocal microscopy. The therapeutic efficacy of this system was evaluated *in vitro* using a MTT assay and *in vivo* after intravenous administration to a murine xenograft model.

Results

The sizes of tocotrienol loaded vesicles were found to be 137 ± 0.169 nm for transferrin-bearing vesicles and 123 ± 0.154 nm for control vesicles. The zeta potential of these vesicles was found to be -36 mV and -40 mV respectively for transferrin-bearing and control vesicles. Transferrin was conjugated to the vesicles at a level of 89 ± 5 % of the initial transferrin added. TRF loading within the vesicles was $44.1 \pm 0.6\%$ of the initial TRF. *In vitro*, the therapeutic efficacy of tocotrienol when encapsulated in transferrin-bearing vesicles was improved by at least 100-fold compared to free tocotrienol and at least 2-fold compared to non-targeted vesicles in T98G, A431 and A2780 cancer cells (i.e. IC_{50} : 0.17 μg/mL, 0.97 μg/mL and 79.49 μg/mL respectively for Tf-vesicles, control vesicles and drug solution in T98G cells). *In vivo*, intravenous administration of tocotrienol encapsulated in transferrin-bearing vesicles led to the regression of well-established tumours, followed by a delayed progression. By contrast, treatment with tocotrienol in solution or encapsulated in control vesicles did not lead to any tumour regression. The treatment was well tolerated in mice, with no weight loss or visible signs of toxicity.

Conclusions

Transferrin-bearing vesicles encapsulating tocotrienol have been successfully prepared. This work corresponds to the first preparation of a tumour-targeted delivery system able to encapsulate tocotrienol. Our findings show that tocotrienol encapsulated in transferrin-bearing vesicles is a highly promising therapeutic system, leading to tumour regression after intravenous administration without visible toxicity.

References

Nesaretnam, K. (2008) *Cancer Lett*. **269**(2): 388-395 (61)

Preparation and evaluation of a novel targeted palm oil vitamin E therapeutic system

Ju Yen Fu and Christine Dufès

Palm oil vitamin E extract known as Tocotrienol-Rich Fraction (TRF) has been shown to exert anti-proliferative and tumour suppressive effects on various cancer cells. However, its therapeutic potential is currently limited by its failure to reach tumours after intravenous administration, without secondary effects on healthy tissues. The objectives of this study are therefore 1) to prepare and characterize novel transferrin-targeted vesicles encapsulating TRF, able to recognize transferrin receptors overexpressed on many cancer cell lines and 2) to evaluate *in vitro* and *in vivo* the therapeutic and targeting efficacies of this therapeutic system.

Upon purification, transferrin-bearing vesicles encapsulating TRF were visualized by transmission electron microscopy and have their size and zeta potential assessed by photon correlation spectroscopy. The TRF loading and transferrin conjugation were respectively analysed by spectrofluorimetry and protein quantification assay. *In vitro*, the TRF uptake by cancer cells overexpressing transferrin receptors after administration of the TRF therapeutic system was assessed by spectrofluorimetry and confocal microscopy. The therapeutic efficacy of this system was investigated *in vitro* by using a MTT assay and *in vivo* after intravenous administration to a murine xenograft model.

In vitro, the therapeutic efficacy of TRF when encapsulated in transferrin-bearing vesicles was improved by at least 100-fold and 2-fold compared to non-encapsulated TRF and control vesicles respectively.
In vivo, the intravenous administration of TRF encapsulated in transferrin-bearing vesicles led to the regression of well-established, vascularized tumours, followed by a delayed progression. By contrast, treatment of the tumours by intravenous administration of TRF encapsulated in control vesicles or administered as a solution did not lead to any tumour regression. The treatment was well tolerated by the mice, with no weight loss or visible signs of toxicity.

This work corresponds to the first preparation of a tumour-targeted delivery system able to encapsulate tocotrienol. Our findings show that TRF encapsulated in transferrin-bearing vesicles is a highly promising therapeutic system, leading to tumour regression of vascularised tumours after intravenous administration without visible toxicity.

Synthesis and evaluation of a novel tocotrienol-based therapeutic system for tumour targeting

Ju Yen Fu[a], Laurence Tetley[b], David R. Blatchford[a] and Christine Dufès[a]

[a]University of Strathclyde, Glasgow and [b]University of Glasgow, Glasgow, UK.

Tocotrienol, a group of compounds present in vitamin E, has gained much attention in recent years for its tumour suppressive properties on cancer cells. Multiple pathways including anti-angiogenesis, p53 activation and apoptosis are among the proposed mechanism of action for the anti-cancer effect of tocotrienol. However, its therapeutic potential was hampered by the limited ability to reach tumours specifically after intravenous administration. In this study, the approach of entrapping tocotrienol in a tumour-targeted delivery system was investigated. Transferrin is an iron transporter whose receptors are often over-expressed in cancer cells due to high iron demand for tumour growth. The conjugation of transferrin to drug delivery systems appeared to be an attractive tool for selective receptor-mediated delivery of therapeutic drugs to tumours. The objectives of this study were therefore to prepare and evaluate the targeting and therapeutic efficacies of transferrin-bearing vesicles entrapping tocotrienol.

Tocotrienol was entrapped in Span 60 vesicles upon heating and probe sonication, prior to transferrin conjugation by cross-linking. Upon purification, vesicles were visualised and characterized for entrapment efficacy, transferrin conjugation efficacy, size and zeta potential. The therapeutic efficacy of this system was evaluated *in vitro* using an MTT assay and *in vivo* after intravenous administration to a murine xenograft model. *In vitro* results showed at least 80-fold improvement in therapeutic efficacy of tocotrienol when entrapped in vesicles. A further 2-fold improvement was observed when vesicles were targeted with transferrin. *In vivo*, marked tumour regression was observed in mice after administration of transferrin-bearing vesicles entrapping tocotrienol. In contrast, no significant advantage was observed in mice treated with control vesicles and free tocotrienol compared to untreated mice. In conclusion, the grafting of transferrin to tocotrienol-loaded vesicles improved the therapeutic potential of tocotrienol, leading to tumour regression of vascularised tumours after intravenous administration without visible toxicity.

Tumor Regression after Intravenous Administration of Tocotrienol Entrapped in Tumor-targeted vesicles

Ju Yen Fu[1], David R. Blatchford[1], Laurence Tetley[2], and Christine Dufès[1]

[1]Strathclyde Institute of Pharmacy and Biomedical Sciences, University of Strathclyde, Glasgow G4 0NR, United Kingdom; [2]Faculty of Biomedical and Life Sciences, University of Glasgow, Glasgow G12 8QQ, United Kingdom.
yen.fu@strath.ac.uk

ABSTRACT SUMMARY

Tocotrienol, a component of the vitamin E, has recently been shown to have antiproliferative effects on cancer cells. However, its inability to specifically reach tumors after intravenous administration limits its therapeutic potential. In order to overcome this problem, we proposed to encapsulate tocotrienol in vesicles bearing transferrin, whose receptors are overexpressed on many cancer cells. The objectives of this study are therefore to prepare transferrin-bearing vesicles entrapping tocotrienol and to evaluate their therapeutic efficacy *in vitro* and *in vivo*.

INTRODUCTION

A component of vitamin E, tocotrienol, has gained much attention in recent years for its tumor suppressive properties on cancer cells[1]. Multiple pathways were shown to be responsible for the anti-cancer effect of tocotrienol, including anti-angiogenesis, activation of p53 and apoptosis[1, 2]. However, its therapeutic potential was limited by its inability to specifically reach tumors after intravenous administration.

In this study, we investigated the approach of encapsulating tocotrienol in a tumor-targeted delivery system for specific delivery of tocotrienol to the tumors. Transferrin is an iron transporter whose receptors are often over-expressed in cancer cells due to the high iron demand for tumor growth[3]. Conjugation of transferrin to drug delivery systems appeared to be an attractive tool for selective receptor-mediated tumor delivery of therapeutic drugs. This strategy has been previously used for several drug and gene delivery systems[4].

The objectives of this study are therefore (1) to prepare and characterize transferrin-bearing vesicles encapsulating tocotrienol and (2) to evaluate *in vitro* and *in vivo* the therapeutic and targeting efficacies of this therapeutic system.

EXPERIMENTAL METHODS

Tocotrienol in the form of tocotrienol rich fraction (TRF) was encapsulated in vesicles composed of Span 60, cholesterol and Solulan C24. Transferrin was then linked to the vesicles by cross-linking, using a method previously described[5]. Purified vesicles were visualized using transmission electron microscopy and characterized using spectrofluorimetry, Lowry protein quantification assay and photon correlation spectroscopy to respectively measure TRF encapsulation efficiency, transferrin conjugation efficiency, vesicle size and zeta potential.

In vitro, the therapeutic efficacy of TRF, either free or entrapped in transferrin-bearing or control vesicles was evaluated on cancer cells over-expressing transferrin receptors (A431 epidermoid carcinoma, T98G glioblastoma and A2780 ovarian carcinoma). Cytotoxicity was determined by means of measuring IC$_{50}$ using MTT assay, while cellular uptake of TRF was assessed quantitatively by spectrofluorimetry and qualitatively by confocal microscopy.

In vivo, treatments equivalent to 10 µg TRF were administered via intravenous tail vein injections to mice bearing subcutaneous A431 tumors. Animal weight and tumor volume were measured daily. The results were expressed as relative tumor growth and the tumor responses were classified according to the Response Evaluation Criteria in Solid Tumor (RECIST) guidelines[6].

RESULTS AND DISCUSSION

TRF-entrapped vesicles showed a mean diameter of 123 nm (polydispersity: 0.154) and zeta-potential of -40 mV, with 44.1 ± 0.6% of TRF loading. Upon transferrin conjugation (89 ± 5% of the initial amount of transferrin added), vesicles diameter increased to 137 nm (polydispersity: 0.169) while zeta potential slightly increased to -36 mV[7]. The negative surface charge on vesicles should be an advantage for minimizing the non-specific interaction with the negatively charged cellular membrane as opposed to cationic vesicles[8]. The combination of active targeting (based on the use of transferrin ligands) and passive targeting (based on the accumulation of particulate systems due to enhanced permeability and retention effect) should provide a tumor-selective targeting strategy.
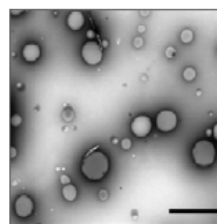
Figure 1. Transmission electron micrographs of TRF-loaded vesicles bearing transferrin (Bar: 1µm)[7].

Upon incubation with cells, the cytotoxicity of TRF, either free or encapsulated in transferrin-bearing and control vesicles, was evaluated and expressed as IC$_{50}$ values in Table 1. At least 80-fold improvement in therapeutic efficacy was observed when TRF was encapsulated in vesicles compared to treatment with TRF solution. A further 2-fold improvement was observed when vesicles were targeted with transferrin compared to control vesicles [7].

Table 1. Cytotoxicity of TRF as free drug or encapsulated in transferrin-vesicles and control vesicles in 3 cell lines (n = 15) [7].

Cell lines	IC$_{50}$ (µg/mL) (Mean ± S.E.M.)		
	Tf-ves.	Ctrl. ves.	Free TRF
A431	0.66 ± 0.08	1.42 ± 0.30	131.06 ± 1.94
T98G	0.17 ± 0.14	0.97 ± 0.48	79.49 ± 0.16
A2780	0.05 ± 0.02	0.11 ± 0.10	10.73 ± 4.36

A marked tumor regression was observed in mice after intravenous administration of transferrin vesicles. This effect was sustained throughout the treatment. In contrast, no significant advantage was observed in mice treated with control vesicles and free TRF compared to untreated mice. All treatments were well tolerated without visible signs of toxicity or weight loss.
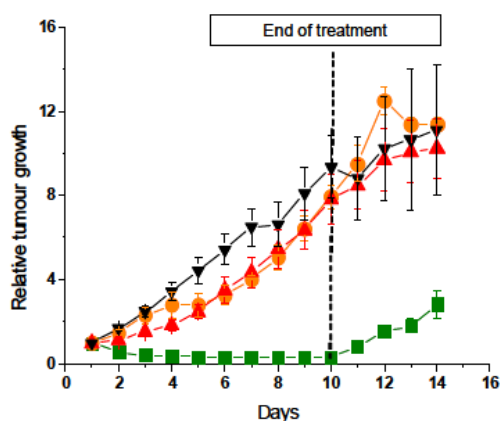
Figure 2. Tumor growth expressed as relative tumor volume (rel. Vol$_{tx}$ = Vol$_{tx}$/Vol$_{t0}$) in a mouse A431 xenograft model after intravenous injection of transferrin-vesicles encapsulating TRF (■), control vesicles encapsulating TRF (●), free TRF solution (▲) and untreated tumors (▼) (n = 5) [7].

CONCLUSION

In conclusion, this work corresponds to the first preparation of a tumor-targeted delivery system able to encapsulate tocotrienol. The grafting of transferrin to tocotrienol-loaded vesicles improved the therapeutic efficacy of tocotrienol to at least 80-fold compared to free tocotrienol *in vitro*. Our *in vivo* study also showed that transferrin-bearing vesicles encapsulating tocotrienol are highly promising therapeutic systems, leading to tumor regression of vascularised tumors after intravenous administration, without visible toxicity.

REFERENCES

1. Nesaretnam K. (2008) Multitargeted therapy of cancer by tocotrienols. *Cancer Lett.*; 269(2): 388-395
2. Miyazawa T., Shibata A., Sookwong P., Kawakami Y., Eitsuka T., Asai A., Okinawa S., Nakagawa K. (2009) Antiangiogenic and anticancer potential of unsaturated vitamin E (tocotrienol). *J. Nutr. Biochem.*; 20: 79-86
3. Daniels T.R., Delgado T., Helguera G., Penichet M.L. (2006) The transferrin receptor part II: targeted delivery of therapeutic agents into cancer cells. *Clin. Immunol.*; 121: 159-176
4. Qian Z.M., Li H., Sun H., Ho K. (2002) Targeted drug delivery via the transferrin receptor-mediated endocytosis pathway. *Pharmacol. Rev.*; 54: 561-587
5. Dufès C., Schätzlein A.G., Tetley L., Gray A.I., Watson D.G., Olivier J.C., Couet W., Uchegbu I.F. (2000) Niosomes and polymeric chitosan based vesicles bearing transferrin and glucose ligands for drug targeting. *Pharm. Res.*; 17: 1250-1258
6. Eisenhauer E.A., Therasse P., Bogaerts J., Schwartz L.H., Sargent D., Ford R., Dancey J., Arbuck S., Gwyther S., Mooney M., Rubinstein L., Shankar L., Dodd L., Kaplan R., Lacombe D., Verweij J. (2009) New response evaluation criteria in solid tumour: Revised RECIST guideline (version 1.1). *Eur. J. Cancer*; 45: 228-247
7. Fu J.Y, Blatchford D.R., Tetley L., Dufès C. (2009) Tumor regression after systemic administration of tocotrienol entrapped in tumor-targeted vesicles, *J. Control. Release*, 140:95-99
8. Mahato R.I., Smith L.C., Rolland A. (1999) Pharmaceutical perspectives of nonviral gene therapy. *Adv. Genet.*; 41: 95-156

227

References

Abd-Elbary, A., El-laithy, H. M., and Tadros, M. I. (2008). Sucrose stearate-based proniosome-derived niosomes for the nebulisable delivery of cromolyn sodium. *Int J Pharm* **357**, 189-198.

Abdelbary, G., and El-Gendy, N. (2008). Niosome-encapsulated gentamicin for ophthalmic controlled delivery. *AAPS PharmSciTech* **9**, 740-747.

Adams, J. U. (2008). Building the bridge from bench to bedside. *Nat Rev Drug Discov* **7**, 463-464.

Agarwal, M. K., Agarwal, M. L., Athar, M., and Gupta, S. (2004). Tocotrienol-rich fraction of palm oil activates p53, modulates Bax/Bcl2 ratio and induces apoptosis independent of cell cycle association. *Cell Cycle* **3**, 205-211.

Aggarwal, S. (2010). Targeted cancer therapies. *Nat Rev Drug Discov* **9**, 427-428.

Ahn, K. S., Sethi, G., Krishnan, K., and Aggarwal, B. B. (2007). Gamma-tocotrienol inhibits nuclear factor-kappaB signaling pathway through inhibition of receptor-interacting protein and TAK1 leading to suppression of antiapoptotic gene products and potentiation of apoptosis. *J Biol Chem* **282**, 809-820.

Alexander, C. (2008). Convergence of synthetic and natural polymers: next generation nanomedicines? *Nanomedicine (Lond)* **3**, 749-751.

Alexis, F., Pridgen, E., Molnar, L. K., and Farokhzad, O. C. (2008). Factors affecting the clearance and biodistribution of polymeric nanoparticles. *Mol Pharm* **5**, 505-515.

Alexis, F., Pridgen, E. M., Langer, R., and Farokhzad, O. C. (2010). Nanoparticle technologies for cancer therapy. In *Drug delivery Handbook of experimental pharmacology* (M. Schafer-Korting, Ed.), pp. 55-86. Springer-Verlag Berlin Heidelberg, Heidelberg.

Alley, M. C., Scudiero, D. A., Monks, A., Hursey, M. L., Czerwinski, M. J., Fine, D. L., Abbott, B. J., Mayo, J. G., Shoemaker, R. H., and Boyd, M. R. (1988). Feasibility of drug screening with panels of human tumor cell lines using a microculture tetrazolium assay. *Cancer Res* **48**, 589-601.

Alsarra, I. A. (2008). Evaluation of proniosomes as an alternative strategy to optimize piroxicam transdermal delivery. *J Microencapsul*, 1-7.

Anwar, K., Iqbal, J., and Hussain, M. M. (2007). Mechanisms involved in vitamin E transport by primary enterocytes and *in vivo* absorption. *J Lipid Res* **48**, 2028-2038.

Arunothayanun, P., Turton, J. A., Uchegbu, I. F., and Florence, A. T. (1999). Preparation and *in vitro/in vivo* evaluation of luteinizing hormone releasing hormone (LHRH)-loaded polyhedral and spherical/tubular niosomes. *J Pharm Sci* **88**, 34-38.

Attwood, D. (2007). Disperse systems. In Pharmaceutics: the design and manufacture of medicines (M. E. Aulton, Ed.), pp. 70-98. Churchill Livingstone Elsevier, Philadelphia.

Azmin, M. N., Florence, A. T., Handjani-Vila, R. M., Stuart, J. F., Vanlerberghe, G., and Whittaker, J. S. (1985). The effect of non-ionic surfactant vesicle (niosome) entrapment on the absorption and distribution of methotrexate in mice. *J Pharm Pharmacol* **37**, 237-242.

Baillie, A. J., Coombs, G. H., Dolan, T. F., and Laurie, J. (1986). Non-ionic surfactant vesicles, niosomes, as a delivery system for the anti-leishmanial drug, sodium stibogluconate. *J Pharm Pharmacol* **38**, 502-505.

Baillie, A. J., Florence, A. T., Hume, L. R., Muirhead, G. T., and Rogerson, A. (1985). The preparation and properties of niosomes--non-ionic surfactant vesicles. *J Pharm Pharmacol* **37**, 863-868.

Baird, R. D., and Kaye, S. B. (2003). Drug resistance reversal--are we getting closer? *Eur J Cancer* **39**, 2450-2461.

Balakrishnan, P., Shanmugam, S., Lee, W. S., Lee, W. M., Kim, J. O., Oh, D. H., Kim, D. D., Kim, J. S., Yoo, B. K., Choi, H. G., Woo, J. S., and Yong, C. S. (2009). Formulation and *in vitro* assessment of minoxidil niosomes for enhanced skin delivery. *Int J Pharm* **377**, 1-8.

Bandak, S., Goren, D., Horowitz, A., Tzemach, D., and Gabizon, A. (1999). Pharmacological studies of cisplatin encapsulated in long-circulating liposomes in mouse tumor models. *Anticancer Drugs* **10**, 911-920.

Bayindir, Z. S., and Yuksel, N. (2010). Characterization of niosomes prepared with various nonionic surfactants for paclitaxel oral delivery. *J Pharm Sci* **99**, 2049-2060.

Beattie, J. R., Maguire, C., Gilchrist, S., Barrett, L. J., Cross, C. E., Possmayer, F., Ennis, M., Elborn, J. S., Curry, W. J., McGarvey, J. J., and Schock, B. C. (2007). The use of Raman microscopy to determine and localize vitamin E in biological samples. *Faseb J* **21**, 766-776.

Beduneau, A., Saulnier, P., and Benoit, J. P. (2007). Active targeting of brain tumors using nanocarriers. *Biomaterials* **28**, 4947-4967.

Bellavance, M. A., Poirier, M. B., and Fortin, D. (2010). Uptake and intracellular release kinetics of liposome formulations in glioma cells. *Int J Pharm* **395**, 251-259.

Bibby, M. C. (2004). Orthotopic models of cancer for preclinical drug evaluation: advantages and disadvantages. *Eur J Cancer* **40**, 852-857.

Bjorneboe, A., Bjorneboe, G. E., and Drevon, C. A. (1990). Absorption, transport and distribution of vitamin E. *J Nutr* **120**, 233-242.

Bogman, K., Erne-Brand, F., Alsenz, J., and Drewe, J. (2003). The role of surfactants in the reversal of active transport mediated by multidrug resistance proteins. *J Pharm Sci* **92**, 1250-1261.

Bouwstra, J. A., and Hofland, H. E. J. (1994). Niosomes. In *Colloidal drug delivery systems* (J. Kreuter, Ed.), pp. 191-218. Marcel Dekker, Inc., New York.

Brigelius-Flohe, R., and Traber, M. G. (1999). Vitamin E: function and metabolism. *Faseb J* **13**, 1145-1155.

Brown, R. E., Anderson, W. H., and Kulkarni, V. S. (1995). Macro-ripple phase formation in bilayers composed of galactosylceramide and phosphatidylcholine. *Biophys J* **68**, 1396-1405.

Cable, C. (1990). An examination of the effect of surface modifications on the physicochemical and biological properties of non-ionic surfactant vesicles. In *Dept of Pharmaceutics*. University of Strathclyde, Glasgow.

Candiani, G., Pezzoli, D., Ciani, L., Chiesa, R., and Ristori, S. (2010). Bioreducible liposomes for gene delivery: from the formulation to the mechanism of action. *PLoS One* **5**, e13430.

Cao, J., Qi, W., and Song, B. (2009). Tocotrienols and the regulation of cholesterol biosynthesis. In *Tocotrienols: vitamin E beyond tocopherols* (R. R. Watson, and V. R. Preedy, Eds.), pp. 237-256. CRC Press Taylor & Francis Group, Boca Raton.

Cardoso, A. L., Simoes, S., de Almeida, L. P., Pelisek, J., Culmsee, C., Wagner, E., and Pedroso de Lima, M. C. (2007). siRNA delivery by a transferrin-associated lipid-based vector: a non-viral strategy to mediate gene silencing. *J Gene Med* **9**, 170-183.

Cassidy, J., and Schätzlein, A. G. (2004). Tumour-targeted drug and gene delivery: principles and concepts. *Expert Rev Mol Med* **6**, 1-17.

Cevc, G., and Richardsen, H. (1999). Lipid vesicles and membrane fusion. *Adv Drug Deliv Rev* **38**, 207-232.

Chakravarthi, S. S., Robinson, D. H., and De, S. (2007). Nanoparticles prepared using natural and synthetic polymers. In *Nanoparticulate drug delivery systems* (D. Thassu, M. Deleers, and Y. Pathak, Eds.), pp. 33-50. Informa Healthcare, New York.

Chan, L. M., Lowes, S., and Hirst, B. H. (2004). The ABCs of drug transport in intestine and liver: efflux proteins limiting drug absorption and bioavailability. *Eur J Pharm Sci* **21**, 25-51.

Chandraprakash, K. S., Udupa, N., Umadevi, P., and Pillai, G. K. (1993). Effect of macrophage activation on plasma disposition of niosomal 3H-methotrexate in sarcoma-180 bearing mice. *J Drug Target* **1**, 143-145.

Chang, P. N., Yap, W. N., Lee, D. T., Ling, M. T., Wong, Y. C., and Yap, Y. L. (2009). Evidence of gamma-tocotrienol as an apoptosis-inducing, invasion-suppressing, and chemotherapy drug-sensitizing agent in human melanoma cells. *Nutr Cancer* **61**, 357-366.

Charman, W. N., Porter, C. J., Mithani, S., and Dressman, J. B. (1997). Physiochemical and physiological mechanisms for the effects of food on drug absorption: the role of lipids and pH. *J Pharm Sci* **86**, 269-282.

Chen, F., Wang, W., and El-Deiry, W. S. (2010). Current strategies to target p53 in cancer. *Biochem Pharmacol* **80**, 724-730.

Cheng, J. X., and Xie, X. S. (2003). Coherent Anti-Stokes Raman Scattering Microscopy: Instrumentation, Theory, and Applications. *J. Phys. Chem. B* **108**, 827-840.

Cheng, W. P., Gray, A. I., Tetley, L., Hang Tle, B., Schätzlein, A. G., and Uchegbu, I. F. (2006). Polyelectrolyte nanoparticles with high drug loading enhance the oral uptake of hydrophobic compounds. *Biomacromolecules* **7**, 1509-1520.

Cheng, W. Y., Fu, M. L., Wen, L. J., Chen, C., Pan, W. H., and Huang, C. J. (2005). Plasma retinol and a-tocopherol status of the Taiwanese elderly population. *Asia Pac J Clin Nutr* **14**, 256-262.

Chiu, Y. L., Ho, Y. C., Chen, Y. M., Peng, S. F., Ke, C. J., Chen, K. J., Mi, F. L., and Sung, H. W. (2010). The characteristics, cellular uptake and intracellular trafficking of nanoparticles made of hydrophobically-modified chitosan. *J Control Release* **146**, 152-159.

Cohn, J. S., Kamili, A., Wat, E., Chung, R. W., and Tandy, S. (2010). Reduction in intestinal cholesterol absorption by various food components: Mechanisms and implications. *Atheroscler Suppl* **11**, 45-48.

Cohn, J. S., Lam, C. W., Sullivan, D. R., and Hensley, W. J. (1991). Plasma lipoprotein distribution of apolipoprotein(a) in the fed and fasted states. *Atherosclerosis* **90**, 59-66.

Conner, S. D., and Schmid, S. L. (2003). Regulated portals of entry into the cell. *Nature* **422**, 37-44.

Connors, K. A. (2002). *A textbook of pharmaceutical analysis*. John Wiley & Sons, Singapore.

Constantinides, P. P., Han, J., and Davis, S. S. (2006). Advances in the use of tocols as drug delivery vehicles. *Pharm Res* **23**, 243-255.

Constantinides, P. P., Lambert, K. J., Tustian, A. K., Schneider, B., Lalji, S., Ma, W., Wentzel, B., Kessler, D., Worah, D., and Quay, S. C. (2000). Formulation development and antitumor activity of a filter-sterilizable emulsion of paclitaxel. *Pharm Res* **17**, 175-182.

Constantinides, P. P., and Wasan, K. M. (2007). Lipid formulation strategies for enhancing intestinal transport and absorption of P-glycoprotein (P-gp) substrate drugs: *in vitro*/*in vivo* case studies. *J Pharm Sci* **96**, 235-248.

Cornaire, G., Woodley, J., Hermann, P., Cloarec, A., Arellano, C., and Houin, G. (2004). Impact of excipients on the absorption of P-glycoprotein substrates *in vitro* and *in vivo*. *Int J Pharm* **278**, 119-131.

Crespan, E., Amoroso, A., and Maga, G. (2010). DNA polymerases and mutagenesis in human cancers. *Subcell Biochem* **50**, 165-188.

Crommelin, D. J. A., and Schreier, H. (1994). Liposomes. In *Colloidal drug delivery systems* (J. Kreuter, Ed.). Marcel Dekker, Inc., New York.

Cunningham, D., Starling, N., Rao, S., Iveson, T., Nicolson, M., Coxon, F., Middleton, G., Daniel, F., Oates, J., and Norman, A. R. (2008). Capecitabine and oxaliplatin for advanced esophagogastric cancer. *N Engl J Med* **358**, 36-46.

da Rocha, A. B., Lopes, R. M., and Schwartsmann, G. (2001). Natural products in anticancer therapy. *Curr Opin Pharmacol* **1**, 364-369.

Daniels, T. R., Delgado, T., Rodriguez, J. A., Helguera, G., and Penichet, M. L. (2006). The transferrin receptor part I: Biology and targeting with cytotoxic antibodies for the treatment of cancer. *Clin Immunol* **121**, 144-158.

Das, S., Das, M., and Das, D. K. (2009). Vitamin E isomers, tocotrienols, in cardioprotection. In *Tocotrienols: vitamin E beyond tocopherols* (R. R. Watson, and V. R. Preedy, Eds.), pp. 285-295. CRC Press Taylor & Francis Group, Boca Raton.

Davis, M. E., Chen, Z. G., and Shin, D. M. (2008). Nanoparticle therapeutics: an emerging treatment modality for cancer. *Nat Rev Drug Discov* **7**, 771-782.

Decuzzi, P., and Ferrari, M. (2008). The receptor-mediated endocytosis of nonspherical particles. *Biophys J* **94**, 3790-3797.

Decuzzi, P., Godin, B., Tanaka, T., Lee, S. Y., Chiappini, C., Liu, X., and Ferrari, M. (2010). Size and shape effects in the biodistribution of intravascularly injected particles. *J Control Release* **141**, 320-327.

D'Emanuele, A., Jevprasesphant, R., Penny, J., and Attwood, D. (2004). The use of a dendrimer-propranolol prodrug to bypass efflux transporters and enhance oral bioavailability. *J Control Release* **95**, 447-453.

Dimitrijevic, D., Lamandin, C., Uchegbu, I. F., Shaw, A. J., and Florence, A. T. (1997). The effect of monomers and of micellar and vesicular forms of non-ionic surfactants (Solulan C24 and Solulan 16) on Caco-2 cell monolayers. *J Pharm Pharmacol* **49**, 611-616.

Ding, Z., Bivas-Benita, M., Hirschberg, H., Kersten, G. F., Jiskoot, W., and Bouwstra, J. A. (2008). Preparation and characterization of diphtheria toxoid-loaded elastic vesicles for transcutaneous immunization. *J Drug Target* **16**, 555-563.

Doi, A., Kawabata, S., Iida, K., Yokoyama, K., Kajimoto, Y., Kuroiwa, T., Shirakawa, T., Kirihata, M., Kasaoka, S., Maruyama, K., Kumada, H., Sakurai, Y., Masunaga, S., Ono, K., and Miyatake, S. (2008). Tumor-specific targeting of sodium borocaptate (BSH) to malignant glioma by transferrin-PEG liposomes: a modality for boron neutron capture therapy. *J Neurooncol* **87**, 287-294.

Dorai, T., and Aggarwal, B. B. (2004). Role of chemopreventive agents in cancer therapy. *Cancer Lett* **215**, 129-140.

Drummond, D. C., Meyer, O., Hong, K., Kirpotin, D. B., and Papahadjopoulos, D. (1999). Optimizing liposomes for delivery of chemotherapeutic agents to solid tumors. *Pharmacol Rev* **51**, 691-743.

Drummond, D. C., Noble, C. O., Hayes, M. E., Park, J. W., and Kirpotin, D. B. (2008). Pharmacokinetics and *in vivo* drug release rates in liposomal nanocarrier development. *J Pharm Sci* **97**, 4696-4740.

Dufès, C., Muller, J. M., Couet, W., Olivier, J. C., Uchegbu, I. F., and Schätzlein, A. G. (2004). Anticancer drug delivery with transferrin targeted polymeric chitosan vesicles. *Pharm Res* **21**, 101-107.

Dufès, C., Schätzlein, A. G., Tetley, L., Gray, A. I., Watson, D. G., Olivier, J. C., Couet, W., and Uchegbu, I. F. (2000). Niosomes and polymeric chitosan based vesicles bearing transferrin and glucose ligands for drug targeting. *Pharm Res* **17**, 1250-1258.

Eastman Chemical Company (2005). Eastman vitamin E TPGS NF: Applications and Properties.

Eavarone, D. A., Yu, X., and Bellamkonda, R. V. (2000). Targeted drug delivery to C6 glioma by transferrin-coupled liposomes. *J Biomed Mater Res* **51**, 10-14.

Eisenhauer, E. A., Therasse, P., Bogaerts, J., Schwartz, L. H., Sargent, D., Ford, R., Dancey, J., Arbuck, S., Gwyther, S., Mooney, M., Rubinstein, L., Shankar, L., Dodd, L., Kaplan, R., Lacombe, D., and Verweij, J. (2009). New response evaluation criteria in solid tumours: revised RECIST guideline (version 1.1). *Eur J Cancer* **45**, 228-247.

Evans, C. L., and Xie, X. S. (2008). Coherent anti-stokes Raman scattering microscopy: chemical imaging for biology and medicine. *Annu Rev Anal Chem (Palo Alto Calif)* **1**, 883-909.

Evans, H. M., and Bishop, K. S. (1922). On the Existence of a Hitherto Unrecognized Dietary Factor Essential for Reproduction. *Science* **56**, 650-651.

Ferrari, M. (2005). Nanovector therapeutics. *Curr Opin Chem Biol* **9**, 343-346.

Ferrari, M. (2010). Frontiers in cancer nanomedicine: directing mass transport through biological barriers. Trends Biotechnol 28, 181-188.

Florence, A. T. and C. Cable (1993). Non-ionic surfactant vesicles (niosomes) as vehicles for doxorubicin delivery. Liposomes in drug delivery. G. Gregoriadis, A. T. Florence and H. M. Patel. Switzerland, Harwood Academic Publishers. 2: 239-253.

Freshney, R. I. (2000). Culture of animal cells: a manual of basic technique. Wiley-Liss, Inc., New York.

Fruehauf, J. P., and Trapp, V. (2008). Reactive oxygen species: an Achilles' heel of melanoma? *Expert Rev Anticancer Ther* **8**, 1751-1757.

Fu, J. Y., Blatchford, D. R., Tetley, L., and Dufès, C. (2009). Tumor regression after systemic administration of tocotrienol entrapped in tumor-targeted vesicles. *J Control Release* **140**, 95-99.

Gabizon, A. A. (2001). Stealth liposomes and tumor targeting: one step further in the quest for the magic bullet. *Clin Cancer Res* **7**, 223-225.

Gannon, C. J., Cherukuri, P., Yakobson, B. I., Cognet, L., Kanzius, J. S., Kittrell, C., Weisman, R. B., Pasquali, M., Schmidt, H. K., Smalley, R. E., and Curley, S. A. (2007). Carbon nanotube-enhanced thermal destruction of cancer cells in a noninvasive radiofrequency field. *Cancer* **110**, 2654-2665.

Gao, Y., Li, L. B., and Zhai, G. (2008). Preparation and characterization of Pluronic/TPGS mixed micelles for solubilization of camptothecin. *Colloids Surf B Biointerfaces* **64**, 194-199.

Gapor, A. (2005). Production of palm-based tocotrienols-enhanced fraction (TEF). In *MPOB Information Series*.

Ghosh, S. P., Hauer-Jensen, M., and Kumar, K. S. (2009). Chemistry of tocotrienols. In *Tocotrienols: vitamin E beyond tocopherols* (R. R. Watson, and V. R. Preedy, Eds.), pp. 85-98. CRC Press Taylor & Francis Group, Boca Raton.

Gianasi, E., Cociancich, F., Uchegbu, I. F., Florence, A. T., and Duncan, R. (1997). Pharmaceutical and biological characterisation of a doxorubicin-polymer conjugate (PK1) entrapped in sorbitan monostearate Span 60 niosomes. *Int J Pharm* **148**, 139-148.

Gómez-Navarro, J., Curiel, D. T., and Douglas, J. T. (1999). Gene therapy for cancer. *Eur J Cancer* **35**, 2039-2057.

Grobmyer, S. R., Iwakuma, N., Sharma, P., and Moudgil, B. M. (2010). What is cancer nanotechnology? In *Cancer nanotechnology, methods in molecular biology* (S. R. Grobmyer, and B. M. Moudgil, Eds.), pp. 1-9. Humana Press, New York.

Gude, R. P., Jadhav, M. G., Rao, S. G., and Jagtap, A. G. (2002). Effects of niosomal cisplatin and combination of the same with theophylline and with activated macrophages in murine B16F10 melanoma model. *Cancer Biother Radiopharm* **17**, 183-192.

Guinedi, A. S., Mortada, N. D., Mansour, S., and Hathout, R. M. (2005). Preparation and evaluation of reverse-phase evaporation and multilamellar niosomes as ophthalmic carriers of acetazolamide. *Int J Pharm* **306**, 71-82.

Gupta, P. N., Mishra, V., Rawat, A., Dubey, P., Mahor, S., Jain, S., Chatterji, D. P., and Vyas, S. P. (2005). Non-invasive vaccine delivery in transfersomes, niosomes and liposomes: a comparative study. *Int J Pharm* **293**, 73-82.

Guthrie, N., Gapor, A., Chambers, A. F., and Carroll, K. K. (1997). Inhibition of proliferation of estrogen receptor-negative MDA-MB-435 and -positive MCF-7 human breast cancer cells by palm oil tocotrienols and tamoxifen, alone and in combination. *J Nutr* **127**, 544S-548S.

Hafid, S. R., Radhakrishnan, A. K., and Nesaretnam, K. (2010). Tocotrienols are good adjuvants for developing cancer vaccines. *BMC Cancer* **10**.

Hait, W. N. (2010). Anticancer drug development: the grand challenges. *Nat Rev Drug Discov* **9**, 253-254.

Handjani-Vila, R. M., Ribier, A., Rondot, B., and Vanlerberghie, G. (1979). Dispersions of lamellar phases of non-ionic lipids in cosmetic products. *Int J Cosmet Sci* **1**, 303-314.

Hao, Y., Zhao, F., Li, N., Yang, Y., and Li, K. (2002). Studies on a high encapsulation of colchicine by a niosome system. *Int J Pharm* **244**, 73-80.

Har, C. H., and Keong, C. K. (2005). Effects of tocotrienols on cell viability and apoptosis in normal murine liver cells (BNL CL.2) and liver cancer cells (BNL 1ME A.7R.1), *in vitro. Asia Pacific Journal of Clinical Nutrition* **14**, 374-380.

Hayes, K. C., Pronczuk, A., and Liang, J. S. (1993). Differences in the plasma transport and tissue concentrations of tocopherols and tocotrienols: observations in humans and hamsters. *Proc Soc Exp Biol Med* **202**, 353-359.

He, L., Mo, H., Hadisusilo, S., Qureshi, A. A., and Elson, C. E. (1997). Isoprenoids suppress the growth of murine B16 melanomas *in vitro* and *in vivo. J Nutr* **127**, 668-674.

Heurtault, B., Saulnier, P., Pech, B., Proust, J. E., and Benoit, J. P. (2003). Physico-chemical stability of colloidal lipid particles. *Biomaterials* **24**, 4283-4300.

Hillaireau, H., and Couvreur, P. (2009). Nanocarriers' entry into the cell: relevance to drug delivery. *Cell Mol Life Sci* **66**, 2873-2896.

Hiura, Y., Tachibana, H., Arakawa, R., Aoyama, N., Okabe, M., Sakai, M., and Yamada, K. (2009). Specific accumulation of gamma- and delta-tocotrienols in tumor and their antitumor effect *in vivo. J Nutr Biochem* **20**, 607-613.

Hofland, H. E., Bouwstra, J. A., Verhoef, J. C., Buckton, G., Chowdry, B. Z., Ponec, M., and Junginger, H. E. (1992). Safety aspects of non-ionic surfactant vesicles: a toxicity study related to the physicochemical characteristics of non-ionic surfactants. *J Pharm Pharmacol* **44**, 287-294.

Holst, C. M., and Oredsson, S. M. (2005). Comparison of three cytotoxicity tests in the evaluation of the cytotoxicity of a spermine analogue on human breast cancer cell lines. *Toxicol In vitro* **19**, 379-387.

Hong, M., Zhu, S., Jiang, Y., Tang, G., and Pei, Y. (2009). Efficient tumor targeting of hydroxycamptothecin loaded PEGylated niosomes modified with transferrin. *J Control Release* **133**, 96-102.

Hosomi, A., Arita, M., Sato, Y., Kiyose, C., Ueda, T., Igarashi, O., Arai, H., and Inoue, K. (1997). Affinity for alpha-tocopherol transfer protein as a determinant of the biological activities of vitamin E analogs. *FEBS Lett* **409**, 105-108.

http://www.atcc.org (2010). Cell Lines and Hybridomas. American Type Culture Collection.

http://www.cancerhelp.org.uk/trials/ (2010). Trials and Research. Cancer Research UK.

http://www.clinicaltrials.gov/ (2010). Clinical Trials. US National Institutes of Health.

http://www.hpacultures.org.uk/ (2010). European Collection of Cell Cultures (ECACC). European Collection of Cell Cultures.

http://www.who.int/topics/cancer/ (2010). Cancer. World Health Organization.

Huang, R. Q., Qu, Y. H., Ke, W. L., Zhu, J. H., Pei, Y. Y., and Jiang, C. (2007). Efficient gene delivery targeted to the brain using a transferrin-conjugated polyethyleneglycol-modified polyamidoamine dendrimer. *Faseb J* **21**, 1117-1125.

Huang, Y., Chen, J., Chen, X., Gao, J., and Liang, W. (2008). PEGylated synthetic surfactant vesicles (Niosomes): novel carriers for oligonucleotides. *J Mater Sci Mater Med* **19**, 607-614.

Huh, K. M., Min, H. S., Lee, S. C., Lee, H. J., Kim, S., and Park, K. (2008). A new hydrotropic block copolymer micelle system for aqueous solubilization of paclitaxel. *J Control Release* **126**, 122-129.

Humecki, H. J. (1995). *Practical Guide to Infrared Microspectroscopy*. Marcel Dekker, New York.

Hussein, D., and Mo, H. (2009). d-Dlta-tocotrienol-mediated suppression of the proliferation of human PANC-1, MIA PaCa-2, and BxPC-3 pancreatic carcinoma cells. *Pancreas* **38**, e124-136.

Iinuma, H., Maruyama, K., Okinaga, K., Sasaki, K., Sekine, T., Ishida, O., Ogiwara, N., Johkura, K., and Yonemura, Y. (2002). Intracellular targeting therapy of cisplatin-encapsulated transferrin-polyethylene glycol liposome on peritoneal dissemination of gastric cancer. *Int J Cancer* **99**, 130-137.

Ikeda, S., Toyoshima, K., and Yamashita, K. (2001). Dietary sesame seeds elevate alpha- and gamma-tocotrienol concentrations in skin and adipose tissue of rats fed the tocotrienol-rich fraction extracted from palm oil. *J Nutr* **131**, 2892-2897.

Immordino, M. L., Dosio, F., and Cattel, L. (2006). Stealth liposomes: review of the basic science, rationale, and clinical applications, existing and potential. *Int J Nanomedicine* **1**, 297-315.

Inokuchi, H., Hirokane, H., Tsuzuki, T., Nakagawa, K., Igarashi, M., and Miyazawa, T. (2003). Anti-angiogenic activity of tocotrienol. *Biosci Biotechnol Biochem* **67**, 1623-1627.

Inoue, S. (1995). Foundations of confocal scanned imaging in light microscopy. In *Handbook of biological confocal microscopy* (J. B. Pawley, Ed.). Plenum Press, New York.

Iqbal, J., and Hussain, M. M. (2009). Intestinal lipid absorption. *Am J Physiol Endocrinol Metab* **296**, E1183-1194.

Ishida, O., Maruyama, K., Sasaki, K., and Iwatsuru, M. (1999). Size-dependent extravasation and interstitial localization of polyethyleneglycol liposomes in solid tumor-bearing mice. *Int J Pharm* **190**, 49-56.

Ishida, O., Maruyama, K., Tanahashi, H., Iwatsuru, M., Sasaki, K., Eriguchi, M., and Yanagie, H. (2001). Liposomes bearing polyethyleneglycol-coupled transferrin with intracellular targeting property to the solid tumors *in vivo*. *Pharm Res* **18**, 1042-1048.

Israelachvili, J. N., Marcelja, S., and Horn, R. G. (1980). Physical principles of membrane organization. *Q Rev Biophys* **13**, 121-200.

James, J. S. (1995). DOXIL approved for KS. *AIDS Treat News*, 6.

Jiang, Q. (2009). Metabolism of tocopherols and tocotrienols and novel functions of their metabolites. In *Tocotrienols: vitamin E beyond tocopherols* (R. R. Watson, and V. R. Preedy, Eds.), pp. 309-330. CRC Press Taylor & Francis Group, Boca Raton.

Jiang, Y. Y., Liu, C., Hong, M. H., Zhu, S. J., and Pei, Y. Y. (2007). Tumor cell targeting of transferrin-PEG-TNF-alpha conjugate via a receptor-mediated delivery system: design, synthesis, and biological evaluation. *Bioconjug Chem* **18**, 41-49.

Jones, D. (2007). Cancer nanotechnology: small, but heading for the big time. In *Nat Rev Drug Discov*, pp. 174-175.

Joosse, A., De Vries, E., van Eijck, C. H., Eggermont, A. M., Nijsten, T., and Coebergh, J. W. (2010). Reactive oxygen species and melanoma: an explanation for gender differences in survival? *Pigment Cell Melanoma Res* **23**, 352-364.

Juturu, V. (2009). Tocopherol and tocotrienols: role in heart disease care and prevention. In *Tocotrienols: vitamin E beyond tocopherols* (R. R. Watson, and V. R. Preedy, Eds.), pp. 219-236. CRC Press Taylor & Francis Group, Boca Raton.

Kamb, A., Wee, S., and Lengauer, C. (2007). Why is cancer drug discovery so difficult? *Nat Rev Drug Discov* **6**, 115-120.

Kannappan, R., Ravindran, J., Prasad, S., Sung, B., Yadav, V. R., Reuter, S., Chaturvedi, M. M., and Aggarwal, B. B. (2010). Gamma-tocotrienol promotes TRAIL-induced apoptosis through reactive oxygen species/extracellular signal-regulated kinase/p53-mediated upregulation of death receptors. *Mol Cancer Ther* **9**, 2196-2207.

Katsanidis, E., and Addis, P. B. (1999). Novel HPLC analysis of tocopherols, tocotrienols, and cholesterol in tissue. *Free Radic Biol Med* **27**, 1137-1140.

Kelf, T. A., Sreenivasan, V. K., Sun, J., Kim, E. J., Goldys, E. M., and Zvyagin, A. V. (2010). Non-specific cellular uptake of surface-functionalized quantum dots. *Nanotechnology* **21**, 285105.

Kelland, L. R. (2004). Of mice and men: values and liabilities of the athymic nude mouse model in anticancer drug development. *Eur J Cancer* **40**, 827-836.

Kepczynski, M., Bednar, J., Kuzmicz, D., Wydro, P., and Nowakowska, M. (2010). Spontaneous formation of densely stacked multilamellar vesicles in dioctadecyldimethylammonium bromide/oleosiloxane mixtures. *Langmuir* **26**, 1551-1556.

Khanna, S., Roy, S., Ryu, H., Bahadduri, P., Swaan, P. W., Ratan, R. R., and Sen, C. K. (2003). Molecular basis of vitamin E action: tocotrienol modulates 12-lipoxygenase, a key mediator of glutamate-induced neurodegeneration. *J Biol Chem* **278**, 43508-43515.

Khanna, S., Roy, S., Slivka, A., Craft, T. K., Chaki, S., Rink, C., Notestine, M. A., DeVries, A. C., Parinandi, N. L., and Sen, C. K. (2005). Neuroprotective properties of the natural vitamin E alpha-tocotrienol. *Stroke* **36**, 2258-2264.

Kircheis, R., Wightman, L., Schreiber, A., Robitza, B., Rossler, V., Kursa, M., and Wagner, E. (2001). Polyethylenimine/DNA complexes shielded by transferrin target gene expression to tumors after systemic application. *Gene Ther* **8**, 28-40.

Kircheis, R., Wightman, L., Schreiber, A., Robitza, B., Rossler, V., Kursa, M., and Wagner, E. (2001). Polyethylenimine/DNA complexes shielded by transferrin target gene expression to tumors after systemic application. *Gene Ther* **8**, 28-40.

Klerk, C. P., Overmeer, R. M., Niers, T. M., Versteeg, H. H., Richel, D. J., Buckle, T., Van Noorden, C. J., and van Tellingen, O. (2007). Validity of bioluminescence measurements for noninvasive *in vivo* imaging of tumor load in small animals. *Biotechniques* **43**, 7-13, 30.

Kobayashi, T., Ishida, T., Okada, Y., Ise, S., Harashima, H., and Kiwada, H. (2007). Effect of transferrin receptor-targeted liposomal doxorubicin in P-glycoprotein-mediated drug resistant tumor cells. *Int J Pharm* **329**, 94-102.

Komiyama, K., Iizuka, K., Yamaoka, M., Watanabe, H., Tsuchiya, N., and Umezawa, I. (1989). Studies on the biological activity of tocotrienols. *Chem Pharm Bull (Tokyo)* **37**, 1369-1371.

Kommareddy, S., and Amiji, M. (2004). Targeted drug delivery to tumour cells using colloidal carriers. In *Cellular drug delivery principles and practice* (D. R. Lu, and S. Øie, Eds.), pp. 181-215. Humana Press, New Jersey.

Kong, G., Braun, R. D., and Dewhirst, M. W. (2000). Hyperthermia enables tumor-specific nanoparticle delivery: effect of particle size. *Cancer Res* **60**, 4440-4445.

Kosowski, A., and Clouatre, D. L. (2009). Vitamin E: natural vs. synthetic. In *Tocotrienols: vitamin E beyond tocopherols* (R. R. Watson, and V. R. Preedy, Eds.), pp. 61-78. CRC Press Taylor & Francis Group, Boca Raton.

Kostanova-Poliakova, D., and Sabova, L. (2005). Anti-apoptotic proteins-targets for chemosensitization of tumor cells and cancer treatment. *Neoplasma* **52**, 441-449.

Kreuter, J. (1994). Nanoparticles. In *Colloidal drug delivery systems* (J. Kreuter, Ed.), pp. 219-342. Marcel Dekker, Inc., New York.

Kumar, K. S., Raghavan, M., Hieber, K., Ege, C., Mog, S., Parra, N., Hildabrand, A., Singh, V., Srinivasan, V., Toles, R., Karikari, P., Petrovics, G., Seed, T., Srivastava, S., and Papas, A. (2006). Preferential radiation sensitization of prostate cancer in nude mice by nutraceutical antioxidant gamma-tocotrienol. *Life Sci* **78**, 2099-2104.

Kunnumakkara, A. B., Sung, B., Ravindran, J., Diagaradjane, P., Deorukhkar, A. A., Dey, S., Koca, C., Yadav, V. R., Tong, Z., Gelovani, J. G., Guha, S., Krishnan, S., and Aggarwal, B. B. (2010). {gamma}-Tocotrienol inhibits pancreatic tumors and sensitizes them to gemcitabine treatment by modulating the inflammatory microenvironment. *Cancer Res* **70**, 8695-8705.

Lasic, D. D. (1991). Kinetic and thermodynamic effect on the structure and formation of phosphatidylcholine vesicles. Hepatology 13, 1010-1012.

Lawson, K. A., Anderson, K., Simmons-Menchaca, M., Atkinson, J., Sun, L., Sanders, B. G., and Kline, K. (2004). Comparison of vitamin E derivatives alpha-TEA and VES in reduction of mouse mammary tumor burden and metastasis. *Exp Biol Med (Maywood)* **229**, 954-963.

Le, T. T., Yue, S., and Cheng, J. X. (2010). Shedding new light on lipid biology with CARS microscopy. *J Lipid Res*.

Lee, C. C., MacKay, J. A., Frechet, J. M., and Szoka, F. C. (2005). Designing dendrimers for biological applications. *Nat Biotechnol* **23**, 1517-1526.

Lesieur, S., and Ollivon, M. (2000). Non-ionic vesicles to micelle transitions. In *Synthetic surfactant vesicles: niosomes and other non-phospholipid vesicular systems* (I. F. Uchegbu, Ed.). pp 49-79. Harwood Academic.

Letchford, K., and Burt, H. (2007). A review of the formation and classification of amphiphilic block copolymer nanoparticulate structures: micelles, nanospheres, nanocapsules and polymersomes. *Eur J Pharm Biopharm* **65**, 259-269.

Levin, N. E., and Clouatre, D. L. (2009). Tocotrienols in vitamin E: hype or science? In *Tocotrienols: vitamin E beyond tocopherols* (R. R. Watson, and V. R. Preedy, Eds.), pp. 13-20. CRC Press Taylor & Francis Group, Boca Raton.

Li, H., Sun, H., and Qian, Z. M. (2002). The role of the transferrin-transferrin-receptor system in drug delivery and targeting. *Trends Pharmacol Sci* **23**, 206-209.

Li, X., Ding, L., Xu, Y., Wang, Y., and Ping, Q. (2009). Targeted delivery of doxorubicin using stealth liposomes modified with transferrin. *Int J Pharm* **373**, 116-123.

Liang, Y., Hilal, N., Langston, P., and Starov, V. (2007). Interaction forces between colloidal particles in liquid: theory and experiment. *Adv Colloid Interface Sci* **134-135**, 151-166.

Lim, E., Modi, K. D., and Kim, J. (2009). In vivo bioluminescent imaging of mammary tumors using IVIS spectrum. J Vis Exp. DOI: 10.3791/1210.

Lindholm, A., Henricsson, S., and Dahlqvist, R. (1990). The effect of food and bile acid administration on the relative bioavailability of cyclosporin. *Br J Clin Pharmacol* **29**, 541-548.

Liu, Y., Peterson, D. A., Kimura, H., and Schubert, D. (1997). Mechanism of cellular 3-(4,5-dimethylthiazol-2-yl)-2,5-diphenyltetrazolium bromide (MTT) reduction. *J Neurochem* **69**, 581-593.

Longhi, A., Ferrari, S., Bacci, G., and Specchia, S. (2007). Long-term follow-up of patients with doxorubicin-induced cardiac toxicity after chemotherapy for osteosarcoma. *Anticancer Drugs* **18**, 737-744.

Lorusso, D., Di Stefano, A., Carone, V., Fagotti, A., Pisconti, S., and Scambia, G. (2007). Pegylated liposomal doxorubicin-related palmar-plantar erythrodysesthesia ('hand-foot' syndrome). *Ann Oncol* **18**, 1159-1164.

Lowry, O. H., Rosebrough, N. J., Farr, A. L., and Randall, R. J. (1951). Protein measurement with the Folin phenol reagent. *J Biol Chem* **193**, 265-275.

Lukyanov, A. N., and Torchilin, V. P. (2004). Micelles from lipid derivatives of water-soluble polymers as delivery systems for poorly soluble drugs. *Adv Drug Deliv Rev* **56**, 1273-1289.

Maeda, H., Bharate, G. Y., and Daruwalla, J. (2009). Polymeric drugs for efficient tumor-targeted drug delivery based on EPR-effect. *Eur J Pharm Biopharm* **71**, 409-419.

Maeda, H., Wu, J., Sawa, T., Matsumura, Y., and Hori, K. (2000). Tumor vascular permeability and the EPR effect in macromolecular therapeutics: a review. *J Control Release* **65**, 271-284.

Makrilia, N., Syrigou, E., Kaklamanos, I., Manolopoulos, L., and Saif, M. W. (2010). Hypersensitivity reactions associated with platinum antineoplastic agents: a systematic review. *Met Based Drugs* **2010**.

Malmsten, M. (2002). *Surfactants and polymers in drug delivery*. Marcel Dekker, Inc., New York.

Malvern Instruments Ltd (2004). Zetasizer Nano Series User Manual.

Marampon, F., Ciccarelli, C., and Zani, B. M. (2006). Down-regulation of c-Myc following MEK/ERK inhibition halts the expression of malignant phenotype in rhabdomyosarcoma and in non muscle-derived human tumors. *Mol Cancer* **5**, 31.

Mardones, P., Strobel, P., Miranda, S., Leighton, F., Quinones, V., Amigo, L., Rozowski, J., Krieger, M., and Rigotti, A. (2002). Alpha-tocopherol metabolism is abnormal in scavenger receptor class B type I (SR-BI)-deficient mice. *J Nutr* **132**, 443-449.

Maruyama, K., Ishida, O., Kasaoka, S., Takizawa, T., Utoguchi, N., Shinohara, A., Chiba, M., Kobayashi, H., Eriguchi, M., and Yanagie, H. (2004). Intracellular targeting of sodium mercaptoundecahydrododecaborate (BSH) to solid tumors by transferrin-PEG liposomes, for boron neutron-capture therapy (BNCT). *J Control Release* **98**, 195-207.

Maruyama, K., Ishida, O., Takizawa, T., and Moribe, K. (1999). Possibility of active targeting to tumor tissues with liposomes. *Adv Drug Deliv Rev* **40**, 89-102.

Matthaus, C., Kale, A., Chernenko, T., Torchilin, V., and Diem, M. (2008). New ways of imaging uptake and intracellular fate of liposomal drug carrier systems inside individual cells, based on Raman microscopy. *Mol Pharm* **5**, 287-293.

McAnally, J. A., Gupta, J., Sodhani, S., Bravo, L., and Mo, H. (2007). Tocotrienols potentiate lovastatin-mediated growth suppression *in vitro* and *in vivo*. *Exp Biol Med (Maywood)* **232**, 523-531.

Medronho, B., Shafaei, S., Szopko, R., Miguel, M. G., Olsson, U., and Schmidt, C. (2008). Shear-induced transitions between a planar lamellar phase and multilamellar vesicles: continuous versus discontinuous transformation. *Langmuir* **24**, 6480-6486.

Miyazawa, T., Shibata, A., Sookwong, P., Kawakami, Y., Eitsuka, T., Asai, A., Oikawa, S., and Nakagawa, K. (2009). Antiangiogenic and anticancer potential of unsaturated vitamin E (tocotrienol). *J Nutr Biochem* **20**, 79-86.

Mizushina, Y., Nakagawa, K., Shibata, A., Awata, Y., Kuriyama, I., Shimazaki, N., Koiwai, O., Uchiyama, Y., Sakaguchi, K., Miyazawa, T., and Yoshida, H. (2006). Inhibitory effect of tocotrienol on eukaryotic DNA polymerase lambda and angiogenesis. *Biochem Biophys Res Commun* **339**, 949-955.

Mizushina, Y., Yoshida, H., and Miyazawa, T. (2009). DNA polymerase inhibition. In *Tocotrienols: vitamin E beyond tocopherol* (R. R. Watson, and V. R. Preedy, Eds.), pp. 141-148. CRC Press Taylor & Francis Group, Boca Raton.

Moghimi, S. M., Hunter, A. C., and Murray, J. C. (2001). Long-circulating and target-specific nanoparticles: theory to practice. *Pharmacol Rev* **53**, 283-318.

Moghimi, S. M., Hunter, A. C., and Murray, J. C. (2005). Nanomedicine: current status and future prospects. *Faseb J* **19**, 311-330.

Monici, M. (2005). Cell and tissue autofluorescence research and diagnostic applications. *Biotechnol Annu Rev* **11**, 227-256.

Morton, C. L., and Houghton, P. J. (2007). Establishment of human tumor xenografts in immunodeficient mice. *Nat Protoc* **2**, 247-250.

Mu, L., Elbayoumi, T. A., and Torchilin, V. P. (2005). Mixed micelles made of poly(ethylene glycol)-phosphatidylethanolamine conjugate and d-alpha-tocopheryl polyethylene glycol 1000 succinate as pharmaceutical nanocarriers for camptothecin. *Int J Pharm* **306**, 142-149.

Mullen, A. B., Baillie, A. J., and Carter, K. C. (1998). Visceral leishmaniasis in the BALB/c mouse: a comparison of the efficacy of a nonionic surfactant formulation of sodium stibogluconate with those of three proprietary formulations of amphotericin B. *Antimicrob Agents Chemother* **42**, 2722-2725.

Munteanu, A., Ricciarelli, R., Massone, S., and Zingg, J. M. (2007). Modulation of proteasome activity by vitamin E in THP-1 monocytes. *IUBMB Life* **59**, 771-780.

Naito, Y., and Yoshikawa, T. (2009). Tocotrienols in altering the expression of adhesion molecules. In *Tocotrienols: vitamin E beyond tocopherols* (R. R. Watson, and V. R. Preedy, Eds.), pp. 149-158. CRC Press Taylor & Francis Group, Boca Raton.

Najlah, M., and D'Emanuele, A. (2007). Synthesis of dendrimers and drug-dendrimer conjugates for drug delivery. *Curr Opin Drug Discov Devel* **10**, 756-767.

Nakagawa, K., Shibata, A., Sookwong, P., and Miyazawa, T. (2009). Angiogenesis inhibition. In *Tocotrienols: vitamin E beyond tocopherols*, pp. 79-84. CRC Press Taylor & Francis Group, Boca Raton.

Nakase, M., Inui, M., Okumura, K., Kamei, T., Nakamura, S., and Tagawa, T. (2005). p53 gene therapy of human osteosarcoma using a transferrin-modified cationic liposome. *Mol Cancer Ther* **4**, 625-631.

Negis, Y., Meydani, M., Zingg, J. M., and Azzi, A. (2007). Molecular mechanism of alpha-tocopheryl-phosphate transport across the cell membrane. *Biochem Biophys Res Commun* **359**, 348-353.

Nesaretnam, K. (2008). Multitargeted therapy of cancer by tocotrienols. *Cancer Lett* **269**, 388-395.

Nesaretnam, K., Ambra, R., Selvaduray, K. R., Radhakrishnan, A., Reimann, K., Razak, G., and Virgili, F. (2004). Tocotrienol-rich fraction from palm oil affects gene expression in tumors resulting from MCF-7 cell inoculation in athymic mice. *Lipids* **39**, 459-467.

Nesaretnam, K., Guthrie, N., Chambers, A. F., and Carroll, K. K. (1995). Effect of tocotrienols on the growth of a human breast cancer cell line in culture. *Lipids* **30**, 1139-1143.

Nesaretnam, K., Selvaduray, K. R., Abdul Razak, G., Veerasenan, S. D., and Gomez, P. A. (2010). Effectiveness of tocotrienol-rich fraction combined with tamoxifen in the management of women with early breast cancer: a pilot clinical trial. *Breast Cancer Res* **12**, R81.

Nesaretnam, K., Wong, W. Y., and Wahid, M. B. (2007). Tocotrienols and cancer: beyond antioxidant activity. *Eur J Lipid Sci Technol* **109**, 445-452.

Niemiec, S. M., Ramachandran, C., and Weiner, N. (1995). Influence of nonionic liposomal composition on topical delivery of peptide drugs into pilosebaceous units: an *in vivo* study using the hamster ear model. *Pharm Res* **12**, 1184-1188.

Noguchi, N., Saito, Y., and Niki, E. (2009). Uptake, distribution and protective action of tocopherol in cultured cells. In *Tocotrienols: vitamin E beyond tocopherols* (R. R. Watson, and V. R. Preedy, Eds.), pp. 159-169. CRC Press Taylor & Francis Group, Boca Raton.

Okahata, Y., Tanamachi, S., Nagai, M., and Kunitake, T. (1981). Synthetic bilayer membranes prepared from dialkyl amphiphiles with nonionic and zwitterionic head groups. *J Colloid Interface Sci* **82**, 401-417.

Olson, B. J., and Markwell, J. (2007). Assays for determination of protein concentration. *Curr Protoc Protein Sci* **Chapter 3**, Unit 3 4.

Paolino, D., Lucania, G., Mardente, D., Alhaique, F., and Fresta, M. (2005). Ethosomes for skin delivery of ammonium glycyrrhizinate: *in vitro* percutaneous permeation through human skin and *in vivo* anti-inflammatory activity on human volunteers. *J Control Release* **106**, 99-110.

Papetti, M., and Herman, I. M. (2002). Mechanisms of normal and tumor-derived angiogenesis. *Am J Physiol Cell Physiol* **282**, C947-970.

Park, S., Lim, J., Chung, S., and Mirkin, C. A. (2004). Self-assembly of mesoscopic metal-polymer amphiphiles. *Science* **303**, 348-351.

Parthasarathi, G., Udupa, N., Umadevi, P., and Pillai, G. K. (1994). Niosome encapsulated of vincristine sulfate: improved anticancer activity with reduced toxicity in mice. *J Drug Target* **2**, 173-182.

Peer, D., Karp, J. M., Hong, S., Farokhzad, O. C., Margalit, R., and Langer, R. (2007). Nanocarriers as an emerging platform for cancer therapy. *Nat Nanotechnol* **2**, 751-760.

Perkel, J. M. (2004). The Ups and Downs of Nanobiotech. *The Scientist* **18**, 14.

Perrie, Y., Barralet, J. E., McNeil, S., and Vangala, A. (2004). Surfactant vesicle-mediated delivery of DNA vaccines via the subcutaneous route. *Int J Pharm* **284**, 31-41.

Perugini, C., Bagnati, M., Cau, C., Bordone, R., Paffoni, P., Re, R., Zoppis, E., Albano, E., and Bellomo, G. (2000). Distribution of lipid-soluble antioxidants in lipoproteins from healthy subjects. II. Effects of *in vivo* supplementation with alpha-tocopherol. *Pharmacol Res* **41**, 65-72.

Peterson, J. K., and Houghton, P. J. (2004). Integrating pharmacology and *in vivo* cancer models in preclinical and clinical drug development. *Eur J Cancer* **40**, 837-844.

Petros, R. A., and DeSimone, J. M. (2010). Strategies in the design of nanoparticles for therapeutic applications. *Nat Rev Drug Discov* **9**, 615-627.

Plumb, J. A. (2004). Cell sensitivity assays: the MTT assay. *Methods Mol Med* **88**, 165-169.

Plumb, J. A., Milroy, R., and Kaye, S. B. (1989). Effects of the pH dependence of 3-(4,5-dimethylthiazol-2-yl)-2,5-diphenyl-tetrazolium bromide-formazan absorption on chemosensitivity determined by a novel tetrazolium-based assay. *Cancer Res* **49**, 4435-4440.

Podda, M., Rallis, M., Traber, M. G., Packer, L., and Maibach, H. I. (1996). Kinetic study of cutaneous and subcutaneous distribution following topical application of [7,8-14C]rac-alpha-lipoic acid onto hairless mice. *Biochem Pharmacol* **52**, 627-633.

Potma, E. O., and Xie, X. S. (2008). Coherent Anti-Stokes Raman Scattering (CARS) Microscopy: Instrumentation and Applications. In *Handbook of Biomedical Nonlinear Optical Microscopy* (B. R. Masters, and P. T. C. So, Eds.), pp. 164-186. Oxford University Press, New York.

Pozo Navas, B., Lohner, K., Deutsch, G., Sevcsik, E., Riske, K. A., Dimova, R., Garidel, P., and Pabst, G. (2005). Composition dependence of vesicle morphology and mixing properties in a bacterial model membrane system. *Biochim Biophys Acta* **1716**, 40-48.

Prasad, Y. V., Puthli, S. P., Eaimtrakarn, S., Ishida, M., Yoshikawa, Y., Shibata, N., and Takada, K. (2003). Enhanced intestinal absorption of vancomycin with Labrasol and D-alpha-tocopheryl PEG 1000 succinate in rats. *Int J Pharm* **250**, 181-190.

Puah, C. W., Choo, Y. M., Ma, A. N., and Chuah, C. H. (2006). Very long chain fatty acid methyl esters in transesterified palm oil. *Lipids* **41**, 305-308.

Qi, Q., Hao, M., Ng, W. O., Slater, S. C., Baszis, S. R., Weiss, J. D., and Valentin, H. E. (2005). Application of the Synechococcus nirA promoter to establish an inducible expression system for engineering the Synechocystis tocopherol pathway. *Appl Environ Microbiol* **71**, 5678-5684.

Qian, Z. M., Li, H., Sun, H., and Ho, K. (2002). Targeted drug delivery via the transferrin receptor-mediated endocytosis pathway. *Pharmacol Rev* **54**, 561-587.

Reddy, L., Odhav, B., and Bhoola, K. D. (2003). Natural products for cancer prevention: a global perspective. *Pharmacol Ther* **99**, 1-13.

Richardson, A., and Kaye, S. B. (2008). Pharmacological inhibition of the Bcl-2 family of apoptosis regulators as cancer therapy. *Curr Mol Pharmacol* **1**, 244-254.

Riehemann, K., Schneider, S. W., Luger, T. A., Godin, B., Ferrari, M., and Fuchs, H. (2009). Nanomedicine--challenge and perspectives. *Angew Chem Int Ed Engl* **48**, 872-897.

Rigotti, A. (2007). Absorption, transport, and tissue delivery of vitamin E. *Mol Aspects Med* **28**, 423-436.

Robertson, D., Hellweg, T., Tiersch, B., and Koetz, J. (2004). Polymer-induced structural changes in lecithin/sodium dodecyl sulfate-based multilamellar vesicles. *J Colloid Interface Sci* **270**, 187-194.

Rodriguez, L. G., Lockett, S. J., and Holtom, G. R. (2006). Coherent anti-stokes Raman scattering microscopy: a biological review. *Cytometry A* **69**, 779-791.

Rogerson, A., Cummings, J., Willmott, N., and Florence, A. T. (1988). The distribution of doxorubicin in mice following administration in niosomes. *J Pharm Pharmacol* **40**, 337-342.

Roxborough, H. E., Burton, G. W., and Kelly, F. J. (2000). Inter- and intra-individual variation in plasma and red blood cell vitamin E after supplementation. *Free Radic Res* **33**, 437-445.

Ruckmani, K., Jayakar, B., and Ghosal, S. K. (2000). Nonionic surfactant vesicles (niosomes) of cytarabine hydrochloride for effective treatment of leukemias: encapsulation, storage, and *in vitro* release. *Drug Dev Ind Pharm* **26**, 217-222.

Sabin, J., Prieto, G., and Sarmiento, F. (2010). Studying colloidal aggregation using liposomes. *Methods Mol Biol* **606**, 189-198.

Sadikot, R. T., and Blackwell, T. S. (2005). Bioluminescence imaging. *Proc Am Thorac Soc* **2**, 537-540.

Saito, Y., Fukuhara, A., Nishio, K., Hayakawa, M., Ogawa, Y., Sakamoto, H., Fujii, K., Yoshida, Y., and Niki, E. (2009). Characterization of cellular uptake and distribution of coenzyme Q10 and vitamin E in PC12 cells. *J Nutr Biochem* **20**, 350-357.

Sakaguchi, N., Kojima, C., Harada, A., Koiwai, K., Emi, N., and Kono, K. (2008). Effect of transferrin as a ligand of pH-sensitive fusogenic liposome-lipoplex hybrid complexes. *Bioconjug Chem* **19**, 1588-1595.

Sakai, M., Okabe, M., Tachibana, H., and Yamada, K. (2006). Apoptosis induction by gamma-tocotrienol in human hepatoma Hep3B cells. *J Nutr Biochem* **17**, 672-676.

Sakai, M., Okabe, M., Yamasaki, M., Tachibana, H., and Yamada, K. (2004). Induction of apoptosis by tocotrienol in rat hepatoma dRLh-84 cells. *Anticancer Res* **24**, 1683-1688.

Sanghvi, R., Evans, D., and Yalkowsky, S. H. (2007). Stacking complexation by nicotinamide: a useful way of enhancing drug solubility. *Int J Pharm* **336**, 35-41.

Sanhai, W. R., Sakamoto, J. H., Canady, R., and Ferrari, M. (2008). Seven challenges for nanomedicine. *Nat Nanotechnol* **3**, 242-244.

Sato, A., Klaunberg, B., and Tolwani, R. (2004). *In vivo* bioluminescence imaging. *Comp Med* **54**, 631-634.

Sausville, E. A., and Burger, A. M. (2006). Contributions of human tumor xenografts to anticancer drug development. *Cancer Res* **66**, 3351-3354, discussion 3354.

Schätzlein, A. G. (2003). Targeting of Synthetic Gene Delivery Systems. *J Biomed Biotechnol* **2003**, 149-158.

Schauss, A. G. (2009). Tocotrienols: a review. In *Tocotrienols: Vitamin E beyond tocopherols* (R. R. Watson, and V. R. Preedy, Eds.), pp. 3-12. CRS Press Taylor & Francis Group, Boca Raton.

ScotPIL Training manual (2006). Small mammals-ScotPIL training.

Seger, R., and Krebs, E. G. (1995). The MAPK signaling cascade. *Faseb J* **9**, 726-735.

Semwogerere, D., and Weeks, E. R. (2005). Confocal microscopy. In *Encyclopedia of biomaterials and biomedical engineering* (G. E. Wnek, and G. L. Bowlin, Eds.). Marcel Dekker, New York.

Sen, C. K., Khanna, S., and Roy, S. (2007). Tocotrienols in health and disease: the other half of the natural vitamin E family. *Mol Aspects Med* **28**, 692-728.

Sen, C. K., Khanna, S., and Roy, S. (2009). Tocotrienols as natural neuroprotective vitamins. In *Tocotrienols: vitamin E beyond tocopherols* (R. R. Watson, and V. R. Preedy, Eds.), pp. 361-378. CRC Press Taylor & Francis Group, Boca Raton.

Sen, C. K., Khanna, S., Roy, S., and Packer, L. (2000). Molecular basis of vitamin E action. Tocotrienol potently inhibits glutamate-induced pp60(c-Src) kinase activation and death of HT4 neuronal cells. *J Biol Chem* **275**, 13049-13055.

Shafer-Peltier, K. E., Haka, A. S., Motz, J. T., Fitzmaurice, M., Dasari, R. R., and Feld, M. S. (2002). Model-based biological Raman spectral imaging. *J Cell Biochem Suppl* **39**, 125-137.

Shah, N., Chaudhari, K., Dantuluri, P., Murthy, R. S., and Das, S. (2009). Paclitaxel-loaded PLGA nanoparticles surface modified with transferrin and Pluronic((R))P85, an *in vitro* cell line and *in vivo* biodistribution studies on rat model. *J Drug Target* **17**, 533-542.

Shah, S., and Sylvester, P. W. (2004). Tocotrienol-induced caspase-8 activation is unrelated to death receptor apoptotic signaling in neoplastic mammary epithelial cells. *Exp Biol Med (Maywood)* **229**, 745-755.

Shchors, K., and Evan, G. (2007). Tumor angiogenesis: cause or consequence of cancer? *Cancer Res* **67**, 7059-7061.

Sheu, M. T., Chen, S. Y., Chen, L. C., and Ho, H. O. (2003). Influence of micelle solubilization by tocopheryl polyethylene glycol succinate (TPGS) on solubility enhancement and percutaneous penetration of estradiol. *J Control Release* **88**, 355-368.

Shibata, A., Nakagawa, K., Sookwong, P., Tsuzuki, T., Oikawa, S., and Miyazawa, T. (2008). Tumor anti-angiogenic effect and mechanism of action of delta-tocotrienol. *Biochem Pharmacol* **76**, 330-339.

Shirode, A. B., and Sylvester, P. W. (2010). Synergistic anticancer effects of combined gamma-tocotrienol and celecoxib treatment are associated with suppression in Akt and NFkappaB signaling. *Biomed Pharmacother* **64**, 327-332.

Silva, G. A., Czeisler, C., Niece, K. L., Beniash, E., Harrington, D. A., Kessler, J. A., and Stupp, S. I. (2004). Selective differentiation of neural progenitor cells by high-epitope density nanofibers. *Science* **303**, 1352-1355.

Simoes, S., Moreira, J. N., Fonseca, C., Duzgunes, N., and de Lima, M. C. (2004). On the formulation of pH-sensitive liposomes with long circulation times. *Adv Drug Deliv Rev* **56**, 947-965.

Simoes, S., Slepushkin, V., Gaspar, R., de Lima, M. C., and Duzgunes, N. (1998). Gene delivery by negatively charged ternary complexes of DNA, cationic liposomes and transferrin or fusigenic peptides. *Gene Ther* **5**, 955-964.

Simone, R., and Palozza, P. (2009). Antioxidant activity of tocotrienols in cells and serum. In *Tocotrienols: vitamin E beyond tocopherols* (R. R. Watson, and V. R. Preedy, Eds.), pp. 99-108. CRC Press Taylor & Francis Group, Boca Raton.

Slichenmyer, W. J., and Von Hoff, D. D. (1990). New natural products in cancer chemotherapy. *J Clin Pharmacol* **30**, 770-788.

Sparreboom, A., Scripture, C. D., Trieu, V., Williams, P. J., De, T., Yang, A., Beals, B., Figg, W. D., Hawkins, M., and Desai, N. (2005). Comparative preclinical and clinical pharmacokinetics of a cremophor-free, nanoparticle albumin-bound paclitaxel (ABI-007) and paclitaxel formulated in Cremophor (Taxol). *Clin Cancer Res* **11**, 4136-4143.

Srivastava, J. K., and Gupta, S. (2006). Tocotrienol-rich fraction of palm oil induces cell cycle arrest and apoptosis selectively in human prostate cancer cells. *Biochem Biophys Res Commun* **346**, 447-453.

Stoscheck, C. M. (1990). Quantitation of protein. *Methods Enzymol* **182**, 50-68.

Strebhardt, K., and Ullrich, A. (2008). Paul Ehrlich's magic bullet concept: 100 years of progress. *Nat Rev Cancer* **8**, 473-480.

Sugano, K., Kataoka, M., Mathews Cda, C., and Yamashita, S. (2010). Prediction of food effect by bile micelles on oral drug absorption considering free fraction in intestinal fluid. *Eur J Pharm Sci* **40**, 118-124.

Sun, W., Wang, Q., Chen, B., Liu, J., Liu, H., and Xu, W. (2008). Gamma-tocotrienol-induced apoptosis in human gastric cancer SGC-7901 cells is associated with a suppression in mitogen-activated protein kinase signalling. *Br J Nutr* **99**, 1247-1254.

Sundram, K., Khor, H. T., Ong, A. S., and Pathmanathan, R. (1989). Effect of dietary palm oils on mammary carcinogenesis in female rats induced by 7,12-dimethylbenz(a)anthracene. *Cancer Res* **49**, 1447-1451.

Suzuki, R., Takizawa, T., Kuwata, Y., Mutoh, M., Ishiguro, N., Utoguchi, N., Shinohara, A., Eriguchi, M., Yanagie, H., and Maruyama, K. (2008). Effective anti-tumor activity of oxaliplatin encapsulated in transferrin-PEG-liposome. *Int J Pharm* **346**, 143-150.

Sylvester, P. W. (2009). Antiproliferative and apoptotic effects of tocotrienols on normal and neoplastic mammary epithelial cells. In *Tocotrienols: vitamin E beyond tocopherols* (R. R. Watson, and V. R. Preedy, Eds.), pp. 119-140. CRC Press Taylor & Francis Group, Boca Raton.

Sylvester, P. W., and Shah, S. (2005). Intracellular mechanisms mediating tocotrienol-induced apoptosis in neoplastic mammary epithelial cells. *Asia Pac J Clin Nutr* **14**, 366-373.

Tan, B., and Mueller, A. M. (2009). Tocotrienols in cardiometabolic diseases. In *Tocotrienols: vitamin E beyond tocopherols* (R. R. Watson, and V. R. Preedy, Eds.), pp. 257-274. CRC Press Taylor & Francis Group, Boca Raton.

Thassu, D., Pathak, Y., and Deleers, M. (2007). Nanoparticulate drug delivery systems: an overview. In *Nanoparticulate drug delivery systems* (D. Thassu, M. Deleers, and Y. Pathak, Eds.), pp. 1-31. Informa Healthcare, New York.

Thermo Fisher Scientific Inc. (2009). Imidoester Crosslinkers: DMA, DMP, DMS, DTBP. *Thermo Scientific Product Instruction.*

Torchilin, V. P. (2000). Drug targeting. *Eur J Pharm Sci* **11 Suppl 2**, S81-91.

Torchilin, V. P. (2005). Fluorescence microscopy to follow the targeting of liposomes and micelles to cells and their intracellular fate. *Adv Drug Deliv Rev* **57**, 95-109.

Torchilin, V. P. (2005). Recent advances with liposomes as pharmaceutical carriers. *Nat Rev Drug Discov* **4**, 145-160.

Torchilin, V. P. (2006). Multifunctional nanocarriers. *Adv Drug Deliv Rev* **58**, 1532-1555.

Torchilin, V. P. (2007). Targeted pharmaceutical nanocarriers for cancer therapy and imaging. *Aaps J* **9**, E128-147.

Torchilin, V. P. (2008). Tat peptide-mediated intracellular delivery of pharmaceutical nanocarriers. *Adv Drug Deliv Rev* **60**, 548-558.

Torchilin, V. P. (2010). Passive and active drug targeting: drug delivery to tumour as an example. In *Drug delivery Handbook of experimental pharmacology* (M. Schafer-Korting, Ed.), pp. 3-53. Springer-Verlag Berlin Heidelberg, Heidelberg.

Traber, M. G., and Kayden, H. J. (1984). Vitamin E is delivered to cells via the high affinity receptor for low-density lipoprotein. *Am J Clin Nutr* **40**, 747-751.

Uchegbu, I. F. (2000). Niosomes and other synthetic surfactant vesicles with anti-tumour drugs. In *Synthetic Surfactant Vesicles: niosomes and other non-phospholipid vesicular systems* (I. F. Uchegbu, Ed.). Harwood Academic.

Uchegbu, I. F., Double, J. A., Kelland, L. R., Turton, J. A., and Florence, A. T. (1996). The activity of doxorubicin niosomes against an ovarian cancer cell line and three *in vivo* mouse tumour models. *J Drug Target* **3**, 399-409.

Uchegbu, I. F., Double, J. A., Turton, J. A., and Florence, A. T. (1995). Distribution, metabolism and tumoricidal activity of doxorubicin administered in sorbitan monostearate (Span 60) niosomes in the mouse. *Pharm Res* **12**, 1019-1024.

Uchegbu, I. F., and Duncan, R. (1997). Niosomes containing N-(2-hydroxypropyl)methacrylamide copolymer-doxorubicin (PK1): effect of method of preparation and choice of surfactant on niosome characteristics and a preliminary study of body distribution. *Int J Pharm* **155**, 7-17.

Uchegbu, I. F., and Florence, A. T. (1995). Non-ionic surfactant vesicles (niosomes): physical and pharmaceutical chemistry. *Advances in Colloid and Interface Science* **58**, 1-55.

Uchegbu, I. F., and Schätzlein, A. (2006). Vesicles prepared from synthetic amphiphiles-polymeric vesicles and niosomes. In *Nanoparticulates as drug carrier* (V. Torchilin, Ed.), pp. 95-124. Imperial College Press, London.

Uchegbu, I. F., Schätzlein, A., Vanlerberghe, G., Morgatini, N., and Florence, A. T. (1997). Polyhedral non-ionic surfactant vesicles. *J Pharm Pharmacol* **49**, 606-610.

Uchegbu, I. F., and Vyas, S. P. (1998). Non-ionic surfactant based vesicles (niosomes) in drug delivery. *Int J Pharm* **172**, 33-70.

Van Hal, D. A., Jeremiasse, E., Junginger, H. E., Spies, F., and Bouwstra, J. A. (1996). Structure of fully hydrated human stratum corneum: a freeze-fracture electron microscopy study. *J Invest Dermatol* **106**, 89-95.

Vanlerberghe, G. (2000). Non-Phospholipid vesicles: Birth or rebirth? In *Synthetic surfactant vesicles: niosomes and other non-phospholipid vesicular systems* (I. F. Uchegbu, Ed.). pp3-8. Harwood Academic.

Varma, M. V., and Panchagnula, R. (2005). Enhanced oral paclitaxel absorption with vitamin E-TPGS: effect on solubility and permeability *in vitro*, in situ and *in vivo*. *Eur J Pharm Sci* **25**, 445-453.

Veikkola, T., Karkkainen, M., Claesson-Welsh, L., and Alitalo, K. (2000). Regulation of angiogenesis via vascular endothelial growth factor receptors. *Cancer Res* **60**, 203-212.

Vistica, D. T., Skehan, P., Scudiero, D., Monks, A., Pittman, A., and Boyd, M. R. (1991). Tetrazolium-based assays for cellular viability: a critical examination of selected parameters affecting formazan production. *Cancer Res* **51**, 2515-2520.

Vivares, E., and Ramos, L. (2005). Polyelectrolyte-induced peeling of charged multilamellar vesicles. *Langmuir* **21**, 2185-2191.

Wacher, V. J., Wong, S., and Wong, H. T. (2002). Peppermint oil enhances cyclosporine oral bioavailability in rats: comparison with D-alpha-tocopheryl poly(ethylene glycol 1000) succinate (TPGS) and ketoconazole. *J Pharm Sci* **91**, 77-90.

Wachsmann-Hogiu, S., Weeks, T., and Huser, T. (2009). Chemical analysis *in vivo* and *in vitro* by Raman spectroscopy--from single cells to humans. *Curr Opin Biotechnol* **20**, 63-73.

Wada, S., Satomi, Y., Murakoshi, M., Noguchi, N., Yoshikawa, T., and Nishino, H. (2005). Tumor suppressive effects of tocotrienol *in vivo* and *in vitro*. *Cancer Lett* **229**, 181-191.

Wagner, E., Curiel, D. T., and Cotten, M. (1994). Delivery of drugs, proteins and genes into cells using transferrin as a ligand for receptor-mediated endocytosis. *Adv Drug Deliv Rev* **14**, 113-135.

Wagner, E. F., and Nebreda, A. R. (2009). Signal integration by JNK and p38 MAPK pathways in cancer development. *Nat Rev Cancer* **9**, 537-549.

Wali, V. B., Bachawal, S. V., and Sylvester, P. W. (2009). Combined treatment of gamma-tocotrienol with statins induce mammary tumor cell cycle arrest in G1. *Exp Biol Med (Maywood)* **234**, 639-650.

Wang, I. C., Tai, L. A., Lee, D. D., Kanakamma, P. P., Shen, C. K., Luh, T. Y., Cheng, C. H., and Hwang, K. C. (1999). C(60) and water-soluble fullerene derivatives as antioxidants against radical-initiated lipid peroxidation. *J Med Chem* **42**, 4614-4620.

Ware, E., Lu, D. R., and Øie, S. (2004). Cellular structure, function, and membrane transport. In *Cellular drug delivery principles and practice* (Ø. S. Lu D.R., Ed.), pp. 9-23. Humana Press, New Jersey.

Watt, I. M. (1997). *The principles and practice of electron microscopy*. Cambridge University Press, Melbourne.

Welsh, D. K., and Kay, S. A. (2005). Bioluminescence imaging in living organisms. *Curr Opin Biotechnol* **16**, 73-78.

Williams, D. B., and Carter, C. (1996). *Transmission electron microscopy: a textbook for material science*. Plenum Press, New York.

Williams, D. B., Carter, C., and Baillie, A. J. (1995). Visceral leishmaniasis in the Balb/C Mouse — a comparison of the in-vivo activity of 5 nonionic surfactant vesicle preparations of sodium stibogluconate. *J Drug Target* **3**, 1-7.

Win, K. Y., and Feng, S. S. (2005). Effects of particle size and surface coating on cellular uptake of polymeric nanoparticles for oral delivery of anticancer drugs. *Biomaterials* **26**, 2713-2722.

Wittgen, H. G., and van Kempen, L. C. (2007). Reactive oxygen species in melanoma and its therapeutic implications. *Melanoma Res* **17**, 400-409.

Wolfensohn, S., and Lloyd, M. (1998). *Handbook of laboratory animal management and welfare*. Blackwell Science, Oxford.

Wong, H. L., Bendayan, R., Rauth, A. M., Li, Y., and Wu, X. Y. (2007). Chemotherapy with anticancer drugs encapsulated in solid lipid nanoparticles. *Adv Drug Deliv Rev* **59**, 491-504.

Wright, S. J., and Wright, D. J. (2002). Introduction to confocal microscopy. In *Methods in cell biology* (B. Matsumoto, Ed.), pp. 2-85. Academic Press, California.

Wu, J., Lu, Y., Lee, A., Pan, X., Yang, X., Zhao, X., and Lee, R. J. (2007). Reversal of multidrug resistance by transferrin-conjugated liposomes co-encapsulating doxorubicin and verapamil. *J Pharm Pharm Sci* **10**, 350-357.

Wu, S. J., and Ng, L. T. (2010). Tocotrienols inhibited growth and induced apoptosis in human HeLa cells through the cell cycle signaling pathway. *Integr Cancer Ther* **9**, 66-72.

Xu, W. L., Liu, J. R., Liu, H. K., Qi, G. Y., Sun, X. R., Sun, W. G., and Chen, B. Q. (2009). Inhibition of proliferation and induction of apoptosis by gamma-tocotrienol in human colon carcinoma HT-29 cells. *Nutrition* **25**, 555-566.

Yan, A., Von Dem Bussche, A., Kane, A. B., and Hurt, R. H. (2007). Tocopheryl Polyethylene Glycol Succinate as a Safe, Antioxidant Surfactant for Processing Carbon Nanotubes and Fullerenes. *Carbon N Y* **45**, 2463-2470.

Yang, Z., Xiao, H., Jin, H., Koo, P. T., Tsang, D. J., and Yang, C. S. (2010). Synergistic actions of atorvastatin with gamma-tocotrienol and celecoxib against human colon cancer HT29 and HCT116 cells. *Int J Cancer* **126**, 852-863.

Yap, S. P., Julianto, T., Wong, J. W., and Yuen, K. H. (1999). Simple high-performance liquid chromatographic method for the determination of tocotrienols in human plasma. *J Chromatogr B Biomed Sci Appl* **735**, 279-283.

Yap, S. P., Yuen, K. H., and Lim, A. B. (2003). Influence of route of administration on the absorption and disposition of alpha-, gamma- and delta-tocotrienols in rats. *J Pharm Pharmacol* **55**, 53-58.

Yap, W. N., Chang, P. N., Han, H. Y., Lee, D. T., Ling, M. T., Wong, Y. C., and Yap, Y. L. (2008). Gamma-tocotrienol suppresses prostate cancer cell proliferation and invasion through multiple-signalling pathways. *Br J Cancer* **99**, 1832-1841.

Yap, W. N., Zaiden, N., Luk, S. Y., Lee, D. T., Ling, M. T., Wong, Y. C., and Yap, Y. L. (2010). *In vivo* evidence of gamma-tocotrienol as a chemosensitizer in the treatment of hormone-refractory prostate cancer. *Pharmacology* **85**, 248-258.

Yi, Y., Kim, J. H., Kang, H. W., Oh, H. S., Kim, S. W., and Seo, M. H. (2005). A polymeric nanoparticle consisting of mPEG-PLA-Toco and PLMA-COONa as a drug carrier: improvements in cellular uptake and biodistribution. *Pharm Res* **22**, 200-208.

Ying, X., Wen, H., Lu, W. L., Du, J., Guo, J., Tian, W., Men, Y., Zhang, Y., Li, R. J., Yang, T. Y., Shang, D. W., Lou, J. N., Zhang, L. R., and Zhang, Q. (2010). Dual-targeting daunorubicin liposomes improve the therapeutic efficacy of brain glioma in animals. *J Control Release* **141**, 183-192.

Yoshida, J., Mizuno, M., and Yagi, K. (1992). Cytotoxicity of human beta-interferon produced in human glioma cells transfected with its gene by means of liposomes. *Biochem Int* **28**, 1055-1061.

Yoshida, Y., and Niki, E. (2009). Antioxidant action of tocotrienols and tocopherols in solution and membranes: chemical and physical effects. In *Tocotrienols: vitamin E beyond tocopherols* (R. R. Watson, and V. R. Preedy, Eds.), pp. 109-118. CRC Press Taylor & Francis Group, Boca Raton.

Yoshioka, T., Skalko, N., Gursel, M., Gregoriadis, G., and Florence, A. T. (1995). A non-ionic surfactant vesicle-in-water-in-oil (v/w/o) system: potential uses in drug and vaccine delivery. *J Drug Target* **2**, 533-539.

Yoshioka, T., Sternberg, B., and Florence, A. T. (1994). Preparation and properties of vesicles (niosomes) of sorbitan monoesters (Span 20,40,60 and 80) and a sorbitan triester (Span 85). *Int J Pharm* **105**, 1-6.

Youk, H. J., Lee, E., Choi, M. K., Lee, Y. J., Chung, J. H., Kim, S. H., Lee, C. H., and Lim, S. J. (2005). Enhanced anticancer efficacy of alpha-tocopheryl succinate by conjugation with polyethylene glycol. *J Control Release* **107**, 43-52.

Yu, L., Bridgers, A., Polli, J., Vickers, A., Long, S., Roy, A., Winnike, R., and Coffin, M. (1999). Vitamin E-TPGS increases absorption flux of an HIV protease inhibitor by enhancing its solubility and permeability. *Pharm Res* **16**, 1812-1817.

Yuan, F., Dellian, M., Fukumura, D., Leunig, M., Berk, D. A., Torchilin, V. P., and Jain, R. K. (1995). Vascular permeability in a human tumor xenograft: molecular size dependence and cutoff size. *Cancer Res* **55**, 3752-3756.

Yuen, K., Ng, B., and Wong, J. (2009). Absorption and disposition of tocotrienols. In *Tocotrienols: vitamin E beyond tocopherols* (R. R. Watson, and V. R. Preedy, Eds.), pp. 297-308. CRC Press Taylor & Francis Group, Boca Raton.

Zhang, L., Chan, J. M., Gu, F. X., Rhee, J. W., Wang, A. Z., Radovic-Moreno, A. F., Alexis, F., Langer, R., and Farokhzad, O. C. (2008). Self-assembled lipid--polymer hybrid nanoparticles: a robust drug delivery platform. *ACS Nano* **2**, 1696-1702.

Zhang, W., Parsons, M., and McConnell, G. (2010). Flexible and stable optical parametric oscillator based laser system for coherent anti-Stokes Raman scattering microscopy. *Microsc Res Tech* **73**, 650-656.

Zhang, Z., Lee, S. H., Gan, C. W., and Feng, S. S. (2008). *In vitro* and *in vivo* investigation on PLA-TPGS nanoparticles for controlled and sustained small molecule chemotherapy. *Pharm Res* **25**, 1925-1935.

Zhao, H., and Yung, L. Y. (2009). Addition of TPGS to folate-conjugated polymer micelles for selective tumor targeting. *J Biomed Mater Res A* **91**, 505-518.

Zou, A., Hoffmann, H., Freiberger, N., and Glatter, O. (2007). Influence of ionic charges on the bilayers of lamellar phases. *Langmuir* **23**, 2977-2984.